RESEARCH DURING 1992-1993 CONCERNING PURPOSEFUL AND INADVERTENT WEATHER MODIFICATION IN ILLINOIS

Precipitation, Cloud Changes, and Impacts (PreCCIP)

by

Stanley A. Changnon, Robert R. Czys, Steven E. Hollinger,
Kenneth Kunkel, Nancy E. Westcott, Robert W. Scott,
Mary Schoen Petersen, Mark Belding, Robin T. Shealy, German Bollero,
Aki Akanbi, Radivan Al-Weshah, and Misganaw Demissie

and

Subcontractors from: Indiana University
South Dakota School of Mines and Technology
Syracuse Research Corporation
Woodley Weather Consultants

Annual Report of Research
During June 1, 1992 - May 31, 1993

NOAA Cooperative Agreement
NA27RA0173-01

Contract Report 560
Illinois State Water Survey
Champaign, Illinois

TABLE OF CONTENTS

INTRODUCTION

The scientific research described herein was conducted within the context of the Precipitation-Cloud Changes and Impacts Project (PreCCIP) of the Illinois State Water Survey. PreCCIP is an ongoing research effort, originally entitled Precipitation Augmentation for Crops Experiment (PACE). The program is in its 13th year of research relating to atmospheric modification

The overall goal of PreCCIP is to understand and measure the modification of atmospheric processes, resulting from inadvertent human activities or purposeful cloud seeding, and the impacts of altered weather and climate conditions on the hydrologic cycle, agricultural activities, and on the social and institutional structure of Illinois. Findings from the PreCCIP research concerning atmospheric processes and the effects of changed conditions are key inputs into a myriad of individual and institutional decisions affecting Illinois. They include major questions about 1) the application of cloud seeding to try to alter precipitation; 2) the magnitude and factors causing inadvertent climate change at the local and regional scales; 3) the types and importance of physical effects and socioeconomic impacts caused by altered weather; and 4) the monitoring, control, and regulation of activities leading to either purposeful or inadvertent modification of weather and climate. PreCCIP embraces a wide range of scientific research including studies of physical processes in the atmosphere, investigations to define how additional summer rain alters a com crop and shifts farm income, and studies of how altered weather conditions affect local, state, and federal activities.

The research described herein was defined on the basis of five major considerations. First has been the findings from past research, which has been structured in a step-by-step approach to develop an understanding of atmospheric processes and their modification. The research was also based upon findings of the most recent results of an ongoing analysis of a 1989 cloud modification experiment. The third factor affecting the research was the status of our understanding of our research on effects of altered weather on various physical and socioeconomic systems. Our staff capabilities and facilities available to the project were a fourth factor influencing the research conducted. The needs for scientific information relating to altered weather and climate in Illinois and the Midwest were a fifth factor in our research endeavors.

The research of PreCCIP in this year focused on three broad topical areas which have been embraced throughout the past five years of the 12-year project. The first is a continuing **study of cloud and precipitation processes.** This is an essential part of understanding how to purposefully modify precipitation in Illinois and the Midwest. Our studies largely completed analyses of the 1989 seeding trials in Illinois.

The second programmatic area of PreCCIP concerned **studies of inadvertent modification of weather and climate conditions** in Illinois and the Midwest. This research has attempted to address major unanswered questions about urban and lake influences on precipitation.

The third area of endeavor related to **studies of the effects of altered weather and climate conditions.** This research embraced studies of impacts on water resources including soil moisture, on agriculture, on the economy, and on government activities.

This report describes the research during a 12-month period which began on June 1, 1992. The research is described by tasks organized under each of the three major programmatic areas.

PURPOSEFUL MODIFICATION OF CLOUDS AND PRECIPITATION

Chapter 1. Summary Of Activities Related To Analysis And Reporting On Results From The 1989 PACE Field Experiment

Summary

An important part of our research related to planned weather modification was continued analysis and reporting on results (task 4) from the exploratory cloud seeding trials conducted in Illinois during the growing season of 1989. The purpose of this chapter is to 1) highlight results from the 1989 experiment, and 2) summarize our efforts to communicate these results.

1. SUMMARY OF 1989 PACE RESULTS

The 1989 PACE experiment produced three major scientific findings. These findings apply to: 1) seeding effects that could be detected in the visual appearance or behavior of the treated cloud, 2) effects on the scale of individual radar echo cores, and 3) effects on radar estimated rainfall at the scale of the multicelled cumulonimbus cloud system.

a. Evaluation of seeding effects based on visual observations

At the end of each flight, the pilot of the meteorological/seeding aircraft, a 20-year veteran in cloud seeding, and the on-board meteorologist-cloud physicist, made independent assessments of which type of treatment the experimental units had received, either Agl or sand. Both persons were totally blind as to the treatments used, and blind to each others guesses. They could only judge the treatment effects by the appearances they expected to see in the rapidly growing upper portions of the cumulus congestus being sampled. Their individual decisions about the type of treatment were made after each flight, along with a record of their reasons for naming the treatment. If they could not show evidence of what they believed was either seeding or no seeding, they could indicate that they were unable to make a decision.

The project's senior radar meteorologist was also involved in a similar experiment. During the analysis of the radar data, and after all treated echo cores had been completely measured, this analyst was asked to examine the data to identify which of the experimental units appeared to have been treated with Agl and which with sand. The analyst could also indicate inability to make a decision. This person was also totally blind to the treatment type. Decisions as to Agl treatment were based on perceptions that the seeded echo behavior, in particular horizontal growth and/or intensity, would conform to a standard reaction.

The treatment identification made by the three individuals for each of the 25 experimental units listed in Table 1. In some cases, the observers and the analyst were unable to make a choice, and these cases are noted. Several instances of indecision occurred during May when rain systems were large and complex.

Table 2 summarizes each individual's choices based only on the cases when each person made a choice. Both observers on the aircraft were very skillful in detecting seeding effects in the

clouds. Interestingly, this shows that the pilot picked 17 of 20 treatments correctly, or 85 percent. The on-board meteorologist also showed positive skill in picking 13 of 19, or 68 percent.

Conversely, the radar analyst picked only 5 of 18 cases correctly. The radar analyst's 28 percent rate of correct identification falls well below chance and reflects no skill. This result suggests use of an incorrect perception of seeding effects, or an inverse cloud response due to seeding. Thus, the expected radar portrayal of the seeded echo behavior was reversed, and a low score by the analyst was in essence "correct," in that it was substantiated by the ensuing analysis of the behavior of seeded clouds.

Also shown in Table 2 are the choices made for the large "A" experimental units, and the smaller "B" experimental units. This breakdown indicates that the pilot and the on-board meteorologist were both extremely skilled in identifying the treatment choices made with the smaller clouds. The pilot's score was perfect, nine for nine, and the meteorologist was 80 percent correct. Both were less accurate on the large cloud choices. This may be attributed to the greater complexity of the large cloud experimental units, which are more difficult to track and observe during and after treatment. They represent much more complicated cloud conditions than the B experimental units. This is also expected because the B experimental units were penetrated two or more times, providing the pilot and the meteorologist with more information on B experimental units than on A experimental units.

The cases when the pilot, the meteorologist, and the analyst could not make a treatment decision showed no preference for either seeded or nonseeded cases, and were almost evenly split for each individual. Inability to decide occurred for several reasons including lack of aircraft contact with treated clouds and the complexity of the sky. In most such cases, the observers reported that they were unable to follow the clouds elements after treatment.

Interpretation of the visual impressions about seeding effects must be made cautiously due to the limited response variables and the relatively small sample size. However, the results of this simple experiment suggest that it was apparently possible for the pilot and the on-board meteorologist to see differences in cloud behavior when Agl was used, but could not see these differences in experimental units when sand was used. This suggests to us that Agl dosages were sufficient to instill some sort of a cloud reaction, and that the sand flares had little effect on the outward appearance of the clouds (i.e. they were truly placebo). However, these first-hand visual observations were not substantiated by the radar meteorologist. That is, the characteristics of the seeded echo cores, as perceived by radar analysis, were generally less indicative of expected behavior (rapid growth and larger tops) than were the sand-treated clouds. Hence, based on the expected primary echo reaction to seeding, the analyst's decisions were in a sense "correct" guesses. One of the important unanswered questions is why the growth of clouds appeared visually but not in the radar data.

b. Results for Individual Echo Cores

Key results are presented for the most suitable clouds, defined as those with a Seedability Index (SI) greater than or equal to 70 percent; and for less suitable clouds, defined as those with SI < 80 percent. These two subgroups were selected for analysis because they provide a fairly large

sample of clouds for each SI filter level chosen. In general, the key findings discussed here for clouds in both subgroups are supported if other SI percentages are selected for analysis.

Table 3 lists key response variables for clouds that met ≥ 70 percent of the seedability criteria. Only one response variable showed a significant difference between the Agl and sand treatments: maximum height. Hence, to the extent that this significant difference did not happen by chance, the response data suggest that the Agl-treated clouds may not have grown as tall as the sand-treated echo cores. Evidence of no other effects on parameters such as area, reflectivity, or brightness, could be found in the data for clouds with SI ≥ 70 percent. This conclusion is clearly opposite from that expected according to the dynamic seeding hypothesis.

Figure la is a graph showing the composite behavior of echo height for clouds with SI ≥ 70 percent. In Figure la, mean echo-core height was computed for only those echo cores that existed at each interpolated observation time relative to treatment. Hence, sample size, shown by the numbers along the bottom of Figure la for either Agl- or sand-treated clouds, changes with time. In Figure la, the Agl-treated echoes observed at 9 minutes prior to treatment are not necessarily the same Agl-treated echoes observed 24 minutes after treatment. Because Figure la allows only for comparison of echoes that were in existence at the observation time, mean values were recomputed using the entire sample of clouds at each interpolated observation time, and these are shown in Figure lb. In this case, a zero height was used for every observation time at which no echo core existed.

Examination of both plots of Figure 1 reveals two important features. First, both methods of computing mean maximum height reveal that for a period of time after treatment the sand-treated clouds were taller than the Agl-treated clouds. Figure la suggests that this difference is greater than one standard measurement error $\left(\frac{\sigma}{\sqrt{n}}\right)$ by 2 to 3 km, for a duration of approximately 30 minutes, beginning at about the time of treatment. The difference between the mean maximum heights of the sand- and Agl-treated clouds is much less dramatic when computed on the basis of a constant sample size (Figure 28b). However, Figure lb suggests that there may have been a short period of time (~12 minutes) when the mean maximum height of the sand-treated clouds exceeded that of the Agl-treated clouds by one standard measurement error.

Figure 2 shows composite diagrams for mean maximum echo-core areas. As can be seen in Figure 2a, mean area growth rates overlap one another beginning almost as early as 21 minutes prior to treatment, and they continue to be similar until about 12 minutes after treatment. After that time the Agl-treated echo cores suddenly decline in mean area, separating the means by more than one standard error. However, mean areas computed on the basis of the entire sample of clouds (Figure 2b) do not show a dramatic difference. Thus, although the "snapshot" of response variables that is offered in Table 3 did not suggest an effect on area, Figure 2 provides weak evidence that there may also have been a negative effect on echo-core area. This finding is also inconsistent with that expected from the dynamic seeding hypothesis.

Figure 3a shows mean maximum reflectivity with time before and after treatment. While Figure 3b gives no indication of a seeding effect on reflectivity, Figure 3a shows faint evidence that there may have been a reduction in reflectivity that roughly corresponds to the time in which Figure 2a suggests a reduction in area. However, the decrease in reflectivity at about 21 minutes

after treatment occurs only briefly, adding to the uncertainty with which a firm conclusion can be drawn.

Figure 4 shows composite diagrams for mean maximum rain flux for echo cores that met ≥ 70 percent of the seedability criteria. These plots are the "noisiest" of the composite diagrams which makes interpretation difficult. However, the plots appear to indicate that both samples of echo cores had similar rain flux from approximately 18 minutes prior to treatment until about 15 minutes after treatment. After this time and corresponding to the decrease in mean echo-core area and reflectivity, rain fluxes for the sand-treated echoes become about one standard error greater than the Agl-treated echoes. This difference persists about 33 to 42 minutes after treatment.

In summary, the evidence presented in Figures 1-4 and in Table 3 does not provide definitive conclusion about what effect, if any, Agl treatment may initially have had on the individual echo cores with SI ≥ 70 percent. However, if there was any effect at all, the evidence suggests that Agl treatment may have been related to a reduction of echo core; height, area, reflectivity, and rain flux. The important conclusion which we arrived at from this analysis was that all of the apparent effects of Agl seeding were contrary to those expected from the dynamic seeding hypothesis, and that reconsideration of the dynamic seeding hypothesis (DSH), its applicability to Illinois clouds and possibly rejection of the DSH in favor of a different seeding hypothesis were warranted.

c. Evaluation of radar estimated rainfall at the scale of the multi-celled system.

The radar-indicated rainfall associated with the large cloud experimental units was subjected to an analysis that compared the Agl- and sand-related rainfall amounts. Each experimental unit was divided into time segments of 15 minutes. The amount of rainfall accumulated during 15-minute segments before treated (BT-15) and after treatment ended (ET + 15) was measured using a radar-rainfall relationship developed for Illinois. The treatment period itself was the only portion of time not fixed in a 15-minute interval during the lifetime of an experimental unit. Because the treatment period for each experimental unit ranged from 15 to 40 minutes, and averaged 30 minutes, a discrete time breakdown was not possible. The rainfall produced in a unit was stated in relation to the time treatment began and ended, however long this period took. Thus, the rainfall "clock" was set to begin with a measurement 15 minutes before treatment and then at 15-minute intervals after the treatment of the unit ended.

The amount of accumulated rainfall was determined for each experimental unit, as shown in Table 4. The amount of rainfall occurring in the extended area, 240 x 240 km square around the radar, was also determined as shown in Table 5.

The median values were determined for the six Agl treatments and the six sand treatments for each of the time segments. The resulting median values were plotted in the upper portion of Figure 5. The units' median values at treatment minus 15 minutes were identical, and they were still similar when treatment began: Agl = 30.8 10^4 m^3 and sand = 24.7 10^4 m^3. However, during the 30 minutes of treatment (the average value), the Agl-related median rainfall value increased rapidly over the median sand value. At the end of the treatment, the median rainfall value for the Agl cases was 182.9 10^4 m^3, as compared to 78.8 10^4 m^3 for sand, which was 2.3 times

higher. In the 30 minutes after treatment ended, the rainfall medians of both Agl- and sand-treated units increased in a generally similar direction, followed by a relative decrease in the rainfall production of the Agl-treated units. The ratios of their differences decreased from 1.47 at ET+30, to 1.2 by ET+60, and to 1.1 by ET+90.

The rainfall results suggest *different conclusions* than did the results for individual echo cores. The accumulated rainfall data for the experimental units treated with Agl showed: 1) an abrupt increase over the sand-treated unit rainfall just after treatment, given that the units started with about the same rainfall amount at BT-15; and 2) a generally decreasing difference between Agl- and sand-related rainfall up to ET+90. This result alone may suggest an enhancement due to Agl treatment, although tests of the differences show probability values of 0.11 to 0.27 for a seeding effect. Hence, this assessment points to the possibility that Agl *may* have had a positive effect on *system* rainfall, in spite of a possible neutral to negative effect on the growth of *individual* clouds that eventually merge with the parent rain system. The extended area results suggest that the Agl-treated units were occurring in convective rainfall situations less favorable for heavy rainfall production than were the sand-treated units. However, we must keep in mind that the determination of rainfall using a radar equation is subject to very large errors which can be up to + 100 percent of the indicated amount, and that the radar-indicated values for the experimental units were not "calibrated" to surface rain gage data because recording rain gages in the study area were insufficient to accomplish such a calibration. Thus, the results of the radar-indicated rainfall amounts are subject to large uncertainty and must be taken with caution.

d. Summary

Because the sample size is small and only applies to a single summers worth of clouds, it is not possible to draw firm conclusions about the effects that Agl seeding may have had on individual clouds or the multi-celled systems that they were associated with. However, the analysis leaves three distinct impressions on which judgments can be made for the direction of future research. First, Agl treatments apparently had an effect on cloud appearance that could be seen, while any effects that sand may have had on cloud appearance could not be noticed. Secondly, if there was a seeding effect on individual echo cores, it was probably opposite or negative. Third, rainfall amounts estimated from radar data on the scale of the meso-scale rain system were weakly positive in spite of the negative effects on individual echo cores. In combination, these results are not at all consistent with that expected from the dynamic seeding hypothesis.

2. COMMUNICATION OF RESULTS

A major activity of research related to planned weather modification has been to bring these results to the attention to those in agriculture, to those in the weather modification community and to those in the atmospheric science community as a whole. To achieve these ends, a number of formal presentations were made to the Illinois Farm Bureau, at the past two annual meetings of the weather modification association, and at the last AMS Symposium on Weather Modification. Another major undertaking during this past year has been the production of an Illinois State Water Survey Bulletin, which is the Water Survey's most prestigious publication. This publication will be distributed through our the state. We also published two refereed articles in the present issue (42nd) *Journal of Weather Modification,* and three scientific papers

were sent to the *Journal of Applied Meteorology*. These provide an in-depth discussion of the results from the 1989 PACE field experiment.

Table 1. Summary by experimental unit of the judgments made by the pilot, in-flight meteorologist, and radar meteorologist of whether AgI or a placebo was used as the treatment material

Experiment unit				*Estimations*		
Number	*Type**	*Date*	*Treatment*	*Pilot*	*In-flight meteorologist*	*Radar meteorologist*
1	B	5/19	AgI	**	**	**
2	A	5/19	P	**	**	AgI√
3	B	5/25	P	**	AgI√	**
4	B	5/30	P	**	AgI√	**
5	A	6/1	AgI	**	AgI	P√
6	B	6/3	P	P	P	AgI√
7	B	6/3	AgI	AgI	AgI	**
8	B	6/12	AgI	AgI	AgI	AgI
9	B	6/12	P	P	P	P
10	B	6/18	P	P	P	**
11	A	6/23	AgI	AgI	**	P√
12	A	6/23	AgI	AgI	AgI	**
13	A	6/23	P	P	AgI√	AgI√
14	B/A	6/27	P	P	P	AgI√
15	B/A	6/27	AgI	AgI	AgI	P√
16	B	7/2	P	P	**	P
17	A	7/8	P	P	**	AgI√
18	A	7/8	AgI	AgI	AgI	P√
19	A	7/11	AgI	AgI	P√	P√
20	A	7/19	P	P	P	AgI√
21	B	7/19	AgI	AgI	AgI	**
22	A	7/23	AgI	P√	P√	AgI
23	A	7/24	P	P	P	P
24	A	7/25	P	AgI√	AgI√	AgI√
25	A	7/25	AgI	P√	**	P√

Notes:

√ Incorrect guess

* A - large clouds; B = small clouds

** Unable to make a decision

Table 2. Summary by experimental unit type of the correctness of judgments made by the pilot, in-flight meteorologist, and radar meteorologist of whether Agl or a placebo was used as the treatment material

	Pilot	*In-Flight meteorologist*	*Radar meteorologist*
Total number of choices of treatment:	20	19	18
Number correct:	17	13	5
Percent correct:	85	68	28
Number of "A" or large cloud choices:	11	9	12
Number correct:	8	5	2
Percent correct:	73	56	17
Number of "B" or small cloud choices:	9	10	6
Number correct:	9	8	3
Percent correct:	100	80	50

Table 3. Response Variables for Clouds with SI > 70% (N = 40)

Responce	Mean		Standard Deviation		Sample Size		p1	p2
Variable	Sand	AgI	Sand	AgI	Sand	AgI		
MaxH10	10.808	8.571	2.713	1.989	26	14	0.010	0.012
MaxA10	80.192	65.643	61.154	55.636	26	14	0.464	0.321
MaxZ	52.623	52.074	13.483	12.167	26	14	0.900	0.734
MaxB	27.700	28.240	6.414	6.496	26	14	0.802	0.691
MXCPdH10	2.538	0.714	2.702	1.541	26	14	0.026	0.025
MXCPdA10	37.000	26.857	57.548	45.951	26	14	0.573	0.734
MXCPdZ	5.035	6.558	12.201	12.754	26	14	0.713	0.810
MXCPdB	2.678	3.262	6.229	6.974	26	14	0.788	0.691
CPMXtMxA	9.519	8.321	14.055	7.677	26	14	0.770	0.533
FEMXtMxA	19.008	16.621	11.129	9.205	26	14	0.497	0.288

$p \leq 5\%$		$p \leq 10\%$		$p > 10\%$	

Table 4. Median radar estimated accumulated rain fall for the Agl and Sand treated experimental units.

	Agl							*Sand*				
Interval	*6/1*	*6/23(1)*	*7/8(2)*	*7/11*	*7/23*	*7/25(2)*	*5/19*	*6/23(3)*	*7/8(1)*	*7/19(1)*	*7/24*	*7/25(1)*
BT-15	17.4	0.8	2.8	3.2	5.0	2.8	2.6	*23*	22.8	13.8	2.8	1.9
BT	95.9	10.0	44.5	13.1	48.3	17.1	20.1	14.9	51.0	69.9	29.2	12.1
ET	261.9	M	242.9	30.6	182.9	24.8	95.9	118.5	583	111.6	61.7	21.1
ET+15	404.9	M	496.7	57.8	205.5	24.5	145.7	232.9	82.0	177.2	113.9	28.1
ET+30	536.1	M	7823	75.2	246.1	24.8	203.6	355.0	112.0	245.7	129.3	40.6
ET+45	647.9	M	940.4	107.2	278.5	24.8	312.2	441.8	117.3	283.7	144.5	49.98
ET+60	743.9	M	1118.1	146.6	285.6	24.8	369.6	479.0	1193	304.7	170.6	56.2
ET+75	823.0	M	1428.1	208.8	291.2	24.8	452.1	495.2	122.8	310.0	199.5	61.4
ET+90	840.6	M	1770.1	331.7	295.5	24.8	519.1	554.0	125.2	320.9	276.7	62.8

Notes:
(1) and (2) refer to the first or second experimental unit on these dates.
M = Missing data.
BT = Beginning of treatment.
ET = End of treatment.

Table 5. Median radar estimated accumulated rain fall for the extended area.

	Agl						*Sand*					
Interval	*6/1*	*6I23*[(1)]	*7/8*[(2)]	*7/11*	*7/23*	*7I25*[(2)]	*5/19*	*6/23*[(3)]	*7/8*[(1)]	*7/19*[(1)]	*7/24*	*7I25*[(1)]
BT-15	3.6	13	3.6	.02	1.0	0.6	9.2	3.8	4.1	7.1	0.8	1.1
BT	16.5	5.3	*22.2*	1.1	7.0	2.5	50.7	17.1	16.2	39.1	5.5	5.1
ET	35.0	M	73.1	4.0	19.0	4.0	126.0	39.2	34.9	612	9.2	10.9
ET+15	59.7	M	109.1	6.6	20.4	4.4	156.2	53.3	52.9	97.3	16.1	12.9
ET+30	87.*5*	M	142.0	8.9	22.7	4.8	180.6	63.9	78.0	1223	18.4	14.1
ET+45	109.7	M	166.6	13.8	24.8	5.4	213.8	73.0	107.9	144.7	23.2	14.8
ET+60	123.6	M	1962	20.5	26.5	5.9	227.5	78.9	136.3	165.5	26.6	15.2
ET+75	145.0	M	231.3	29.3	27.9	6.3	248.1	84.6	169.8	193.7	29.9	15.7
ET+90	152.7	M	282.5	40.1	30.1	6.9	261.8	90.0	197.0	2103	39.6	16.3

NOTES:
(1) and (2) refer to the first or second experimental unit on these dates.
M = Missing data.
BT = Beginning of treatment.
ET =Ending of treatment.

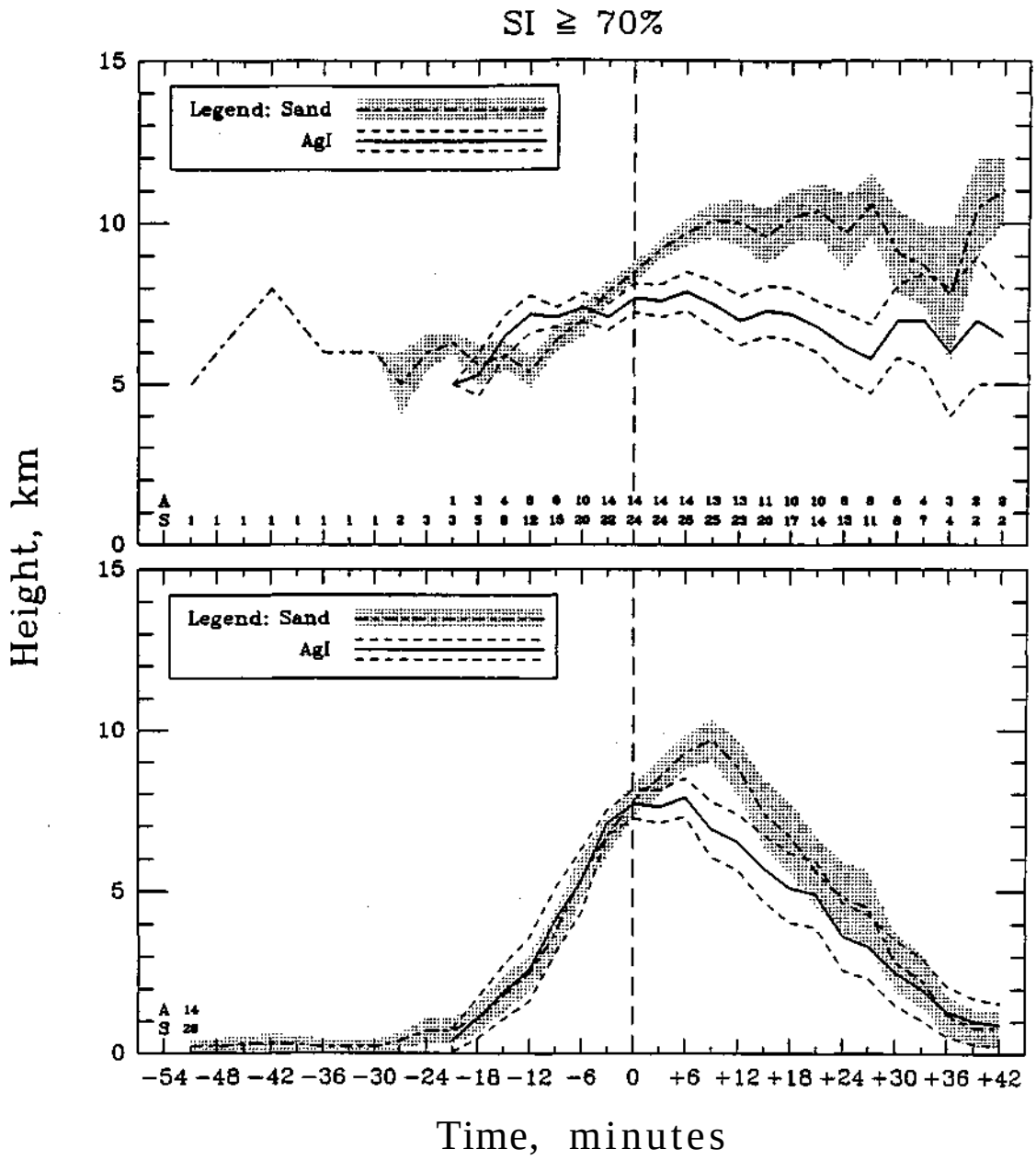

Figure 1. Composite diagram showing variation of echo core height with time for echo cores having a Seedability Index ≥ 70%.

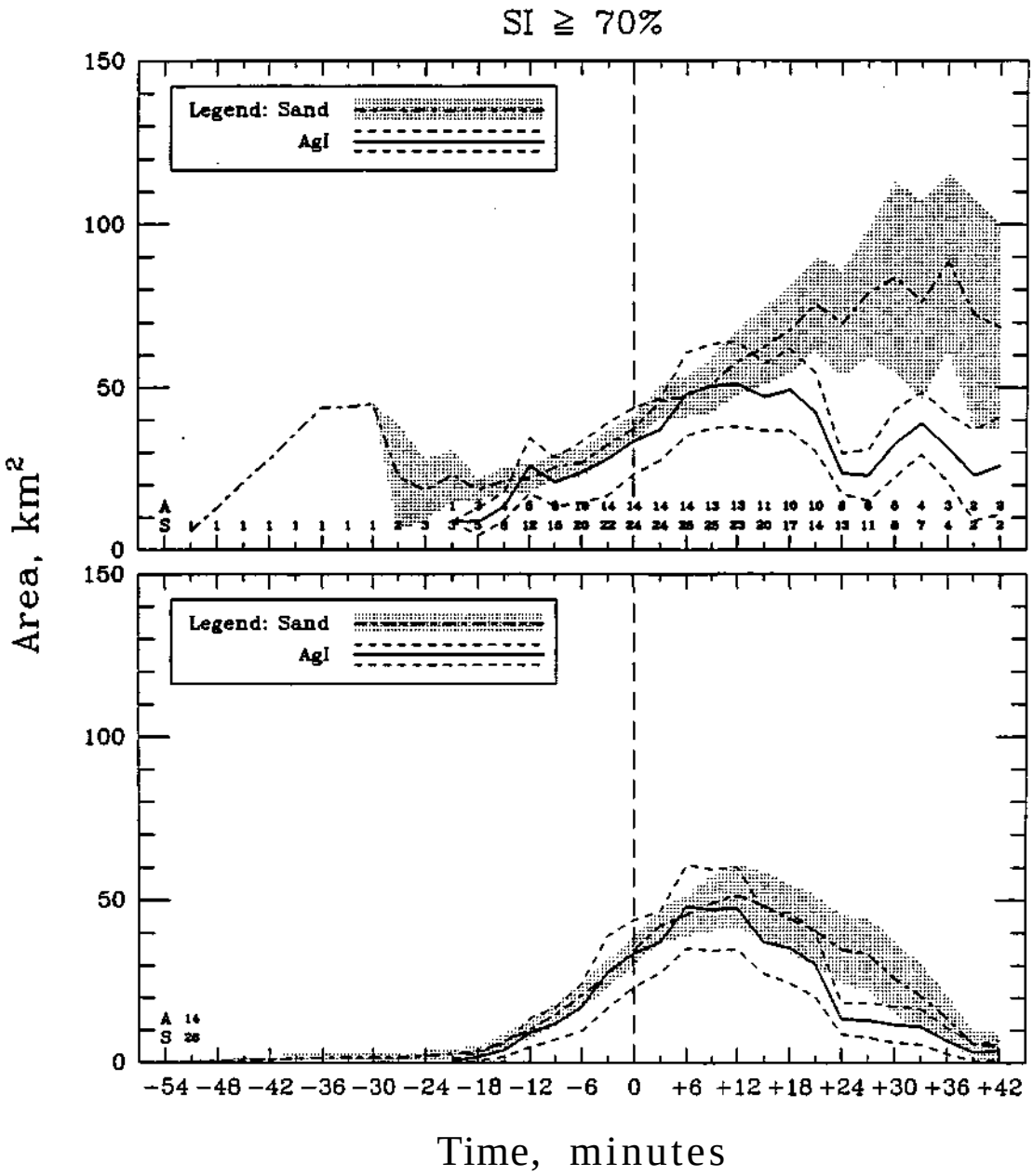

Figure 2. Composite diagram showing variation of echo core area with time for echo cores having a Seedability Index ≥ 70%.

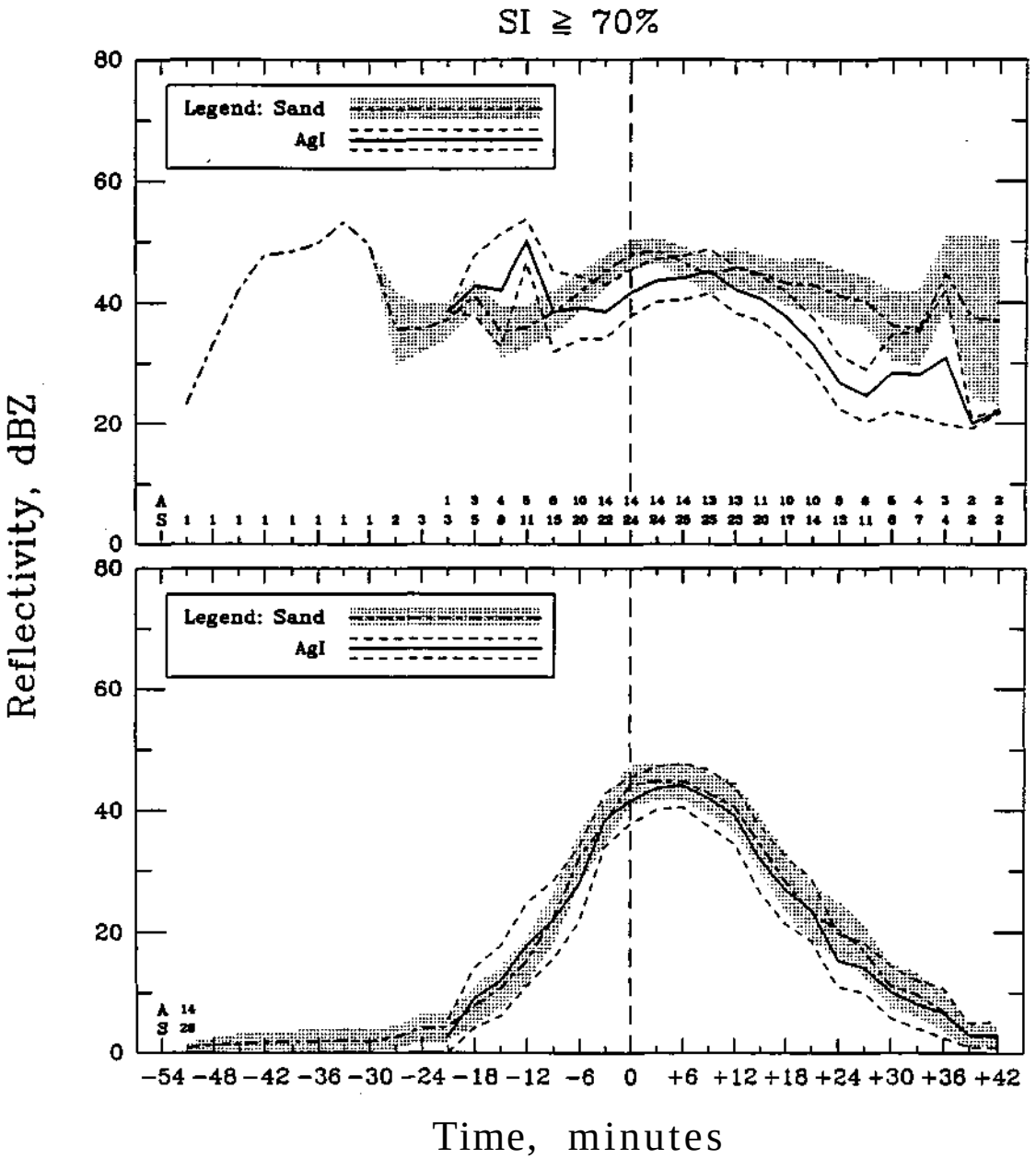

Figure 3. Composite diagram showing variation of echo core reflectivity with time for echo cores having a Seedability Index ≥ 70%.

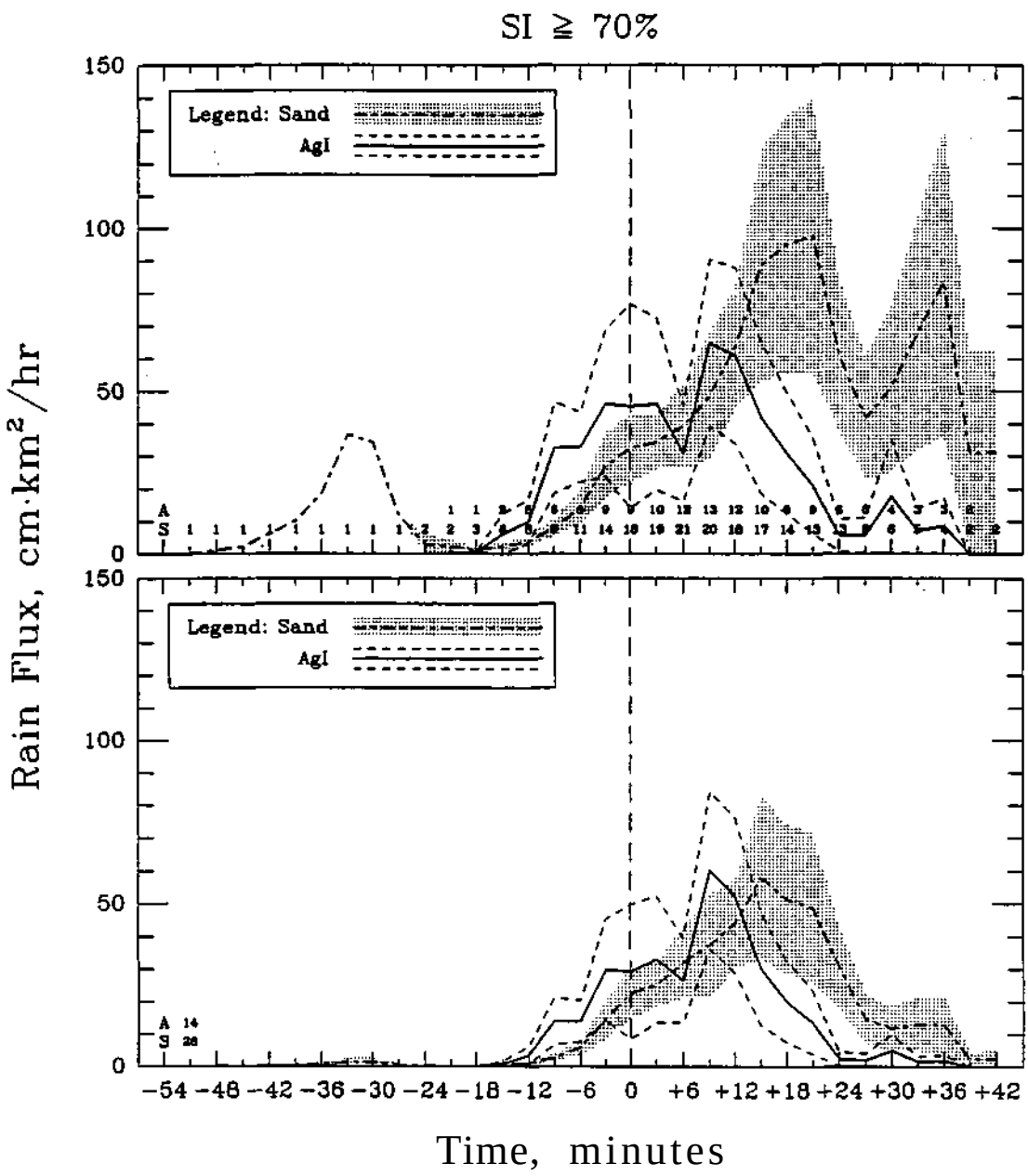

Figure 4. Composite diagram showing variation of echo core rain flux with time for echo cores having a Seedability Index ≥ 70%.

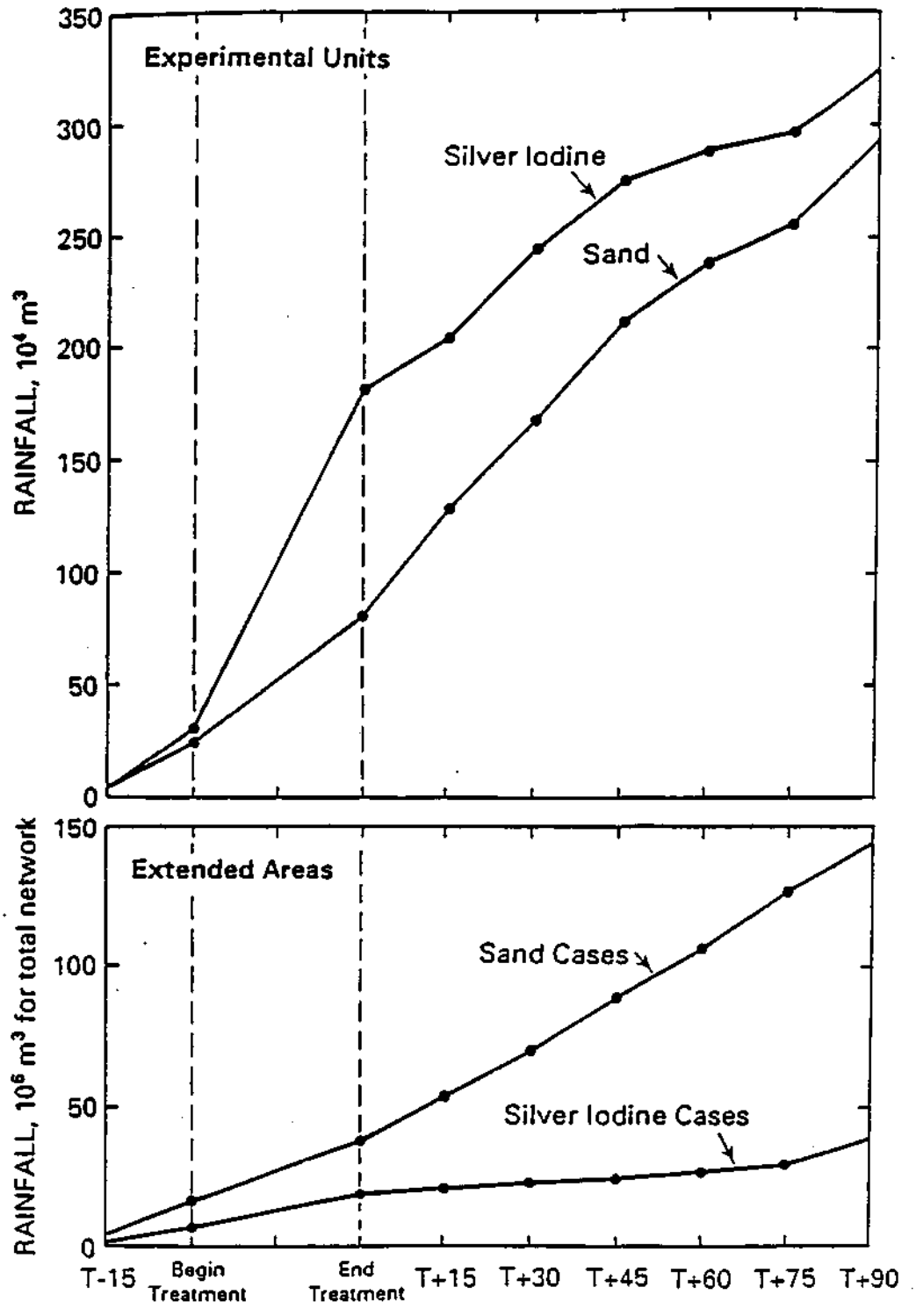

Figure 5. Variation with time relative to seeding of median radar estimated rainfall for experimental units (upper) and the network (lower) as a whole.

Chapter 2. Observational Study Of The Initiation Of Ice In The Warm Based Illinois Cumulus Congestus Of The 1989 PACE Field Program

Summary

Basic scientific understanding about natural warm-based convective clouds, how ice may naturally originate, and how the natural origination of ice may be altered by glaciogenic cloud seeding which may in turn should have effects on cloud dynamics. During this research period, we completed an analysis of microphysical data obtained at the -10°C level during the 1989 PACE field experiment. This analysis focused on the initiation of ice. There were several important findings. Our observations indicate that- ice probably originates from the direct freezing of supercooled drizzle and rain drops- indicated by a high correlation between concentrations of supercooled drizzle and rain drops and concentrations of "first" graupel. We found that there is no correlation between estimated cloud top temperature and the concentration of ice - indicating that ice nuclei are either unimportant or their influence is masked by some other mechanism. Examination of data from 2D optical array probes revealed a large number of images which resemble those that may have been cast by the shadow of two precipitation-size drop frozen together upon contact. This possibility was examined under the belief that these "double," or "dumbbell" shaped images may have occurred in the 2D image records because of the colocation of two precipitation-size drops in the laser beam of the optical array probe. Using theory for particle coincidence in FSSP data, we determined that the number of double images observed in the 1989 PACE 2D data set were too numerous to have occurred by "coincidence." This finding supports the collision-freezing hypothesis developed for PACE clouds; that is ice may originate from the collision of supercooled drizzle and rain drops in the evolution of rain by a supercooled coalescence process. However, for this mechanism to be viable, the collision rate between supercooled drizzle and rain drops must be sufficiently large such that the production of ice from collisions can be accounted for. Existing theory for collision rates for precipitation-size drops was used with the 1989 PACE microphysical data to determine if rates are large enough to account for observed concentrations of ice. This analysis revealed that only a small fraction, less than 10%, of the collisions must result in freezing for a collision-freezing mechanism to explain first ice concentrations. Therefore, the possibility of a first ice mechanism can not be ruled out on the basis of this evidence.

1. INTRODUCTION

Ice has been observed in some types of clouds at temperatures warmer and concentrations higher than if heterogeneous nucleation acted alone. Dobson (1949) was probably the first to report indirect evidence that detectable concentrations of ice crystals in his cloud chamber occurred at temperatures much colder than indicated by observations earlier made by Findeisen (1942). Since these early observations, there has been a large number of field studies that have also encountered discrepancies between concentrations of "first" ice and ice nuclei. Mossop (1970, 1985a) has provided excellent reviews of the state of knowledge about the origin and concentration of ice in clouds. Although a substantial amount of progress has been made toward understanding the initiation and evolution of ice in clouds, wide gaps still exist in our knowledge about this subject

Three mechanisms are widely recognized as being responsible for the conventional production of primary ice in clouds: 1) heterogeneous nucleation; 2) secondary or multiplication processes; and, 3) homogeneous nucleation. The proposed research will focus on another ice nucleation mechanism that has received limited attention, but may potentially be very important in clouds with an active coalescence process. This mechanism has been referred to as "dynamic" or "mechanical" ice nucleation (Chalmers 1961, Chalmers 1964, Gitlin and Lin 1969, Goyer et al. 1965).

It is well known that the primary mechanism for precipitation initiation in deep, warm based convective clouds is by a warm-rain process (Langmuir 1948). Radar observations in the humid Midwest have indicated that approximately 50% of first echoes form at temperatures totally warmer than 0°C, and that another 40% straddle the 0°C isotherm (Battan 1953, Braham and Dungey 1978). As an updraft carries a cloudy parcel of air containing drizzle and raindrops to temperatures colder than 0°C, a "warm-rain" process involving supercooled drops must proceed, and it is collisions between supercooled drizzle and rain drops that may result in the origin of ice in the type of clouds that were studied in the 1989 PACE field program.

2. ICE INITIATION IN THE PRESCENCE OF SUPERCOOLED DRIZZLE AND RAINDROPS

Much of what is known about the origin of ice in deep convective clouds with active coalescence processes has been inferred from observations taken around the humid midwest (Koenig 1963, Brown and Braham 1963, Braham 1964, Czys 1991, and Czys and Petersen 1992a), Florida (Hallett et al. 1978, Sax et al. 1979, and Willis and Hallett 1991), west Texas (Jurica and Scro 1985), and South Africa (Bruintjes et al. 1987) A large number of additional findings very relevant to ice initiation have been made from measurements of maritime clouds around Australia (Mossop et al. 1968, Mossop et al. 1970, Mossop et al. 1972, and Mossop 1985b), and mostly around the Pacific Northwest (Hobbs 1969, Hobbs and Rangno 1985, Hobbs and Rangno 1990, and Rangno and Hobbs 1991).

There were a number of key findings initially reported from Project Whitetop (Braham 1964, and Koenig 1963) that have held true to this day, which are very relevant to the proposed research:

1) ice initiates at temperatures as warm as -5°C usually in the form of frozen precipitation-size drops and graupel;

2) ice concentrations are 10 to 1000 times higher than expected from conventional measures of ice nuclei (Fig. 1);

3) there is little or no dependence of first ice concentration on cloud top temperature (Fig. 1);

4) ice usually does not appear until after supercooled drizzle and rain drops are present, and;

5) ice concentrations are positively correlated with concentrations of supercooled drizzle and raindrops (Figs. 2 and 3).

3. "MECHANICAL" OR "DYNAMIC" ICE NUCLEATION

The fact that ice can be mechanically nucleated in supercooled water was demonstrated many years ago when Barnes (1906) showed that water in a glass vessel could be caused to freeze at -3 or -4°C if it was agitated by shaking. Young and Van Sicklen (1913) found that the crude mechanical shock of a "hammer" (~37 g) falling a few millimeters on to a "anvil" submerged in bulk water would cause ice to nucleate. Dorsey (1948) reported that water in a sealed glass bulb could be easily supercooled to -14°C. Sharp tapping on the bulb's exterior and sloshing had no effect, but violent splashing caused freezing.

The first reference to the possibility that ice may nucleate from collisions between supercooled drops in clouds may have occurred following Blanchard's (1957) presentation at the First Conference on Clouds and Precipitation. There, L.J. Battan asked if attempts were made to produce supercooled drop collisions in the vertical wind tunnel to explore the possibility that collision may "accelerate freezing." E.J. Workman, referring to the works of Reynolds, then commented, "If one could form the union of two drops which are so structurally organized as to be unable to freeze themselves, then the disorder which would be introduced by bringing these drops into coalescence might account for or favor freezing of supercooled droplets in thunderstorms even when they (presumably the droplets) are quite small."

Almost a decade later, Hobbs (1965) speculated that supercooled droplets in natural fogs may freeze on collision. Alkezweeny (1968) reported that two 1 mm diameter supercooled drops suspended from strings had an enhanced probability of freezing when they were brought into contact.

Alkezweeny (1969) may have been the first to uncover observational evidence of a collision-freezing mechanism in replicator data (see Fig. 4). In presenting this data, Alkezweeny has indicated that frozen droplets with diameters greater than about 50 μm can easily be distinguished from liquid droplets of the same or larger diameter because the latter tend to splash upon impacting the replicator substrate. Of course, the replicator data of Alkezweeny is not absolute evidence that the drops froze in collision prior to their sampling, but this report motivated examination of 2DC and 2DP image data [that were collected during the 1989 field program of the Precipitation Augmentation for Crops Experiment (Changnon et al. 1991)] for shapes that may have been cast by the shadows of two drops frozen together on contact.

In Fig. 5 one example can be found of an image (arrow) that may have been cast by two drops frozen together. The possibility that this "double image" may be related to the coresidence of two precipitation-size particles in the 2D laser beam has been considered. Following the discussion by Baumgardner et al. (1985) about coincidence problems in FSSP data, the probability that two particles will be collocated in the sample volume of the laser beam can be computed from the integral

$$P_t = \int_0^{t_1} \beta e^{-\beta t} dt = 1 - e^{-\beta t_1} \quad (1)$$

where ß is the mean expected inter arrival rate of the particles and t_1 is the average transit time of the particle through the laser beam. In Eq. 1, the mean inter arrival rate can be found from

$$ß = N_o W L_D v \quad (2)$$

where N_Q is the "actual concentration", W is the beam width, L_D is the length of the DOF, and v is the true air speed. According to specifications we have for the 2DC probe used in the 1989 PACE field program, a value of 0.432 cm^2 was used for the sample area (WxL_D). True air speed was approximately 100 m s^{-1}, and we compute (Czys and Petersen 1992b) that N_0 = 0.001 cm . A value for the average transit period, t_l, was obtained from the ratio of the beam width to the true airspeed, or t_1 = 0.08 cm / 10^4 cm s^{-1} = 8.0 x 10^{-6} s. Substitution of these values in the right hand side of Eq. 1 yields

$$P_t = 3.456 \text{x} 10^{-5} \quad (3)$$

Thus, there is roughly one chance in approximately 30,000 image frames of finding two precipitation-size drops collocated.

During the course of the 1989 PACE field experiment, a total of approximately 120,000 2DC image frames were obtained (where we did not count streakers and artifacts, but included zero area and one diode images to obtain a conservative estimate). Thus, based on the grand total number of images there was a chance of finding on the order of four images frames depicting the shadow of two collocated particles. In comparison, a total of 75 double images were identified in the 2DC image records and 21 found in the 2DP image records, many times more than would be expected by "coincidence". Therefore, the argument of particle collocation does not account for all of the 2DC double images that were found in the 1989 PACE 2DC image data.

The 1989 PACE 2D image records obtained at temperatures colder than 0°C were carefully examined for other images of the dumbbell type shown in Fig. 5. When such an image was found the maximum dimension (diameter) of each particle in the couplet was estimated and recorded to a computer file using software designed for this task (Czys and Petersen, 1992b). The size data for the double-images are plotted in Fig. 6 as open diamonds. Alkezweeny's data are plotted as the solid squares, and is in fairly good agreement with the 1989 PACE observations. Another interesting feature of Fig. 6 is that both the 1989 PACE and Alkezweeny observations fall outside the area where theory (shading) would predict mechanical ice nucleation by cavitation (Czys 1989). However, this might be attributed to the possibility that higher energy collisions result in coalescence-freezing, and that newly coalesced drops would form a spherical shape upon freezing which would go detected as a drop or a graupel in the 2D data.

4. COLLISION RATES AND FREEZING PROBABILITIES

For a collision-freezing mechanism to be viable, natural collision rates and collision-freezing probability must be within realistic limits. Following the theoretical work of Rogers (1989), the rate at which drops collide with other drops can be estimated from

$$P_1 = \frac{3}{2}\frac{\pi \, E \, k \, n_0^{\,2}}{\lambda^5}, \quad [\text{collisions s}^{-1}\text{m}^{-3}] \tag{4}$$

where E is the collection efficiency, $k = 4X10^3$ s^{-1} is a constant related to parameterization of drop fall speed, and X and n_0 are the slope and the intercept, respectively, of the raindrop size distribution. For this calculation, we have assume a Marshall-Palmer (1948) size distribution with $n_0 = 0.08$ cm^{-4} and have obtained a value of $\lambda = 24.8$ cm^{-1} from

$$Z = \frac{720 n_0}{\lambda^7} \times 10^{12}, \quad [\text{mm}^6\text{m}^{-3}] \tag{5}$$

assuming a reflectivity of 40 dBZ (i.e. $Z=10^4$ mm^6 m^{-3}). Substitution of values into Eq. 4 yields

$$P_1 = 12.8 \text{ s}^{-1} \text{ m}^{-3}. \tag{6}$$

For a cloudy parcel of air containing supercooled drizzle and raindrops, raising from the 0°C level to where it is observed (say the -10°C level for this example), than the transit time (t) to reach the observation level is given by $\Delta z/U$, where Δz is the depth of the 0 to -10°C layer, and U the mean rate of rise of the parcel. Assuming that the collision rate remains constant over the transit time, the concentration of ice (N_I) that should be present at the observation level from a collision-freezing mechanism may be estimated by

$$N_I = P_1 \tau \, f_p \tag{7}$$

where f_p is the collision-freezing probability. If t = 500 s (2000 m/4 m s^{-1}) then Eq. 7 reduces to

$$N_I = 6400 \, f_p \quad \left[\frac{\text{collisions}}{\text{m}^3} \cdot \frac{\text{freezes}}{\text{collision}}\right] or \left[\text{m}^{-3}\right] \tag{8}$$

From Eq. 8 we see that a freezing probability of 10 percent would result in an estimated ice concentration of about .5 e^{-1}, and that a freezing probability of approximately 75 percent would result in a concentration of about 5 e^{-1}; both of which are in the range of observed "first" ice concentrations.

Thus, this rough estimate suggests that a collision-freezing mechanism can not be ruled on the basis of inadequate numbers of collisions or unrealistically high freezing probabilities. Furthermore, a collision-freezing mechanism would also fit other aspects of the observational evidence: ice would appear only after the production of supercooled drizzle and rain drops; and

concentrations would be dependent on concentrations of supercooled precipitation-size drops, but would not be dependent on temperature.

5. CONCLUSIONS

Deep, warm-based convective rain clouds, characterized by moderate updrafts and appropriate initial CCN spectra, typically produce raindrops by coalescence before or shortly after cloud top passes above the 0°C level. The production of rain involving interactions between supercooled drizzle and rain drops must proceed even though temperatures are colder than 0°C. Under these conditions observations indicate that ice originates at temperatures warmer and concentrations higher than expected from heterogeneous nucleation alone. If a fraction of the interactions in self-collection (Berry and Reinhardt 1974) resulted in freezing, then collision rates and collision-freezing probabilities do not have to be unrealistic to account for the type and concentration of ice.

6. REFERENCES

Adam, J.R., R. Cataneo, and R.G. Semonin, 1971: The production of equal and unequal size droplet pairs. *Rev. ScL Instrum.,* 42,1847-1849.

Alkezweeny, AJ., 1968: The fragmentation of freezing water droplets in free fall. Ph.D. *thesis,* University of Washington, 88 pp.

Alkezweeny, A J., 1969: Freezing of supercooled water droplets due to collision. *J. Atmos. ScL,* 8, 994-995.

Barnes, H.T., 1906: *Ice Formation.* J. Wiley, 260 pp.

Battan, L.J., 1953: Observation on the formation and spread of precipitation in convective clouds. *J. Meteor.,* 10, 311-324.

Baumgardner, D., W. Strapp, J.E. Dye, 1985: Evaluation of the Forward Scattering Spectrometer Probe. Part II: Corrections for Coincidence and dead-time losses. *J. Atmos. Ocean. Technol.,* 2, 626-632.

Berry, E.X, and R.L. Reinhardt, 1974: An analysis of cloud drop growth by collection: Part I-IV. *J. Atmos. ScL,* 31,1814-1831, 2118-2135.

Blanchard, D.C. 1957: The supercooling, freezing and melting of giant waterdrops at terminal velocity in air. *Artificial Stimulation of Rain,* New York, Peraamon Press, 427 pp

Blanchard, D.C, 1969: Electrostatic field and freezing. *Science,* **133,** 1672.

Braham, R.R., Jr., 1964: What is the role of ice in summer rain-showers? *J. Atmos. ScL,* 21, 640-645.

Braham, R.R., Jr., and M.J. Dungey, 1978: A study of urban effects on radar first echoes. *J. Atmos. Sci.,* 17, 644-654.

Brown, E.N., and R.R. Braham, Jr., 1963: Precipitation particle measurements in cumulus congestus. *J. Atmos. Sci.,* 20, 23-28.

Bruintjes, R.T., AJ. Heymsfield, and T.W. Krauss, 1987: An examination of double plate ice crystals and the initiation of precipitation in continental cumulus clouds. *J. Atmos. Sci.,* 44, 1331-1349.

Chalmers B., 1961: The growth of ice in supercooled water. Edgar Marburg Lecture, *Amer. Soc. Testing Mater. Proc,* 1-9.

Chalmers, B., 1964: *Principles of Solidification.* New York, Wiley, 86-89.

Changnon, S.A., R.R. Czys, R.W. Scott, and N.E. Westcott, 1991: The Illinois precipitation modification program. *Bull. Amer. Meteor. Soc,* 72, 587-604.

Czys, R.R., and H.T. Ochs, 1988: The influence of charge on the coalescence of water drops in free fall. *J. Atmos. Sci.,* 45, 3161-3168.

Czys, R.R., 1989: Ice initiation by collisional forcing in warm-based cumuli. *J. Appl. Met.,* 28, 1098-1104.

Czys, R.R., 1991: A preliminary appraisal of the microphysical nature and seedability of warm-based midwestem clouds at -10°C.*J. Weat. Mod.,* 23, 1-17.

Czys R.R. and M.S. Petersen, 1992a: Observations of first ice in Illinois cumulus. Preprints 11th International Conference on Clouds and Precipitation. Montreal, Canada.

Czys, R. R. and M. S. Petersen, 1992b: A roughness detection technique for objectively classifying drops and graupel in 2D image records. *Jour. Atmos and Ocean Tech., 9,* 242-257.

Czys, R.R., 1993: Preliminary Laboratory Results On The Coalescence Of Small Precipitation-Size Drops Falling Freely in a Refrigerated Environment. *J. Atmos. Sci.,* in review.

Dobson, G.M.B., 1949: Ice in the atmosphere. *Quart. J. R. Met. Soc,* 75, 117-130.

Dorsey, N.E. 1938: The freezing of supercooled water. *Trans. Amer. Phil. Soc,* 38, 247-328.

Findeisen, W., 1942: Ergebnisse von Wolken - und Niederschlags-beobachtungen bei Wetterkundungesflugen uber See. Reichsamt f. Wetterdienst Forsch. u. Erfahrungsberichte, B. No. 8, 3-12.

Gitlin S.N., and S. Lin, 1969: Dynamic nucleation of the ice phase in supercooled water. 7. *Appl. Phys.,* 40, 4761-4767.

Goyer, G.G., T.C. Nhadra, and S. Gitlin, 1965: Shock induced freezing of supercooled water. *J. Appl. Met.,* 4, 156-160.

Hallett, J., R.I. Sax, D. Lamb, and A.S. Ramachandra Murty, 1978: Aircraft measurements of ice in Florida cumuli. *Quart. J. Roy. Meteor. Soc,* 104, 631-651.

Hobbs, P. V., 1965: The aggregation of ice particles in clouds and fogs at low temperatures. *J. Atmos. ScL,* 22, 296-300.

Hobbs, P.V., 1969: Ice multiplication in clouds. *J. Atmos. ScL,* 26, 315-318.

Hobbs P.V., and A.L. Rangno, 1985: Ice particle concentrations in clouds. *J. Atmos. Sci.,* 42, 2523-2549.

Hobbs, P.V. and A.L. Rangno 1990: Rapid development of high ice particle concentrations in small polar maritime cumuliform clouds. *J. Atmos. Sci.,* 47, 2710-2722.

Jayaratne, O.W., and B J. Mason, 1964: The coalescence and bouncing of water drops at an air/water interface. *Proc. Roy. Soc (London),* A280, 545-565.

Jurica, G.M., and K.D. Scro, 1985: Microphysical properties of cumulus congestus clouds observed during Texas HIPLEX. *Pro. Fourth WMO Conf. on Weather Modification,* Honolulu, World Meteor. Org., 363-368.

Koenig, L.R., 1963: The glaciating behavior of small cumulonimbus clouds. *J. Atmos. Sci.,* 20, 29-47.

Langmuir, I., 1948: The production of rain by a chain reaction in cumulus clouds at temperatures above freezing. J. *Meteor.,* 5,175-192.

Marshall, J.S., and W. McK. Palmer, 1948: The distribution of raindrops with size. *J Meteor.,* 5, 165-166.

Mossop, S.C., R.E. Ruskin, and KJ. Heffernan, 1968: Glaciation of a cumulus at approximately -4°C. *J. Atmos. ScL,* 25, 889-899.

Mossop, S.C., 1970: Concentrations of ice crystals in clouds. *Bull. Amer. Meteor. Soc,* 51, 474-479.

Mossop, S.C., A. Ono, and E.R. Wishart, 1970: Ice particles in maritime clouds near Tasmania. *Quart. J. Roy. Meteor. Soc,* 96, 487-508.

Mossop, S.C., R.E. Cottis, and B.M. Bartlett, 1972: Ice crystal concentrations in cumulus and stratocumulus clouds. *Quart. J. R. Met. Soc,* 98, 105-123.

Mossop, S.C., 1985a: The origin and concentration of ice crystals in clouds. *Bull. Amer. Meteor. Soc,* 66, 264-273.

Mossop, S.C., 1985b: Microphysical properties of supercooled cumulus clouds in which an ice particle multiplication process operated. *Quart. J. Roy. Meteor. Soc,* 111, 183-198.

Ochs, H.T., R.R. Czys, and K.V. Beard, 1986: Laboratory measurements of coalescence efficiencies for small precipitation drops. *J. Atmos. ScL,* 43,225-232.

Ramamurty, M., R.M. Rauber, B.P. Collins, P.C. Kennedy, and W.L. Clark, 1991: UNIWIPP: A University of Illinois field experiment to investigate the structure of mesoscale precipitation in winter storms. *Bull. Amer. Meteor. Soc,* 72, 764-776.

Rangno, A.L., and P.V. Hobbs, 1991: Ice particle concentrations and precipitation development in small polar maritime cumuliform clouds. *Quart. J. Roy. Meteor. Soc,* 117, 207-241.

Sax, R.I., J. Thomas, M. Bonebrake, and J. Hallett, 1979: Ice evolution within seeded and non-seeded Florida cumuli. *J. Appl. Met.,* 18, 203-214.

Willis, P.T., and J. Hallett, 1991: Microphysical measurements from an aircraft ascending with a growing isolated maritime cumulus tower. *J. Atmos. Sci.,* 48, 283-300.

Young, S.W., and WJ. Van Sicklen, 1913: The mechanical stimulus to crystallization. *Amer. Chem. Soc. J.,* 35, 1067-1078.

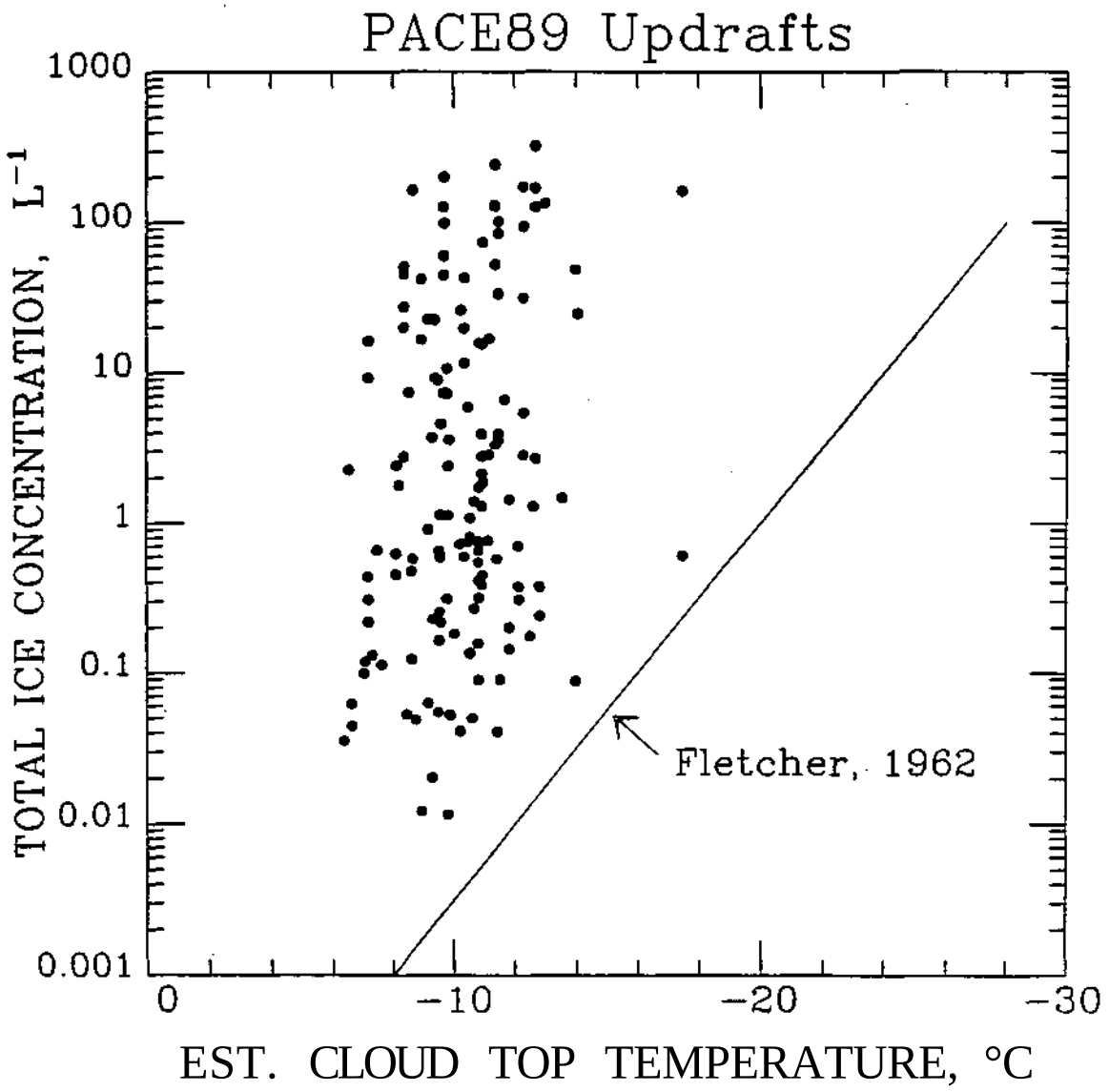

Figure 1. Estimated cloud top temperature versus total (2DC + 2DP) ice concentration observed in the updrafts of deep, warm-based clouds that were sampled during the 1989 PACE field experiment.

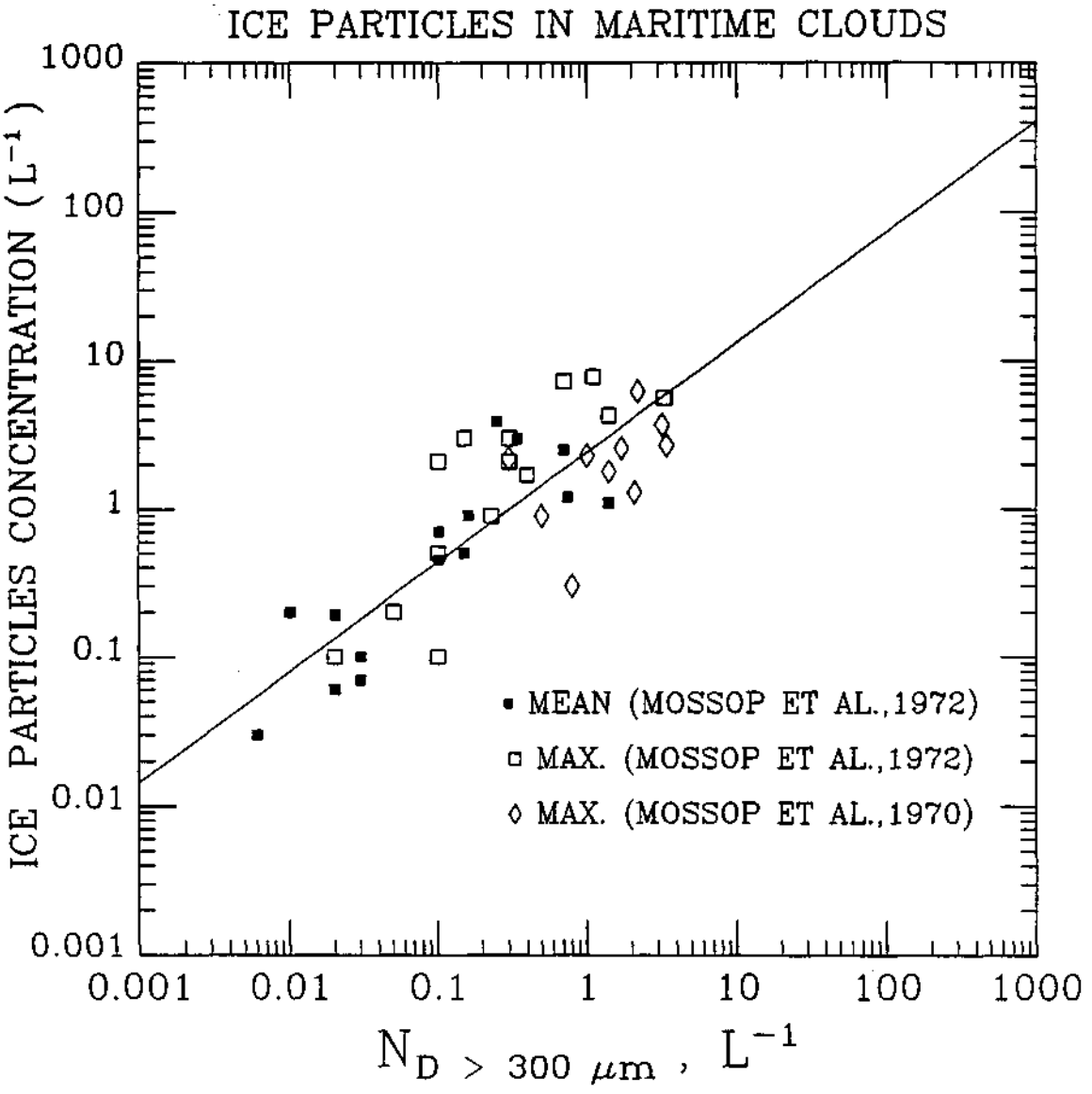

Figure 2. Relationship between concentration of supercooled drizzle and rain drops ($N_{D>300}$ μm) and ice concetration for maritime clouds measured around Australia.

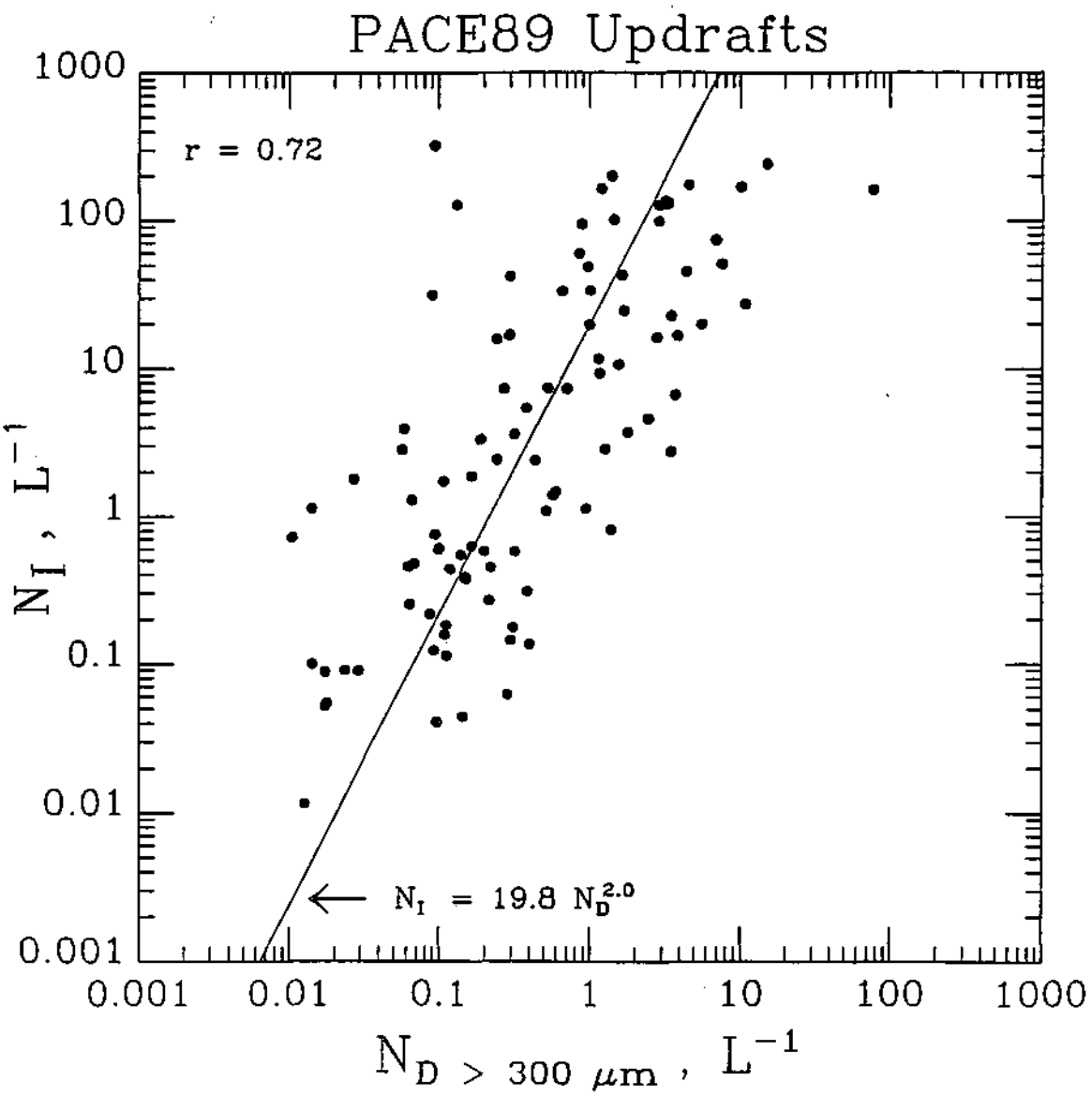

Figure 3. Relationship between concentration of supercooled drizzle and rain drops ($N_{D>300}$ μm) and ice concentration in the updrafts of deep, warm-based clouds sampled during the 1989 PACE field experiment.

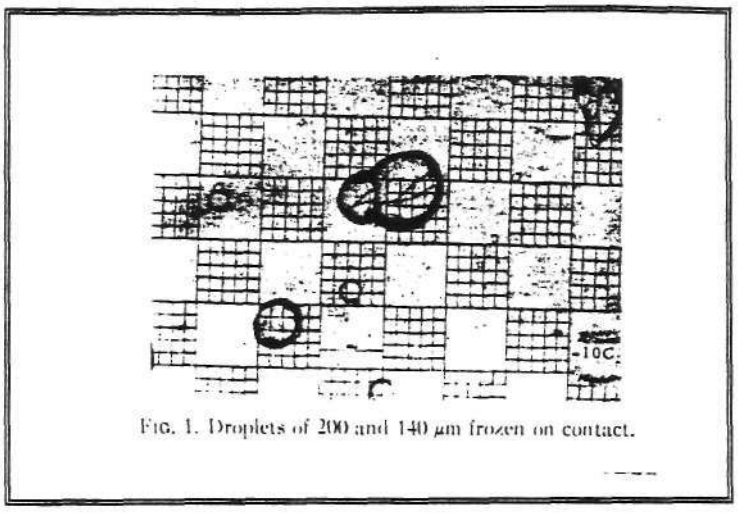

FIG. 1. Droplets of 200 and 140 μm frozen on contact.

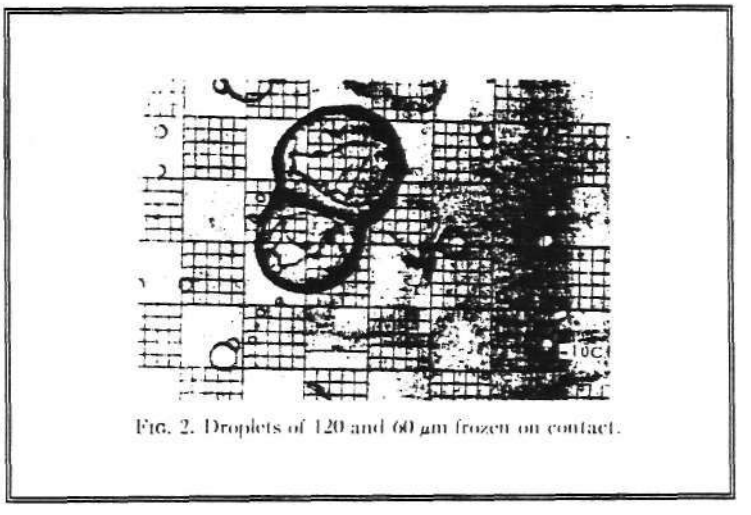

FIG. 2. Droplets of 120 and 60 μm frozen on contact.

Figure 4. Examples of double images that were reported by Alkezweeny (1969).

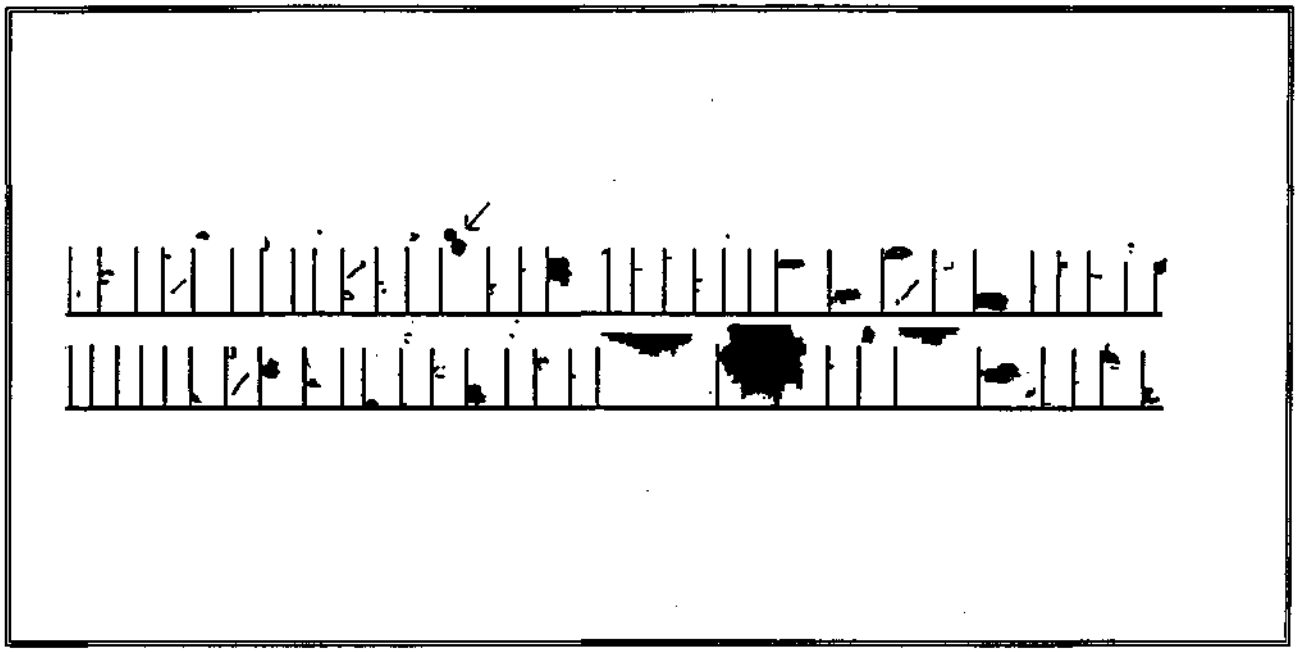

Figure 5. An example (arrow) of the type of double images that were found in the 2DC and 2DP field data obtained in updraft at -10°C for clouds sampled in the 1989 PACE field experiment.

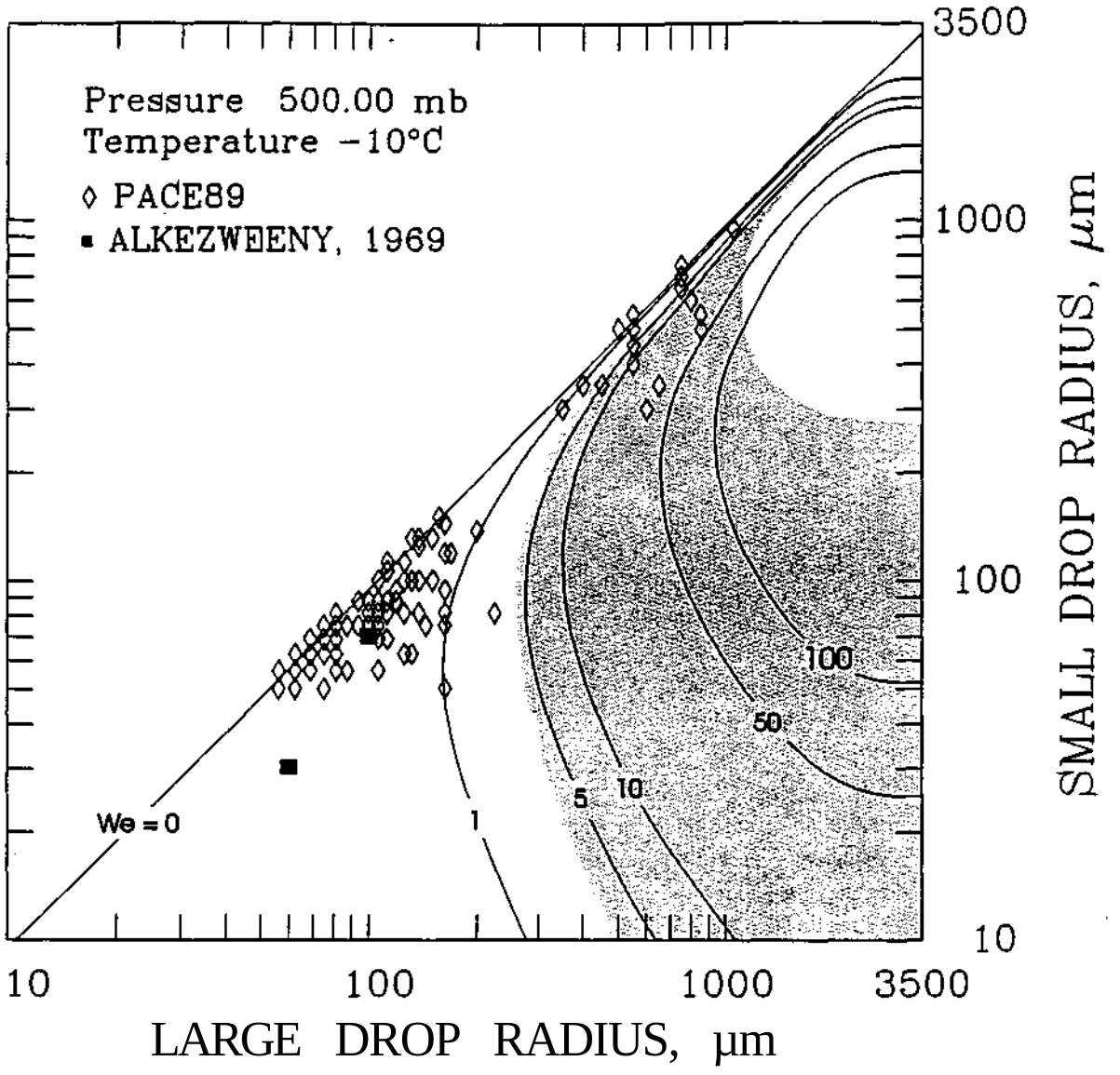

Figure 6. Plot of size data for double images identified in the 2D images from the 1989 field experiment. Shaded area indicates region where the impact pressure may be large enough to cause cavitation (see Czys 1989).

Chapter 3. Preliminary Laboratory Results On The Coalescence Of Small Precipitation-Size Drops Falling Freely In A Refrigerated Environment

Summary

Results from a set of laboratory observations of collisions between small precipitation-size drops falling freely at terminal velocity in a refrigerated collision chamber that were taken during this research period are presented. These experiments were conducted as part of investigations into the possibility that supercooled drops may freeze when they collide. In these experiments, the average radius of the size-pair was a 353 μm and 306 μm. Air temperatures ranged from 20°C to -15°C. Drop temperatures ranged from 20°C to approximately 2°C. Experimentation revealed that the coalescence efficiency increased from approximately 42% for mean drop temperatures between 20°C and ~10°C to about 81% for mean drop temperatures between -10°C and 2°C. A particularly interesting finding was an abrupt increase in coalescence efficiency, rather than gradual, at a mean drop temperature of about 10°C. A reduction in drop deformation during impact due to a dramatic increase in viscosity with decreasing temperature is considered as a mechanism which can act to promote coalescence. Reduction of drop deformation, which can be expressed by a non-dimensional Weber number, and the temperature dependency of the drop surface tension and fall speed is also examined as an explanation for the results. The abrupt increase in coalescence efficiency requires further investigation. The extent to which these results may be extended to collection processes in clouds remains uncertain, because of the effect that reduced pressure can have on deformation through drop fall speed and interaction time, and because the drops were not at thermal equilibrium. The results of this experiment do point to the need for further investigation in which free fall drop collisions are produced at thermal equilibrium, and at lower pressures, and that precipitation processes involving drizzle and raindrops may be considerably more complicated than previously suggested by experiment.

1. INTRODUCTION

Coalescence first received acceptance as an important mechanism for the production of rain in certain types of clouds with the work of Langmuir (1948), although Findeisen (1939) may have been the first to consider but reject this mechanism as "contrary to experience." It is also widely accepted that the production of rain by coalescence is not restricted to clouds with tops totally warmer than 0°C (Byers and Braham, 1949; Battan 1.953; Braham 1964; Braham and Dungey 1978). Implicit with emerging conceptual and numerical models of rain production by coalescence is that there may be physical factors in addition to those directly related to collision geometry (i.e. impact angle, closure velocity, etc.) that may effect the outcome of drop collisions as a cloudy parcel raises to colder temperature and lower pressure.

Because of the importance of drop interactions in the production of rain, the collision/coalescence process has received a great deal of attention in atmospheric research, resulting in a growing body of information about how drop collisions might result in clouds,

along with data on how certain physical factors might influence collision results. But, almost all the experiments have been conducted at room temperature and pressure. Furthermore, the quantity of data from experiments most realistically representing conditions for drop collisions in clouds has been limited by experimental complexity, and the time that it takes to obtain a statistically meaningful sample size.

Though progress has been slower than desirable, inquiry at room temperature and pressure has well established that the intervening air presents a barrier to coalescence in the form of a thin air film which must be ruptured before the near drop surfaces can make contact (see for example, Deraguin and Kussakov 1939; Shiskim 1964; Jones and Wilson 1978). Otherwise, the drops may bounce apart if the interaction time is short compared to the film drainage time, or they may temporary coalesce if the interaction time is about the same as the film drainage time and if the rotational energy is sufficient to pull the drop masses apart. The effect of the air film to hinder coalescence in favor of bounce or temporary coalescence has been well documented in experiments with drop streams impacting bulk water surfaces (Jayarante and Mason 1964), in experiments with two streams of equally sized drops impacting at oblique angles (Brazier Smith et al. 1972; Park 1970), in pendent drop experiments (Whelpdale and List 1971; Levin and Machnes 1977), and in experiments where isolated collisions were produced between dissimilarly sized drops initially falling freely at terminal velocity (Ochs et al. 1986; Czys and Ochs 1988; and Ochs et al. 1991).

Laboratory experimentation has also established that the coalescence of water drops can be promoted if the drops carry sufficient amounts of charge (Rayleigh 1879; Telford et al. 1955; Plumlee 1964; Jayarantne and Mason 1964; Welpdale and List 1971; Sartor and Abbott 1972; Sartor and Abbott 1968; and Dayan and Gallily 1975), and that results for free fall collisions organize according to the mean relative difference in surface charge between the large and small drop (Czys and Ochs, 1988; and Laird et al. 1992). Most studies of electric field effect have focused on promotion of drop collision rather than coalescence, although in some cases it might be inferred that electric field may also aid coalescence (Abbott 1975; Plumlee and Semonin, 1965; Telford and Thorndike 1961; Schlamp et al. 1976; and Goyer et al. 1960). Thresholds for electrostatic effects appear to be in the range of values expected in electrified clouds, but experimental results show as much dependence on how well natural collision forces have been simulated, as on the collision parameters themselves. The effect of relativity humidity on coalescence is not yet well understood, with experiments thus far providing mixed results (see for example, Prokhorov, 1954, Canlas 1960; Lindblad 1964, and Park 1970). The effect of pressure and temperature has received very limited attention with work by Canlas (1960) where results might indicate that coalescence may be promoted with decreasing pressure, but hindered as air temperatures decreases below that of the laboratory. List and Fung (1981) found that the types of breakup for a single drop size pair were no different at 50 kPa then at 100 kPa.

This paper reports preliminary results of an experiment in which isolated collisions were produced between dissimilarly sized drops falling freely at near terminal velocity in a refrigerated collision chamber.

2. EXPERIMENTAL APPARATUS

The single jet, dual drop size configuration used for this investigation is depicted in Fig. 1, and consists of a water reservoir, heat exchanger, cylindrical vibrating orifice drop generator, refrigerated collision chamber, temperature sensors, and digital control circuitry. Figure 2 is a photograph showing the refrigerated collision chamber and computerized control system. The refrigerated collision chamber was approximately 25.5 cm along each interior side; and 200 cm tall. The collision chamber was constructed from 1.25 cm thick Plexiglas, and was insulated by 10.2 cm of extruded polystyrene insulation. The interior of the chamber was cooled by a single evaporator coil mounted to one of the chamber walls. A 1/4 horsepower compressor previously used in an NCAR ice nucleus counter was used as the cooling unit. Temperature in the chamber could be controlled from 20 to approximately -20°C by manually adjusting an expansion value. Air temperature was measured using a set of 10 vertically spaced thermocouples monitored by a digital thermocouple display system.

Deionized water containing a slight amount of $NaNO_3$ (to improve conductivity) was supplied to the drop generator from a pressurized 210 liter polyethylene drum. The water was filtered and then fed through a heat exchanger for precooling before traveling through insulated tubing to the drop generator where it exited as a liquid jet. A photograph showing the liquid jet with capillary waves exiting the base of the drop generator and breaking into a stream of uniformly sized drops is shown in Fig. 3. When the precooler was used, water temperature near where the jet exited the drop generator was measured to be between 6° and 8°C, using a micro-thermocouple inserted into the tubing 5 cm above the drop generator base.

Mechanical vibrations from a cylindrical piezoelectric crystal caused the jet to break up into a stream of uniformly sized drops. The drop generator was improved over that used by Czys and Ochs (1988) by using stainless steel for the tubing assembly. Dissimilarly sized drops were produced by the method of Adam et al. (1971). The method of regularly switching between two excitation frequencies to produce alternating packets of dissimilarly sized drops has been reported by Ochs et al. (1986, see their Fig. 1). In this method, a square wave voltage of a high frequency was applied to the crystal for a prescribed period of time, creating a "packet" of small drops. This action was followed by applying a low frequency square wave voltage to the crystal for another period of time, and resulted in a "packet" of large drops. By periodically switching between periods of excitation frequency, alternating streams of small and large drops were produced from the single jet of the drop generator.

Most of the drops were charged using a cylindrical charging electrode placed around the point of jet breakup. The stream of charged drops was deflected as it passed between vertically aligned high voltage electrodes (see Fig. 1). A high speed switching circuit made it possible to switch between the charging voltage and a much lower voltage for a moment in time that coincided with the creation of one drop. This action resulted in the production of a minimally charged drop which was not deflected as it passed between the high voltage electrodes, and thus fell through the collision chamber. The digital controls were first set to allow a small drop to be created with minimal charge followed by the creation of a large

drop with minimal charge. The time between selection of a minimally charged large and small drop was set so that the large drop overtook the small drop at a level in the collision chamber chosen to ensure that both drops were within *5%* of terminal velocity.

Streak/strobe photography was used to record the collision events (see Czys and Ochs 1988 for examples). The drops were illuminated from behind by an incandescent lamp angled approximately 45° above the camera lens axis in a vertical plane perpendicular to the film plane. In this lighting orientation the drops focus the light from behind to a point on the portion of the drops facing the camera. As the drop pairs passed by the exposed film, streak lines were recorded corresponding to their fall trajectory. To aid in distinguishing between collision results, the drops were also illuminated by a single flash of a strobe light positioned approximately 45° to the side of the lens axis in a horizontal plane. The strobe flash was set to occur to illuminate the drops below the level where the large drop would, on average, overtake the small drop. From this strobe lighting configuration, the entire outline of the drop(s) was exposed on the film.

3. DATA COLLECTION AND REDUCTION

To simplify procedures in these preliminary experiments, a single camera was used to record collision events. Therefore, critical offset for coalescence was not established as was done in Czys and Ochs (1988) using two cameras viewing collision events from orthogonal positions. As a consequence, coalescence efficiencies were computed from counts of events assuming two different models of collision geometry, each representing extreme cases in the orientation of the drops to the film plane of the camera.

In the first collision geometry model (model I), collisions were assumed to occur between drops in a horizontal collision cross section area aligned with the lens axis and perpendicular to the film plane. Figure 4 is a schematic diagram showing the horizontal collision cross-section in the plane of drop interaction for collision model I. As Fig. 4 illustrates, the offset (distance) between the drops before collision and angle of offset (Y) to the film plane were both assumed to occur randomly. Therefore, the coalescence efficiency e is simply obtained from the ratio of the number of coalescence (N_C) to the total number of collision events (N_T). In the second more restrictive collision geometry model (model II), drop collisions were assumed to occur solely in the plane parallel to the film plane. Hence, the collision offset was assumed to occur randomly, but the angle of the offset to the film plane was assumed to be zero. Therefore, the coalescence efficiency under these assumptions was approximated by e^2.

Initial experiments were conducted without measuring drop charge, assuming that careful vertical alignment of the drop stream perpendicular to the horizontal electric field between the high voltage electrodes would be sufficient to consistently result in drops with low charge. However, this does not guarantee the lowest possible drop charge (Ochs et al. 1991). In these experiment, collisions were first photographed at room temperature, exposing approximately 90 to 120 frames of film. Refrigeration of the collision chamber was initiated, and then data were typically collected several times during the day while the chamber cooled. The cooling rate of the chamber was nonlinear, cooling at an approximate

rate of 10°C hr^{1} from 20°C to 0°C, 5° hr^{1} from 0°C to -10°C, and 2.5° hr^{1} from -10 to -15°C.

Drop temperatures were computed using a 1D heat and mass transfer model, including the effect of ventilation. Drop temperatures were computed based on the vertical distribution of temperature in the chamber at the time of observation, the size of the large and small drops, temperature of the drops upon entering the chamber, and fall speed profile of the drops. Model results for a 310 and 350 μm radius drops entering the chamber at 10°C are shown in Fig. 5. The observational level was 110 cm from the chamber top. A limiting factor in these experiments is that it becomes impossible to produce collisions for distance greater than approximately 110 cm because the drops meander slightly as they fall rather than following straight-line trajectories. Also note in Fig. 5 that the temperature profile is stably stratified and that this helped to suppress vertical air motions within the chamber. Collisions were photographed over a short period of time, usually 10 to 15 minutes at any particular temperature. Therefore, uncertainties in drop temperature related to changes in chamber temperature were about ±2.0°C as indicated by the vertical temperature record kept for each experimental trial.

Results from the first series of experiments were so unusual that additional experimental trials were conducted in which drop charge was measured. These experiments were carried out in order to address concerns that initial results were somehow related to an unaccounted electrical effect rather than related to temperature. In the second set of experiments, drop charge was measured using an electrometer capable of measuring charges down to approximately $10"^{15}$ Coulombs (± $4x10^{-15}$ Coulombs). In this series of experiments, a set of measurements were made of the charge on the large and small drops immediately before and after each sequence of photographs at a specified temperature. This was done to ensure that charge on both drops did not change by amounts that might be suspected of influencing collision outcome. It was not possible to make the charge measurements without first opening an access door and inserting the electrometer. This resulted in introduction of humid laboratory air into the refrigerated chamber during several times over the course of observations. The temperature distribution in the chamber would rapidly recover from the introduction of warm air because was over designed for chamber cooling. However, with each charge measurement and because of a small amount of leakage of laboratory air into the chamber, frost increasingly accumulated on the evaporation coils reducing their capacity to cool the chamber. Therefore, drop temperatures in the experimental runs with charge measurement are not as cold as those in the first set of experiments.

4. Results

Tables 1 and 2 list experiment conditions and results from the series of experiments without and with drop charge measurements, respectively. Listed in both Tables is a run identification letter, calculated mean drop temperature (°C), drop radius (urn), the number of photographed coalescences (N_C), bounces (N_B), and total collision events ($N_T = N_C + N_B$). Coalescence efficiency calculated assuming model I (ε) and model II (e^2) collision geometry are also listed along with measurement uncertainties (A£ = $\pm k(N_T)[\varepsilon(1-\varepsilon)/N_T]^{1/2}$)

where k is a function of the number of observations, and the standard deviation is given by the square root of the means for a dichotomous sample (see Blalock 1972). Table 2 also lists the mean absolute value of relative drop charge ($|Q_R-Q_r|$) which has been found to be an acceptable way to present collision results for charged drops in free fall (Czys and Ochs 1988).

Figure 6 is a plot of coalescence efficiency (e) versus mean drop temperature for all the runs listed in Table 1 (open circles) and Table 2 (closed circles). Vertical lines are $\pm\Delta E$. The prominent feature of Fig. 6 is the marked jump of coalescence efficiency from about 42% to 81% at a mean drop temperature of approximately 10°C. The overlap of coalescence efficiencies in the transition zone is probably do to temperature measurement uncertainties which have since been reduced.

The results shown in Fig. 6 are also rather noisy and this may have occurred for at least two reasons. The first reason is related to the possibility that in striving to optimize collision rate, it is possible to inadvertently adjust the experiment to favor direct central (coalescence) or glancing (bounces) collisions. It is also possible to inadvertently synchronize film exposure with one type of collision event over another by inadvertently miscuing camera triggering which can just as easily act to maintain synchronization with a certain collision result as to restore randomness, as' has been the case in other free fall drop experiments (Ochs et al. 1986).

5. Discussion

An assessment of the relative drop charges in this experiment has led to the conclusion that the results are probably not directly related to some sort of electrostatic effect. As indicated by the general scatter in Fig. 7, which is a plot of coalescence efficiency versus relative drop charge, there is no correlation (r_c=0.06) between coalescence efficiency and charge in this experiment, while coalescence efficiency was found to be much more highly correlated (r_c=0.65) with temperature. A further indication that charge was not a direct factor in these results is that the two largest relative charges had coalescence efficiencies which were among the lowest of the group. Therefore, relative drop charge can not be used to completely explain the high coalescence efficiencies at lower temperatures in this experiment. However, the larger relative charges in this experiment (those greater than approximately $3x101^{-13}$) are near the minimum required to cause coalescence that has been reported by Sartor and Abbott (1972) and Howard and Crosby (see Park 1971) from experiments with two nearly vertical drop streams impacting at a slight angle. This suggests that future experimentation into temperature effect on coalescence should be conducted at much lower relative charges than reported here to better remove the possibility of charge effects in the results.

Temperature may effect the process of coalescence of the freely falling drops in this experiments by altering drop deformation which aids trapping of the air film between the approaching drop surfaces. If the air film is not sufficiently thinned and ruptured, the colliding drops do not make contact and will bounce apart. Therefore, any change in the

physical conditions of the collision that would reduce deformation could potentially contribute to increased coalescence.

In these experiments, temperature reduction may have promoted coalescence by reducing the deformation because of a large increase in the viscosity (η) of the drops. Table 3 shows that the viscosity of water increases by 80% from its value at 20°C to 0°C. An increase in viscosity will increase the shear stress, and be particularly effective in reducing deformation for less direct impact angles where drop collisions tend to result in bounce. Thus, drops at low temperature resist deformation and thereby have a higher coalescence efficiency.

Drop deformation in free fall collision can also be viewed from the perspective of the non-dimensional Weber number (We) which is the ratio of impact pressure to surface tension:

$$We = \rho_w r \Delta V \sigma^{-1} \qquad (1)$$

where p_w is the density of water, AV the impact velocity, σ the surface tension of water, and the deformation radius, r, is scaled to the radius of the small drop (Ochs et al 1986). As Eq. 1 implies, there should be more deformation in drop collisions characterized by larger Weber number. As Table 3 shows, surface tension increases with decreasing temperature, while the terminal velocity (Beard 1976, 1977) of the large and small drop decrease disproportionately, consequently resulting in a decrease in impact velocity. Hence, the interaction time increases allowing for increased thinning of the air film at the same time as the surface tension increases. Considered in combination, the change in a and AV translate into a modestly large decrease in We, approximately 7 percent for this experiment. Therefore, while changes in viscosity are much larger, potential influences other collision parameters represented in We should not be ignored because they also can contribute to deformation reduction which would favor coalescence at the expense of bounce.

The fact that the coalescence efficiency shows an abrupt increase at low temperature is not well understood. This result may be conceptually related to the possibility that a threshold exists that must be overcome before the air film is thinned sufficiently for rupture, allowing coalescence to proceed. Until this threshold is crossed, either by less deformation, more interaction time or both, coalescence efficiency remains unaffected, even though viscosity, surface tension, and impact velocity have changed in way that should aid coalescence. The lack of a gradual change in critical angle for coalescence with increasing relative drop charge is another example coalescence efficiency do not always change gradually with gradual changes of the collision conditions (Czys and Ochs 1988).

The possibility that drop evaporation somehow aided coalescence also can not be ruled out. However, recent evidence reported by Ochs et al. (1992) have revealed a small effect to promote bounce rather than coalescence as relative humidity decreases.

Also consider that the increase of coalescence efficiency with drop cooling may not directly apply to drop coalescence process in clouds because of the strong influence that pressure and temperature have on drop fall speed and deformation, respectively. Table 4 illuminates this point by showing the temperature and pressure dependence of each collision parameter. The important differences between Table 4 and 3 are the large and slightly disproportionate increase in terminal velocity, and consequential large increase in impact velocity and Weber number with decreasing temperature and pressure. These changes are favorable to bounce and temporary coalescence because more deformation and less interaction time may occur in clouds as temperature and pressure decrease (assuming of course that pressure decrease does not have some unaccounted influence in air film drainage). In addition to the need for other observations at different drop sizes and size ratios, very difficult future experiments are warranted in which pressure, temperature, charge, and velocity are well known and controlled parameters.

6. CONCLUSIONS

Coalescence efficiency was found to change in unexpected ways in laboratory experiments where isolated collisions were produced between cooled drops that averaged in size of 353 and 306 μm in radius. The experiments are unique because they are the first in which cooled drops of known and controlled charge were falling freely at terminal velocity before collision. No other data exists on the coalescence efficiency of cooled drops in free fall at terminal velocity. The laboratory results indicate that coalescence efficiency sharply rises from 42% to 81% at a mean drop temperature of approximately 10°C. This behavior may be related to changes in drop deformation and interaction time that combine to favor coalescence at cold temperatures (and room pressure) because these changes favor air film drainage. The sudden rather than gradual change in coalescence efficiency needs further experimental study. A comparison of collision parameters calculated assuming laboratory and mid-tropospheric pressure suggests that coalescence efficiency may decrease in raising parcels of cloudy air that may be related to a decrease in interaction time and an increase in drop deformation which would accompany disproportionate increases in large and small drop terminal velocity, assuming that the effect drop viscosity does not outweigh the influence of these other physical factors. While these results only apply to one pair of drop sizes, they do suggest that caution be exercised in simply assuming that coalescence efficiency does not change as temperature decreases with vertical cloud growth. In addition to needing data at other drop sizes and size ratios, future more difficult experiments are warranted in which pressure and temperature are simultaneously controlled to resolve the interplay between film drainage mechanisms that are temperature and pressure dependent. Clearly, the process of drop coalescence in clouds is considerably more complicated than even previous careful experimentation has indicated, and thus the adequacy of customary assumptions about warm rain process at colder than room temperatures is called into question.

7. REFERENCES

Adam, J.R., R. Cataneo, and R.G. Semonin, 1971: The production of equal and unequal size droplet pairs. *Rev. ScL Instrum.,* 42,1847-1849.

Blalock, H.M., Jr., 1972: *Social Statistics.* Second Edition. McGraw-Hill, New York, New York, 583 pp.

Battan, L.J., 1953: Observation on the formation and spread of precipitation in convective clouds. *J. Meteor.,* 10, 311-324.

Beard, K.V., 1976: Terminal velocity and shape of cloud and precipitation drops aloft. *J. Atmos. ScL,* 33,851-864.

Beard, K.V., 1977: Terminal velocity adjustment for cloud and precipitation drops aloft. *J. Atmos. Sci,* 34,1293-1298.

Braham, R.R., Jr., 1964: What is the role of ice in summer rain-showers? *J. Atmos. Sci,* 21, 640-645.

Braham, R.R., Jr., and M.J. Dungey, 1978: A study of urban effects on radar first echoes. *J. Atmos. ScL,* 17, 644-654.

Brazier-Smith, P.R., S.G. Jennings, and J. Latham, 1972: The interaction of falling water drops: coalescence. *Proc. Roy. Soc. London,* A326, 393-408.

Byers, H.R., and Braham, R.R., Jr., 1949: The thunderstorm: Report of the thunderstorm project. Washington, DC.: US. Government Printing Office.

Canlas, D.C., 1960: An experimental investigation on the effects of ambient pressure, temperature, and relative humidity on the coalescence of water drops. Ph.D. *thesis,* New York University, 64 pp.

Czys, R.R., 1987: A Laboratory study of interactions between small precipitation-size drops in free fall. Ph.D. *thesis,* University of Illinois, Urbana, Illinois, 131 pp.

Czys, R.R., and H.T. Ochs, 1988: The influence of charge on the coalescence of water drops in free fall. J. *Atmos. ScL,* 45, 3161-3168.

Dayan, N., and I. Gallily, 1975: On the collection efficiency of water droplets under the influence of electric forces I: Experimental, charge-multipole effects. *J. Atmos. ScL,* 32, 1419-1429.

Derjaguin, B., and M. Kussakov, 1939: Anomalous properties of thin polymolecular films. *Acta Physicochim,* 10, 153-174.

Findeisen, W., 1939: Zur Frage der Regentropfenbildung in reinen Wasswewolken. *Met Z.*, 56, 365.

Foote, G.B., 1975: The water drop rebound problem: Dynamics of collision. *J. Atmos. Sci.*, 32, 390-402.

Goyer, G.G., J.E. McDonald, F. Baer, and R.R. Braham, 1960: Effects of electric fields on water-droplet coalescence. *J. Appl. Met.,* 17, 442-445.

Jayaratne, O.W., and B J. Mason, 1964: The coalescence and bouncing of water drops at an air/water interface. *Proc. Roy. Soc (London),* A280, 545-565.

Jones, A.F., and S.D.R. Wilson, 1978: The film drainage problem in droplet coalescence. *J. Fluid Meck,* 87, 263-288.

Ochs. H.T., N.F. Laird, D J. Holdridge, D.E. Schaufelberger, and J.Q. Feng, 1992: Effects of relative humidity on the coalescence of small precipitation drops in free fall. Proceedings of the 11th International Conference on Clouds and Precipitation. Montreal, Canada, 21-22.

Laird, N.F., H.T. Ochs III, D J. Holdridge, D.E. Schaufelberger, R.R. Czys, and J.Q. Feng, 1992: Effects of charge on the coalescence of small precipitation drops at terminal velocity. Proceedings of the 11th International Conference on Clouds and Precipitation. Montreal, Canada, 23-26.

Langmuir, I., 1948: The production of rain by a chain reaction in cumulus clouds at temperatures above freezing. *J. Meteor.,* 5,175-192.

Levin, Z., and B. Machnes, 1977: Experimental evaluation of the coalescence efficiency of colliding water drops. *Pure Appl. Geophys.*, 115, 845-867.

Lindblad, N.R., 1964: Effects of relative humidity and electric charge on the coalescence of curved water surfaces. *J. Colloid Sci,* 19, 729-743.

List, R., and C. Fung, 1982: The effect of pressure on the breakup of one pair of raindrops. *Atmos.-Ocean,* 20,17-27.

Ochs, H.T., D.E. Schaufelberger, and J.Q. Feng, 1991: Improved coalescence efficiency measurements for small precipitation drops. *J. Atmos. Sci.*, 48, 946-951.

Ochs, H.T., R.R. Czys, and K.V. Beard, 1986: Laboratory measurements of coalescence efficiencies for small precipitation drops. *J. Atmos. Sci.,* 43, 225-232.

Park, R.W., 1970: Behavior of water drops colliding in humid nitrogen. Ph. D. *thesis,* University of Wisconsin, Madison, Wisconsin, 577 pp.

Plumlee, H.R., 1964: Effects of electrostatic forces on drop collision and coalescence in air. Charged Particle Res. Lab. Rept. CPRL-8-64, Illinois State Water Survey, Urbana, 101 pp.

Plumlee, H.R., and R.G. Semonin, 1965: Cloud droplet collision efficiency in electric fields. *Tellus,* 17, 356-364.

Prokhorov, P.S., 1954: The effects of humidity deficit on coagulation processes and the coalescence of liquid drops. *Discussions Faraday Soc,* 18, 41-51.

Rayleigh, Lord, 1879: The influence of electricity on colliding water drops. *Proc. Roy. Soc,* 28, 406-409.

Sartor, J.D., and C.E. Abbott, 1972: Some details of coalescence and charge transfer between freely falling drops in different electrical environments. *J. Rech Atmos., 6,* 479-493.

Sartor, J.D., and C.E. Abbott, 1968: Charge transfer between uncharged water drops in free fall in an electric field. J. *Geophys. Res.,* 73, 6415-6423.

Shiskim, N.S., 1964: Clouds, Precipitation and Thunderstorm Electricity. Gimiz, Leningrad.

Plumlee, H.R., and R.G. Semonin, 1965: Cloud droplet collision efficiency in electric fields. *Tellus,* 17, 356-364.

Telford, J.W., N.S. Thorndike, and E.G. Bowen, 1955: The coalescence between small water drops. *Quart. J. Roy. Meteor. Soc,* 81, 241-250.

Whelpdale, D.M., and R. List, 1971: The coalescence process in raindrop growth. *J. Geophys. Res.,* 76, 2836-2856.

Table 1. Summary of experiment conditions and results for runs with unknown drop charge.

Run	T_D °C	R μm	r μm	N_C	N_B	N_T	ε %	ε^2 %	Δε %
f	18	364	316	15	105	120	13	1	±5
g	18	357	310	67	36	103	65	42	±9
d	17	353	312	12	71	83	14	2	±7
g	15	357	310	28	42	70	40	16	±11
f	15	364	316	62	52	114	54	29	±9
g	15	357	310	53	58	111	48	22	±9
f	14	364	316	57	69	126	45	20	±8
g	13	357	310	40	61	101	40	15	±9
g	13	357	310	22	39	61	36	13	±12
d	12	353	312	65	0	65	100	100	±10
d	11	353	312	80	2	82	98	95	±3
f	11	364	316	25	0	25	100	100	±10
b	11	345	304	35	54	89	39	15	±10
c	10	354	303	59	68	127	46	21	±8
e	10	349	309	60	47	107	56	31	±9
e	5	349	309	87	7	94	93	85	±5
c	4	350	303	112	0	112	100	100	±10
a	3	327	294	34	9	43	79	62	±12
b	3	345	304	119	42	161	74	54	±6
e	3	349	309	30	0	30	100	100	±10
c	3	347	313	133	7	140	95	90	±3
a	2	327	294	154	12	166	93	86	±3

Table 2. Summary of experiment conditions and results for runs with known drop charge.

Run	T_D °C	R μm	r μm	$\|QR-Q_r\|$ coulombs	N_C	N_B	N_T	e %	ε^2 %	$\pm\Delta\varepsilon$ %
h1	19	352	310	$8.3x10^{-14}$	21	19	40	53	27	15
h2	19	352	310	$2.4x10^{-13}$	12	23	35	34	11	16
i1	18	348	304	$3.9x10^{-13}$	5	37	42	12	1	10
jl	18	341	297	$7.5x10^{-14}$	21	39	60	35	12	12
k1	18	356	301	$2.0x10^{-13}$	24	37	61	39	15	12
11	17	355	310	$2.3x10^{-14}$	17	36	53	32	10	12
ml	17	377	310	$2.6x10^{-13}$	29	48	77	38	14	10
k2	12	356	301	$1.4x10^{-13}$	35	49	84	42	17	10
k3	12	356	301	$l.lx10^{-13}$	36	69	105	34	11	9
k4	12	356	301	$8.7x10^{-13}$	29	39	68	43	18	11
h3	12	352	310	$1.5x10^{-13}$	41	7	48	85	72	10
h4	12	352	310	$1.5x10^{-13}$	57	33	90	63	40	9
i2	12	348	304	$1.4x10^{-13}$	74	13	87	85	72	7
i3	12	348	304	$1.9x10^{-13}$	81	4	85	95	90	4
i4	12	348	304	$1.5x10^{-13}$	40	47	87	46	21	11
13	10	358	310	$2.7x10^{-13}$	36	37	73	49	24	10
j2	11	341	297	$1.6x10^{-13}$	50	8	58	86	74	8
j3	11	341	297	$3.5x10^{-14}$	39	47	86	45	20	10
j4	11	341	297	$1.2x10^{-13}$	77	6	83	93	86	5
14	10	355	310	$2.3x10^{-14}$	15	15	30	50	25	18
12	10	355	310	$2.7x10^{-13}$	79	4	83	95	90	4
m2	10	377	310	$2.6x10^{-13}$	72	0	72	100	100	10
m3	10	377	310	$2.5x10^{-13}$	88	0	88	100	100	10

Table 3. Temperature dependence of collision parameters computed for drops 350 μm and 300 μm radius.

Temp. °C	poise	a $m s^{-1}$	VR $m\ s^{-1}$	V_r $m\ s^{-1}$	AV $m s^{-1}$	WE	P kPa
20	0.010	73.0	291.7	249.2	42.5	0.74	95
15	0.011	73.8	291.4	249.0	42.4	0.73	95
10	0.013	74.6	291.0	248.8	42.2	0.72	95
5	0.015	75.3	290.6	248.6	42.0	0.70	95
0	0.018	76.1	290.2	248.4	41.8	0.69	95
%Δ	80%	4	-1.0	-0.3	-1.6	-6.8	

Table 4. Temperature and pressure dependence of collision parameters computed for drop 350 and 300 μm radius.

Temp. °C	σ ms^{-1}	V_R ms^{-1}	V_r m	ΔV s^{-1}	WE ms^{-1}	P kPa
20	73.0	291.7	249.2	42.5	0.74	95
15	73.7	302.3	258.1	44.2	0.79	85
10	74.6	314.7	268.5	46.2	0.86	75
5	75.3	329.5	280.9	48.6	0.94	65
0	76.1	337.9	288.0	49.9	0.98	60
%Δ	4	16	16	17	32	

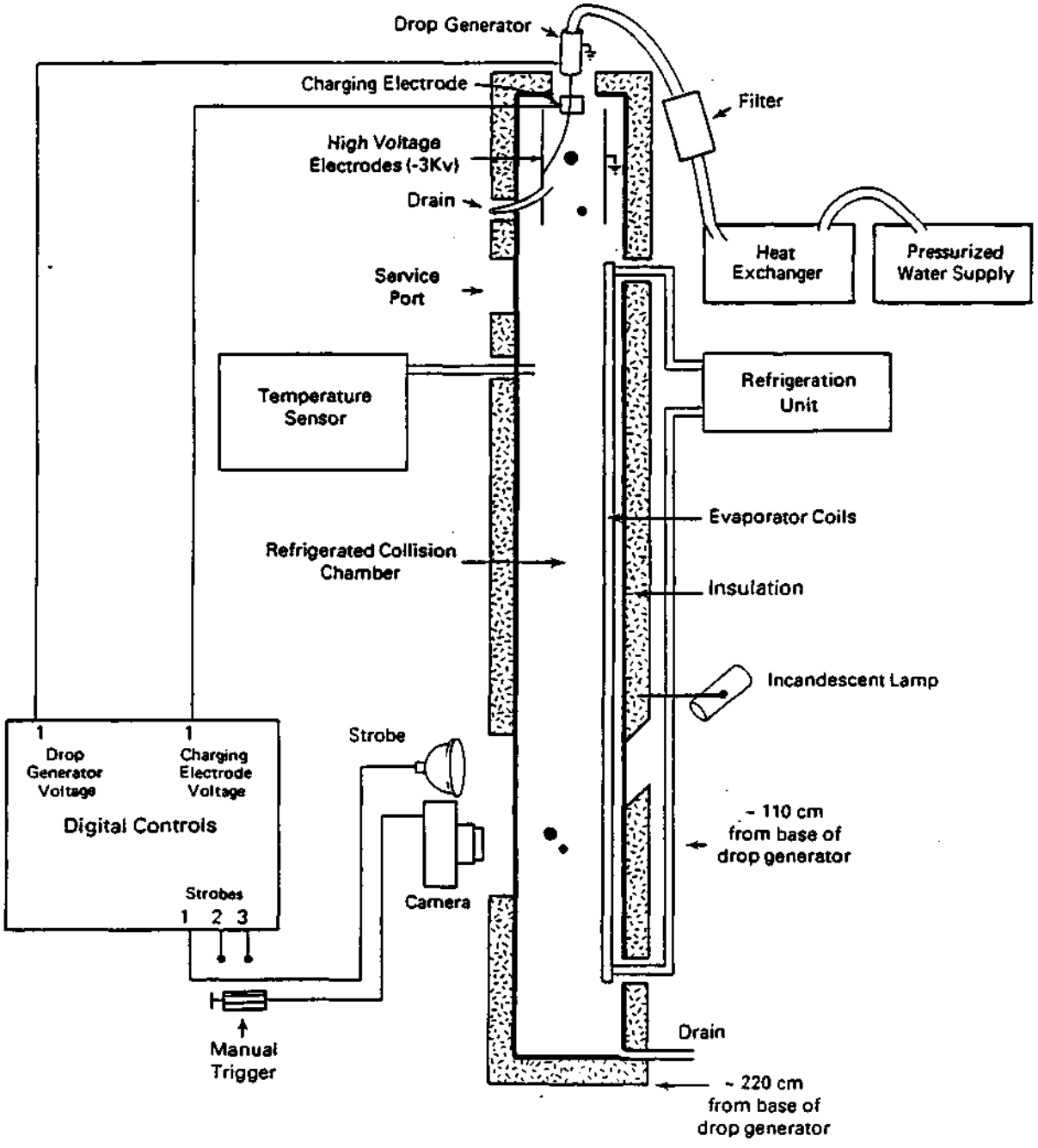

Figure 1. Schematic diagram of the refrigerated drop collider system.

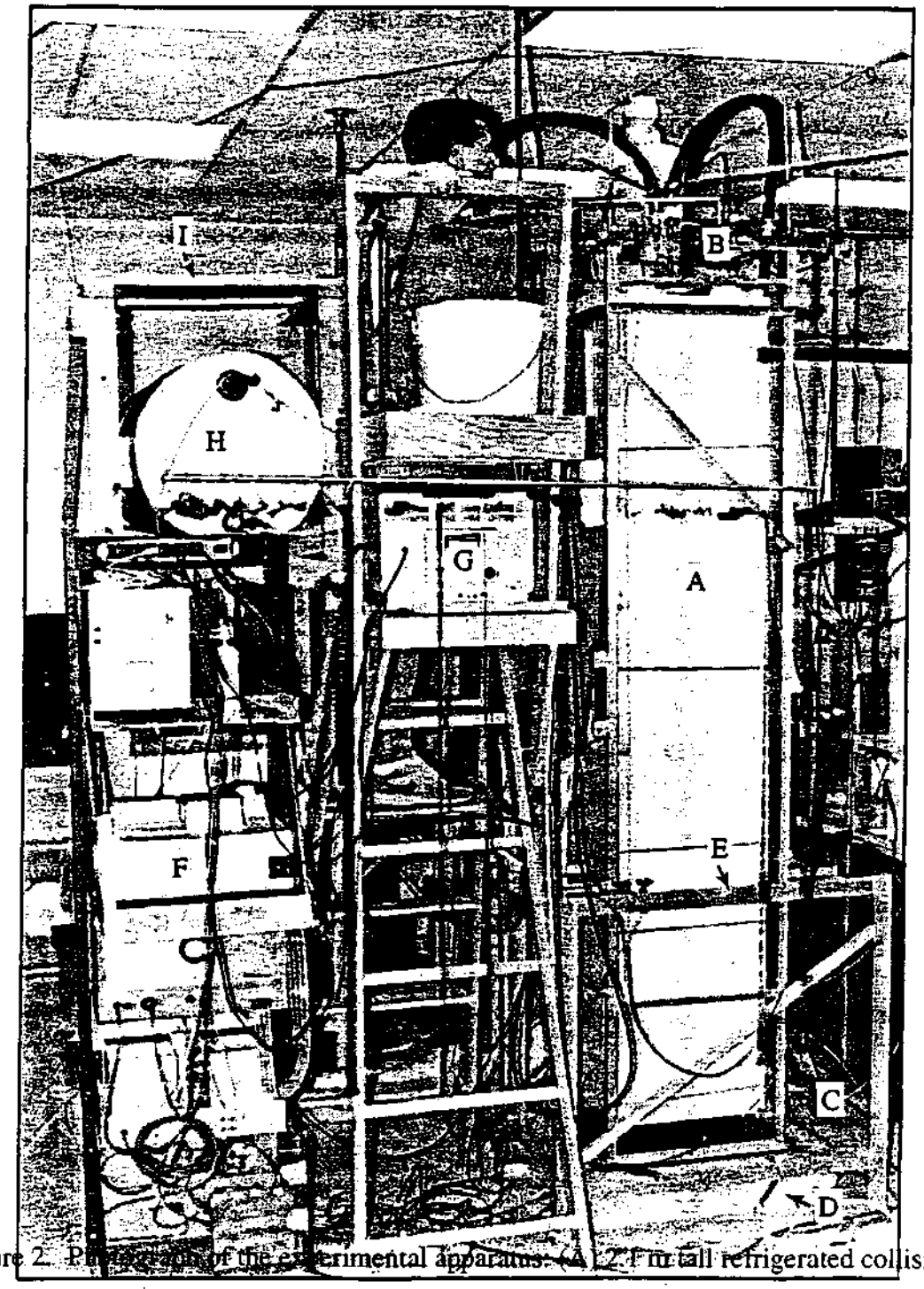

Figure 2. Photograph of the experimental apparatus: (A) 2.1 m tall refrigerated collision chamber, refrigeration unit adapted from an NCAR ice nucleus counter is located to the right and is not shown, (B) drop generators and mounting hardware, (C) "floating" drop generator support structure, (D) vibration isolation platform, (E) chamber support stand, (F) back of computer control system, (G) back of computer monitor, (H) water reservoir for drop generator "B", and (I) water reservoir stand.

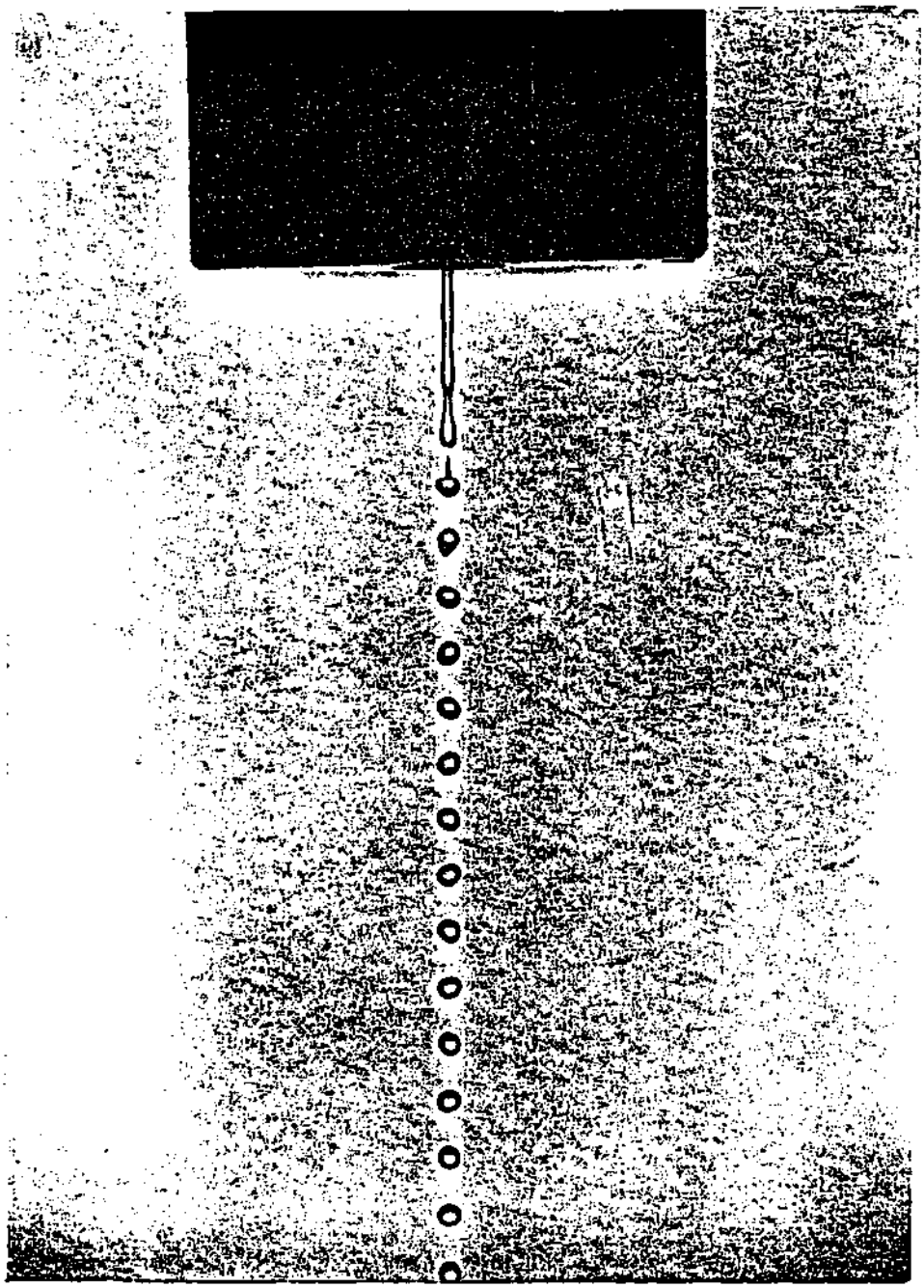

Figure 3. Macro-photograph of the water jet issuing from the drop generator. The diameter of the drop generator base is 1.4 cm.

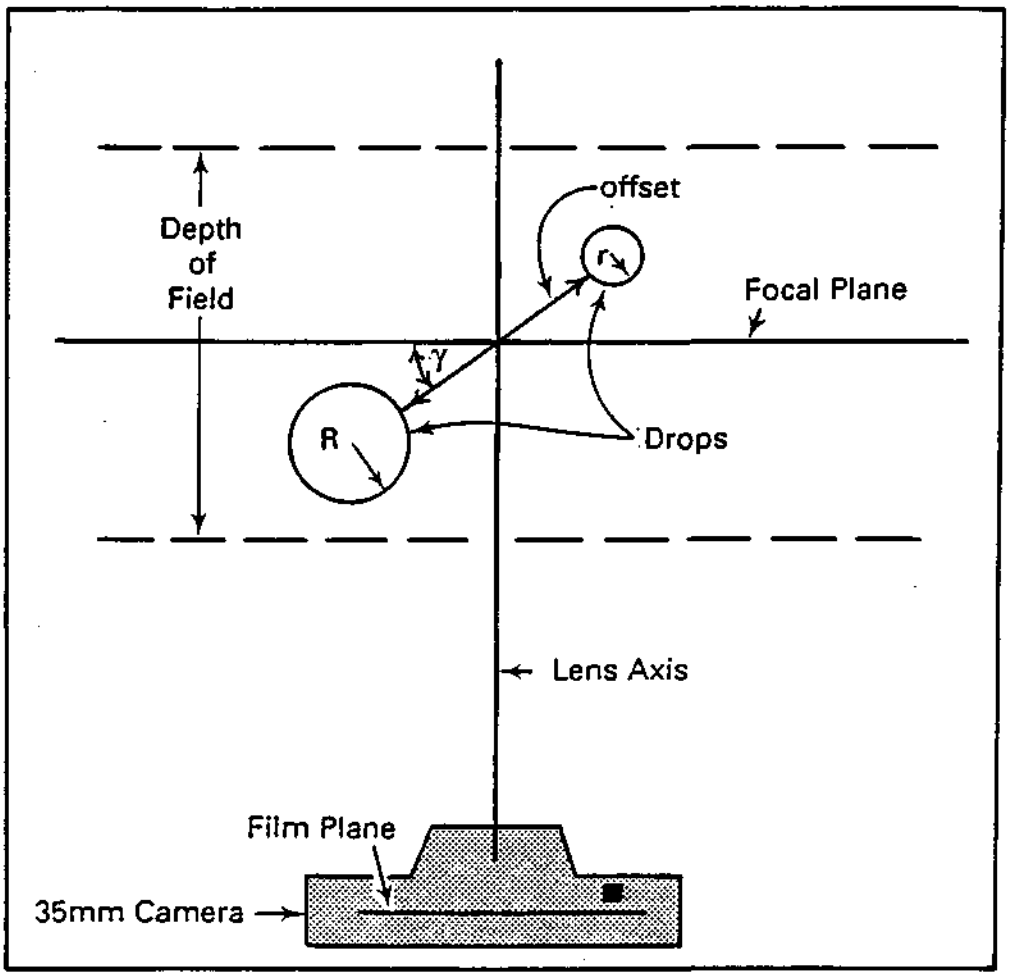

Figure 4. Diagram of the horizontal collision cross-section in the plane of drop interaction and the view of the camera.

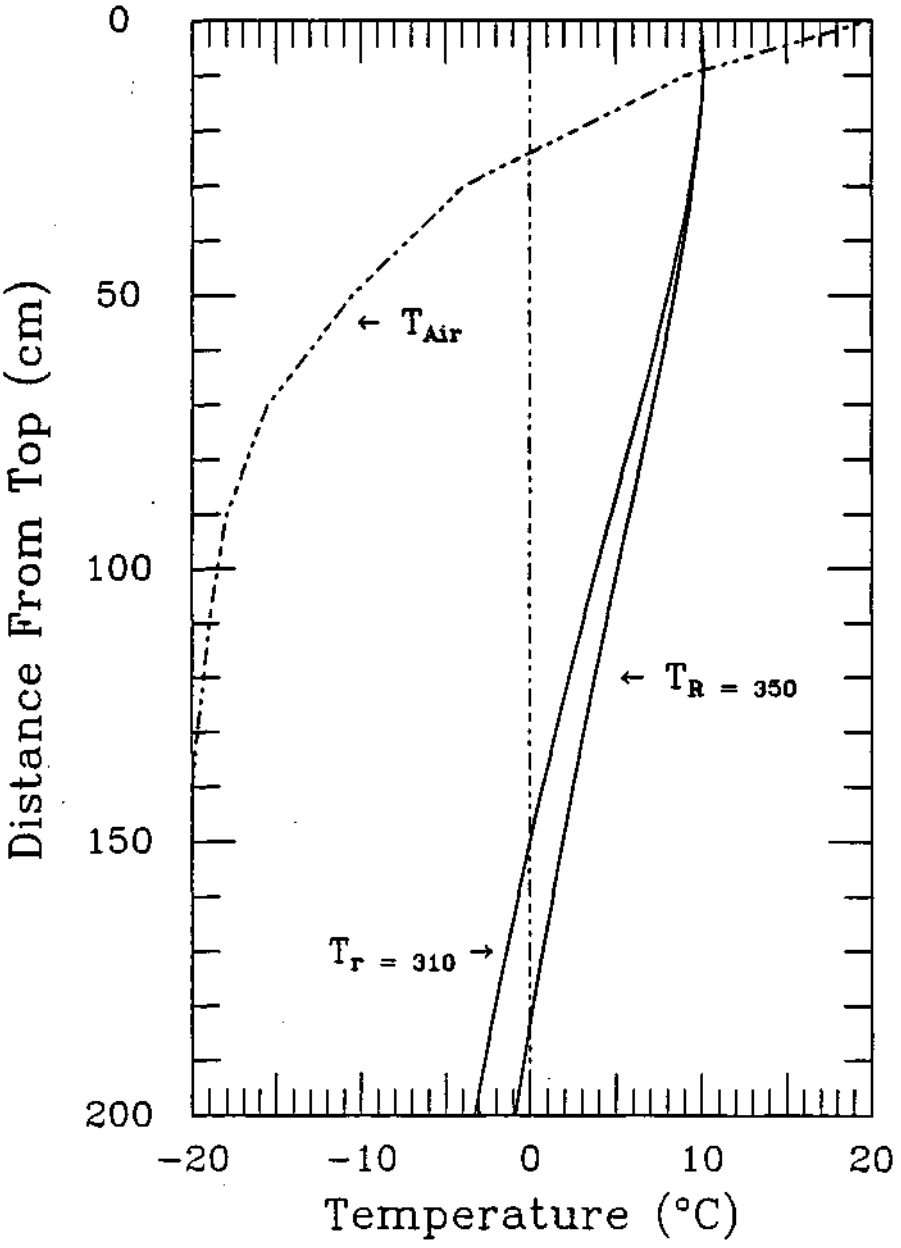

Figure 5. Vertical profile of air temperature (T_{Air}) and the computed temperature for drops 350 (T_R) and 310 (T_r) μm radius respectively in the refrigerated collision chamber.

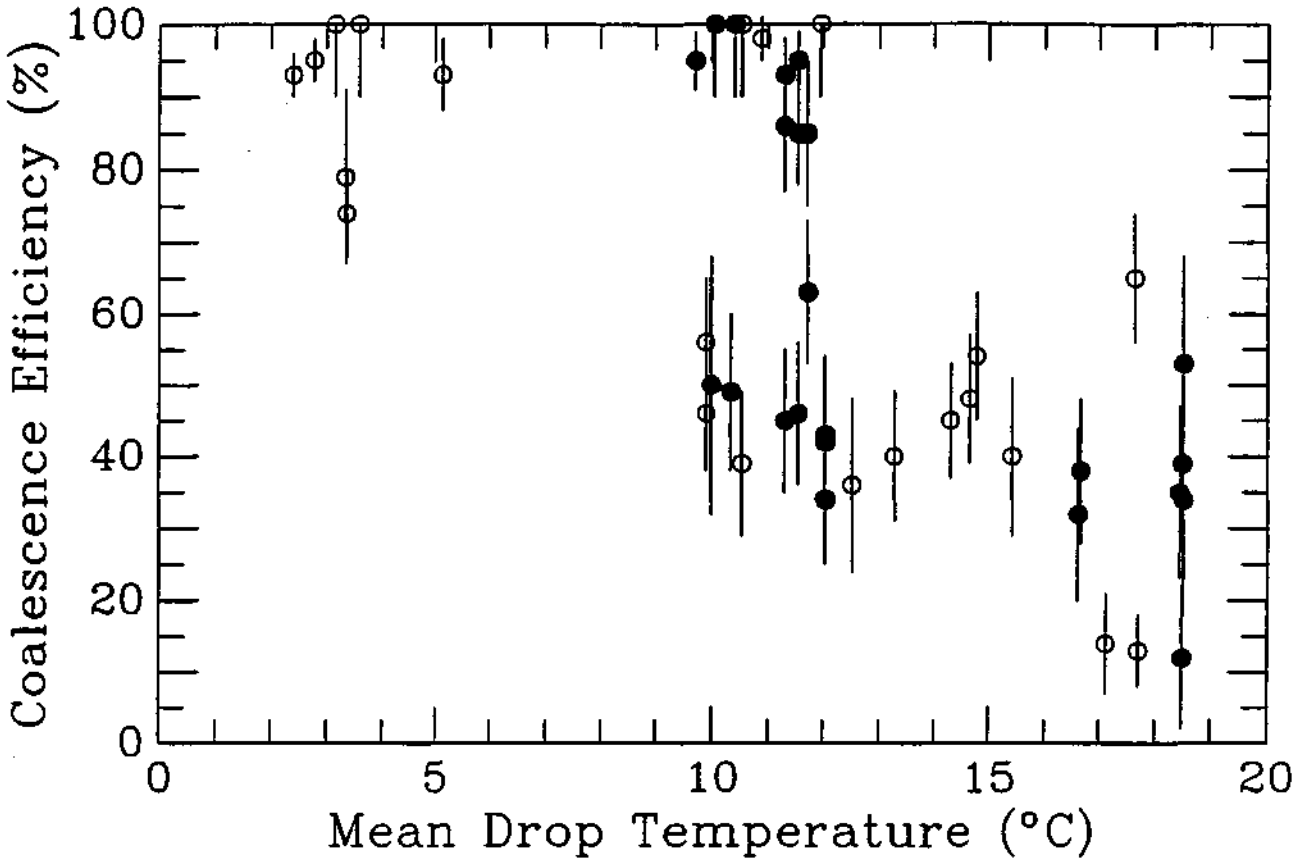

Figure 6. Experimentally determined coalescence efficiency versus mean drop temperature.

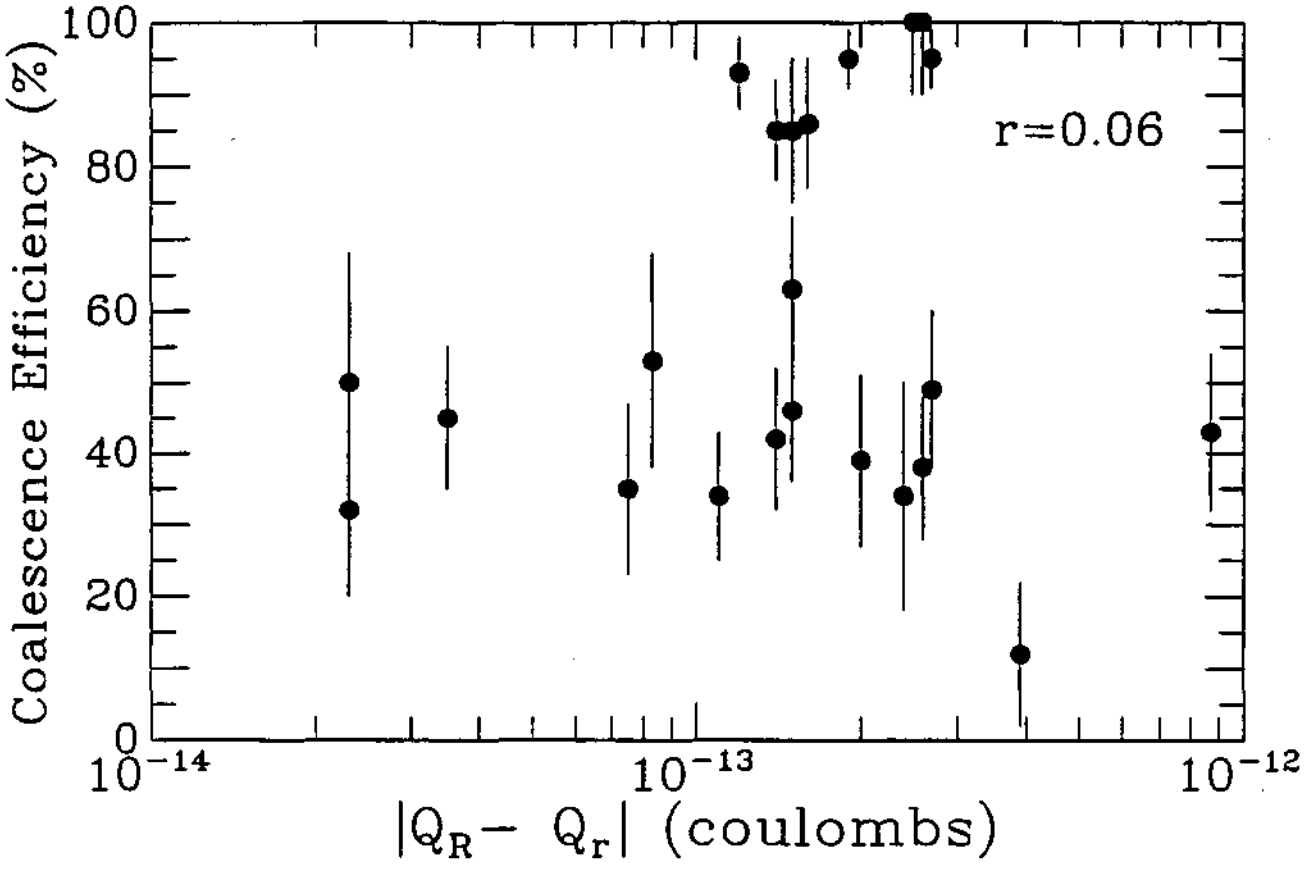

Figure 7. Experimentally determined coalescence efficiency versus relative drop charge.

Chapter 4. Numerical Simulations Of Raindrop Temperature Relevant To Mitigating Heavy Ice Accumulations By Cloud Seeding In Freezing Rain Storms

Summary

This research was conducted as part of our on going task to investigate for scientifically sound, socially acceptable, planned weather modifications strategies that may be of benefit to Illinois. This work represents a new area of interest that focuses upon the cloud seeding potential of cold season clouds to convert supercooled drizzle and rain drops to ice during their fall to earth and thereby mitigate destructive accumulations of ice at the earth's surface. The example used was the lower atmospheric conditions associated with a major ice storm that affected east-central Illinois in 1990. This was a noteworthy sign for its a large impact on the natural setting, and public and private property in east-central Illinois. As discussed later this, investigation also has implications for avioding dangerous aircraft icing regions.

For this investigation, a one-dimensional computer model was developed and used to simulate the temperature of freely falling raindrops. The model includes the effects of ventilation and mass transfer on the disposal and redistribution of latent and sensible heat, and the effects of mass transfer on drop size and fall speed. Model results showed that the temperature and humidity profiles for the subcloud region were favorable for the production of supercooled drops, and that the amount of supercooling is proportional to drop size - phenomena that should be important contributing factors to damaging ice accumulations. From the storm sounding, we speculate that precipitation may have evolved from cold cloud processes near cloud top, to a coalescence process at mid- and lower-level cloud regions, and to the development of supercooled rain beneath cloud base. Therefore, the 1990 ice storm appears to be an example of supercooled drops freezing on slightly warmer surfaces, rather than "warm" drops impacting upon freezing surfaces.

A modified version of the model was developed and used to simulated rain drop freezing in this event to determine if the sounding profile would have permitted the production of sleet. These model runs suggest that the cold air layer near ground level would have been sufficient for complete freezing of raindrops smaller than 1 mm diameter, while larger raindrops would only have only partially solidified before reaching the earth. The results of this investigation indicate that the conditions beneath cloud base may, in many events, permit the production of sleet. However, further research is warranted into the effect that artificially freezing populations of supercooled drizzle and rain drops may have on meso-scale circulations, as information fundamental to developing a seeding hypothesis to ameliorate severe ice storms.

1. INTRODUCTION

The temperature of liquid drops and other hydrometeors is often neglected in the study of cloud and precipitation processes because the particles tend to be small, exhibit little thermal inertia, and experience only small spatial temperature gradients. Thus, near thermal equilibrium states are readily maintained with the environment air. However, there are a number of situations when the importance of drop temperature can not be ignored. For one example, in the study of drop evaporation, Kinzer and Gunn (1951) demonstrated that small drops can reach an equilibrium temperature nearly equal to that of a well ventilated wet-bulb in the same

environment. In an investigation of the shattering of freezing drops, where the amount of dissolved gas and equilibrium conditions are important, Hobbs and Alkezweeny (1968) showed that the temperature of larger cloud droplets in free fall (D = 100 urn) may lag behind a linear temperature gradient of 0.5°C cm^{-1} by as much as 1°C. The possibility that regions of ultrahigh supersaturation can exist in clouds where some of the particles are not in thermal equilibrium has also been considered as a possible mechanism for enhancing the initiation of ice in some types of clouds (Gagin 1972, Gagin and Nozyce 1984, Fakuta and Lee 1986). Donaldson and Stewart (1993) have drawn attention to the importance of particle temperature in the development of fog from melting and freezing precipitation.

The potential importance of drop temperature in freezing rain and ice storms has not received explicit attention, although these events have been the subject of a number of studies. Calloway (1959) investigated the meteorology and climatology of glaze ice, meteorological characteristics of ice storms, and their geographic distributions within and outside the United States. Other studies of freezing rain events have primarily focused on attendant synoptic and mesoscale conditions (Stewart and Patenaude 1988, Mahaffy 1961, Parker and Harrison 1967, Kirk 1967, Koolwine 1975, Young 1978), unusual circumstances (Turner and Marriot 1988), and possible effects of melting precipitation on mesoscale circulations (Wexler et al. 1954, Lin and Stewart 1986, Moore and Stewart 1986, Szeto et al. 1988a, Szeto et al. 1988b, and Raga et al. 1993). Huffman and Norman (1988) proposed the concept of a "supercooled warm rain process" as a possible precipitation mechanism in freezing rain events.

This chapter presents the first calculations relevant to the importance of raindrop temperature in the sub-cloud layer of an ice storm that caused destructive ice accumulations. It focuses on the thermodynamic conditions that must exist for heavy ice accumulations at the earth's surface. To place this work into perspective, this article begins with a description of the impact of the 1990 Valentines Day ice storm on east-central Illinois, and the accompanying synoptic weather conditions. A qualitative description of the 1D numerical model used to calculate the temperature of falling raindrops is then presented. (A detailed description of the physical principles applied in the models, and a list of variable names and definitions are given in the appendices.) Results are given for liquid drizzle and rain drops along with an assessment of the importance of ventilation and mass transfer on drop temperature, and the sensitivity of drop temperature at the earth's surface to the structure of the vertical temperature profile in the sub cloud region. Results are also presented for simulations of rain drop freezing made from curiosity to determine if the vertical temperature structure would have permitted the production of sleet if an ice nucleation mechanism had operated.

2. IMPACT OF THE EVENT

The 1990 Valentine's Day ice storm affected the weather over much of the west, central, and eastern United States. This particular three day event (14-16 February 1990) occurred during four independent atmospheric field projects based from the Rocky mountains to the eastern Great Lakes (see Martner et al. 1992 for a summary). It produced a variety of severe weather including: heavy snowfall, freezing rain, thunderstorms, hail, and tornadoes. Preliminary estimates indicate that 35 states were affected resulting in $120 million in property damage.

In east-central Illinois, the ice storm began on 14 February 1990 at about 2200 UT (1600 LT). According to observations taken at the Champaign, Illinois, National Weather Service cooperative station located on the grounds of the Illinois State Water Survey, three rain episodes occurred during the night. Precipitation ended at approximately 1300 UT (0700 LT) the morning of 15 February 1990 with measured accumulations in excess of 3.3 cm (liquid equivalent). The ice storm caused severe damage to the local arboriculture and brought daily human activities to a near standstill. Nearly 15,000 residences were left without electrical power. East-central Illinois was declared a federal disaster area with an excess of $12 million of damage to public and private property.

An example of the damage to the local tree population and the significant ice loads on major tree trunks and limbs are shown in Fig. 1. Notice that surfaces with low heat capacity, such as branches, blades of grass, bushes, etc., accumulated ice; while surfaces with high heat capacity, such as concrete streets, did not. This occurrence was associated with above-freezing temperatures (> 0°C) that persisted in the region for several days prior to the storm. A close-up photograph of ice accumulation on tree branches of about 1 to 1.5 cm diameter is shown in Fig. 2. Ice accumulations reached 0.13 to 0.64 cm. The facts that the ice was clear rather than opaque and that there was very little evidence of icicling suggest the collection and rapid freezing of liquid precipitation.

3. WEATHER CONDITIONS

Fig. 3 shows the surface weather conditions for Wednesday, 14 February, 1990, at 1300 UT (0700 LT). A cold front had passed through east-central Illinois, and in the next several hours it would orient parallel to the southwestern upper-level flow, resulting in a typical overrunning precipitation pattern. Surface temperatures south of the front were warmer than 0°C, while those just behind the front were around 0°C with very light northeast winds. A NCAR/CLASS sounding taken during the evening of 14 February 1990 as part of the field operations of the University of Illinois Winter Precipitation Program (UNIWIPP) is shown in Fig. 4 (Ramamurthy et al. 1991). The interesting feature of the sounding is the existence of a cold air layer near ground level at 990 to 925 mb with a warm air layer above at 925 to 710 mb. In the cold air layer, temperatures reached a minimum of about -4°C, while temperatures aloft were around +8°C. Cloud bases were estimated to be approximately 1 km (895 mb), and cloud tops extended to 9 km (300 mb). Hence, the clouds that developed over east-central Illinois not only had tops that protruded into air colder than 0°C, they also had substantial mid-level regions that were warmer than the melting temperature of ice. Although no aircraft observations were taken around east central Illinois during this event, it is reasonable to suspect that precipitation evolved by a coalescence process in addition to cold cloud processes near cloud top.

4. MODEL DESCRIPTION

The temperature distribution inside a water drop during free-fall depends on the thermal resistance of the water drop, the heat transfer between the drop and the surrounding air, the mass transfer between the drop and the surrounding air, and the rate at which heat is carried away into the environment. Thermal resistance, which determines how the water drop reacts to changes in its environment, decreases with increasing thermal conductivity, as do specific heat capacity and

the density of water. Two mechanisms that dominate the heat transfer process are convection (diffusion plus ventilation) and mass transfer (i.e., either evaporation or condensation). Convective transfer means heat flux between the drop and the external flow. Mass transfer directs heat toward or away from the drop, depending on environmental humidity and other factors. Both mechanisms are highly dependent on drop size and the moist thermophysical properties of the environment.

For simplicity, the unsteady one-dimensional (1D) heat diffusion equation was used to compute the temperature distribution within a freely falling liquid drop. The time step and grid spacing varied with drop size, and were chosen to be small enough to resolve the rate of temperature and humidity changes as they apply to each drop size. The model was based on an implicit scheme. The initial selection of time-step was based on that computed for an explicit scheme, and then refinements were made until the solution converged.

Unless otherwise stated, volume average drop temperatures calculated from the computed internal temperature distribution of the drop are presented. As input, the model used initial drop diameter and initial drop height above the ground. Any arbitrarily chosen environmental temperature and humidity profile can be used with the model. At each time step, a computation was made of the amount of heat conducted through the drop (if an internal temperature gradient exists) and into the environment, if the drop happens to be warmer than the environment. Of course, the direction of heat conduction reverses if the gradient reverses.

The computation accounted for the ventilation that occurs when heat is carried away from the drop by external flow (Beard and Pruppacher 1971). The drop surface temperature was modified depending on whether condensation or evaporation occurred during the time step. Changes in drop surface temperature then were allowed to propagate into and away from the drop. An adjustment was also made in drop terminal velocity as drop size changed. Thus, for a drop initially wanner than a subsaturated environment, its temperature would be affected by heat loss to the air by conduction, in addition to cooling by evaporation or warming by condensation, in the presence of ventilation and depending on the difference between drop surface temperature and environmental dew-point temperature.

The model did not take into account the effects of internal circulation or drop oscillation on the internal temperature distribution. These factors are probably negligible for drops smaller than 2.0 mm diameter. For larger drops, the effect of internal circulation tends to be compensated by the effect of oscillation (Pruppacher and Rasmussen 1979). Heat conduction was assumed to be radially symmetric.

Other important assumptions were that: 1) the initial temperature of the drop was uniform; 2) the change in water density (as drop temperature changed) did not change the volume of the drop - only mass transfer was allowed to change drop size; 3) the thermal properties were constant inside the drop; and 4) the drop was spherical. Finally, the model did not include simulation of drop collection, nor did it take into account the net effect of the drop population on the environment.

5. MODEL RESULTS FOR LIQUID DRIZZLE AND RAINDROPS

Calculations were made for drops in the size-range from 0.1 to 5 mm diameter. Doppler radar observations taken as part of UNIWIPP during the ice storm suggest median drop diameters of 1 or 2 mm. In each calculation, a drop's prescribed fall began at 1600 m above sea level. In each calculation, the drop was assumed to be initially at thermoequilibrium with the environment air and falling at terminal velocity. Model results for the drop's temperature at the ground (200 m above sea level) were found to be insensitive to initial drop temperature, according to test runs on drops of various sizes in which initial drop temperatures were as much as 5°C warmer than the air.

Table 1 summarizes selected model results and shows that drops smaller than 0.4 mm diameter completely evaporate before reaching the ground. A 0.1 mm drop falls only 57 m, while drops of 0.2 and 0.3 mm diameter fall 376 and 887 m, respectively, before completely evaporating. In these calculations, complete evaporation was specified as a drop size smaller than 10 μm diameter. Table 1 also shows that drops that reach the ground are supercooled, and the amount of supercooling increases with greater drop diameter. For comparison, the temperature at the earth's surface was 0°C. Thus, for the drops to be in thermal equilibrium, they would have had to be 0°C. The amount of supercooling may have been nearly 1.0°C for a 3.0 mm drop. Hence, increases in supercooling with drop size may have been an important factor contributing to heavy ice accumulation in the Valentine's Day ice storm.

Figure 5 shows model results for a 0.5 mm liquid drop. As can be seen in the figure, after only a short fall, the drop attains a steady-state temperature very nearly equal to the wet-bulb temperature of its environment. This occurs because small drops have very short thermal relaxation times which permit near-instantaneous response to changes in the temperature and humidity of the environment. Upon reaching the earth's surface, the calculation indicates that the drop is supercooled a few tenths of a degree.

Figure 6 shows model results for a 2 mm drop. A drop of this size does not closely follow changes in air temperature and humidity. As the drop progresses from its initial point on the sounding, its temperature lags behind changes in air temperature. At no particular time does the surface temperature of the drop exactly equal the dew-point temperature of the air. Upon reaching the earth, it is supercooled nearly 0.5°C. A particularly interesting feature in Fig. 6 is that at the lowest part of the fall (from 250 to 200 m), the average computed temperature of the drop is colder than the dew-point temperature of the air, a condition that would permit drop growth (and warming) by condensation, even though the environment is subsaturated.

Figs. 5 and 6 suggest several important implications that are related to the unique structure of the temperature profile. First, a substantial volume of "warm" cloud probably existed during this winter storm, in which precipitation could have evolved by a coalescence process. Secondly, drop supercooling did not occur in-cloud, but rather in subcloud regions, where air temperatures were colder than 0°C. These conditions favored increased supercooling with drop size and heavy ice accumulations. In fact, atmospheric regions with supercooled drizzle and raindrops present particularly hazardous regions for aircraft icing (Politovich 1989). These regions are hazardous because large drops tend to spread away from deiced portions of the wings. Ice accumulations at these wing locations cannot be removed, resulting in drastic reductions in

aircraft performance (Sand et al. 1984). Thus, model results suggest that dangerous regions of supercooled liquid can exist outside of cloud regions and that, if it is not possible to land, aircraft caught in subcloud regions of supercooled rain may find safety by ascending into warm (T > 0°C) cloud aloft, a practice just opposite to conventional.

6. MODEL RESULTS FOR VARIATIONS ON THE NATURAL CONDITIONS

This section describes the results of the application of the heat and mass transfer model to various natural conditions. Three primary variations on the natural conditions were investigated. First was the relative importance of conduction, ventilation, and mass transfer in determining drop temperature. Secondly, the model was used to determine the sensitivity of final drop temperature to changes in the minimum temperature of the cold air in the 200 to 800 m layer near the ground. This run was conducted to determine if a slightly warmer air layer would result in a warmer final drop temperature. This condition potentially can affect the rate of ice accumulation by lengthening the time required for the liquid to freeze. In the third variation, the model was modified to simulate drop freezing as a heuristic exercise to determine if the sounding conditions would have permitted the production of sleet. The sensitivity of the final liquid/solid drop condition to ice nucleation temperature was also examined.

a. Relative importance of ventilation and mass transfer

It is well known that the external flow exerts a strong influence on the transport of heat and vapor toward or away from an object. Thus, several model runs were performed to explore and quantify the relative importance of ventilation and mass transfer on drop temperature during fall and in determining ground-level temperature, which is the temperature that is relevant to ice accumulation. Two variations on the complete model were run for drops in the size range of 0.1 to 5.0 mm diameter: variation 1) runs without mass transfer and no ventilation effects on heat transfer, and variation 2) runs with ventilation effects on heat transfer but no mass transfer. Table 1 lists final drop temperatures for these runs and expectedly reveals that mass transfer has a profound effect on drop survivability and drop temperature. As can be seen from the runs without mass transfer, all drops survived the fall from 1600 m to the ground; while in the run with mass transfer, drops in the size range from 0.1 to 0.3 mm completely evaporate. Hence, the long-appreciated importance of drop mass transfer is evident in moistening subcloud regions.

This cursory investigation also indicated, not unexpectedly, that ventilation has a large influence on drop temperature. In the absence of ventilation, heat transfer toward or away from the drop is solely governed by conduction in each medium. Drop temperature profiles at different altitudes (Fig. 6) clearly indicate that a significant temperature difference develops between the drop and the environment, particularly as drop size increases. For smaller drops with small thermal inertia, the mechanism of conduction is almost sufficient for the drop to closely follow changes in the sounding temperature as it falls. Larger drops with greater thermal inertia do not change temperature readily. Results for runs without ventilation and mass transfer (Table 1) also indicate that the temperature of large drops at ground level are well in excess of 0°C. Hence, ventilation makes a major contribution to drop supercooling at ground level.

Mass transfer also modifies drop temperature by bringing the surface temperature of the drop to nearly that of the dew-point temperature for subsaturated environments. As shown in the

previous section, special combinations of drop size, temperature lag, and vertical sounding structure can produce conditions favorable for condensation in a subsaturated environment. This finding further illustrates that all three mechanisms, heat transfer, mass transfer and ventilation are required to bring freely falling larger drops into full moist thermodynamic equilibrium with the environment, at least for drops falling in the subcloud region of the Valentine's Day ice storm.

b. Sensitivity to the temperature profile in the lower atmosphere

Several model runs were made to obtain an appreciation for the sensitivity of final drop temperature to the structure of the lower cold-air layer. A primary interest in these runs was to determine if a slightly warmer sounding would have resulted in drop temperatures warmer than 0°C at the earth's surface, and thereby determine if ice accumulations would have been less severe. Figure 7 shows how the sounding was modified for three model runs; one assuming that the minimum temperature, roughly located at 650 m, was 1°C colder than observed and model runs assuming that the minimum temperature was 1 and 2°C warmer than observed. Simulations were made under the later assumption to determine if it would have been possible for drop temperatures at the earth's surface to be warmer than 0°C, and thus, mitigate or advert ice accumulations. The simulation for the colder minimum temperature was made for the opposite reason.

Table 2 lists average drop temperatures at ground level for the observed and modified soundings. Increases in the minimum temperature of the cold air layer near the earth's surface are shown to have little effect on average drop temperature at ground level for drops with diameters smaller than about 1 mm. The ground-level average temperatures of larger drops are influenced by up to several tenths of a degree centigrade. These results indicate another important aspect of the breadth of the drop size spectrum. Not only does drop supercooling increase with drop size, but drop temperature at ground level is strongly influenced by the coldness of the air through which it has traveled. Hence, model results suggest that the structure of the cold-air layer is an important factor to consider in freezing rain events if raindrops of larger than about 1 mm diameter are expected.

c. *Simulations of drop freezing*

The one-dimensional heat and mass transfer model was modified to simulate raindrop freezing. These simulations were performed to determine the extent to which the temperature structure in the lower atmosphere was conducive to partial or complete freezing of the rain drops had an ice nucleation mechanism operated. Drop freezing was modeled as the two-stage process described in Pruppacher and Klett (1980). In the first stage, an ice shell was assumed to form almost immediately around the outer surface of the drop. In this stage, the release of latent heat from fusion causes the drop to warm to near 0°C, and the thickness of the initial ice shell was modeled to be limited by initial warming. Because the drop cannot warm to temperatures in excess of 0°C, approximately $\Delta T c_p / h_{sg}$ of the drop mass initially freezes (Hallett 1964, King 1975). In the second stage, the ice shell propagates inward at a rate governed by the rate at which the latent heat of freezing can be disposed of into the surrounding air. If the environment were isothermal, thickening of the ice shell would reduce the rate of latent heat disposal. The temperature of the partially frozen drop remains near 0°C until the conversion of liquid to solid is complete.

Model calculations were performed for drops in the size range from 0.1 to 5 mm diameters, and results are given in Table 3. Results for 0.5 and 2 mm drops are shown in Figs. 8 and 9, respectively. In this numerical simulation, nucleation was assumed to occur when the average drop temperature reached -2.5°C. Model runs were performed under the assumption of several other nucleation temperatures, and the results are also presented in Table 3 for comparison. Figures 8 and 9 show that the temperature of the drop immediately warmed to almost 0°C as a result of the release of the latent heat of fusion. The drop remained near 0°C until it completely crystallized. As the model calculations suggest in Fig. 8, a 0.5 mm liquid drop completely transforms into ice after only a short fall distance, after which time the heat and mass transfer problem follows that with the physical properties of an ice sphere. After complete freezing, no further fusional latent heat release occurs, and the drop eventually cools to a temperature between that of the air and the frost point of the environment. Thus, drop temperature is once again simply governed by conduction, ventilation, and mass transfer, but follows the thermophysical behavior of ice. Model results shown in Fig. 9 suggest that complete freezing of a 2 mm drop does not occur before it reaches ground level. The fraction of the drop that is ice by volume is only 55%. Hence, latent heat release continued throughout the entire fall of the drop, so that the drop temperature is near 0°C at the time it reaches ground level.

Results from several model runs in which the nucleation temperature was assumed to be -1, -2.5, and -4°C are presented in Table 3. For drops smaller than 2.0 mm, varying the nucleation temperature had relatively little effect on the calculated fraction of drop that was ice at the earth's surface. For example, computations for drops from 0.4 to 1.0 mm and a nucleation temperature of -1°C showed that they become 100% ice before reaching the earth's surface. The model produced approximately the same results for a -2.5°C nucleation temperature. However, as Table 3 indicates, drops larger than about 2 mm with an assumed nucleation temperature of -4°C never nucleated ice in the model because they never achieved the assumed ice nucleation temperature. This implies that if the natural atmosphere acts to nucleate ice in supercooled rain, then the character of the precipitation population that would eventually reach the earth's surface would be highly dependent on the ice nucleation temperature, the breadth of the drop size spectrum, and the thermal dynamic structure of the cold-air layer.

7. CONCLUSIONS

A one-dimensional heat and mass transfer model was used to study the temperature and freezing behavior of drizzle and raindrops assuming the thermodynamic conditions observed during the 1990 Valentine's Day freezing rain storm that affected east-central Illinois. The vertical structure of the sounding suggests that atmospheric conditions were conducive to the production of rain by a coalescence process in addition to cold cloud processes near cloud top. Model results suggest that conditions were very favorable for supercooling drizzle and raindrops below cloud base. Furthermore, conditions favored increased supercooling with drop size. This factor, along with factors such as rainfall rate and persistence, may have contributed to the damaging ice accumulations. The sounding of the 1990 Valentine's Day ice storm may be typical of freeezing rain stroms, and thus recognition of similar features may assist in forecasting these events.

Sensitivity studies suggest that minor changes in the temperature of the lower cold layer may produce only minor changes in final drop temperature for diameters smaller than 1.0 mm. These calculations showed that for certain meteorological situations, it is not appropriate to assume that the hydrometeors are in thermal equilibrium with their environment, and that it is possible for precipitation from cloud regions where a coalescence processes operates to result in supercooled rain. An important unresolved question related to the Valentine's Day ice storm has to do with the absence or lack of an ice nucleating mechanism that would have resulted in sleet at the ground, rather than supercooled rain.

The one-dimensional heat and mass transfer model was modified to simulate raindrop freezing to explore for the liquid/solid characteristic of the precipitation at the ground had ice nucleation occurred. The model applied to the observed sounding showed that drizzle-size drops completely freeze within a few hundred meters of fall, and thereby may reach the earth as sleet. However, larger raindrops do not completely freeze prior to reaching the earth, and thus may reach the earth as hydrometeors with an outer ice shell and inner liquid. These sensitivity model studies of the mass fraction of the drop that potentially can transform to ice before reaching ground level indicate that if the ice nucleation temperature is too cold, some of the hydrometeors may reach the earth as a mixture of liquid and solid.

8. REFERENCES

Beard, K.V., and H.R. Pruppacher, 1971: A wind tunnel investigation of the rate of evaporation of small water drops falling at terminal velocity in air. *J. Atmos. Sci.,* 28, 1455-1464.

Calloway, C.C., 1959: Glaze: Its Meteorology and Climatology, Geographical Distribution, and Economic Effects. Tech. Rep. EP-105, Environmental Protection Research Division, Quartermaster Research & Engineering Center, U.S. Army, Natick, MA.

Donaldson, N.R., and R.E. Stewart, 1993: Fog induced by mixed-phased precipitation. *Atmos. Res.,* 29, 9-25.

Dye, J.E., and P.V. Hobbs, 1968: The influence of environmental parameters on the freezing and fragmentation of suspended water drops. *J. Atmos. Sci.,* 25, 82-96.

Fukuta, N., and H J. Lee, 1986: A numerical study of the supersaturation field around growing graupel. *J. Atmos. Sci.,* 43,1833-1843.

Gagin, A., 1972: The effect of supersaturation on the ice crystal production by natural aerosols. *J. Rech. Atmos.,* 6 ,175-185.

Gagin, A., and H. Nozyce, 1984: The nucleation of ice crystals during the freezing of large supercooled drops. 7. *Rech. Atmos.,* 18, 119-129.

Gerald, C.F., and P.O. Wheatley, 1984: *Applied Numerical Analysis.* Addison-Wesley Publishing Company, Inc., Reading, MA, 579 pp.

Hallett, J., 1964: Experimental studies of the crystallization of supercooled water. *J. Atmos. Sci.*, 21, 671-682.

Hobbs, P.V., and AJ. Alkezweeny, 1968: The fragmentation of freezing water droplets in free fall. J. *Atmos. ScL, 25,* 881-888.

Huffman, GJ., and G.A. Norman, 1988: The supercooled warm rain process and the specification of freezing precipitation. *Mon. Wea. Rev.*, 116, 2172-2182.

Incropera, F.P., and D.P. DeWitt, 1985: *Fundamentals of Heat and Mass Transfer.* Wiley, New York, 802 pp.

Kays, W.M., and M.E. Crawford, 1980: *Convective Heat and Mass Transfer.* McGraw-Hill, Inc., New York, 420 pp.

Kinzer, G.D., and R. Gunn, 1951: The evaporation, temperature and thermal relaxation-time of freely falling waterdrops. *J. Meteor.*, 8, 71-83.

King, W.D., 1975: Freezing rates of water droplets. 7. *Atmos. ScL,* 32, 403-408.

Kirk, T.H., 1967: The synoptic conditions attending an occurrence of freezing drizzle. *Meteo. Mag.,* 96,112-115.

Koolwine, T., 1975: Freezing Rain. MS thesis, Dept. of Physics, University of Toronto, Ontario, Canada, 92 pp.

Lin, C.A., and R.E. Stewart, 1986: Mesoscale circulation initiated by melting snow. *J. Geophys. Res.,* 91, 13299-13302.

Mahaffy, F.J., 1961: The ice storm of 25-26 February 1961 at Montreal. *Weatherwise,* 241-244.

Mariner, B.E., R.M. Rauber, R.M. Rasmussen, E.T. Prater, and M.K. Ramamurthy, 1992: Impacts of a destructive and well-observed cross-country winter storm. *Bull. Amer. Meteor. Soc,* 73, 169-172.

Moore, G.W.K., and R.E. Stewart, 1986: The coupling between melting and convective air motions in stratiform clouds. 7. *Geophys. Res.,* 90,10659-10666.

Parker, G., and A.A. Harrison, 1967: Freezing drizzle in south-east England on 20 January 1966. *Meteo. Mag.,* 96, 108-112.

Politovich, M.K., 1989: Aircraft icing caused by large supercooled droplets. *J. Appl. Meteor.,* 28, 856-867.

Pruppacher, H.R., and J.D. Klett, 1980: *Microphysics of Clouds and Precipitation.* D. Reidel Publishing Company, Boston, MA, 714 pp.

Pruppacher, H.R., and R. Rasmussen, 1979: A wind tunnel investigation of the rate of evaporation of large water drops falling at terminal velocity in air. *J. Atmos. Sci.,* 36, 1225-1260.

Raga, G.B., R.E. Stewart, and N.R. Donaldson, 1993: Microphysical characteristics through the melting region of a midlatitude winter storm. *J. Atmos. Sci,* 48, 843-855.

Ramamurthy, M.K., R.M. Rauber, B.P. Collins, M.T. Shields, P.C. Kennedy, and W.L. Clark, 1991: UNIWIPP: A University of Illinois field experiment to investigate the structure of mesoscale precipitation in winter storms. *Bull Amer. Meteor. Soc.,* 72, 764-776.

Ranz, W., and W. Marshall, 1952: Evaporation from drops, *Chem. Eng. Prog.,* 48, 141-146.

Sand, W.R., W.A. Cooper, M.K. Politovich, and D.L. Veal, 1984: Icing conditions encountered by a research aircraft. *J. Climate Appl. Meteor.,* 23,1427-1440.

Stewart, R.E., and L.M. Patenaude, 1988: Rain-snow boundaries and freezing precipitation in Canadian east coast winter storms. *Atmos.-Ocean,* 28, 377-398.

Szeto, K.K., C.A. Lin, and R.E. Stewart, 1988a: Mesoscale circulations forced by the melting of snow in the atmosphere, Part I: Basic simulations and dynamics., 7. *Atmos. Sci.,* 45, 1629-1641.

Szeto, K.K., R.E. Stewart, and C.A. Lin, 1988b: Mesoscale circulations forced by the melting of snow in the atmosphere, Part II: Application to meteorological features. *J. Atmos. Sci.,* 45, 1642-1650.

Turner, D.W., and D.J. Marriott, 1988: An unusual example of freezing rain. *Meteor. Mag.,* 117, 255-257.

Wexler, R., RJ. Reed, and J. Honig, 1954: Atmospheric cooling by melting snow. *Bull. Amer. Meteor. Soc,* 35, 48-51.

Woo, S., and A.E. Hamielec, 1971: A numerical method of determining the rate of evaporation of small water drops falling at terminal velocity in air. *J. Atmos. Sci.,* 28,1448-1454.

Young, W.R., 1978: Freezing Precipitation in the Southeastern United States. MS thesis, Texas A&M University, 123 pp.

Table 1. Summary of key model results.

Initial Drop Diameter (mm)	0.1	0.2	0.3	0.4	0.5	0.7	1.0	2.0	3.0	4.0	5.0
Complete Model											
With ventilation and mass transfer											
Final Drop Diameter (mm)	0.00	0.00	0.00	0.23	0.40	0.64	0.96	1.985	2.98	3.98	4.98
Final Drop Phase	V	V	V	L	L	L	L	L	L	L	L
Final Drop Temperature (C)	7.8	6.4	-2.5	-0.00	-0.01	-0.04	-0.10	-0.46	-0.97	-1.44	-1.70
Variation 1											
Without ventilation and mass transfer											
Final Drop Phase	L	L	L	L	L	L	L	L	L	L	L
Final Drop Temperature (C)	-0.00	-0.00	-0.01	-0.02	-0.05	-0.17	-0.65	0.26	3.59	5.32	6.17
Variation 2											
With ventilation, without mass transfer											
Final Drop Phase	L	L	L	L	L	L	L	L	L	L	L
Final Drop Temperature (C)	-0.00	-0.00	-0.00	-0.01	-0.01	-0.03	-0.07	-0.40	-0.92	-1.18	-1.02
Fall Distance (m)	57	376	887	1400	1400	1400	1400	1400	1400	1400	1400
Fall Time (sec)	424	916	1115	1052	747	500	350	212	172	157	152

L Liquid phase

V Vapor phase

Table 2. Final drop temperatures showing the sensitivity to minimum sounding temperature.

	Minimum Sounding Temperature, °C			
	Observed	+1	+2	-1
Diameter, mm				
0.5	-0.01	-0.01	-0.01	-0.02
1.0	-0.10	-0.08	-0.08	-0.10
2.0	-0.45	-0.35	-0.33	-0.46
3.0	-0.97	-0.76	-0.65	-1.00
4.0	-1.44	-1.12	-0.88	-1.48
5.0	-1.70	-1.27	-0.96	-1.75

Table 3. Percent of drop that was ice at the earth's surface showing the sensitivity of final drop phase to nucleation temperature.

	Ice Nucleation Temperature, °C		
Diameter, mm	-1.0	-2.5	-4.0
0.5	100	100	100
1.0	100	98	52
2.0	57	55	50
3.0	29	27	0
4.0	17	14	0
5.0	10	6	0

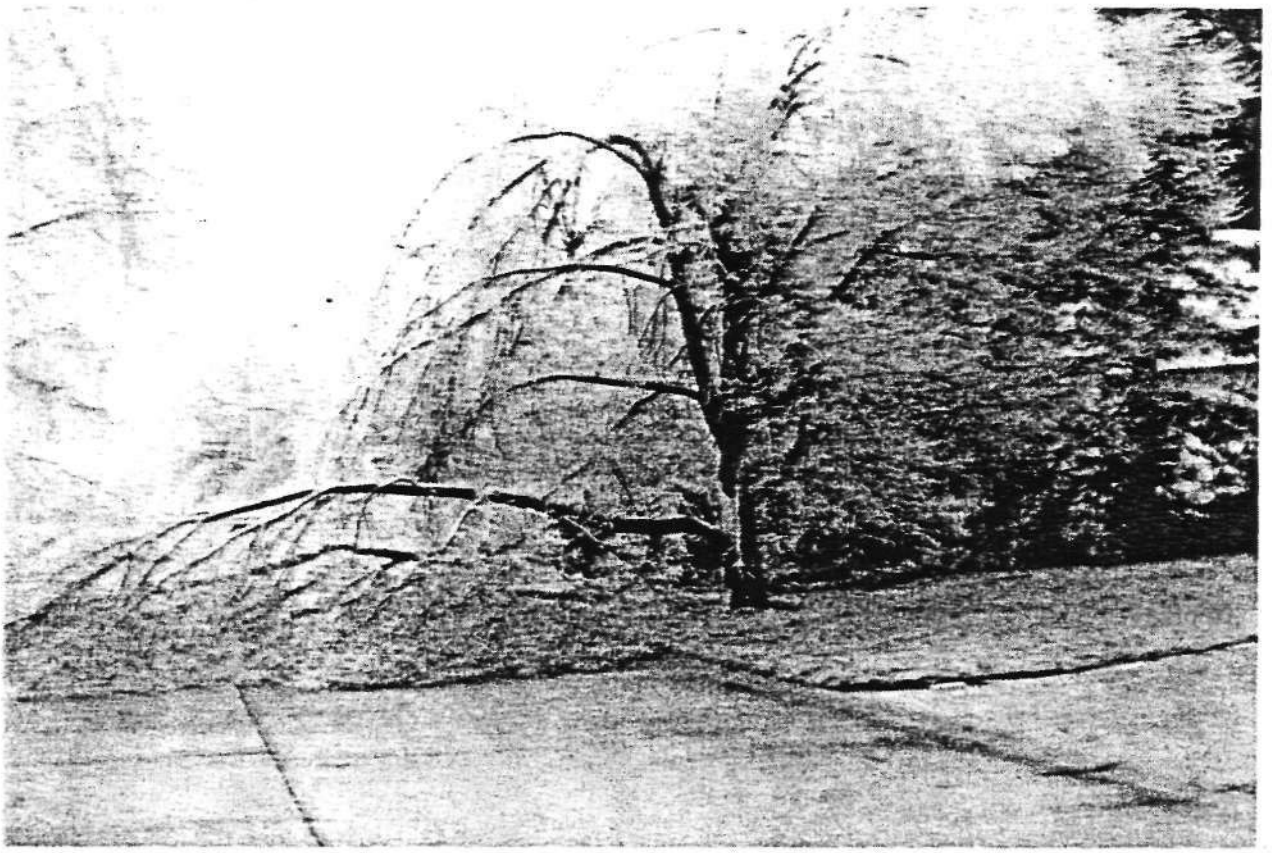

Figure 1. Typical damage to local arboriculture.

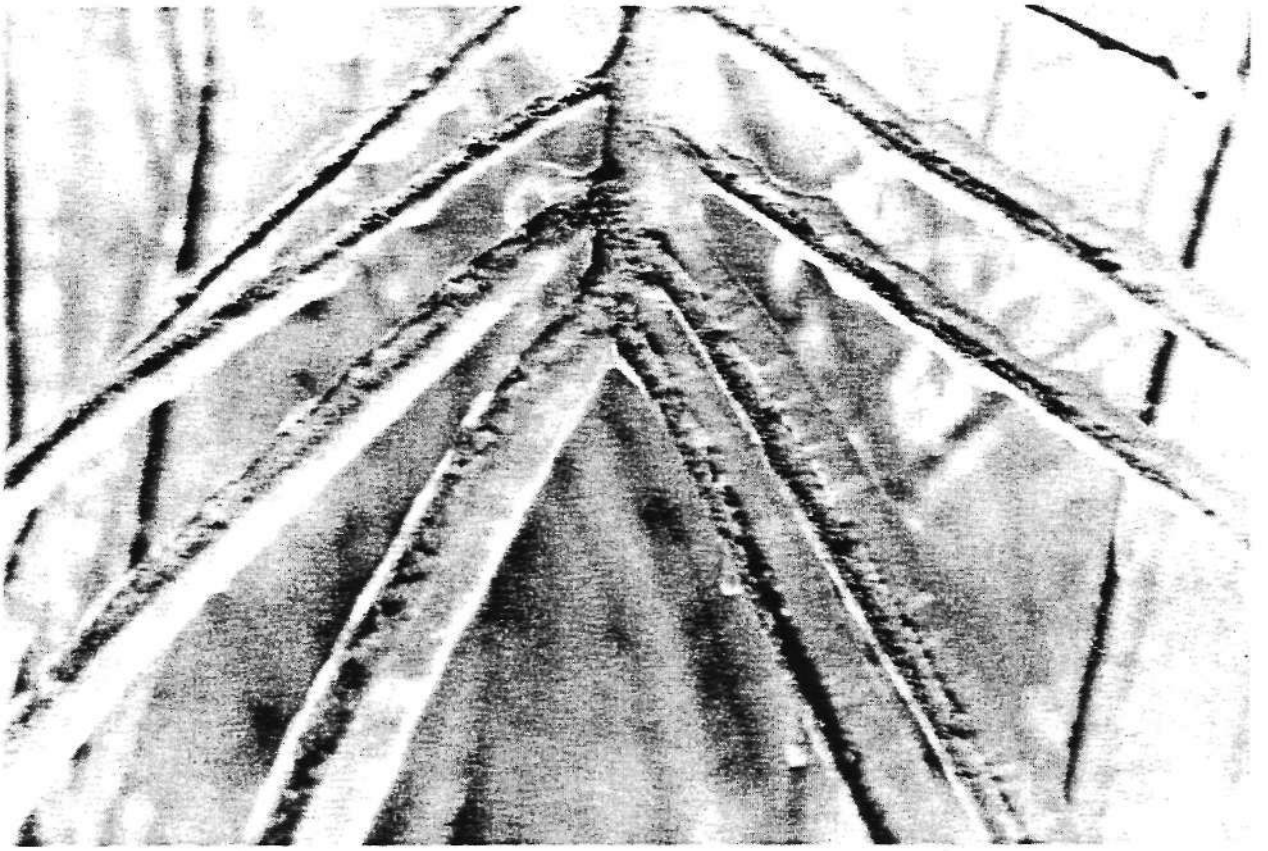

Figure 2. Heavy ice accumulations on tree branches.

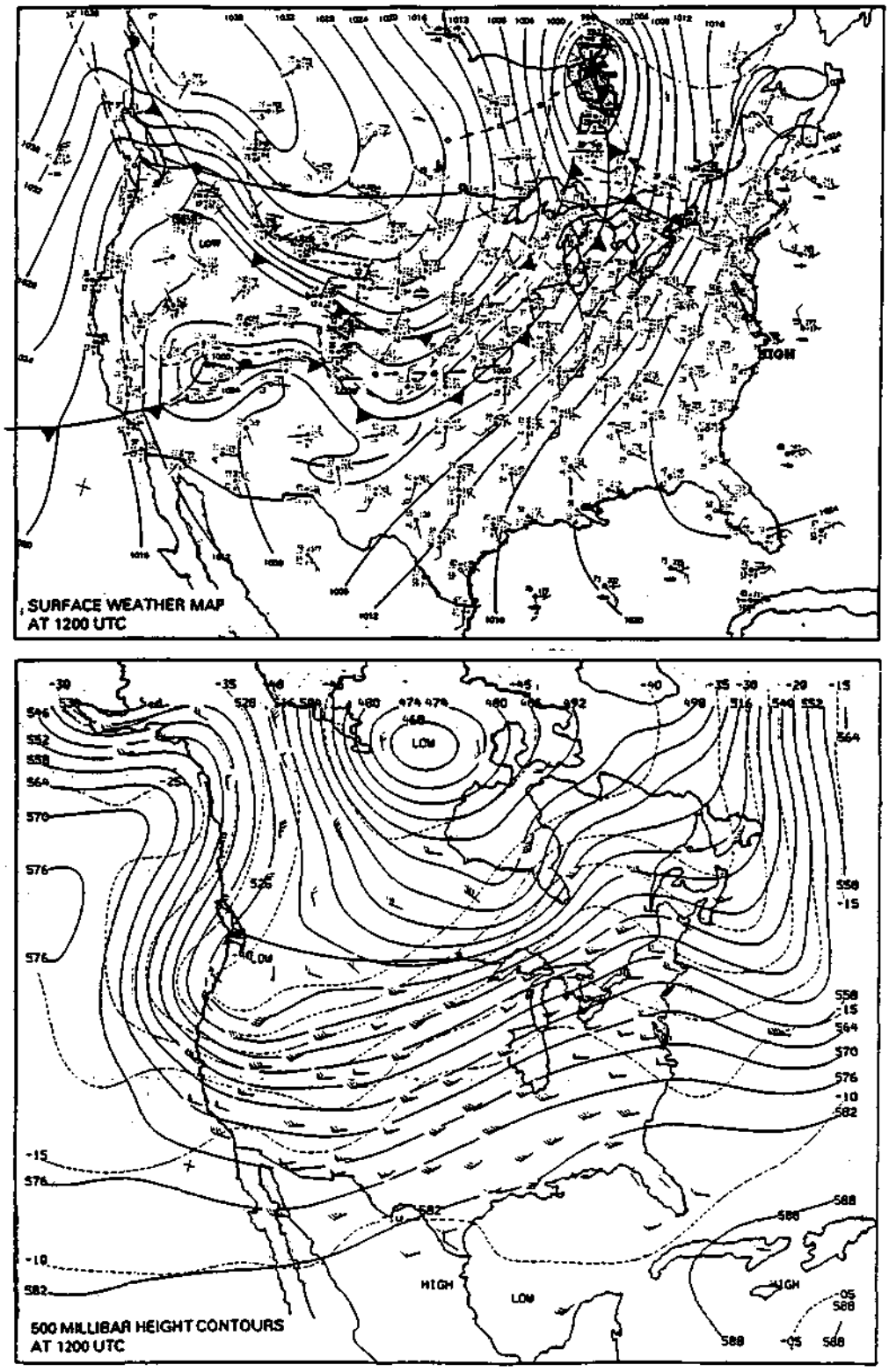

Figure 3. Surface and 500-mb weather conditions for Wednesday, 14 February 1990 (From the Daily Weather Map Series).

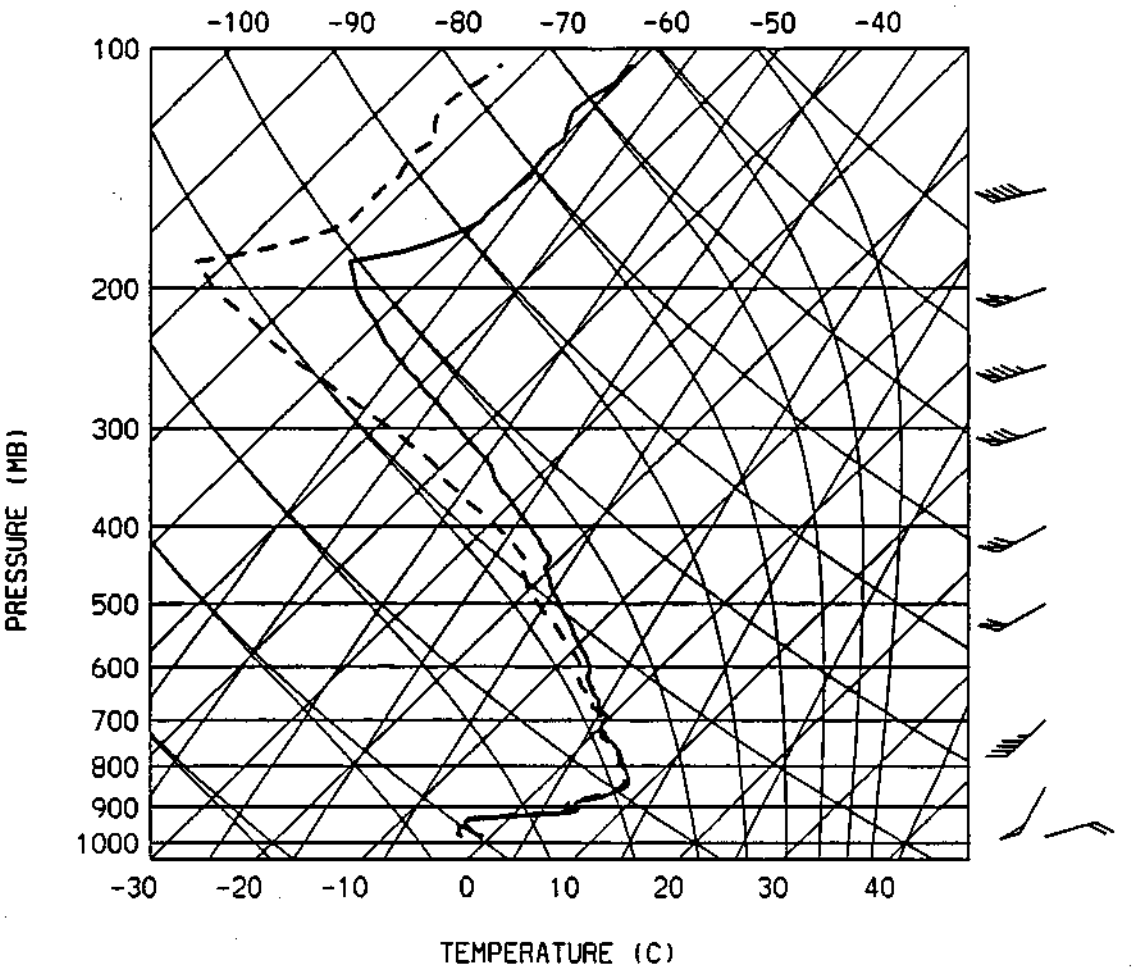

Figure 4. Skew T/Log P diagram showing NCAR/CLASS sounding released from Willard Airport on 14 February 1990 at 1800 LT. Solid line = air temperature, dashed line = dew-point temperature.

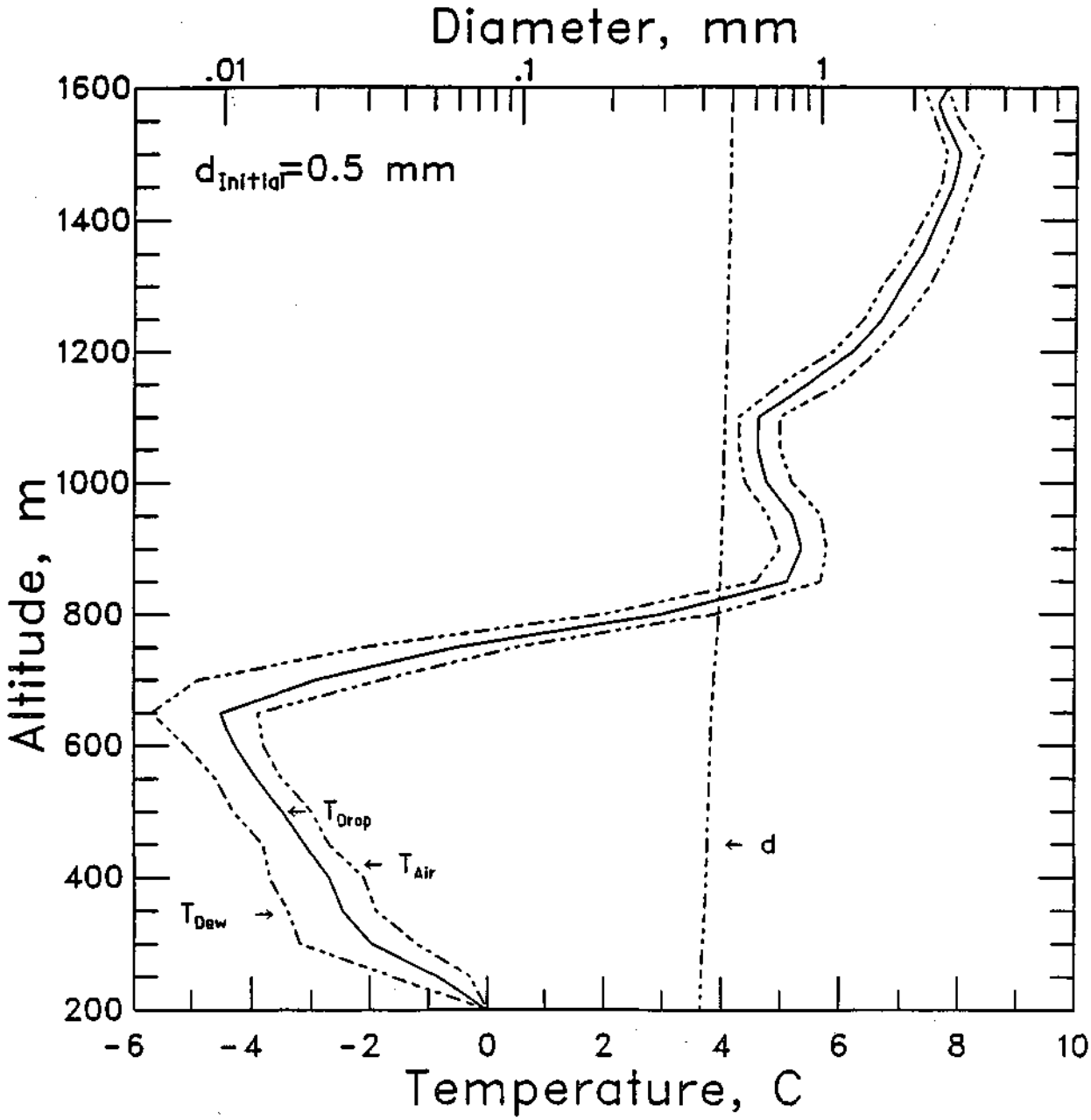

Figure 5. Model results for a drop of 0.5 mm initial diameter.

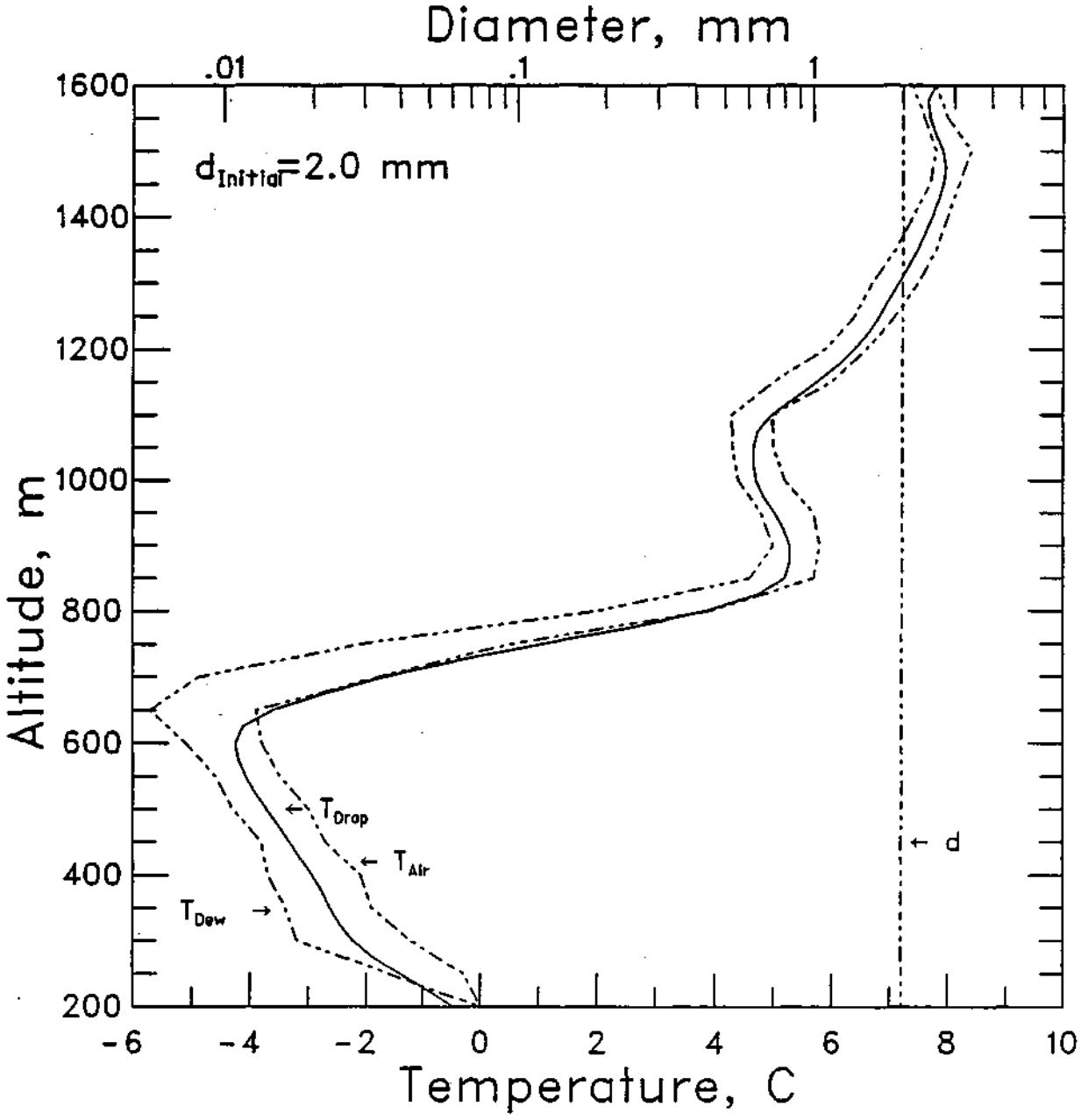

Figure 6. Model results for a drop of 2.0 mm initial diameter.

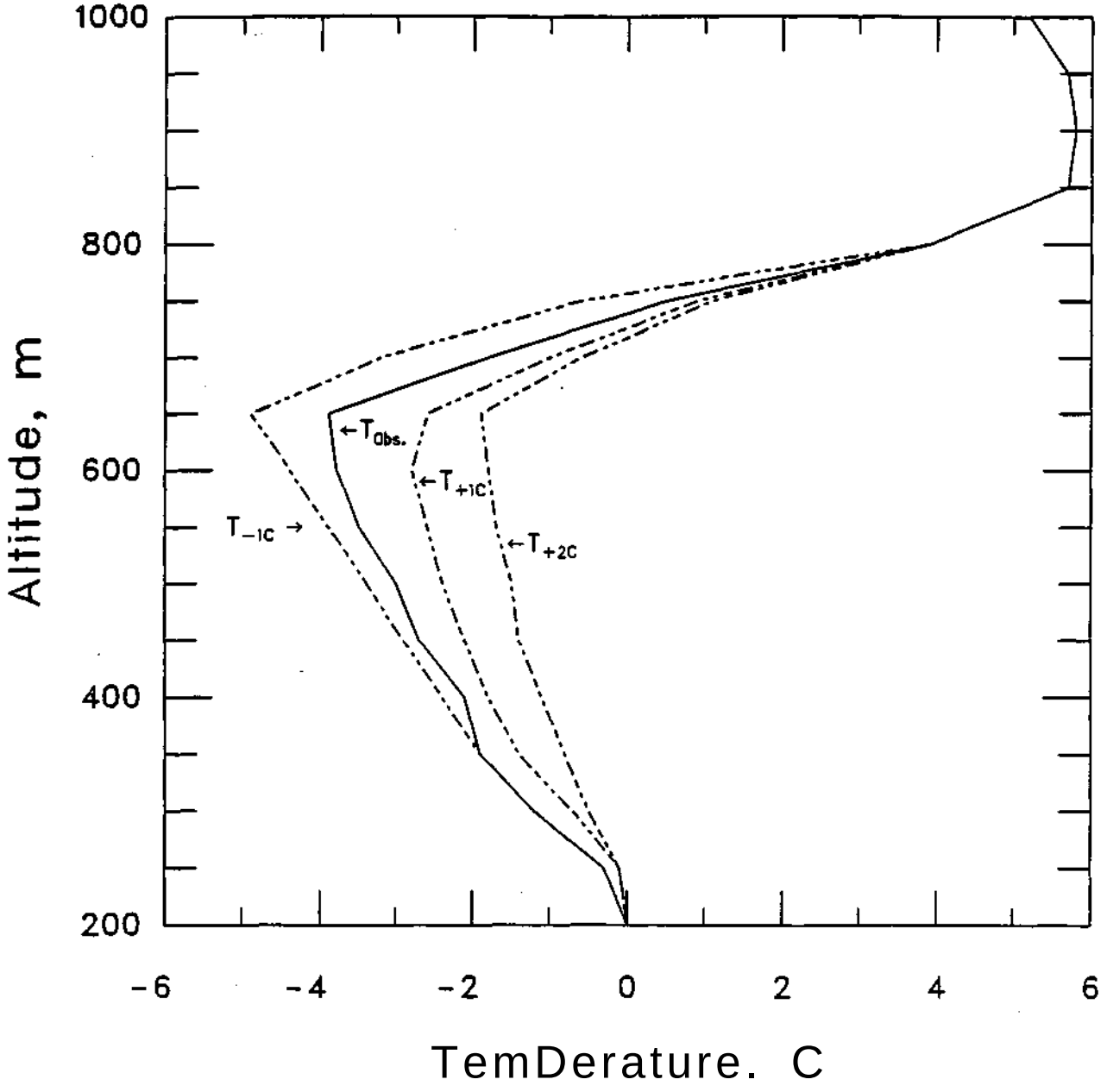

Figure 7. The observed sounding (T_{Obs}), and intentionally modified soundings used in the drop temperature sensitivity studies assuming the minimum temperature at approximately 650 m was about 1°C colder (T_{-1C}), 1°C warmer (T_{+1C}), and 2°C warmer (T_{+2C}).

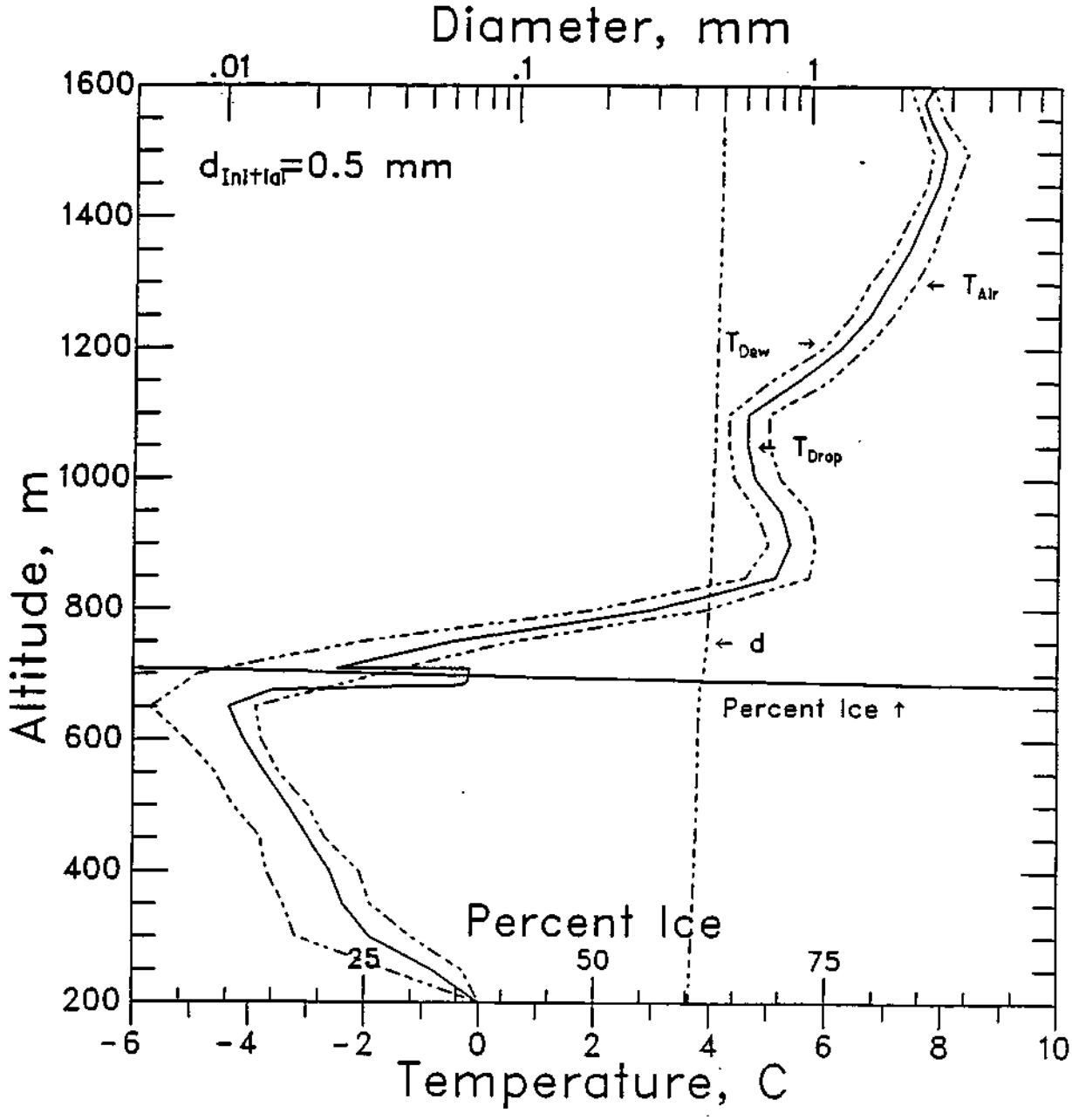

Figure 8. Model results for a drop of 0.5 mm initial diameter, assuming freezing occurs when the drop reaches an average temperature of -2.5 °C.

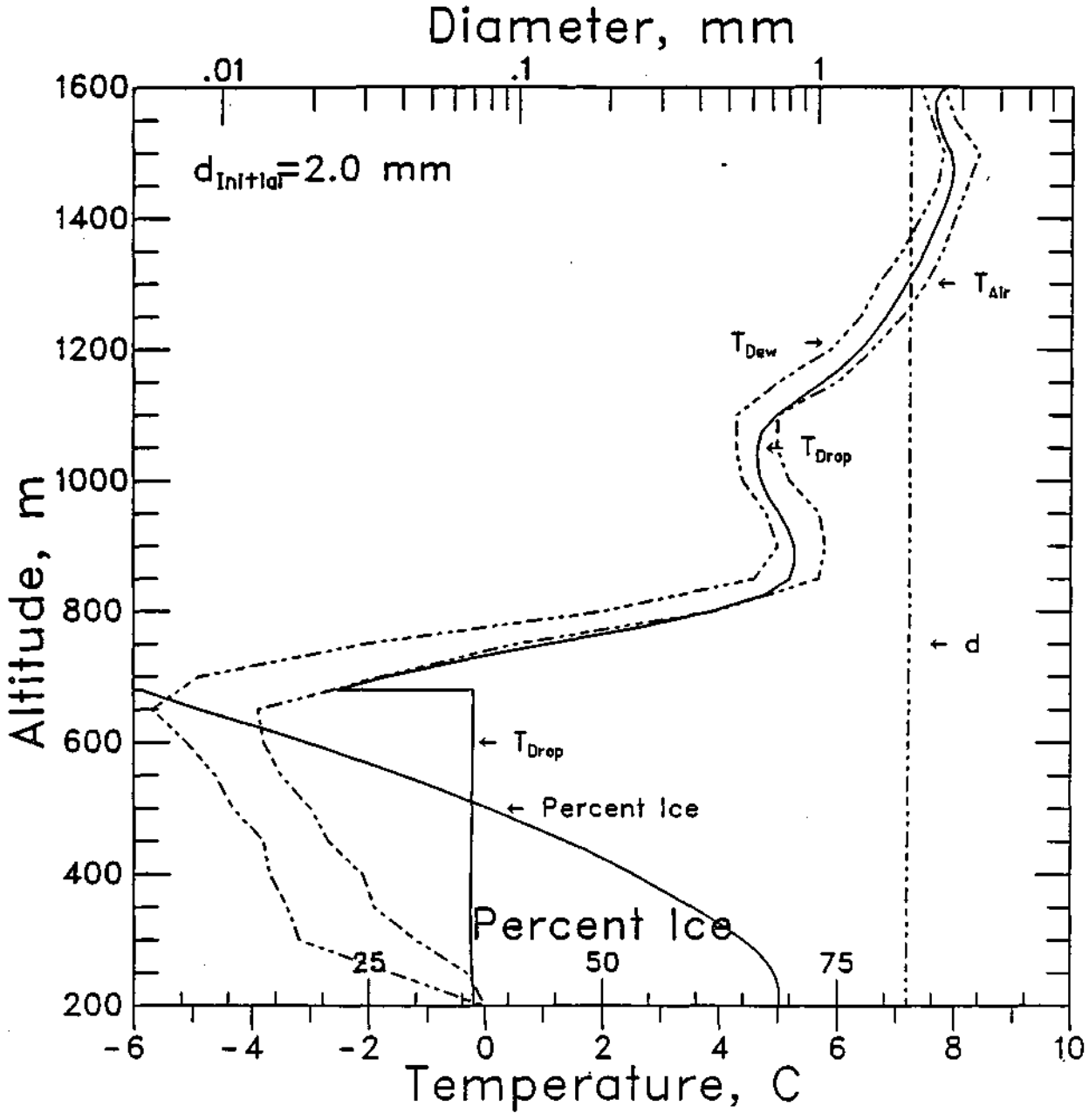

Figure 9. Model results for a drop of 2.0 mm initial diameter, assuming freezing occurs when the drop reaches an average temperature of -2.5 C.

LIST OF APPENDICES

APPENDIX A

List of Symbols

c_p	specific heat capacity
d	diameter of drop
D	diffusivity
f_v	ventilation factor defined by Eq. 18
h	heat transfer coefficient or enthalpy
h_{sf}	latent heat of melting
h_{sg}	latent heat of sublimation
m	mass fraction
m	mass flow rate
m	mass flux
N_{Pr}	Prandtl number
Nu	Nussult number
N_{Re}	Reynolds number
N_{Sc}	Schmidt number
q''	heat flux
r	spatial coordinate
R	radius of drop
t	time coordinate
t^*	nondimensional time coordinate defined by Eq. 4 or Eq. 24
T	temperature
T^*	nondimensional temperature defined by Eq. 3 or Eq. 23
u	velocity
x	nondimensional spatial coordinate defined by Eq. 2 or Eq. 22
a	thermal diffusivity
λ	heat conductivity
v	kinematic viscosity
p	density

subscripts

0	initial condition
conv	convection
mt	mass transfer by evaporation/condensation
i	inner
ice	ice
i/w	ice/water interface
m	air-vapor mixture
max	maximum
min	minimum

o	outer
s	drop surface
subl	sublimation
t	time coordinate
v	vapor
w	water
co	environment condition

APPENDIX B

Theoretical Model Description

1. The heat conduction problem

Following the discussion of Incropera and Dewitt (1985), the equation governing unsteady one-dimensional heat diffusion in a spherical coordinates system (0 < r < R) can be written in nondimensional form as:

$$\frac{\partial T_w^*(x,t^*)}{\partial t^*} = \frac{\partial^2 T_w^*(x,t^*)}{\partial x^2} + \frac{2}{x}\frac{\partial T_w^*(x,t^*)}{\partial x}, \tag{1}$$

with the nondimensional parameters defined as:

$$x = \frac{r}{R}, \tag{2}$$

$$T_w^*(r,t) = \frac{T_w(r,t) - T_{\infty,0}}{T_{\infty,\min} - T_{\infty,0}}, \tag{3}$$

$$t^* = \frac{\alpha_w t}{R^2}, \tag{4}$$

$$\alpha_w = \frac{\lambda_w}{\rho_w c_p}. \tag{5}$$

Symbol definitions have been given in Appendix A. The left-hand side of Eq. 1 represents the rate of change of internal energy of the medium per unit volume. From conservation of energy, the left-hand side is equal to the net heat flux into the control volume.

Equation 1 presents a classic boundary value problem depending on the physical boundary conditions and initial time. For this problem these conditions were:

$$\frac{\partial T_w^*(x=0,t^*)}{\partial x} = 0, \tag{6}$$

$$\frac{\partial T_w^*(x=1,t^*)}{\partial x} = -\frac{Rq_w''}{\lambda_w(T_{\infty,\min} - T_{\infty,0})}, \tag{7}$$

where q''_w is the heat flux conducted from the drop to the environment. Eq. 6 is the symmetric boundary condition, which states that initially there is no temperature gradient at the center of a water drop. Equation 7 is the boundary condition for a convective and evaporating surface at r - R. The heat flux conducted out of water drop q''_w, which must be disposed of and carried away into the environment can be written as:

$$q''_w = q''_{conv} + q''_{mt}, \tag{8}$$

where q''_{conv} is the heat flux to be dissipated from the drop to the environment due to heat convection, and q''_{mt} is the dissipated heat flux due to evaporation/condensation. The initial condition for the heat diffusion equation is:

$$T^*_w(x, t^* = 0) = \frac{T_{w,0} - T_{\infty,0}}{T_{\infty,\min} - T_{\infty,0}}, \tag{9}$$

which states that the initial drop temperature is uniform throughout the drop.

2. Convective Cooling

The heat flux q''_{conv} from a water drop to the environment due to convection may be expressed by Newton's law of cooling as:

$$q''_{conv} = h[T_w(r = R, t) - T_{\infty,t}], \tag{10}$$

where h is the average convective heat transfer coefficient for the entire surface, $T_w(r = R,t)$ is the surface temperature of water drop at time t, and $T_{co.t}$ is the environment temperature at time t. Thus, q''_{conv} results from a temperature difference between the drop and the

environment flow field. The average convective heat transfer coefficient can be expressed as:

$$h = \frac{\lambda_m Nu}{2R}, \tag{11}$$

where λ_m is the thermal conductivity of the air-vapor mixture and Nu is the Nussult number.

For a freely falling liquid water drop, the correlation of Ranz and Marshall (1952) has sometimes been used to obtain the Nussult number. However, Beard and Pruppacher (1971) found that Ranz and Marshall's correlation overestimated the Nussult and/or Sherwood numbers, which might be due to the fact that the glass capillary was used to suspend the drops in their experimental setup. Beard and Pruppacher (1971) obtained improved parameterization of Nu from laboratory experiments with freely suspended drops in a wind tunnel. Their experimental results for drop diameters in the range of 40 to 1200 μm showed that:

$$Nu = 2\begin{cases} 1.00 + 0.108(N_{Re}^{1/2} N_{Pr}^{1/3})^2, (N_{Re}^{1/2} N_{Pr}^{1/3}) < 1.4 \\ 0.78 + 0.308(N_{Re}^{1/2} N_{Pr}^{1/3}), (N_{Re}^{1/2} N_{Pr}^{1/3}) \geq 1.4 \end{cases}, \tag{12}$$

where N_{PT} = v / a is the Prandtl number defined as the ratio of the kinematic viscosity v to the thermal diffusivity a of water vapor in air and N_{Re} = 2 Ru_{co} /v is the Reynolds number given as the ratio of the product of drop diameter (2i?) and external flow velocity to the kinematic viscosity. This relationship was found to be in good agreement with the numerical results of Woo and Hamielec (1971). In addition, Pruppacher and Rasmussen (1979) investigated the evaporation rate of large water drops falling at terminal velocity in air. Their results showed that the applicable range of Eq. 12 can be extended to drop diameters up to 5000 μm.

3. Evaporative cooling

a. Mass transfer in a quiescent environment

The assumptions made in calculating the evaporative flux of water vapor from the stationary drop to the surroundings were: 1) one-dimensional quasisteady system; 2) the flux of water from or to the drop does not change the conditions of the environment; and 3) thermodynamic equilibrium is reached at the drop surface. Hence, following the discussion of Kays and Crawford (1980) the water vapor species equation for a two-component mixture of water vapor and air (for R < r < CO) using a one-dimensional spherical coordinate system can be written as:

$$\rho_m u_m \frac{dm_v}{dr} - \frac{1}{r^2}\frac{d}{dr}\left(r^2 \rho_m D \frac{dm_v}{dr}\right) = 0, \tag{13}$$

where m_v is the mass fraction of water vapor, p_m is the density of the mixture, u_m is the bulk velocity of the mixture, and D is the diffusivity of water vapor in air. The boundary conditions for the water vapor species equation were:

$$m_v(r = R) = m_{v,s}, \tag{14}$$

$$m_v(r \to \infty) = m_{v,\infty}, \tag{15}$$

where $m_{v,s}$ is the mass fraction of vapor at the water drop surface, and $m_{v,co}$ is the mass fraction of vapor at the environment. By considering mass conservation at the water drop surface and the solution of the species equation (Eq. 13), the evaporation rate of mass from the water drop surface to the sounding can be written as:

$$\dot{m}_{mt,0} = 4\pi\rho_m DR \ln\left(\frac{1-m_{v,\infty}}{1-m_{v,s}}\right). \qquad (16)$$

Finally, the heat flux from a stationary water drop to the water-air interface that provided the energy required to evaporate the water can be written as:

$$q''_{mt,0} = \dot{m}''_{mt,0}(h_w - h_m), \qquad (17)$$

where h_w is the enthalpy of the liquid water, and h_m is the enthalpy of the vapor-air mixture at the drop surface.

b. Mass transfer in a convective environment

The effect of convection on the mass transfer from a water drop to the surroundings due to the drop's motion was approximated by means of a ventilation coefficient, f_v, defined by:

$$f_v = \frac{m_{mt}}{\dot{m}_{mt,0}}, \qquad (18)$$

where m_{mt} is the evaporation rate of a moving drop, and $m_{mt.0}$ is the evaporation rate of a stationary drop. For water drops evaporating in air during free-fall, the value of f_v has been found experimentally (Beard and Pruppacher 1971; Pruppacher and Rasmussen 1979) to be:

$$f_v = \begin{cases} 1.00 + 0.108(N_{Sc}^{1/3} N_{Re}^{1/2})^2, (N_{Sc}^{1/3} N_{Re}^{1/2}) < 1.4 \\ 0.78 + 0.308(N_{Sc}^{1/3} N_{Re}^{1/2}), (N_{Sc}^{1/3} N_{Re}^{1/2}) \geq 1.4 \end{cases}, \qquad (19)$$

where $N_{Sc} = v/D$ is the Schmidt number given as the ratio of the kinematic viscosity v to the diffusivity D of water vapor in air. With the ventilation factor f_v, the latent heat required to evaporate the liquid water q''_{mt}, was obtained from:

$$q''_{mt} = f_v \dot{m}''_{mt,0}(h_w - h_m) = f_v q''_{mt,0}. \tag{20}$$

4. Simulation of drop freezing

When ice nucleates within a supercooled drop, complete solidification occurs in two major stages (see for example, Pruppacher and Klett, 1980; Dye and Hobbs, 1968). In the first stage, a small fraction of liquid water is frozen and releases latent heat, which almost immediately raises the temperature of the whole drop to near 0°C. In this stage, a thin ice shell forms over the surface of the drop. In the second stage, the drop freezes radially inward at a speed depending on the rate at which latent heat can be disposed of into the environment, a physical effect that becomes increasingly limited as the ice shell thickens.

For this model formulation, it was assumed that a dendrite formed uniformly during the initial freezing stage, and that the initial freezing time was negligible compared with the freezing time for the second stage. The rate of freezing in the second stage was determined by the heat flux transferred away from the ice shell to the environment. Assuming that inward propagation of the ice shell is radially symmetric, then the unsteady heat diffusion equation for the ice shell ($R_i < r < R_0$) may be written as:

$$\frac{\partial T^*_{ice}(x,t^*)}{\partial t^*} = \frac{\partial^2 T^*_{ice}(x,t^*)}{\partial x^2} + \frac{2}{x + \dfrac{R_i}{R_o - R_i}} \frac{\partial T^*_{ice}(x,t^*)}{\partial x}, \tag{21}$$

with the nondimensional parameters defined as:

$$x = \frac{r - R_i}{R_o - R_i}, \tag{22}$$

$$T^*_{ice}(r,t) = \frac{T_{ice}(r,t) - T_{\infty,0}}{T_{\infty,\min} - T_{\infty,0}}, \tag{23}$$

$$t^* = \frac{\alpha_{ice} t}{\left(R_o - R_i\right)^2}, \tag{24}$$

$$\alpha_{ice} = \frac{\lambda_{ice}}{\rho_{ice} c_{p_{ice}}}, \tag{25}$$

where R_i is the inner radius of the ice shell (i.e ice/water interface) and R_0 is the outer radius of the ice shell (i.e. ice/air interface). Symbol definitions have been given in Appendix A. The left-hand side of Eq. 21 represents the rate of change of internal energy of the ice shell per unit volume. From conservation of energy, the left-hand side is equal to the net heat flux into the ice shell.

The boundary conditions for this problem were:

$$T^*_{ice}(x = 0, t^*) = \frac{T_{i/w} - T_{\infty,0}}{T_{\infty,\min} - T_{\infty,0}}, \tag{26}$$

$$\frac{\partial T^*_{ice}(x = 1, t^*)}{\partial x} = -\frac{(R_o - R_i) q''_{ice}}{\lambda_{ice}(T_{\infty,\min} - T_{\infty,0})}, \tag{27}$$

where q''_{ice} is the heat flux conducted through the ice shell to the environment. Eq. 26 is the boundary condition at the ice/water interface, which states that the ice temperature at the inner radius is the ice/water interface temperature. The ice/water interface temperature is chosen to be -0.2 °C according to Dye and Hobbs (1968). Equation 27 is the boundary condition for a convective and sublimating surface at $r = R_0$. The heat flux conducted out of ice shell q''_{ice}, which must be disposed of and carried away into the environment can be written as:

$$q''_{ice} = \dot{m}''_{subl} h_{sg} + h[T_{ice}(R_o, t) - T_\infty(t)], \tag{28}$$

where m''_{subl} is the rate of mass flux of ice due to sublimation, h_{sg} is the latent heat of sublimation, and h is the heat transfer coefficient. After the temperature profile of the ice shell was determined, the inner edge of the ice shell (R_i) was calculated by Eq. 29,

$$\left(1-\frac{c_{p_w}(T_{il w}-T_w)}{h_{sf}}\right)\rho_w h_{sf}\frac{dR_i}{dt}=-\lambda_{ice}\frac{\partial T_{ice}(R_i,t)}{\partial r}, \tag{29}$$

while the outer edge of the ice shell (R_0) was calculated using:

$$\frac{dR_o}{dt}=\frac{1}{4\pi R_o^2\rho_{ice}}\dot{m}_{subl}. \tag{30}$$

5. Finite difference solution of the heat diffusion equation

Because the calculation allowed conditions in the environment air to change at each time step, the unsteady heat diffusion equations (Eqs. 1 and 21) were solved by the finite difference method. The heat diffusion equation was discretized by the first order forward time and second order implicit central space differencing scheme. A set of simultaneous algebraic equations was formed after the discretization. Results from the convective heat and mass transfer analysis provided the boundary conditions for the heat diffusion equations. The resulting system equation for each time step was then solved by the LU decomposition method (Gerald and Wheatley, 1984) to obtain the temperature distribution inside the water drop as a function of time.

Chapter 5. Numerical Simulation of the Cloud Seeding of a Warm Base Illinois Convective Cloud with and without Ice Multiplication Active

Harold D. Orville, Fred J. Kopp, Richard D. Farley
Institute of Atmospheric Sciences
South Dakota School of Mines and Technology
501 E. St. Joseph Street
Rapid City, South Dakota 577001-3995

Summary

Seeding simulations on a moderately vigorous, warm base, convective cloud produced a strong initial signal if ice multiplication was not active; no signal otherwise. Even though a strong effect was produced in the initial graupel field, no effect on the total rainfall was produced. The results lead to speculation about the effects of hygroscopic seeding of continental, cold base clouds. The large drops formed by the seeding could establish an ice multiplication process leading to cloud ice (and the resultant precipitating ice) at temperatures even higher than those due to ice-phase cloud seeding (such as silver iodide).

1. INTRODUCTION

This chapter reports on the results of numerical simulations of cloud seeding effects. This case treats the ice phase seeding of a moderately vigorous warm base convective cloud, similar to those active convective clouds observed on the Precipitation Augmentation for Crops Experiment (PACE) project conducted by the Illinois State Water Survey. Our only other cloud seeding simulation of a warm base convective cloud was reported on in an earlier WMA Journal paper (Orville et al., 1989) and involved clouds from the Cooperative Huntsville Meteorological Experiment (COHMEX). An important difference in this current experiment is the simulations.

2. CLOUD DESCRIPTION

The atmospheric sounding from 23 June 1989 taken at the Willard Airport, Savoy, Illinois, was used as input to the cloud model. This day produced large convective clouds that were well observed by aircraft and radar. Clouds grew to 10 km and more. Cloud base temperatures were + 15°C at a height of about 1.5 to 2.0 km. The sounding is shown in Fig. 1(a) and (b). Light winds were present as indicated in Fig. 1(b). Observations indicated a large number of cloud droplets and a broad droplet distribution. We used a number concentration of 972 droplets per cubic centimeter and a relative dispersion of 0.473 in the cloud model runs based on the observations.

Three experimental units were obtained on this day. Two received treatment with silver iodide and one with sand (a placebo case).

3. BRIEF CLOUD MODEL DESCRIPTION

The model used in this study is a two-dimensional, time-dependent cloud model (Orville and Kopp, 1977; Lin et al., 1983) with bulk water microphysics and 200 m grid intervals over a 20 km by 20 km domain. Cloud seeding simulations employ techniques described in Hsie et al. (1980), Kopp et al. (1983), and Orville et al. (1984). The model is anelastic and uses a vorticity/stream function approach to obtain the velocity field. Chen and Orville (1980) provide additional information on the dynamic framework of the model.

The bulk water microphysical method is based on concepts suggested by Kessler (1969). Our model divides water and ice hydrometeors into five classes: cloud water, cloud ice, rain, snow, and high density precipitating ice (graupel/hail). Rain, snow, and graupel/hail, which are assumed to follow inverse exponential size distributions, possess appreciable terminal fall velocities. Cloud water and cloud ice have zero terminal velocities and thus travel with the air parcels. These five classes of hydrometeors interact with each other and water vapor through a variety of crude parameterizations of the physical processes of condensation/evaporation, collision/coalescence and collision/aggregation, accretion, freezing, melting, and deposition/sublimation. The microphysical processes and parameterizations employed in the bulk water model are discussed in detail by Wisner et al. (1972), Orville and Kopp (1977), and Lin et al. (1983).

The model was run with autoconversion (coalescence) activated and primary ice initiation at -20°C. Freezing of rain drops begins as early as -5°C. Cloud seeding was simulated assuming a drop of silver iodide flares. The silver iodide creates ice crystals starting at -5°C, but is more effective as the temperature lowers. The results from the seeding were compared with a run in which no seeding was simulated. In addition, two other runs were made with ice multiplication simulated, as described in Alexic et al. (1989). One of the runs was seeded, one was unseeded. The important point to realize is that the ice multiplication routine generates cloud ice in the temperature region -3°C to -8°C if graupel is present. The efficiency of the process depends on the amount of cloud liquid in droplets larger than 25 μm in diameter.

4. PRELIMINARY CLOUD MODEL RESULTS

4.1 Normal Cases (No Ice Multiplication)

Figure 2 shows the development of the clouds in the unseeded and the seeded run, without ice multiplication active. A mean convergence value of 5×10^{-5} s^{-1} was superimposed in the lower atmosphere, no convergence in the middle atmosphere, and divergence of equal magnitude to the convergence in the upper atmosphere. This leads to upward vertical motions of a few cm/s in the domain and for a tendency for the thermals in the lower atmosphere to merge. The atmosphere becomes more unstable under convergence conditions in the lower atmosphere. There was ample evidence from the synoptic conditions for this day to use convergence in the model.

The figure and all of its panels cover the period from 57 min to 84 min. The solid line denotes the cloud outline (100% relative humidity); the dashed lines, the streamlines (units of kg m^{-2} s^{-1}); the dots are rain mixing ratios; the S's are snow; and the asterisks are hail mixing ratios. Threshold values are 1.0 kg^{-1} for the rain and hail and 0.5 g kg-1 for the snow. The left column panels are for the unseeded case; the right column ones for the seeded case. The first panel for the seeded case at 57 min shows the initial distribution of the silver iodide, an assumed drop of flares. The quantity of Agl is 100 g/km in the y-direction.

Precipitation in the unseeded case forms primarily and initially from the coalescence of cloud water to rain water. An extensive rain field is obvious at 60 min of simulated real time. A small amount of graupel/hail had formed at 57 min, but the quantity was too small to show up on these graphs. Snow and graupel appear by 63 min as the cloud top passes the -20°C level (7 km, 0°C is at about 4 km and -10°C at 5.6 km). The snow field is above the rain field, but some graupel/hail is falling through the rain. Precipitation reaches the ground at about 69 min, and a substantial microburst is produced thereafter (about 25 m s^{-1} horizontal wind speed difference at the ground). The cell has produced most of its precipitation fallout by 81 min. Nearly 22 mm peak depth of rain is produced. Remnants of the cell persist until 93 min and later.

Ice precipitation in the seeded case begins much differently than in the unseeded case. The panel at 60 min shows the upper part of the cloud almost completely filled with snow and graupel/hail. This has happened because of the interaction of the artificially produced ice crystals with the rain. Small amounts of rain interacting with the ice crystals produce snow in the model; large values of rain content interacting with ice crystals produce graupel/hail in the model cloud. Small areas of rain are present at the melting level on either side of the cloud at about the 4 km level. The precipitation develops rapidly and falls towards the ground, reaching the ground a minute or two before the rain in the unseeded case. At later times, the seeded case produces a very light shower from a small cloud in the center of the domain. As might be expected, the radar reflectivity pattern shows the earlier development of graupel/hail also. A difference of 10 dB exists at the early stages of precipitation development.

The total amount of precipitation accumulated on the ground is nearly identical in the two cases, although the seeded case produced its precipitation slightly sooner (see Figs. 3, 4, and 5). Even though the supercooled rain was transformed to precipitating ice rapidly, no strong dynamic effect of the seeding was detected. One to two g kg^{-1} of rain were rapidly transformed to ice. The extra heating (0.5°C) was evident in the temperature graphs, but was not enough to alter the dynamics of the cloud significantly. That may only have occurred if a mid-level capping inversion had been present.

Figures 3 and 4 show the accumulated rain and graupel/hail on the ground versus time. About 65 K tons/km of precipitation are produced; 98% of it is rain. Figure 5 shows the distribution of the rain on the ground in the unseeded and seeded runs. Slight redistribution of the rain is evident.

Figure 6 indicates some of the main differences in the production of precipitation in the two cases. The unseeded case shows the formation of rain starting at about 57 minutes after model start-up (simulated real time). The ice precipitation begins at 61 minutes, graupel showing up a little before the snow. This is caused by the formation of graupel through the freezing of rain, while the initial formation of snow awaits the initiation of cloud ice.
The picture is different for the seeded case. Rain begins as before via coalescence, but the Agl seeding at 57 minutes produces artificial ice crystals which then interact with the rain to form snow and graupel. The graupel/hail peaks at about 64 minutes, about 2 minutes earlier than in the unseeded case. The graupel/hail falls into the melting layer after 63 minutes forming rain which, after 66 minutes, mimics the production of rain in the unseeded case.

These results indicate that the initial rain formation in the unseeded case is from coalescence of cloud water to rain and then growth of the rain by collection of the cloud. This growth peaks at about 62 minutes and then begins to drop off. The surge in the rain production starting at 66 minutes is due to the fallout and melt of graupel and is common to both unseeded and seeded cases.

4.2 Ice Multiplication Active

Figure 7, provided to us by the ISWS, indicates that the presence of ice in the updrafts of the PACE clouds depends in part on the presence of large drops, drops with diameters greater than 300 μm. Consequently, we rain two cases simulating the physics of the Hallett-Mossop ice process, as parameterized by Alexic et al. (1989). Figure 8 presents the main result. Ice multiplication in the unseeded case masks any effect of cloud seeding in this case. This is due to the presence of large drops (rain) in the updrafts of the cloud, the freezing of some of the rain to produce some graupel, and the interaction of the graupel with the cloud water droplets (numerous and with a broad relative dispersion). This produces cloud ice at a relatively warm temperature (-5°C) and leads to snow and further graupel production. The seeded case has a nearly undetectable effect; one additional snow symbol appears in the cloud in this figure.

Figure 9 shows the formation of cloud ice in (1) the unseeded case - no ice multiplication; (2) the seeded case with ice multiplication; and (3) the unseeded case with ice multiplication active. There is nearly a one kilometer height difference between the cases, and a significant difference in cloud temperature at the height where the initial cloud ice appears. The seeded case with ice multiplication shows up intermediate to the two other cases because of its greater mixing ratio values (nearly three orders of magnitude greater). These results would indicate that no differences would be found in the precipitation production of the seeded and unseeded cases with ice multiplication active, which is indeed what resulted.

5. SUMMARY AND SPECULATION

The numerical simulation of this relatively vigorous convective cloud has resulted in some added insight into the complexities of the seeding process and its effects on clouds — at least numerical clouds. The seeding test on the cloud without an ice multiplication process active led to some

very clear seeding signals near the time of seeding, but not in the final precipitation on the ground. The signals were rapid transformation of the rain to ice precipitation and a rapid increase in the radar reflectivity. Very slight changes in the vertical velocity were evident, and a change in the cloud temperature was positive in the seeded cloud. The results with ice multiplication activated in the model code showed a nearly complete masking of the seeding effect, and no significant differences between the seeded and unseeded cloud at any time.

These results are different from those of Orville et al. (1989) where a very vigorous seeded cloud showed less rain than its unseeded counterpart, while a moderate shower cloud (seeded) showed a positive effect from the seeding. However, no ice multiplication was simulated in the earlier study.

A less vigorous warm base convective cloud may show some effects of ice phase seeding, even with an ice multiplication process active. Further studies are certainly warranted, and another case from the PACE data set is scheduled for study.

These results lead to speculation regarding the hygroscopic seeding of continental type cold base convective clouds. Such seeding may lead to early appearance of ice in the cloud. The results shown above indicate that cloud ice appears lowest in the cloud when ice multiplication is active. The hygroscopic seeding of a continental cold base cloud could lead to the formation of large drops which could then freeze to form graupel. This could activate an ice multiplication process in limited regions of the cloud which would then initiate ice in a relatively warm portion of the cloud. We plan to test this concept on some of the numerical simulations that we have conducted previously.

These results are model dependent and have been obtained on one case from the PACE data set. The bulk water microphysics develop precipitation too soon once a precipitation species is formed. The concepts evolving from these studies should be tested in more detailed microphysical models, whenever possible.

6. REFERENCES

Alexic, N.M., R.D. Farley, and H.D. Orville, 1989: A Numerical Cloud Model Study of the Hallett-Mossop ice Multiplication Process in Strong Convection. Atmos. Res., 23, 1-30.

Chen, C-H., and H.D. Orville, 1980: Effects of Mesoscale Convergence on Cloud Convection. J. Appl. Meteor., 19, 256-274.

Hsie, E-Y., R.D. Farley, and H.D. Orville, 1980: Numerical Simulation of Ice-Phase Convective Cloud Seeding. J. Appl. Meteor., 19, 950-977.

Kessler, E., 1969: On the Distribution and Continuity of Water Substance in Atmospheric Circulations. Meteor. Monogr., 32. 84 pp.

Kopp, FJ., H.D. Orville, R.D. Farley, and J.H. Hirsch, 1983: Numerical Simulation of Dry Ice Seeding Experiments. J. Climate Appl. Meteor., 22, 1542-1556.

Lin, Y-L., R.D. Farley, and H.D. Orville, 1983: Bulk Parameterization of the Snow Field in a Cloud Model. J. Climate Appl. Meteor., 22, 1065-1092.

Orville, H.D., and FJ. Kopp, 1977: Numerical Simulation of the Life History of a Hailstorm. J. Atmos. Sci., 34, 1596-1618. [Reply: J. Atmos. Sci., 35, 1554-1555.]

Orville, H.D., FJ. Kopp, R.D. Farley, and R.B. Hoffman, 1989: The Numerical Modeling of Ice-Phase Cloud Seeding Effects in a Warm-Base Cloud: Preliminary Results. J. Wea. Modif., 21, 4-8.

Orville, H.D., R.D. Farley, and J.H. Hirsch, 1984: Some Surprising Results from Simulated Seeding of Stratiform-Type Clouds. J. Climate Appl. Meteor., 23, 1585-1600.

Wisner, C.E., H.D. Orville, and C.G. Myers, 1972: A Numerical Model of a Hail-Bearing Cloud. J. Atmos. Sci., 29, 1160-1181.

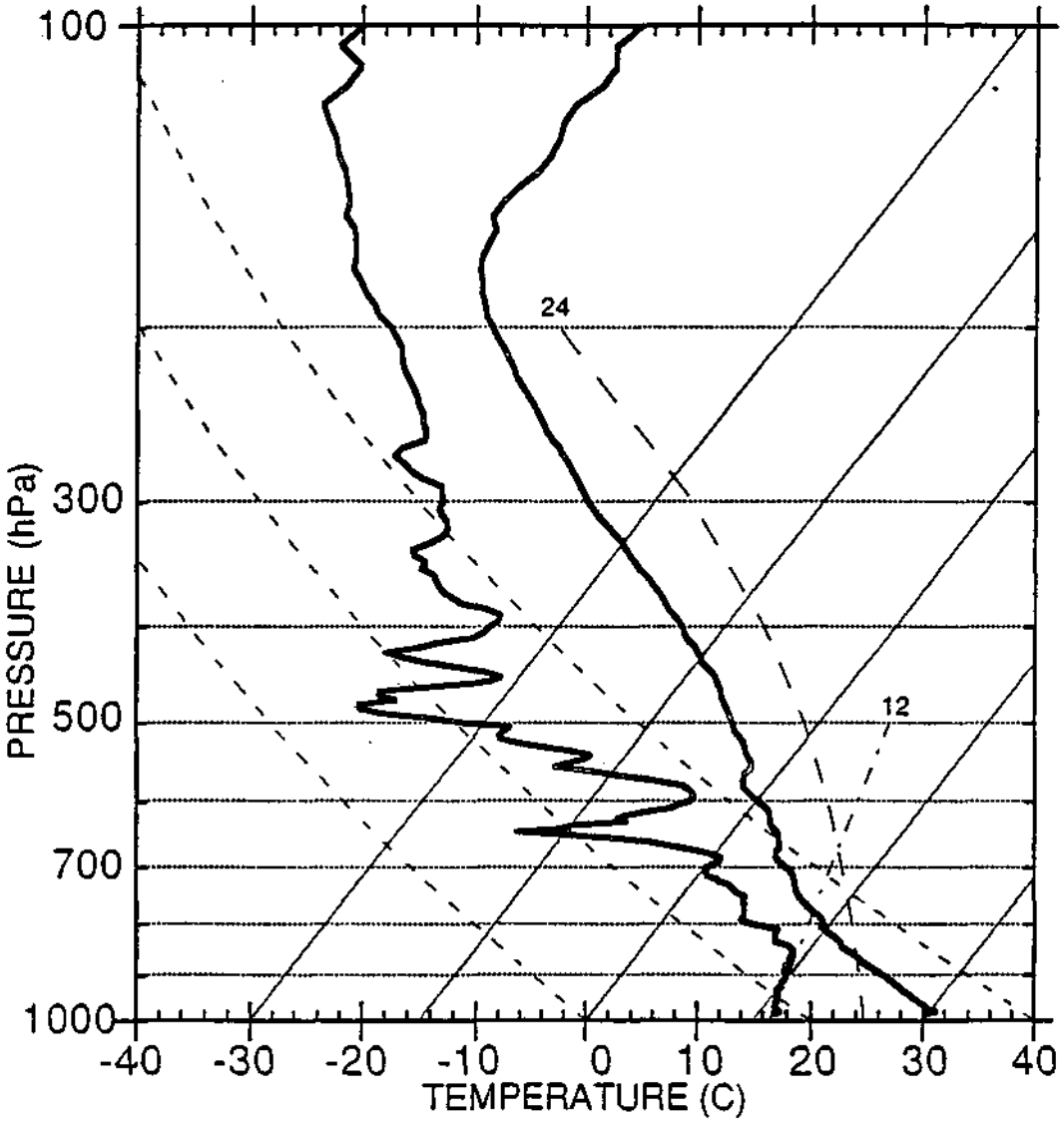

Figure 1a. The atmospheric sounding for 1252 CDT on 23 June 1989, Willard airport. Skew T-log p for temperature and moisture variables.

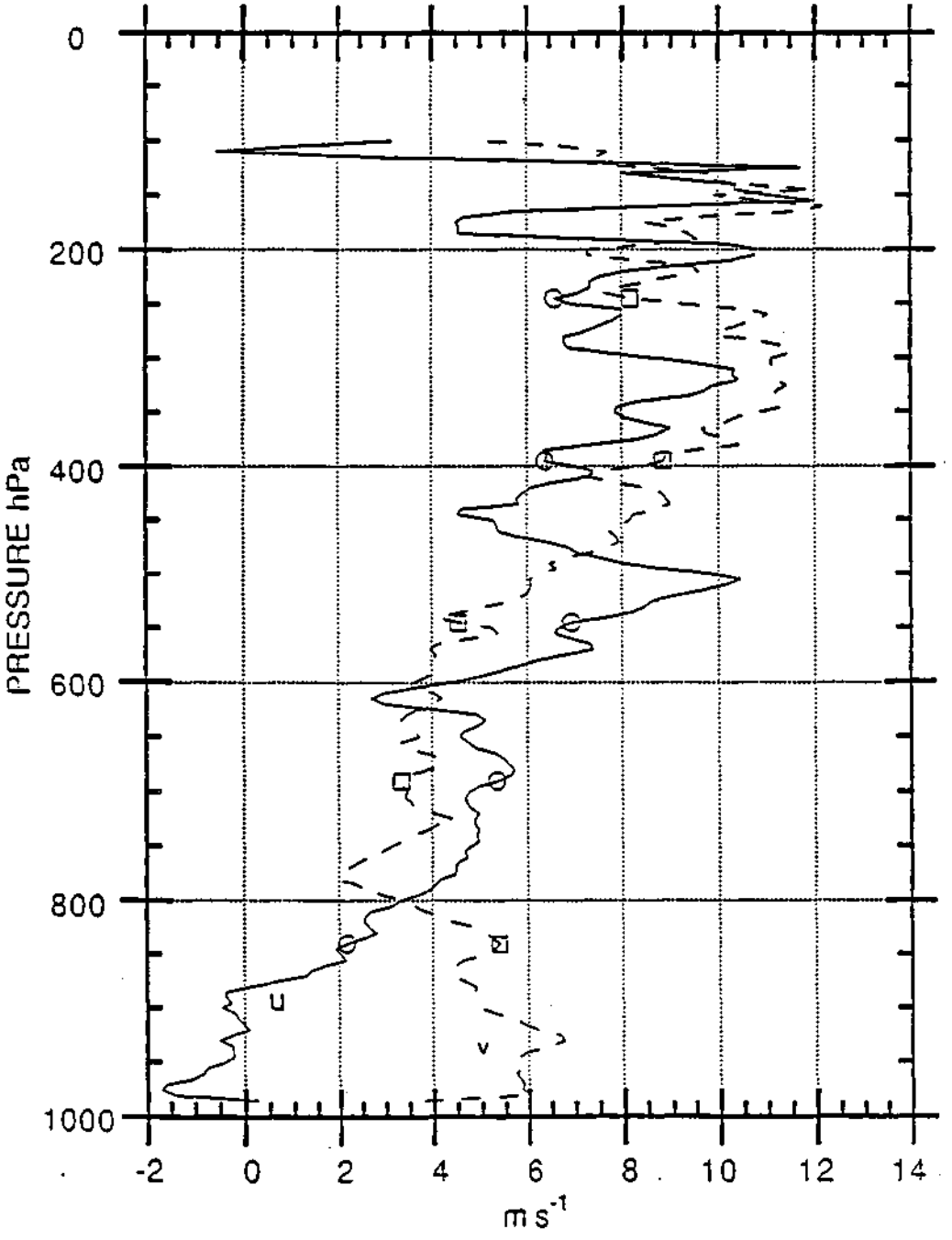

Figure 1b. The atmospheric sounding for 1252 CDT on 23 June 1989, Willard airport. Winds U (west, positive), and V (south, positive).

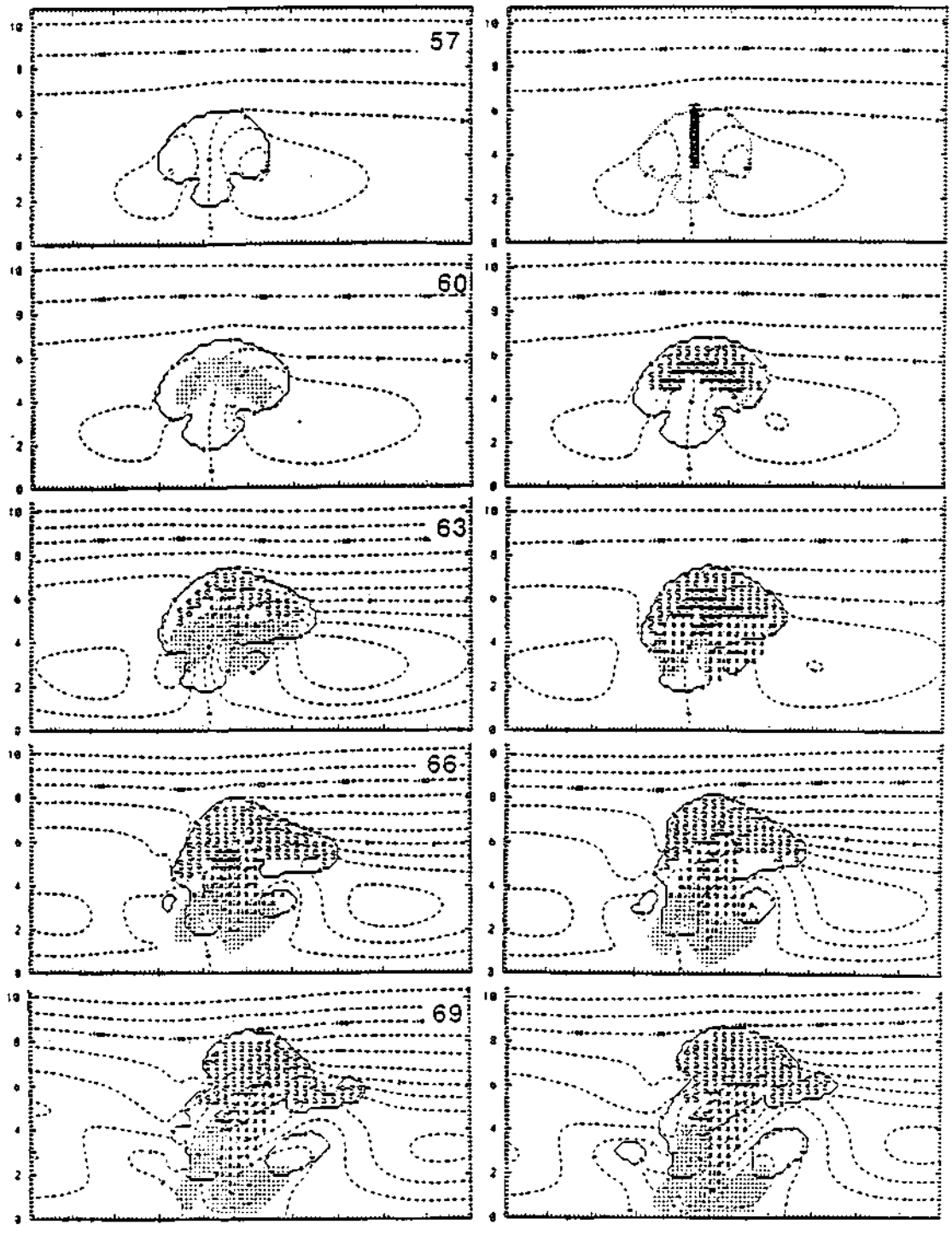

Figure *2.* Cloud history for the unseeded (left column) and seeded (right column) cases. The model domain covers 20 km in the horizontal and 20 km in the vertical, but the top is cut off at 10 km in this depiction. Dashed lines are streamlines; solid lines outline the cloud; dots indicate regions of rain greater than 1 g kg^{-1}; S is snow greater than 0.5 g kg^{-1}; * is hail greater than 1 g kg^{-1}. At 57 min, no precipitation is yet visible in the unseeded case; and in the seeded case, the solid vertical bar outlines the initial pattern of the seeding material that is in the cloud at this time.

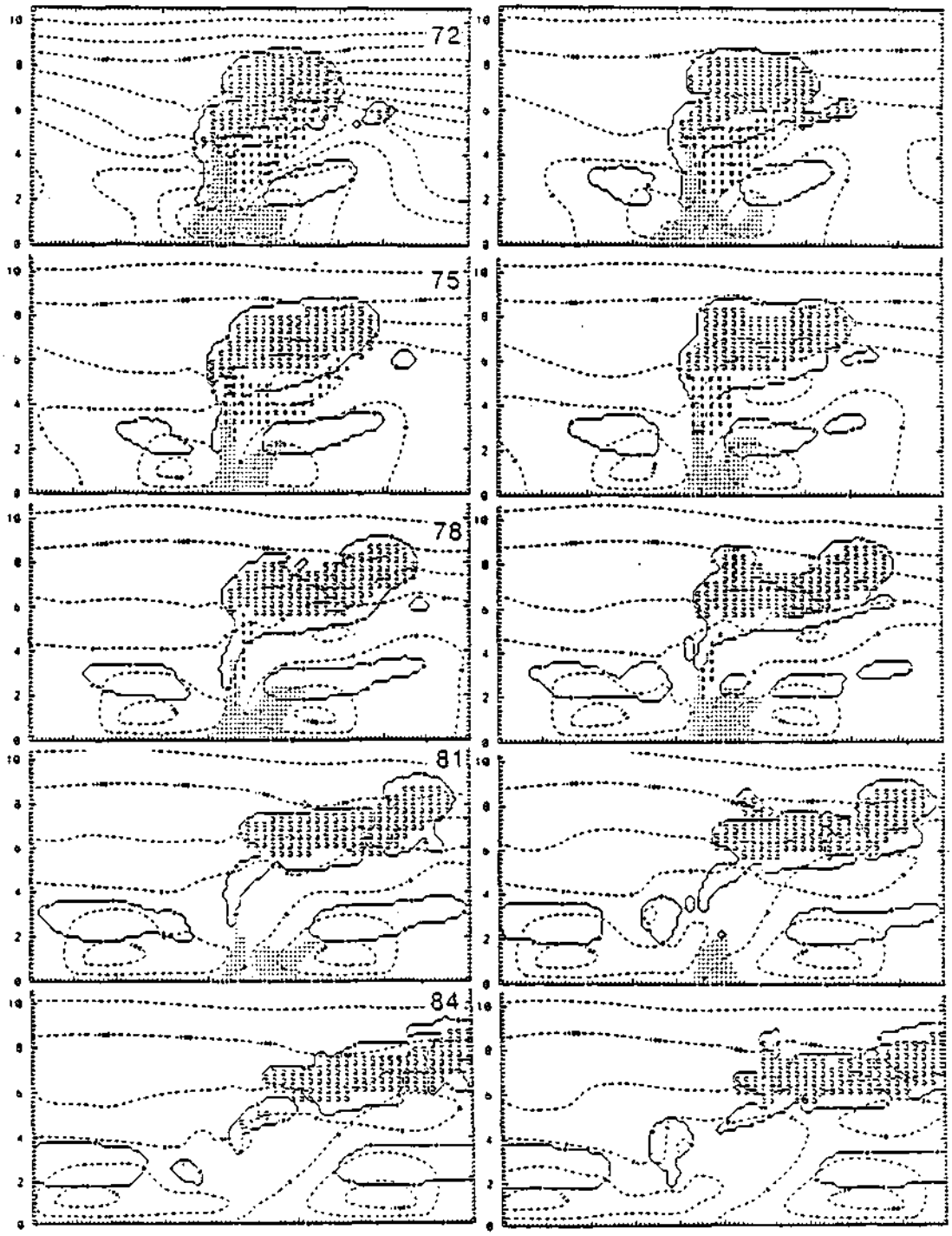

Figure 2. Continued

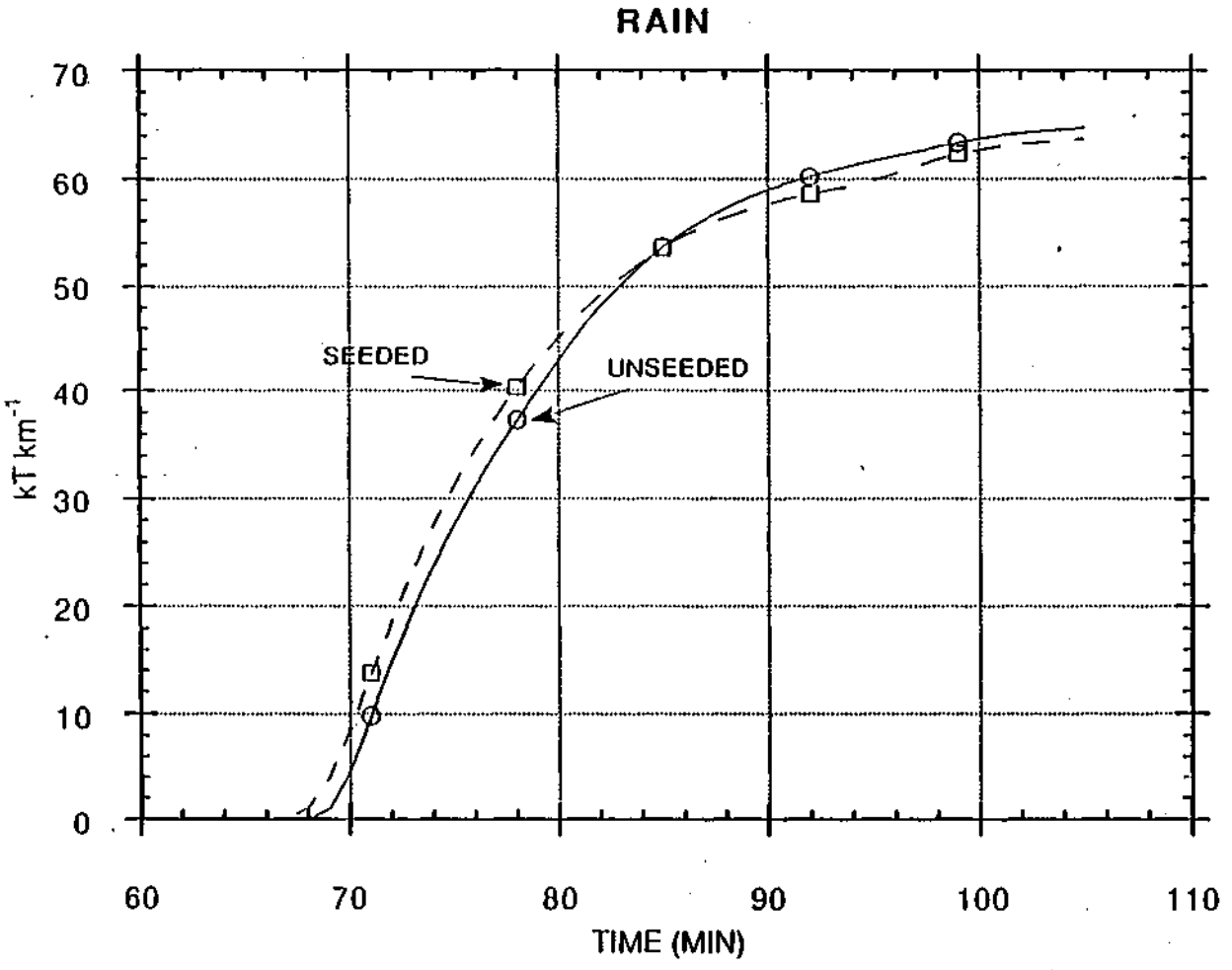

Figure 3. Rain in kilolons per kilometer on the ground simulated in the model. The per kilometer refers to the unresolved third dimension (all dependent variables are assumed constant in the y-direclion).

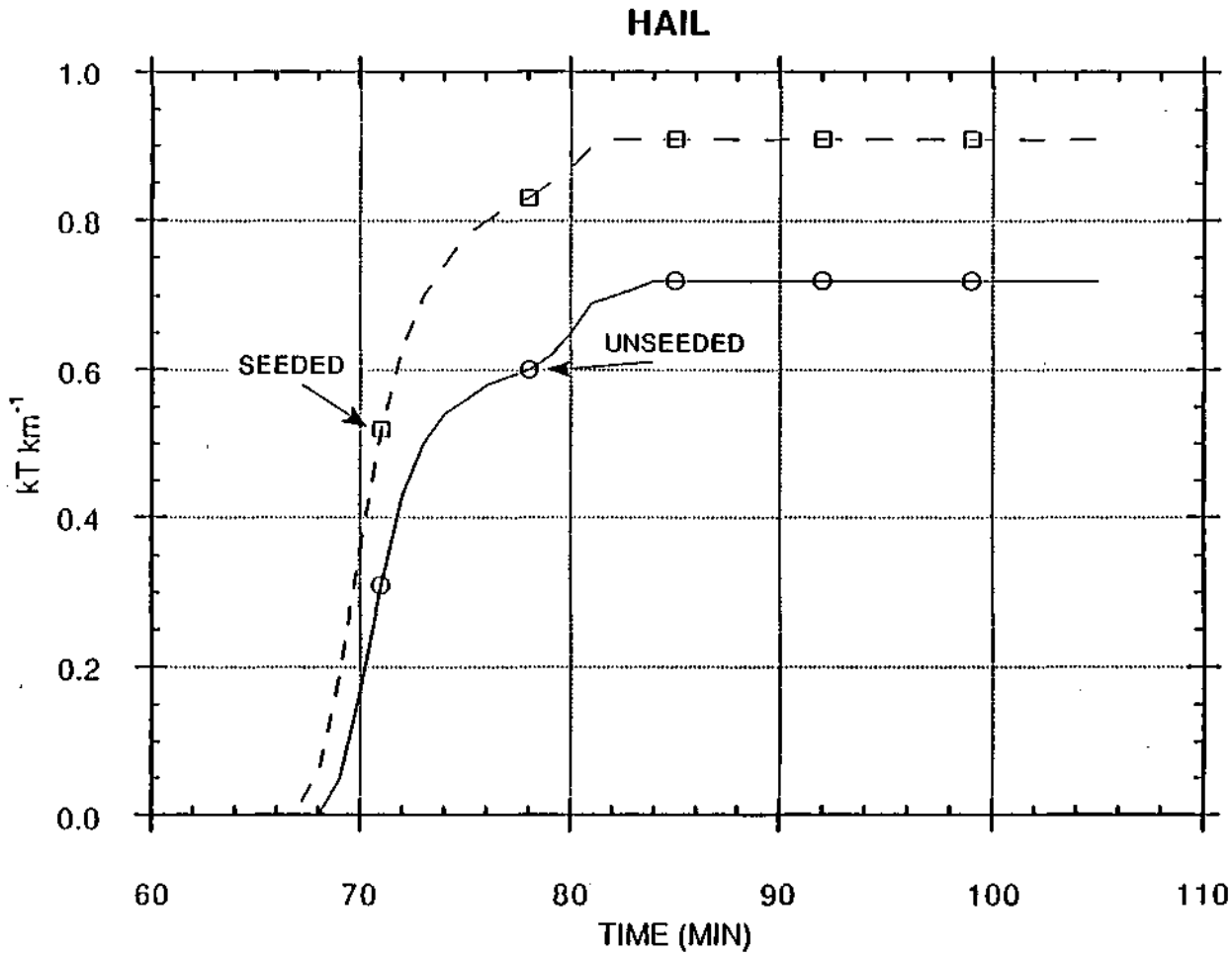

Figure 4. Hail in kilotons per kilometer on the ground (as in Figure 3).

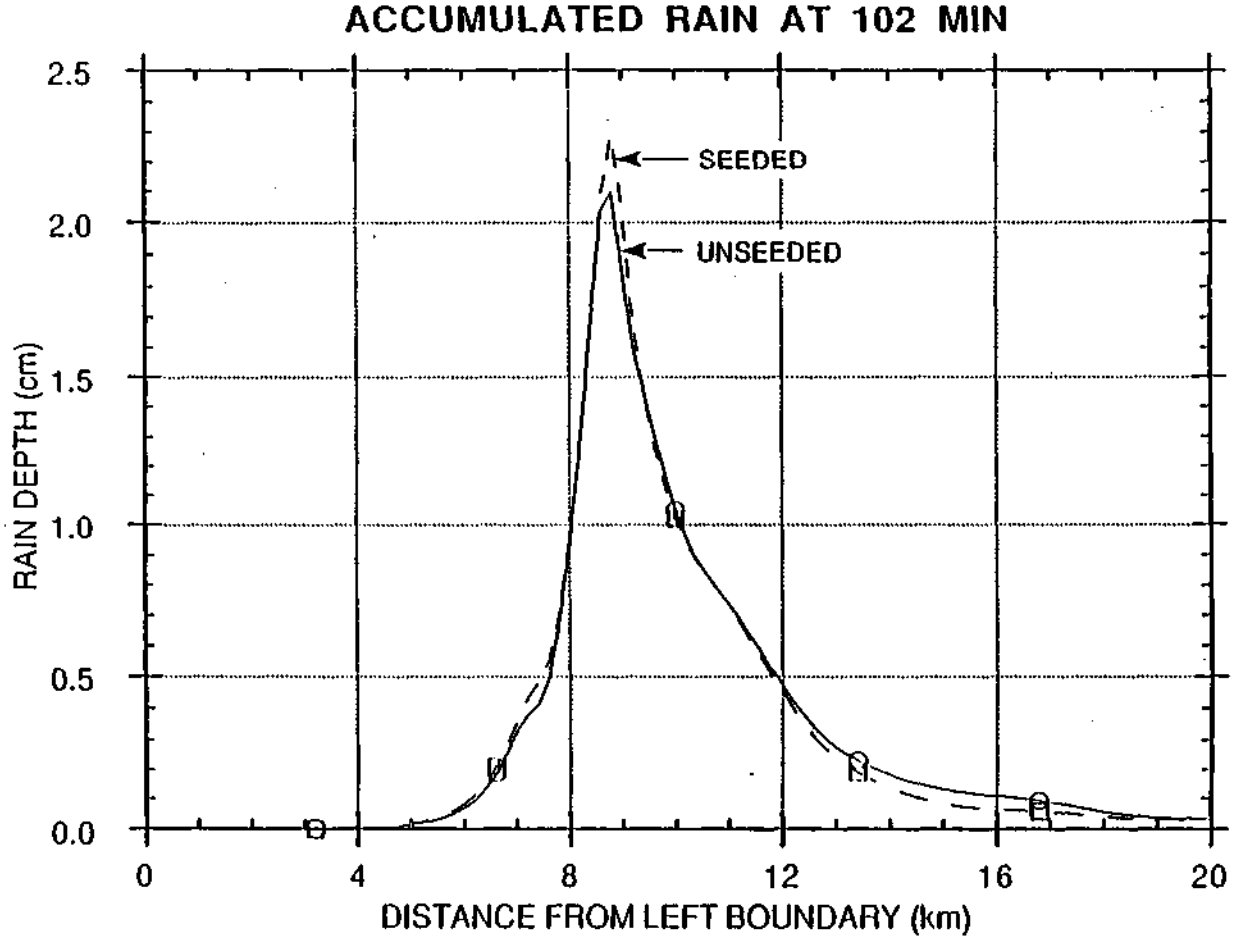

Figure 5. Rainfall on the ground as measured by a rain gage at 102 minutes.

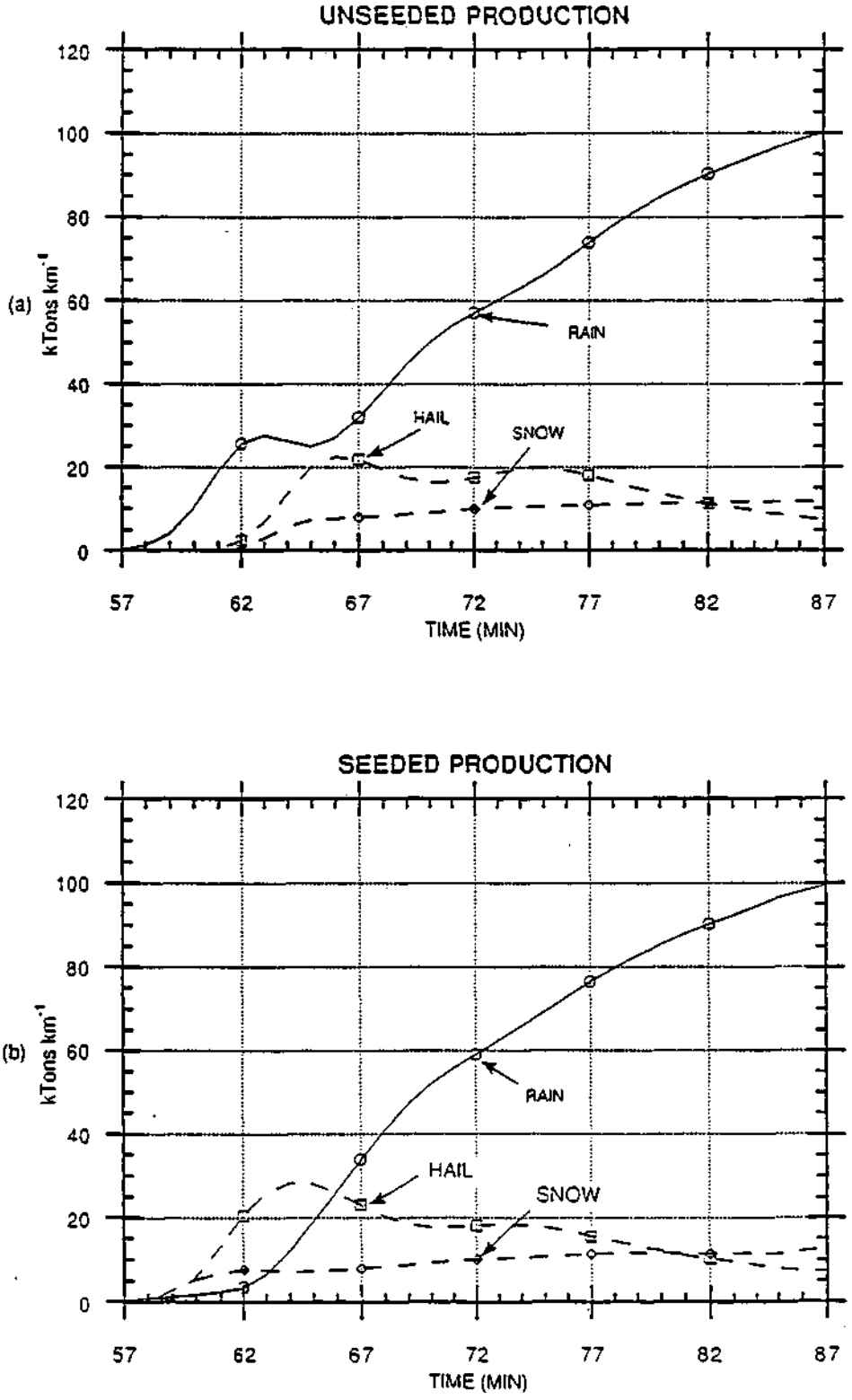

Figure 6. Production of precipitation in kilotons per kilometer (as in Figure 3). The curves for rain, hail, and snow are given vs. time. Note that the rain is converted to hail in the seeded case initially.

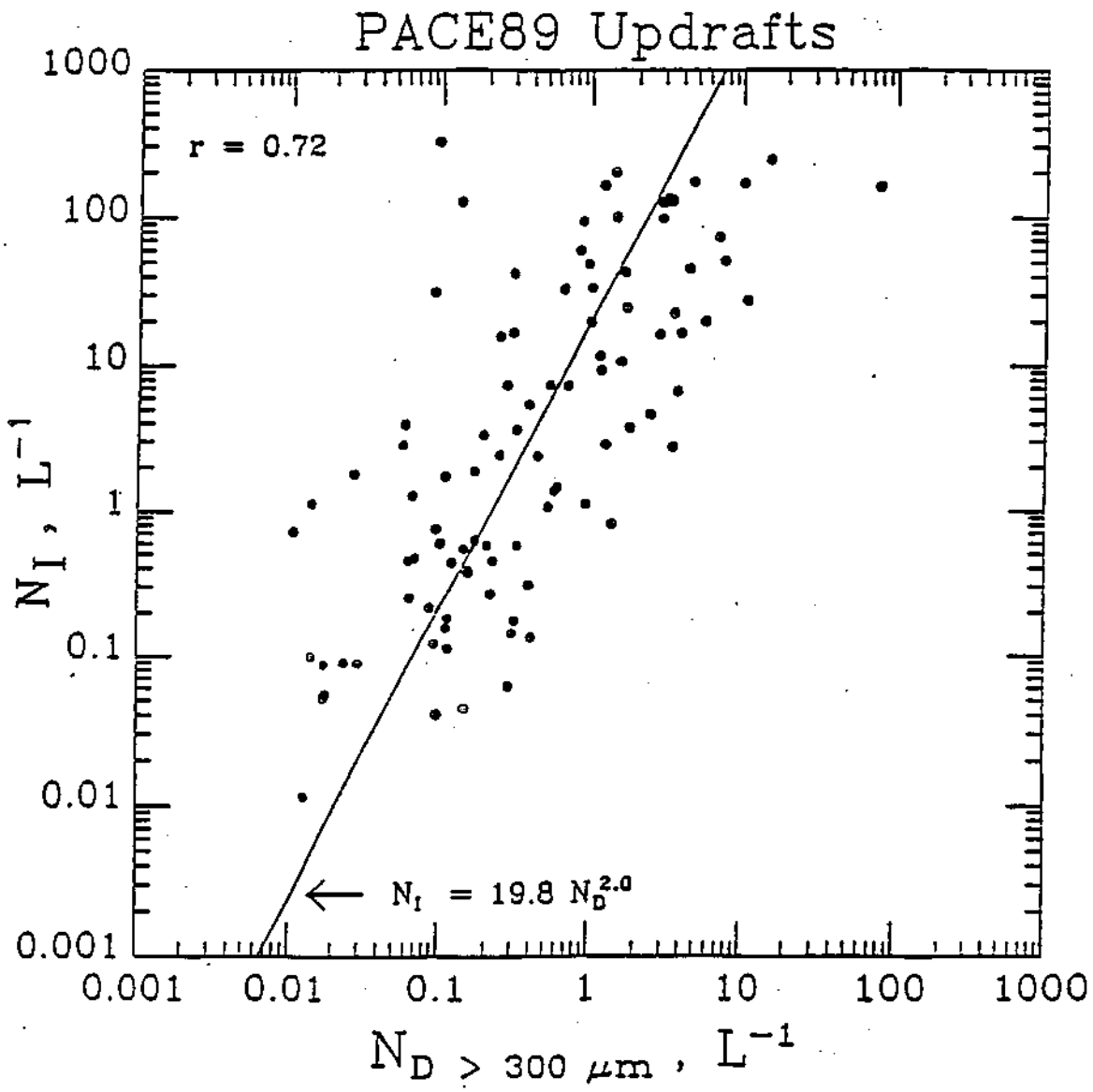

Figure 7. Number of ice particles vs. number of drops >3.00 µm.

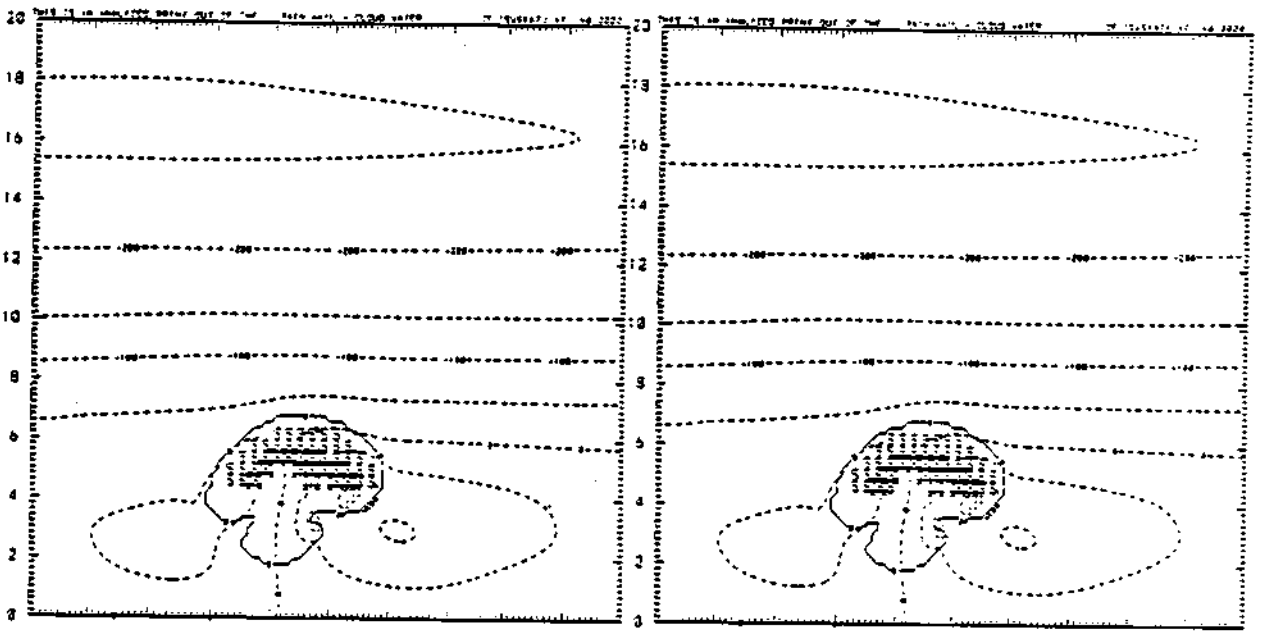

Figure 8. As in Figure 2, except for the ice multiplication case at 60 min. Left panel is for the unseeded case; right is seeded.

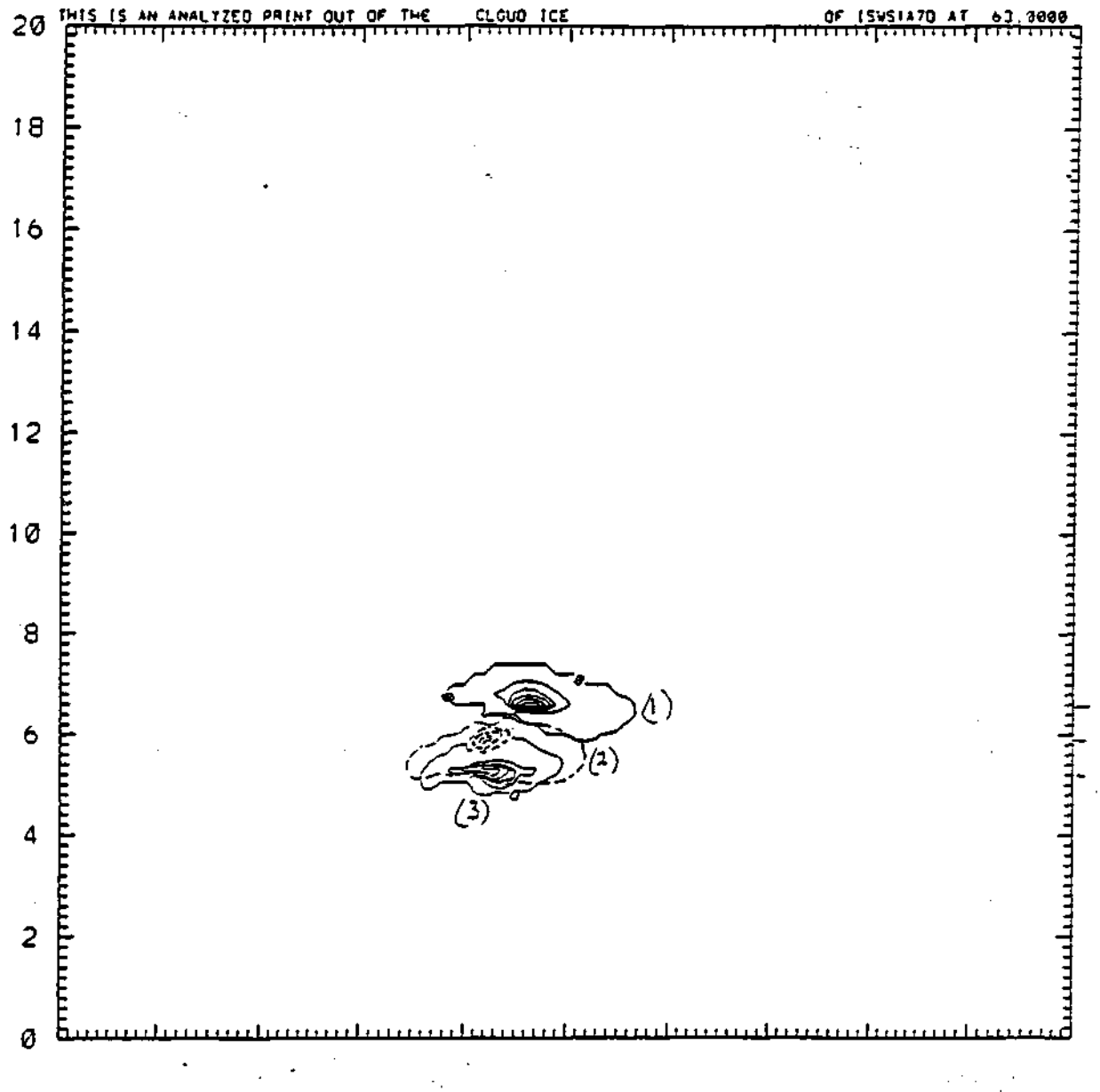

Figure 9. Cloud ice patterns at 57 min showing the initial location of significant amounts of cloud ice in the (1) unseeded/unactivated ice multiplication case; (2) the seeded/activated ice multiplication case (dashed line); and (3) the unseeded/activated ice multiplication case. Note that only the lower left portion of the grid is shown in this figure.

INADVERTENT MODIFICATION OF THE ATMOSPHERE

Chapter 6. The Climatic Impacts of Contrails

David J. Travis and Andrew M. Carleton
Climate and Meteorology Program
Department of Geography
Indiana University

1. BACKGROUND

Proper identification of the abundance and areal coverage of jet condensation trails (contrails) is critical towards gaining an understanding of their association with climate and influence on radiation transfer. This research was one of the 13 tasks (#8) proposed for this 2-year period. Previous research, of both an empirical (e.g. Carleton and Lamb, 1986; DeGrand, 1991) and theoretical (e.g. Appleman, 1953; Scorer, 1978) nature, indicates that contrails often form within or near natural cirrus environments. For this reason, they are often obscured from below and can be "hidden" within from satellite identification above. Even during clear sky conditions, surface contamination can limit the satellite detection of all but the brightest and most linear contrails. It has become necessary, therefore, to develop methods which can enhance the satellite contrail signal.

Lee (1989) demonstrates a method that enhances the contrail signal by utilizing the "split-window" of the Advanced Very High Resolution Radiometer (AVHRR) on board the NOAA Polar Orbiters. The calibrated radiance values from infrared (IR) channel 4 (11 μm) can be subtracted from those of channel 5 (12 μm) to produce images that reveal contrails more distinctly than from either channel separately. Lee (1989) demonstrates this method by successfully applying it to three sample scenes. It has not yet, however, been tested on a large number of scenes having a wide variety of surface and cloud conditions.

An additional consideration for those using satellite data to study contrails is that the analyst is often required to make subjective decisions. This poses a potential problem, owing to the wide variety of contrail morphological characteristics, to the consistency of their identification especially when cloud and surface contamination exists. In addition, previous techniques have proven to be laborious and limitations must, therefore, be placed on the amount of data processed. More recently, however, the increased availability of digital satellite data has provided the opportunity to develop computer-based "objective" methods which can analyze large data sets in a relatively short amount of time.

A method developed by Englestaad et al (1992) utilizes the Lee (1989) contrail-enhanced "differenced" images to objectively identify contrails exclusively using computer techniques. A three-stage algorithm, utilizing user-prescribed parameters, searches for the bright, nearly-straight

line segments which characterize contrails. Though Englestaad et al (1992) successfully applied the procedure to several test scenes, it also has not been tested on a large number of scenes having a wide range of conditions. Both the Lee (1989) and Englestaad et al (1992) methods will be tested here.

2. OBJECTIVES

The primary purpose for this study is to identify the utility of the Lee (1989) and Englestaad et al (1992) methods for use in a large-sample study of AVHRR digital data scenes of contrails. The utility will be assessed by weighing the amount of time required to complete the procedures against their benefits. The specific objectives are as follows:

1. Determine the magnitude of contrail enhancement (Lee 1989) and its variation over a wide range of conditions.

2. Determine the accuracy of the contrail identification method (Englestaad et al, 1992) and the sensitivity to changes in the user-selected input parameters which defines a contrail.

Besides for completing our database and updating additional computer hardware and software requirements, we have focused in this, our second of this three-year study, on developing a proper methodology which can objectively identify contrails using a large sample of digital AVHRR data. The results here are critical towards obtaining a set of reliable and comprehensive conclusions concerning the climatic impacts of contrails. The final phase, utilizing this methodology, will be completed in the upcoming year (August 1993-July 1994)

3. SELECTION OF AVHRR SCENES

A total of ten scenes, covering most of the U.S. and adjacent coastal waters, east or west of the Mississippi River, were selected from the available database, all from the NOAA-9 satellite, and then subdivided into a total of 16 scenes (Table 1). Each scene was prescreened to ensure that contrails were evident within. In addition, each was classified by surface type (e.g. land, water) and by cloud amount. Cloud coverage was divided into three categories:

1. Mostly clear (less than 1/4),

2. Partly cloudy (1/4-3/4), and

3. Mostly cloudy (greater than 3/4).

Each scene was no larger than 512 x 512 pixels (1.1 km) in size since this is the maximum that can be processed using the Englestaad (1992) method.

Table 1

Day	*Time*	*Latitude/Longitude*	*Sky*	*SFC*
04	2024	36N 81W	1	*L*
04	0900	36N 81W	1	L
07	1953	37N 80W	3	L
07	1953	37N 80W	2	L
15	2008	38N 80W	2	L
15	2008	38N 80W	1	L
15	2008	38N 80W	2	L
16	1957	38N 80W	1	L
96	2041	40N 85W	1	L
97	2216	37N 105W	1	W
97	2216	37N 105W	3	L
97	2216	37N 95W	3	L
102	2309	45N 120W	3	W
102	2309	45N 120W	3	W
103	2258	45N 120W	2	W
112	1929	36N 81W	3	L

4. OBJECTIVE 31 - TEST OF THE LEE (1989) METHOD

To test the Lee (1989) method, each scene was first inspected visually to identify the number of contrails evident. Visual analysis was completed four times separately for each scene, once in each vertical and horizontal direction across the screen, and then the average number was calculated and recorded. Contrails were identified as bright, linear features not oriented consistently with the prevailing "natural" cloud flow. This method is detailed in carleton and Lamb (1986) and has been successfully utilized in a number of "hard copy" imagery studies (e.g. Detwiler, 1983; DeGrand, 1991).

Following the visual analysis, each scene was processed using the Lee (1989) contrail-enhancement procedure. Following this procedure, all scenes were again visually inspected to identify the number of contrails present. Each was inspected four times in a similar fashion to that prior to enhancement and then the average value calculated. The number of identified contrails was then compared to the number seen prior to enhancement. Finally, a Student's t-test was completed to determine whether any change in the number of identified contrails was significant.

5. OBJECTIVE #2 - ENGLESTAAD (2992) METHOD

To determine the utility of the Engelstaad et al (1992) method it was concluded, a priori, that the most critical aspect of this procedure is the consistency of the user prescribed input parameter settings for contrail definition. In order for a procedure such as this to be a useful tool for analyzing a large number of AVHRR scenes, a relatively consistent set of parameters must be available to accomplish the task in all or most situations. Otherwise, the analyst must determine the appropriate parameter settings for each scene which can require an inordinate amount of time. In addition, subjective decisions may be required to determine the "best" parameter settings which offsets the "objectivity" of the computer analysis. The goal here then is to determine the "best" group of parameter settings, by comparing the number of computer identified contrails to those seen visually, for the range of the 16 scenes. This method was originally developed by Englestaad et al (1992) specifically for the purpose of inspecting those scenes which had been pre-processed with the Lee (1989) "enhancement" procedure. For this reason, our test scenes were processed similarly here as well.

a. Parameter Settings

The parameter settings that are utilized in the Englestaad et al (1992) algorithm pre-specify the definition of each of the following:

a. Minimum Temperature - Controls the threshold of minimum temperature difference between a group of pixels for "ridge" identification.

b. Local Ridge - Controls the threshold of orientation difference between all ridges (on the entire screen) and each individual ridge.

c. Global Ridge - Controls the threshold of orientation difference between all "local" (128 x 128 pixel) ridges and each individual.

d. Minimum Brightness - Controls the threshold of brightness difference between all ridges and each individual ridge.

Through trial and error, it was concluded that the most efficient method of determining the "best" parameter settings was to adjust parameters a, b, and c by increments of ten and parameter d by increments of one. All parameter settings were started from a value zero and each adjustment was done while holding the others constant. Adjustments were completed until the proper parameter settings were obtained where the computer identified the exact (or nearly exact) same contrails that were evident by visual inspection.

It was anticipated that more than one group of "best" parameter settings would become evident due to the wide range of cloud, surface, and contrail characteristics associated with each scene. The analysis was completed, therefore, with the hope that specific groups of parameter settings

could be identified for specific scene situations and then applied to similar scenes with confidence.

6 RESULTS: LEE (1989) METHOD

Tests of the level of contrail enhancement using the Lee (1989) method yields impressive results (Table 2). In nearly all scenes the number of contrails identified after the enhancement (Band 4-5) was greater than the number prior (Brand 4). The only exceptions to this are those occurring during clear (or nearly clear) sky conditions and those located over water where none or only small amounts of contrail enhancement are noted. The procedure is most efficient at enhancing contrails located over land especially when hidden within "natural" clouds.

Table 2

Day	*Tune*	*Band 4*	*Band 4-5*	*%Inc*	*Sky*	*SFC*
04	2024	39	47	21	1	L
04	0900	4	7	75	1	L
07	1953	12	25	108	3	L
07	1953	11	18	64	2	L
15	2008	38	43	13	2	L
15	2008	35	35	0	1	L
15	2008	29	29	0	2	L
16	1957	9	12	33	1	L
96	2041	13	20	54	1	L
97	2216	7	9	29	1	W
97	2216	9	27	200	3	L
97	2216	10	24	140	3	L
102	2309	7	9	29	3	W
102	2309	7	7	0	3	W
103	2258	2	2	0	2	W
112	1929	10	18	80	3	L

A Student's t-test indicated that when considering all 16 scenes the level of enhancement is significant at the 0.01 level. This demonstrates that the Lee (1989) method does provide a significant enhancement of the contrail signal and suggests that they may be much more abundant than we have previously been aware, especially within clouds. It is important to note that even where enhancement is not significant there is no decrease of the number of contrails identified. This points out that the method does not inhibit the signal in any fashion but only enhances it. The authors also note that during the analysis the method appeared to enhance the total length

and width of those contrails evident prior to enhancement. This suggests that the method does not only enable more contrails to be identified but also better reveals those already seen. For these reasons, it is concluded that this method should indeed be applied to all AVHRR data sets when attempting to identify and analyze contrails.

7. RESULTS: ENGLESTAAD ET AL (1992) METHOD

A total of approximately 150 runs of the Englestaad et al (1992) algorithm were required to identify the "best" parameter settings (Table 3) for the 16 AVHRR scenes (about ten per scene).

Table 3

Day	*Tune*	*Parameter Settings*	*Sky*	*SFC*
04	**2024**	**20, 80, 80, 5**	**1**	**L**
04	**0900**	**120, 80, 80, 3***	**1**	**L**
07	**1953**	**130, 80, 80, 3**	**3**	**L**
07	**1953**	**100, 60, 80, 3**	**2**	**L**
15	**2008**	**120, 60, 60, 3**	**2**	**L**
15	**2008**	**130, 60, 80, 3**	**1**	**L**
15	**2008**	**120, 80, 60, 5**	**2**	**L**
16	**1957**	**100, 40, 60, 3**	**1**	**L**
96	**2041**	**40, 80, 80, 3**	**1**	**L**
97	**2216**	**60, 60, 80, 5**	**1**	**W**
97	**2216**	**100, 80, 80, 3**	**3**	**L**
97	**2216**	**80, 80, 80, 3**	**3**	**L**
102	**2309**	**120, 80, 80, 3***	**3**	**W**
102	**2309**	**100, 80, 80, 5**	**3**	**W**
103	**2258**	**80, 60, 60, 3**	**2**	**W**
112	**1929**	**120, 80, 80, 3***	**3**	**L**

During the analysis it quickly became evident that the algorithm is extremely sensitive to the parameter input values. In some scenes, especially those containing many contrails (>10), only a small change in one parameter setting yielded a change in the number of identified contrails from 0 to as many as 30. Only three of the 16 scenes had the same "best" input parameter settings (highlighted with an asterisk) and those had no specific temporal (i.e. time of day or year), cloud, or surface similarities.

Of the four parameter settings, the most sensitive appears to be the "minimum temperature"

variable. This is not surprising since it provides the threshold for initial ridge detection which is extremely dependent on the heterogeneity of the clouds and surface within. A flat surface (e.g. ocean) having little cloud will require a much lower threshold for ridge detection then one over land having clouds. The remaining parameters are primarily used to dictate how the ridges, once specified, are characterized. Though these aren't as sensitive to variations, they still did not demonstrate any consistency between scenes.

One must, therefore, question the reliability of this method for identification of contrails across a wide range of scenes. It appears the only means for reliable contrail identification is to treat each scene separately and determine the best parameter settings. The amount of time required and the fact that these decisions would be based ultimately on the visual inspection of the screen suggests that this is not a beneficial task. As a result, we have concluded that this method will not be utilized during the final year of this project.

8 CONCLUSIONS

The results from this study have demonstrated the utility of the Lee's (1989) "contrail enhancement" method for use in a large-scale jet contrail study. The procedure enhances contrails in nearly all situations especially when over land and within cloud. In addition, other morphological characteristics such as contrail length and width appear to be better defined after enhancement. The results also suggest that contrails may be more abundant than originally known, especially within clouds. The enhancement procedure provides one of the few methods to confirm or reject this hypothesis.

The Englestaad et al (1992) method is very sensitive to the user-specified "contrail definition" parameter settings. The greatest sensitivity appears to be associated with the "minimum temperature" threshold which responds greatly to variations in surface and cloud heterogeneity. In our opinion, this method is not suitable for a large-scale study of jet contrails.

9. ACKNOWLEDGMENTS

The authors would like to thank both Tom Lee and Mark Engelstaad for providing the necessary algorithms for each method and offering valuable comments.

10 REFERENCES

Appleman, H.. 1953. The Formation of Exhaust Condensation trails by Jet Aircraft. Bull. Am. Met. Soc, 72, 752-761.

Carleton, A.M.. and P.J. Lamb, 1986. Jet Contrails and Cirrus Cloud: A Feasibility Study Employing High Resolution Satellite Imagery. Bull. Am. Met. Soc, 67, 301-309.

DeGrand, J.Q., 1991. A Satellite-Derived Mid-Season Climatology of Jet Condensation trails: April 1977-October 1979. M.A. Thesis, Indiana University.

Detwiler, A., 1983. Effects of Artificial and Natural Cirrus. Clouds on Temperatures Near the Ground. J. Wea. Mod., 15, 45-55.

Englestaad, M., Sengupta, S.K., Lee, T., and Welch, R.M., 1992. Automated Detection of Jet Contrails Using the AVHRR Split Window. Int. J. Remote Sensing, Vol. 13, No. 8, 1391-1412.

ERDAS, Inc., 1991. Erdas Field Guide, ERDAS Inc., Atlanta, GA, 394 pp.

Lee, T., 1992. Jet Contrail Identification Using the AVHR Infrared Split Window. Jour. App. Met., Vol. 28, 993-995.

Scorer, R.S., 1978. Environmental Aerodynamics. Ellis Horwood Limited Pub., 488 pp.

U.S. Department of Commerce, 1991. NOAA Polar Orbiter Data. NOAA-NESDIS-NCDC-SDSD, 200 pp.

Chapter 7. Satellite-Estimated Summer Rainfall for Lakes Michigan, Superior and Huron for 1988, 1989 and 1990: The Accuracy of the Rainfall Estimates

William L. Woodley
Woodley Weather consultants
Littleton, Colorado 80127

and

John Augustine
National Severe Storms Laboratory
Boulder, Colorado 80303

Summary

The Griffith/Woodley satellite rain estimation technique was used to estimate convective rainfall over Lakes Michigan, Superior, and Huron and surrounding land areas for June, July, and August in 1988, 1989, and 1990. This is a new approach for the estimation of rainfall over this region. Previous methods have included:

1. use of raingages along or just inland from the shore,

2. use of limited island gage data and comparisons with shoreline gages to develop ratios that are applied elsewhere, and

3. radar techniques.

Most past approaches agree that, on the average, decreases in precipitation occur over the Great Lakes during the warm season and increases occur in the cold season. However, the differences between the estimates from the methods is significant, particularly from hydrologic considerations.

This study resolved the summertime uncertainties. The full report (available if desired) is the second and last report of the series dealing with Great Lakes rainfall. This task was task #9 in our plan of research. The first report addressed the rationale for the study, the methodology and the initial results. This second report updated the results of the first report, presented additional analyses and focused on their accuracy by comparing them to raingage measurements around the lakes.

As discussed in the first report, the rain estimates for the nine months of study were made using hourly, full-resolution, geosynchronous, infrared satellite imagery, which was available in digital form. It was then navigated to an earth-located coordinate system at full spatial resolution of nominally 8 km at the satellite subpoint. The navigation was performed on the visible data and is accurate to one visible pixel (1 km). The rain estimates were then made according to the

procedures that have been described previously. A perspective correction was applied to the hourly rain estimates to account for the large viewing angle at high latitudes before the rainfall was apportioned on the earth's surface. Two apportionment schemes were tested with the coldest 10 percent of the cloud, defined by the -20° C isotherm, receiving between 30 and 50 percent of the total estimated rainfall.

All satellite rain estimates were compared on an hourly, daily, and monthly basis to measured rainfall in a 10,300 km^2 recording raingage network near Detroit, Michigan. This was done to determine the accuracy of the rain estimates and to derive an adjustment for the satellite rain estimates for areas elsewhere. The satellite rain estimates were typically about a factor of two greater than the corresponding gage measurements for monthly and for whole summer measurements. This result was expected because constants derived in Florida were applied to Midwestern convective systems. These satellite versus gage comparisons for the Detroit network were then used to adjust the satellite estimates of rainfall over the Great Lakes and surrounding land areas. This adjustment greatly improved the accuracy of the satellite rainfall estimates over regions away from the calibration raingage network.

The study verifies that the rainfall amounts over Lake Michigan and Lake Superior are less than upwind over land values, regardless of the stratification. The mean summer land versus water percentage rainfall differences are -15 and -23 percent for Lake Michigan and Lake Superior, respectively, before partitioning further by day and by night The day (0600 to 1800 CST) versus night (1800 to 0600 CST) partition within the overall summer indicates rather small variability for Lake Michigan (-17 percent during the day and -13 percent at night). The situation is reversed, however, for Lake Superior with an apparent greater deficit of rainfall over the lake at night (-33 percent) than during the day (-11 percent).

The monthly percentage differences are quite uniform month-to-month for Lake Michigan, ranging from -14 to -16 percent, but larger and highly variable for Lake Superior. The mean percentage difference for Lake Superior is as large as -38 percent for July and as small as -5 percent for August. The differences by year are also more variable for Lake Superior, ranging between -10 percent and -36 percent, than for Lake Michigan, which had values ranging between -10 and -17 percent.

Only limited comparisons between the satellite rain estimates and raingage ground truth were made in the first report, implying that, while one might have confidence in the relative land versus water rainfall differences, confidence in the absolute values of the rainfall estimates might not be warranted. This notion is largely dispelled in the second report.

To assess the accuracy of the summer-season satellite rainfall estimates, they were compared systematically to gage-measured rainfall over nine Midwestern states after first being adjusted by the Detroit raingage network. It was noted subsequently that the seasonal satellite-derived values agree best with the corresponding gage values for states close to the adjusting Detroit raingage network, especially for Michigan, Wisconsin, and Illinois, where the ratios of satellite to gage rainfalls are near unity (i.e. 1.00). The seasonal agreement in Iowa and Minnesota is

fairly good as well (i.e. within 6 percent). The method underestimated the summer rainfall in Missouri, Indiana, Ohio, and Kentucky by 15 to 20 percent.

This excellent agreement between gage and satellite mean summer rain values for both Michigan and Wisconsin suggests that, due to their close proximity to the lakes, the mean summer satellite-derived rainfalls for Lakes Michigan, Superior, and Huron are potentially accurate to within 5 percent. The analyses indicate, however, that the individual monthly satellite-derived lake values are less accurate relative to the gages. This suggests that some further gage adjustment would be necessary to improve the accuracy of the monthly lake values.

The best method of increasing the accuracy of the monthly satellite lake rainfall estimates was the use of statewide comparisons between satellite and raingages to adjust the satellite estimates of lake rainfall. In essence, therefore, the states served as proxies for the Detroit network. This scheme was tested by using the state adjustments to adjust the satellite-estimated rainfall in nearby states, which served as surrogate lakes. The satellite rainfalls in these surrogate lakes were then compared to their gage-measured rainfall before and after the adjustment. This process produced good satellite and gage agreement in most instances. As examples, 66 and 80 percent of the monthly comparisons were within 20 and 30 percent, respectively, of the gage standard. The mean error for all monthly comparisons was 21 percent.

The states of Michigan and Wisconsin were then used to adjust the monthly and seasonal satellite estimates of lake rainfalls to obtain final best estimates for these water bodies. In the period of study (i.e. summers 1988, 1989, and 1990) it appears that Lake Superior received the most mean summer rainfall (9.38 in.), followed by Lake Michigan (8.92 in) and then Lake Huron (7.40 in). Lake Michigan had virtually the same rainfall as the state of Michigan in this time period, while Lake Huron, exclusive of the North Channel and Georgian Bay, had 21 percent less rainfall than this state. Lake Superior, on the other hand received about 5 percent more rainfall than the state of Michigan, which is affected by the lakes themselves under most flow regimes.

All lakes received much less rainfall than Wisconsin, which is upwind of the lakes to the west and southwest and unaffected by the lake suppression under most summer weather patterns. The mean summer lake deficits relative to Wisconsin are 22, 16, and 47 percent for Lakes Michigan, Superior, and Huron, respectively, for the period of investigation. The full report from Woodley Consultants, for this research, is available at the Illinois State Water Survey.

This study suggests enormous potential for the combined use of satellite imagery and raingages for the estimation of Great Lakes rainfall. It is recommended that additional summer rain estimation be made in order to stabilize the results. It is recommended further that the potential of the methodology to assist in the management and modelling of the Great Lakes system be investigated.

Chapter 8. Impact of Urban Areas on Cloud-to-Ground Lightning Flash Frequency

1. INTRODUCTION

A number of investigations have examined the effect of urban areas on the initiation and enhancement of rainfall. This research task was identified in our proposal as Task 10. Observations made in the St. Louis area during project METROMEX (1971-1975) revealed that frictional, thermodynamic, and microphysical factors can enhance the development and growth of convective clouds (Changnon et al, 1981). The warm and aerodynamically rough urban surfaces promote increased mixing and convection within the boundary layer. Observations of low-level convergence (Ackerman, 1978) and numerical simulations (Hjelmfelt, 1982) of the St. Louis area indicated that urban effects could lead to positive vertical velocities over and downwind of the urban area. Changnon et al. (1981) found a 15% increase in precipitation over and downwind of St. Louis. This urban effect on rainfall was not observed in all storms, however, but was most apparent in larger, organized convective storms. The results of the 3-year Chicago Area Project (CAP, 1976-1978), corroborated the rainfall results of the St. Louis study, in that summer rainfall over and downwind of the city was increased by 15%, with the increases again most apparent in the larger storms (Changnon, 1980).

Additionally, a climatological study of rainfall, thunder and hail indicated an increase in thunderstorm activity in 7 of 9 U.S. cities, with the effect sometimes extending 50 km downwind (Huff and Changnon, 1973). There was an indication that the increase in the number of days with thunder might be related to the size of the urban area.

The objective of this study was to further examine the effect of urban areas on thunderstorms, in the Chicago and St. Louis areas, and on 14 other cities which span a wide range of sizes, populations, pollution characteristics and topographic features. The data employed by this study are cloud-to-ground (abbrev. Cg) lightning flash observations from the National Lightning Detection Network (NLDN). In particular, this study compares the change in frequency of Cg lightning flashes (of negative and positive polarity) in the area immediately upwind of the cities, to that of the cities themselves, and to an area immediately downwind of the cities.

2. DATA ANALYSIS

Lightning data for the years 1989 to 1992 were obtained from the archive of the NLDN. In the midwest area, this network utilizes data from lightning detectors (wide band, magnetic direction finders) operated by GeoData Services and by The National Severe Storms Laboratory. Cummins, et al., (1992), in a performance analysis of the NLDN, estimated that for 1992, location accuracies were about 2 to 4 km (at least 50 % of the flashes were within 2 to 4 km), with a detection efficiency of 80 to 90% within the midwest. For earlier years, location accuracy estimates could have ranged from at best, 2 to 4 km and at worst, 8 to 16 km, and detection efficiencies from 70 - 90 %. Azimuthal site errors were evaluated annually (Orville, 1987),

however, and should have contributed minimally to location errors, making the worst case accuracy estimate unlikely.

Initially, 19 midwestern cities with metropolitan populations exceeding 500,000 were selected for study. However, even under optimal conditions, a random azimuthal error of 1 to 2° can be expected (Krider et al., 1976) and thus the accuracy of the flash location is in part dependent on the number of direction finders sensing the lightning flashes. Thus, two cities (Cleveland and Nashville) were eliminated from the analysis, because of the low number of detectors located within 400 km of urban center (5 and 4, respectively). The results for Cleveland also may have been complicated by lake effects. Lake Erie, along the north shore of Cleveland appears to have suppressed convection over Cleveland during these 4 summers. Memphis also was eliminated, as a theoretical projection of the average observable number of sensors reporting lightning was less than 4 for that area, as it was for Cleveland and Nashville (Cummins, et al, 1992).

Lightning data was extracted for the region within 120 km of 16 large midwestern cities (Table 1). The urban boundaries were delineated by the corporate limits of the cities, as derived from the 1987 Rand McNally Cosmopolitan World Atlas. The urban areas ranged in size from 288 to 2928 km^2. While even the smaller cities have a diameter larger than that of the worst case location accuracy, it might be argued that more weight should be placed on the results of the largest 8 cities (Table 1).

The lightning data were summed (number of flashes, return strokes) or averaged (amplitude of the first return stroke) over 4 x 4 km grid squares. Grid boxes encompassed by the city, upwind and downwind areas were delineated. As the prevailing storm motion for these cities has a strong westerly component, the results from the downwind area to the east of the city and from the upwind area to the west of the city are presented. The upwind and downwind areas each include double the grid points of the urban area and have widths comparable to the diameters of the cities. Since the urban effects observed in St. Louis were most pronounced in the summer months, this analysis is based on June, July and August data.

3. **RESULTS**

3.1 Storm Definition and Storm Frequency

The lightning storms within 120 km of each city were defined in a simple way, as an event which had 5 or more Cg flashes, with the flashes separated from all other flashes by more than one hour. No attempt was made to include a spatial limit on the location of flashes within each storm. The storms ranged in flash occurrence, from 5 to 35,000 flashes.
The storms were grouped by the frequency of flashes per storm. Results presented here are for the storms or portions of storms which occurred within the upwind west, downwind east and/or urban areas, grouped by storm type and for the total sample of storms occurring in these areas (Table 2).

3.2 Flash Frequency

It appears that for some cities, the total number of Cg flashes are more frequent over and downwind of the urban area than for the west upwind area (Tables 3, 4). The pluses in Tables 3 and 4, refer to west-to-east increases in flash frequency and the minuses to decreases, both significant at the 5% level. Statistical significance for differences in the median and distribution of the change in flash frequency was determined using a two-sided Wilcoxon Rank Sum Test. In looking at the total number of flashes for all storms, 12 of the 16 urban areas showed an increase in flash frequency over the city and 13 showed an increase over the downwind area to the east.

The small storms ("A" in Tables 3 and 4) averaged only .3 flashes per 16 km^2, and represent only a few events. While the large "D" and "E" storms averaged 45 and 26 flashes per 16 km^2, respectively, they also represent only a few events. Caution should be taken in considering statistically significant values in these categories, and in considering significant values for all storms when they are dominated by significant differences in the D and E categories. The average number of flashes observed per 16 km^2 for the 4 summers of data was 2.8 for the "B" storms, and 36 for the "C" storms. Emphasis here is placed on the results for the C storms (500-5,000 flashes) which have both a moderately large flash density and a large sample of storms.

The results for Chicago and St. Louis areas generally agree with those of past studies, in that the urban area appeared to enhance convection over and downwind of the cities. An increase of 22% was observed in the number of flashes produced by C storms over Chicago, and 36% over St. Louis (Table 5). The downwind area as compared to the upwind area also increased for both cities, by 23% for Chicago and by 136% for St.Louis (Table 5). An enhancement of urban and downwind lightning flash frequency for C storms also was found for Dallas-Fort Worth, Kansas City and Milwaukee. The amount of lightning activity downwind of St.Louis and Dallas-Fort Worth were considerably greater than the increase over their urban centers.

All of the large cities except Detroit and Cincinnati showed some indication of increased lightning frequency over the city, and all but Minneapolis-St.Paul and Cincinnati showed an increase downwind of the city. Except for Omaha, the eight smaller cities showed little change in lightning frequency for the C storms over the city. However, five of these cities did show an increase in lightning immediately downwind of the city.

3.3 Possible Factors Relating to Flash Increases

A cursory examination of the results were made with regard to elevation, metropolitan and urban populations, city size, estimates of CCN concentration, and with respect to topographic features in and around the urban areas. Mean elevations were determined for 2 km x 2 km grid boxes within 120 km of city center for the 3 largest cities, within 75 km for the next 5 largest cities, and within 60 km for the smallest 8 cities. The topographic features noted were the presence of one of the Great Lakes which can often act to suppress summertime convection, or a major river

which can act as a source of moisture, or the location of the urban area in a broad depression. The 1988 urban and metropolitan populations were obtained from the 1990 World Almanac. Annual averages of PM10 (particulate matter with aerodynamic diameters smaller than 10 um) and sulfur dioxide (SO_2), were used as gross indicators of cloud condensation nuclei (CCN) concentrations (US EPA, National Air Quality and Emissions Trends Report, 1989, 1990).

For each of the cities (including urban, upwind and downwind areas), there appeared to be no correlation between elevation and frequency of Cg flashes for the 5 storm categories, for the total group of storms, or for the location of the first 5 or 50 flashes from each storm. Additionally, no consistent relationship could be found between topographic features present and lightning frequency.

Only St. Louis exceeded the expected EPA annual mean criteria of 50 ugm^3 for PM10 in both 1989 and 1990 (Table 6). Chicago, Kansas City, and Omaha had the next highest values of PM10 for these two years. None of the cities exceeded the annual mean criteria of .03 ppm for SO_2 in 1989 and 1990. Generally, the cities covering a wider area and with a larger population had larger annual values of PM10 and SO_2, and consistently had larger urban and downwind values of cloud-to-ground flashes. Dallas-Fort Worth, Cincinnati and Detroit were notable exceptions. While enhanced lightning activity over and downwind of Dallas-Fort Worth was in evidence, it was "cleaner" than the other large cities. Both Detroit and Cincinnati were relatively dirty, but showed no effect or a negative effect on lighting activity. Changnon, et al., (1981) indicated that CCN levels in St. Louis were elevated and altered the cloud drop distribution by increasing the number of small drops. Additionally, ultra-giant CCN also were observed in St. Louis. The presence of some large CCN in combination with the large number of small CCN may have enhanced Hallet-Mossop (1974) ice multiplication processes, resulting in the enhanced glaciation of clouds. However, even in St. Louis, no direct relationship was found between CCN levels and enhanced rainfall.

Values of the percent change in lightning flash frequency from upwind west to the urban area, and from the upwind west to the downwind areas are presented in Fig. 1 and 2, respectively, for the C storms. Open circles refer to statistically significant changes. From these data, it does not appear that the size of the city greatly impacted the magnitude of the urban effect, as had been suggested by the results of Huff and Changnon, 1973). Similarly, no relationship was found between lightning frequency differences and population.

Results from the METROMEX project indicated that increased numbers of cumulus congestus clouds were found over St. Louis during the period from 0900 to 2400 LDT. To determine whether this effect could be observed in the lightning data, the location of the first 50 flashes from all storms were examined. No indication was found of a greater number of storms initiating over the urban area.

The St. Louis results also indicated that echoes were able to grow to greater heights over and downwind of the urban area during the afternoon hours when the maximum interaction occurs between the urban heat island and the unstable air flowing across it (Changnon et al., 1981). An

examination of lightning frequency during the period from 1200 to 2100 LDT was made (Table 7). It was found that 9 of the 16 cities showed a statistically significant increase in lightning, ranging from 15 to 76%, over the urban area, and 12 cities showed an increase between 17 and 89%, downwind of the urban area. When only the afternoon "C" storms were considered (Table 8), similar results were found. Based on METROMEX and CAP results, while the urban area may initiate new cloud growth, the largest effects are upon existing rainstorms that pass over the city.

In at least 8 of the cities, a larger effect was observed downwind of the city than over the city. This observation, may indirectly support the low theta-e theory. This theory suggests that the ingestion by storms of lower (by 2 to 4 °C) theta-e air typically found in urban areas would decrease the strength of updrafts and allow suspended precipitation to fall to the ground (Changnon, 1981). It is possible that the larger downwind effects found for many of these cities may be due in part to rainstorms, already invigorated by the urban area itself, being additionally fueled by higher theta-e air found downwind of the city.

4. CONCLUSIONS

An examination of the summertime lightning flash frequency over and downwind of 16 central United States cities for 4 years, suggests that indeed convection is enhanced over and downwind of some major urban areas as suggested by earlier studies. However, because of the paucity of samples in the very small and very large storm categories, more years of data are required to delineate specific conditions under which this enhancement occurs. In the mean time, to more clearly determine the underlying processes resulting in this urban effect, a case study approach may be warranted.

5. REFERENCES

Ackerman, B., 1978: Regional Kinematic Fields. Summary of METROMEX, Vol. 2. Causes of Precipitation Anomalies. ISWS Bulletin 63, Urbana, 165-205.

Changnon, S.A., 1980: Evidence of urban and lake influences on precipitation in the Chicago area, J. Appl. Meteor., 19, 1137-1159.

Changnon, S.A., Jr., R.G. Semonin, A.H. Auer, R.R. Braham, Jr., and J.M. Hales, 1981: METROMEX: A Review and Summary. Meteorological Monographs, Amer. Meteor. Soc, 18, 181 p.

Cummins, K.L., W.L. Hiscox, A.E. Pifer, and M.W. Maier, 1992: Performance analyses of the U.S. National Lightning Detection Network, Preprint, 9th Intl. Conf. on Atmos. Electricity (expanded paper),

Hallet, J. and S.C. Mossop, 1974: Production of secondary ice particles during the riming

process. Nature, 24, 26-28.

Hjelmfelt, M.R., 1982: Numerical simulation of the effects of St. Louis on mesoscale boundary layer airflow and vertical air motions: Simulations of urban vs. non-urban effects. J. Appl. Meteor., 21, 1239-1257.

Huff, F.A., and S.A. Changnon, 1973: Precipitation modification by major urban areas. Bull. Amer. Meteor. Soc., 54, 1220-1232.

Krider, E.P., R.C. Noggle and M.A. Uman, 1976: A gated wideband magnetic direction finder for lightning return strokes. J. Appl. Meteor., 15, 301-306.

Orville, R.E., Jr., 1987: An analytical solution to obtain the optimum source location using multiple direction finders on a spherical surface. J. Geophy. Res., 92, 10877-10886.

Table 1. The size and 1988 population of cities examined for possible urban effects on lightning frequency.

City	Metropolitan Population	Urban Population	Urban Area (km^2)
Chicago	8,180,900	2,977,520	2,298
Detroit	4,620,200	1,035,920	2,224
Dallas-Ft.Worth	3,766,100	1,671,430	1,248
Minh.-St.Paul	2,387,500	603,780	960
St. Louis	2,466,700	403,700	864
Cincinnati	1,728,500	370,480	752
Milwaukee	1,571,700	599,380	736
Kansas City	1,575,400	438,950	704
Indianapolis	1,236,600	727,130	592
Columbus	1,344,300	569,570	544
Louisville	967,000	281,880	544
Wichita	483,100	295,320	432
Oklahoma City	963,800	434,380	400
Tulsa	727,600	368,300	336
Omaha	621,600	353,170	320
Toledo	616,500	340,760	288

Table 2. Number of storms or partial lightning storms for 16 central U.S. cities, for June-August 1989-1992.

Number of Flashes		Mean	Std.Dev.
A:	5-50	17	10
B:	51 - 500	41	10
C:	501 - 5,000	63	10
D:	5,001 - 15,000	16	6
E:	> 15,000	2	2
	All Storms	138	25

Table 3. Significant change in Cg Flash frequency from the upwind to the urban area, for storms grouped by flash frequencies of: A) 5-50, B) 51-500, C) 501-5,000, D) 5,001-15,000, E) >15,000, and for all storms. Increases in urban area are +, and decreases are -.

City	A	B	C	D	E	All
Chicago		+	+	-	+ **	+
Detroit				- *	o	
Dallas-Ft.Worth		-	+		o	+
Minn.-St.Paul		-	+	*	o	+
St. Louis		+	+	+	- **	+
Cincinnati	-	-			-	
Milwaukee		-	+	- *	+ **	+
Kansas City		+	+	+	- **	+
Indianapolis					+	+
Columbus				+	+	+
Louisville		+			+	+
Wichita				+	**	+
Oklahoma City					+ **	+
Tulsa	+	+			o	
Omaha			+	+	+ **	+
Toledo				*	+**	

* based on ≤ 10 storms
o no storms in this category
** based on 1-3 storms

Table 4. Significant change in Cg Flash frequency from the upwind to the downwind area, for storms grouped by flash frequencies of: A) A 5-50, B) 51-500, C) 501-5,000, D) 5,001-15,000, E) > 15,000, and for all storms. Significant increases in the downwind area are +, and decreases are -.

City	A	B	C	D	E	All
Chicago		-	+	-	+ **	+
Detroit			-	*	o	-
Dallas-Ft.Worth	-		+	+	o	+
Minn.-St.Paul	+	-		+ *	o	+
St. Louis		+	+	-	- **	+
Cincinnati	-				-	-
Milwaukee		-	+	*	**	+
Kansas City		+	+	+	**	+
Indianapolis				+	+	+
Columbus			+	+	+	+
Louisville		+	+		+	+
Wichita		+	+	+	**	+
Oklahoma City		+		+	+ **	+
Tulsa		-	+	+	o	+
Omaha		+	+	+	+ **	+
Toledo		+		*	- **	-

* based on < 10 storms
o no storms in this category
** based on 1-3 storms

Table 5. Mean number of Cg Flashes per 16 km^2 found in the upwind west areas, and expressions of the differences between the area in the city and areas upwind and downwind of the city, significant changes (indicated by shading) in frequency of Cg Flashes from the upwind to the urban area and in Cg frequency from the upwind to the downwind area, for "C" storms (500 to 5,000 flashes).

		(City - Upwind/ Upwind)		(Downwind - Upwind/ Upwind)	
City	Upwind Flashes	% Change	P-value	% Change	P-value
Chicago	26	22.4	.000	23.2	.000
Detroit	35	3.2	.491	-20.0	.000
Dallas-Ft.Worth.	27	97.5	.000	109.8	.000
Minn.-St.Paul	30	26.3	.000	7.1	.488
St. Louis	23	35.6	.000	136.3	.000
Cincinnati	59	8.2	.086	4.4	.414
Milwaukee	20	40.8	.000	26.6	.001
Kansas City	29	46.7	.000	57.7	.000
Indianapolis	43	24.3	.308	16.1	.559
Columbus	34	- 6.8	.337	40.7	.000
Louisville	41	18.0	.282	53.8	.000
Wichita	40	10.5	.071	30.4	.000
Oklahoma City	37	13.3	.078	8.7	.072
Tulsa	38	- 9.4	.436	13.8	.014
Omaha	40	12.7	.043	20.2	.000
Toledo	37	- 6.1	.073	-24.1	.126

Table 6. Factors that might lead to changes in lightning flash frequency: topographic features, and increases in cloud condensation nuclei estimated by the annual average (1989 and 1990) of PM10 and SO_2.

City	Topography	PM10 (ug/m^3) 1989, 1990	SO_2 (ppm) 1989, 1990
Chicago	Lake (do,E)	48,45	.011, .010
Detroit	Lake (do,E;up,S)	52,35	.015, .018
Dallas-Ft.Worth	River (NW/SE)	36,35	.005, .006
Minn.-St.Paul	River (W/E)	33,34	.010, .010
St. Louis	River (W/E)	76,82	.018, .015
Cincinnati	River (W/E)	45,35	.016, .017
Milwaukee	Lake (do,E)	40, 35	.007, .007
Kansas City	River (S/N)	47,43	.006, .004
Indianapolis	Bowl	43,38	.014, .013
Columbus	Bowl	40,35	.010, .008
Louisville	Bowl	38,36	.012, .012
Wichita	Bowl	31, 30	--- , .009
Oklahoma City		27,29	.006, .004
Tulsa		36,27	.007, .012
Omaha	River (S/N)	46,44	.002, .002
Toledo	Lake (do,E)	--,26	.008, .007

Table 7. Mean number of Cg Flashes per 16 km^2 found in the upwind west areas, significant changes (indicated by shading) in frequency of Cg Flashes from the upwind to the urban area and in Cg frequency from the upwind to the downwind area, for storms occurring during the period from 1200 to 2100 LDT.

		(City - Upwind/ Upwind)		(Downwind - Upwind/ Upwind)	
City	Upwind Flashes	% Change	P-value	% Change	P-value
Chicago	40	-4.5	.060	-0.1	.688
Detroit	38	-12.5	.004	-14.8	.000
Dallas-Ft.Worth.	40	55.4	.000	42.4	.000
Minn.-St.Paul	12	76.2	.000	80.8	.000
St. Louis	56	43.2	.000	36.0	.000
Cincinnati	121	- 8.4	.226	- 3.9	.680
Milwaukee	21	51.7	.000	88.9	.000
Kansas City	35	22.4	.000	69.0	.000
Indianapolis	73	9.4	.100	22.9	.000
Columbus	86	17.5	.003	56.3	.000
Louisville	79	15.4	.039	50.5	.000
Wichita	39	18.7	.001	16.7	.000
Oklahoma City	23	48.4	.000	82.1	.000
Tulsa	36	11.5	.315	28.7	.007
Omaha	23	13.6	.178	37.1	.000
Toledo	59	-32.3	.008	-38.9	.000

Table 8. Mean number of Cg Flashes per 16 km^2 found in the upwind west areas, significant changes (indicated by shading) in frequency of Cg Flashes from the upwind to the urban area and in Cg frequency from the upwind to the downwind area, for "C" storms (500 to 5,000 flashes) occurring during the period from 1200 to 2100 LDT.

		(City - Upwind/ Upwind)		(Downwind - Upwind/ Upwind)	
City	Upwind Flashes	% Change	P-value	% Change	P-value
Chicago	16	2.1	.378	12.7	.419
Detroit	18	- 8.6	.166	-23.8	.000
Dallas-Ft.Worth.	11	175.2	.000	166.5	.000
Minn.-St.Paul	9	69.8	.000	28.2	.001
St. Louis	11	71.3	.000	192.9	.000
Cincinnati	41	-17.1	.001	14.3	.710
Milwaukee	10	68.7	.000	57.3	.000
Kansas City	11	32.0	.010	88.8	.000
Indianapolis	25	-13.2	.242	4.0	.742
Columbus	20	26.0	.025	100.7	.000
Louisville	28	31.0	.072	68.5	.000
Wichita	18	8.0	.554	14.6	.006
Oklahoma City	15	67.7	.000	77.3	.000
Tulsa	20	- 7.8	.861	- 8.5	.552
Omaha	10	68.2	.000	55.0	.000
Toledo	27	-33.1	.046	-40.2	.001

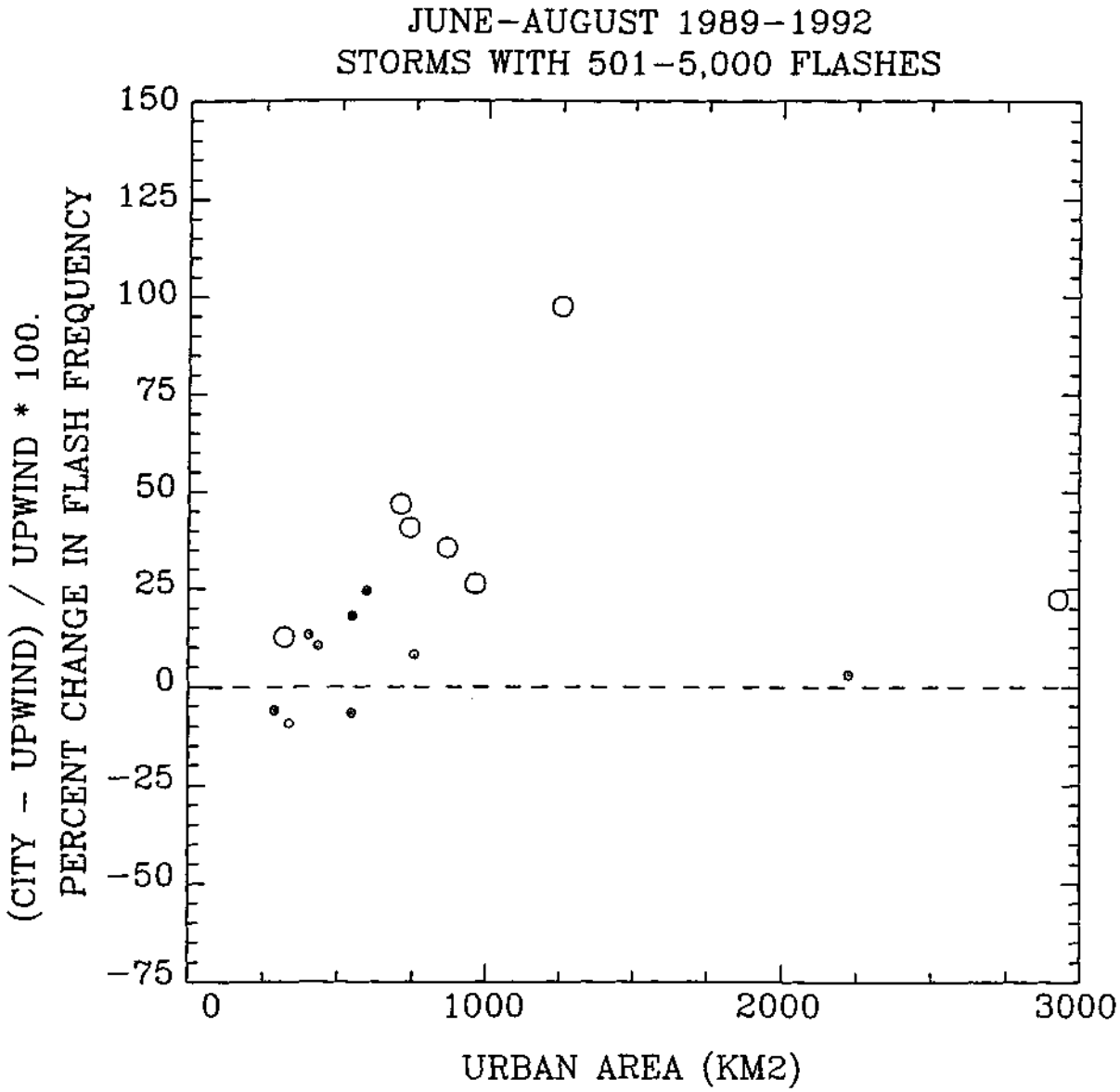

Figure 1. Percent change in Cg Flash Frequency from the upwind to the urban area vs. urban area for 16 Midwestern cities.

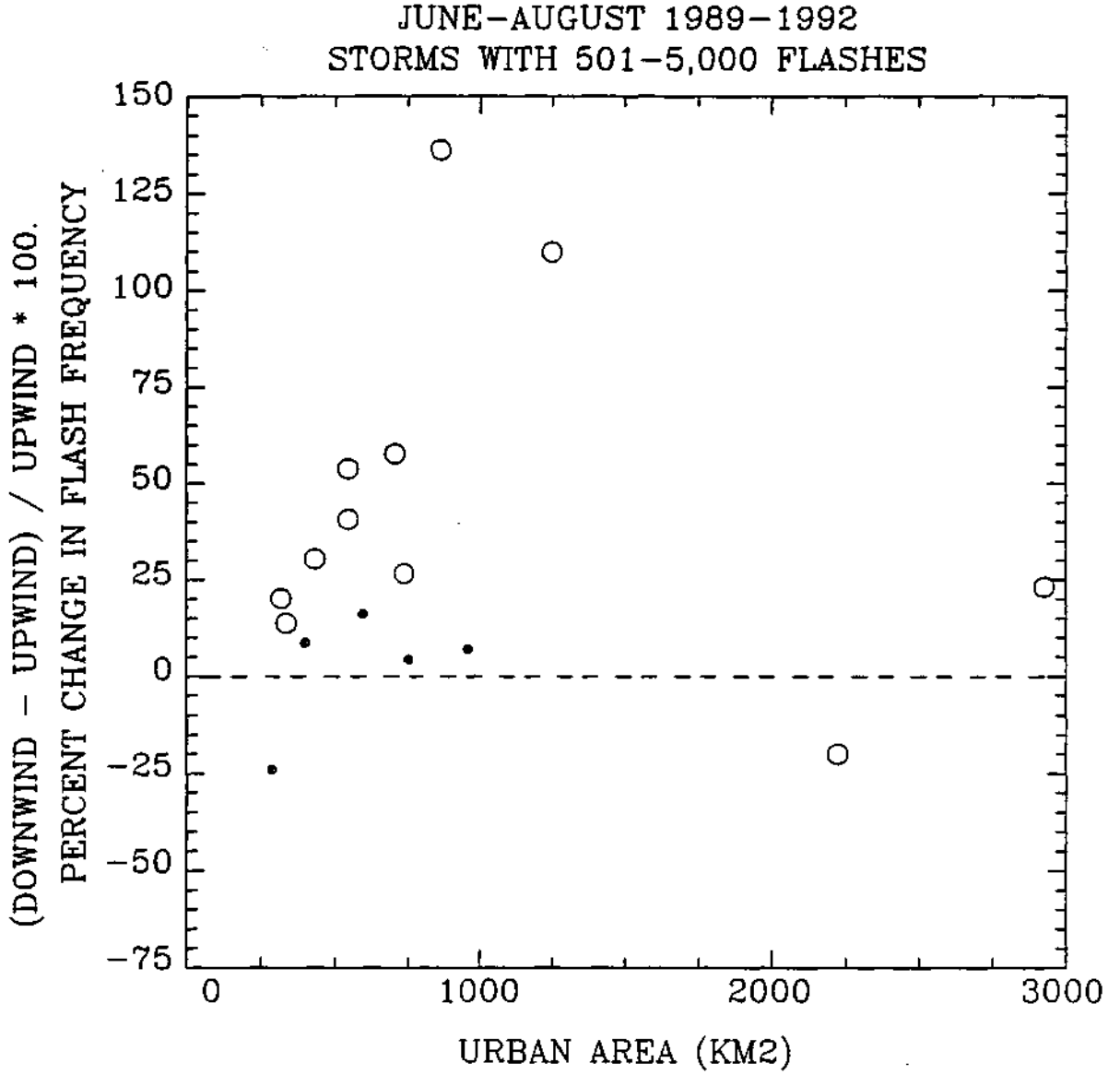

Figure 2. Percent change in Cg Flash Frequency from the upwind to the downwind area vs. urban area for 16 Midwestern cities.

Chapter 9. Seasonal Rainfall and Soil Temperature Impacts on Corn Growth and Yield

1. INTRODUCTION

During the summers of 1987 through 1991, experiments in rain shelters were conducted to evaluate the impact of increased rainfall on corn (Zea mays L.) yields in east-central Illinois (Hollinger and Changnon, 1993). The increases in rainfall were designed to simulate the effects of enhanced rainfall due to cloud seeding in typical dry, average and wet summers. Results of that study showed that increased rainfall resulted in larger grain yields. However, the increase in yields due to more rain during the typical dry, average, and wet summers were small compared to the variability of corn yields among the five years. In each of the five summers the same amount of rain was received on the same days of the year during the months of June, July and August. Analysis of the yield data in relation to other weather variables revealed that temperature during the first 30 days of corn growth was highly correlated with final yield. This research was conducted as part of Task 11 of the one-year project.

Various studies have shown that temperature can greatly affect corn yields when the corn plant is pollinating (Herrero and Johnson, 1980) and during the two weeks following pollination when the kernels are developing (Jones et al., 1981, 1984, 1985). Lehenbauer (1914) demonstrated the effect of temperature on corn leaf elongation. Since that time many studies have demonstrated the relationship between temperature and the rate of corn development. However, most of the research on the temperature effects on com have focused on corn development and not corn growth[1] and final yield. The growing degree day concept (Cross and Zuber, 1972) and later work by Coelho and Dale (1980) have demonstrated that the rate of corn development is highly correlated to temperature. However, there are no studies that relate corn growth and final yield to the temperature experienced by the plant during its early growth stages.

It has been long accepted that the two to four weeks around corn pollination is the most critical period for rainfall in determining corn grain yield. Most studies have related the rainfall response of corn to the calendar (Runge, 1968; Huff and Changnon, 1972). A major problem with this approach is that the corn crop is never planted at exactly the same time each year, and the temperature regime under which it is grown can either lengthen or shorten, in days, a given

[1]Corn development is defined as the rate of leaf initiation and elongation, stem elongation, and tassel and ear initiation and development. Corn growth is defined as the accumulation of dry matter in the various plant compartments. While corn growth and development are highly correlated, the number of leaves and ears are determined by the genetic makeup of the plant. The final size of the leaves, stems, and ears is greatly affected by the environment in which the corn plant grows.

growth stage. Thus, the response of corn yield to a calendar period, while informative, does not allow for fine tuning of either weather modification for rainfall enhancement, or water application through irrigation.

The objectives of the 1992 research were to determine 1) how early season temperature affect canopy development and its effect on yield, and 2) the growth stage during which corn responds most to water applications.

2. METHODS

Two experiments were established in the spring of 1992. The first experiment was designed to study the effects of soil and air temperature on early corn growth and development and the effect on final yield. The second experiment was to study the effects on final yield of no rainfall, rainfall equal to 50 percent of evapotranspiration, and 100 percent of evapotranspiration during different corn growth stages.

2.1. Soil and Air Temperature Effects.

The experiment was conducted at the University of Illinois Agronomy South Farm at Urbana-Champaign to evaluate the response of corn growth and developmental characteristics under different soil and air temperatures during the period from planting to the 5-leaf stage. Air temperature treatments were established by planting the corn on two different dates. Soil temperature was controlled using warm and cool water circulating through copper pipes buried next to the corn rows.

The experiment was set up in a randomized complete block split-plot design. Dates of planting were assigned to main plots and treatments to sub-plots. Individual experimental units were 2 rows 76 cm apart by 6 m long. Ten plants were randomly selected within each replication and non-destructive measurements taken on the same plants throughout the season.

2.2.1. Agronomic Methods.

The plot area where the experiment was established consisted of two separate experimental areas that had experienced different cropping histories. The west plot area (Figure 1) had corn planted on it in both 1990 and 1991, while the east plot area had soybeans planted on it in 1990 and was fallow during the summer of 1991. Because the corn crop was to be hand planted and preparation of the soil required physical contact between the workers hands and the soil, no root worm treatment was applied to the plots before planting. Root worm control was affected using Lorsban 4E at a rate of 7 liter per hectare (1/ha) after a severe outbreak of root worms was observed in early July.

Corn hybrid Pioneer 3379 was hand planted on 11 May and 4 June at a population of 68,325 seed ha^{-1}. After emergence the plants were thinned to a spacing of one plant every 20 cm. Before planting, the plots were fertilized with 224 kilogram per hectare (kg per ha) of nitrogen

(N), 56 kg per ha of phosphorus (P), and 168 kg per ha of potassium (K). Weeds were controlled by hand cultivation throughout the growing season.

Plant stage, individual leaf area, plant height, stem major and minor axis, and leaf senescence were observed three times per Week from emergence to the 5-leaf stage, and once a week afterwards until complete leaf senescence. At tasseling, final height, the length of each internode, and the dimensions of the internode major and minor axes were recorded. To reduce the amount of leaf handling the length and width of each leaf still in the whorl and not fully emerged at the previous observation date were the only leaves measured. Once the collar of a leaf had emerged from the whorl and the leaf measurements taken, the leaf was not measured again.

Leaf area (L_a) was calculated based on the leaf length (L_1), maximum width (L_w,), and a correction factor (McKee, 1964) as

$$L_a = 0.75 L_1 L_w. \quad (1)$$

The whole plant leaf area on each sampling date was computed by summing all the individual leaf areas. Based on the statistical design, using the mean procedure (PROC MEANS) in SAS (SAS, 1992), mean leaf areas were calculated for each treatment at each sampling date throughout the season.

Growing Degree Days (GDD) were calculated using the Modified Growing Degree formula (MGDD) (Cross and Zuber, 1972). From planting to the fifth leaf stage, GDD were computed using the soil temperature from each treatment. After the soil temperature treatments were shut off the GDD calculations were based on the air temperature.

The plants that had been repeatedly measured during the growing season were harvested separately, and the following variables recorded: number of ears per plant, number of kernel rows per ear, average number of kernels in a row, weight of the whole ear, mass of the grain from each ear, the mass of 100 kernels, and plant biomass. In addition, the grain yield of all the plants in each experimental unit was included to determine the overall plot yield.

Statistical analysis was done using the general linear model procedure (GLM) in SAS.

2.2.2. Soil Temperature Control.

The treatments consisted of maintaining the temperature of the soil surrounding the corn growing point at 5°C above and below ambient temperature. Therefore, the experiment had three treatments: ambient (control); warm (5°C above ambient); and cool (5°C below ambient). The temperature was controlled until the 5-leaf stage after which the growing point was assumed to be above the soil surface. Once above the surface of the soil the growing point is mainly affected by the air temperature.

Soil temperatures were maintained using a hydronic system. Ambient soil temperatures were monitored and the warm and cool soil temperature treatments were maintained 5°C above and 5°C below the ambient soil temperature. Soil temperature was monitored by thermocouple arrays placed in the ambient and temperature treated rows. A datalogger sampled each sensor array once every ten seconds; calculated separate average values for all ambient, warm and cool arrays; and sent appropriate control signals to the heating and cooling systems.
The heating system consisted of a 208 liter drum with a 4500 watt, 240 volt heating element installed in the lower portion of the tank. Water was circulated by a pump through the tank at a rate of 113. 1 m^{-1} through a 2.54 cm ID PVC pipe distribution network and then through 6.1 meter long 1.27 cm ID copper pipes buried next to the planted rows. Water return flow was routed through a second 2.54 cm ID PVC pipe system back to the 208 liter tank.

The cooling system consisted of a 208 liter drum and 240 volt 3 phase 63.24 MJ chiller. The water circulation system was identical to the that used for the heating system. A separate water loop circulated cold water through the chiller to carry away waste heat removed from the circulating water supply.

Copper pipe was buried in the planted rows with the bottom of the copper pipe 1 cm above and to the side of the corn seed. The top of the copper pipe was 2 cm below the surface of the soil. A thermocouple was installed every 1.5 meters along the copper pipe on the same side and at a depth of 2.54 cm in the ambient, heated, and cooled planting rows. These 5 thermocouples were connected in parallel to form an array whose output signal represented the average temperature along each copper pipe.

The sensor arrays were constructed of 30 gauge, type T thermocouple wire with each junction water sealed with a coating of silicone glue and heat shrink tubing. Five junction leads were connected in parallel to a single lead wire that ran to a multiplexer. The junction of the five thermocouple leads was sealed with silicone glue and heat shrink tubing. Individual thermocouples were installed in the rows adjacent to copper pipe by using a 5 cm length of 0.635 cm diameter rigid plastic tubing to act as a support to hold the thermocouple probe at a distance from the copper pipe equal to the space between the seed and the copper pipe.

The copper pipes in the heated and cooled rows were connected to their respective circulation system. The copper pipes in the ambient rows were not connected to any circulation system. Thus all measured rows had identical physical obstructions to the individual plant's growth. The datalogger, a Campbell Scientific CR10, was connected to two multiplexers that facilitated the sampling of all 48 sensor arrays. After the arrays were measured by the datalogger, their values were averaged by cool, ambient, and warm group. The resulting numbers were used to maintain appropriate water temperatures in the respective circulating systems.

Control signals from the data logger were routed to optioisolated relays that controlled all equipment with the system. The two water pumps were separately turned on and off through manual software control to facilitate maintenance of the system. The heating element was switched under automatic software control by two control lines through two optoisolated relays.

The chiller was automatically controlled by the data logger software through a single control line and optoisolated relay. Optical isolation of the chiller and heater was necessary to protect the data logger from power surges during lightning storms.

2.2. Rainfall during Different Growth Stages.

Two rain shelters (Banwart, 1987, 1988; Changnon and Hollinger, 1988) were used to protect a total of 72 plots from all natural summer rainfall. Water was then applied to the plots at periodic intervals through the season. Water application dates were selected based on a climatological distribution of most likely rain dates (Table 1). When consecutive rain days occurred in the climatological sequence, water was applied on only one of the days. The first water application was made on the first "rain" day after planting. The total amount of water applied to each plot changed throughout the growing season depending upon the growth stage, and evapo-transpiration since the last watering.

The rain shelters were originally designed for a single rainfall rain treatment on each plot throughout the growing season. As designed, the plumbing in the rain shelters would need to be changed manually as the crop grew. Therefore, the rain shelters were modified by adding electrically operated shut off valves to control the amount of water applied to each of the plots. A computer program was written to monitor flow sensors and compute the quantity of water applied to each plot and determine when each nozzle should be shut off. The modification allowed two people to easily apply the water treatments without having to physically change the plumbing each time the crop advanced to another growth stage.

A fractional factorial experiment was set up in rain shelters. Two levels of water (no water, and water equal to evapo-transpiration [ET]) were applied to each plot during the first three corn growth stages (planting to tassel initiation, tassel initiation to ear initiation, and ear initiation to end of row set). Three water treatments (no water, water equal to 50 percent of ET, and water equal to 100 percent of ET) were applied during the growth stages of end of row set to silking, silking to end of lag phase, and end of lag phase to maturity. The total number of combinations of water treatments and growth stages was seventy-two; therefore, there was no replication of treatments in the experiment. The extremes of treatments were one plot with no water applied from planting to maturity, and one plot with water applied at the rate of 100 percent of ET during each growth stage.

The plots were planted on 4 June 1992. Seeds were planted at a spacing of approximately 10 cm using a mechanical planter. After emergence the plants were thinned to a final population of 64,200 plants per hectare (plants/ha). Before planting, the plots were fertilized with 224 kilogram per hectare (kg/ha) of nitrogen (N), 56 kg/ha of phosphorus (P), and 168 kg/ha of potassium (K). The plots were irrigated approximately one week before planting to ensure an adequate soil moisture supply in the profile before planting the crop.

At maturity, 2.44 meters (m) of the center two rows of each plot were harvested to determine the total grain yield. The components that make up the final grain yield--number of rows per ear,

number of kernels per row, and kernel mass— and vegetative mass were also measured.

2.3. Weather Monitoring.

Air temperature, relative humidity, solar radiation, and wind speed and direction were all monitored at the Illinois Climate Network automated weather station located at the Illinois State Water Survey Research Center 1 km west of the rain shelter and plot area. Rainfall was monitored at the plot area. However, in neither of these experiments was the total rain at the plots that important. All the natural rain was kept off the rain shelter plots after the corn was planted, and the soil temperature treated plots were irrigated so that water stress would not impact the plots. The only reason for monitoring the rainfall was for completeness of the weather record.

3. RESULTS

The results of both experiments are presented below. Response of the corn plant to the soil and air temperature treatments are provided first, followed by the response of final yield to rainfall during six different growing stages.

3.1. Soil and Air Temperature Effects

Results showing the accuracy of the soil temperature treatments, the response of yield and yield components to the date of planting and soil temperature treatments, and the response of leaf emergence and size to the soil temperature treatments are presented in this section.

3.1.1. Accuracy of Soil Temperature Treatments

The procedure used to maintain the soil temperature treatments did not require complex modeling of the soil heat capacity or conductivity, because the actual soil temperatures were being monitored and the temperature continuously modified. Time lags existed in the system therefore a constant 5°C temperature difference from ambient was not expected. The greatest deviations from the 5°C treatments in the first date of planting were approximately 1°C (Figure 2a). Soil temperature treatment control of the second date of planting was not as good (Figure 2b). Deviations from the desired treatment temperatures were as large as 13°C (Table 2).

3.1.2. Yield and Yield Components

The corn yields and the yield components that make up the corn yield are analyzed to evaluate the effects of the date of planting and the soil temperature treatments.

3.1.2.1. Date of Planting Effect.

Analysis of variance (Anova) indicates that overall yield, number of rows (NROWS), number of kernels per row (NKERN), mass of 100 kernels (W100KERN), total ear weight (TEARW), and

total kernel weight (TKERNELW) were significantly affected by the date of planting (Table 3). The total kernel weight is the average weight of the grain on each ear, while total ear weight includes both the grain, cob, and husk of the ear.

Overall corn yields for the first date of planting (DOP 1) were significantly higher than the second date of planting (DOP 2). The yield components reveal the effect of date of planting on how the total yield was obtained. NROWS, NKERN, and W100KERN means for DOP 1 were significantly greater than DOP 2. Moreover, TEARW and TKERNELW means were significantly greater for DOP 1 compared to DOP 2. Date of planting did not significantly affect either the total vegetative mass (BIOMASS) or the number of ears per plant (NEARS). However, the first date of planting had smaller plants with an average of more ears per plant than the second date of planting.

3.1.2.2. Soil Temperature Treatment Effect

Anova indicates that the mean overall yield, NROWS, NKERN, W100KERN, TEARW, and TKERNELW were affected by the treatments (Table 4). The overall yields, NROWS, NKERN, and TKERNELW means of the warm and the ambient treatments were not significantly different, but both the ambient and warm treatment means of each of the variables were significantly greater than the cool treatment. The cool treatment W100KERN mean was significantly higher for the cool treatment compared to the warm and the ambient treatments. W100KERN means were not significantly different between the warm and ambient treatments. TEARW means for the warm and cool treatments were significantly different. However, the ambient treatment mean was not significantly different from either the cool or warm treatment.

Even though the ambient and warm temperature treatments for the above variables were not significantly different, there was a trend to more rows per ear, kernels per row, total ear weight, and total grain mass per ear with warmer soil temperature during the period from planting to the 5-leaf stage. The mass of 100 kernels tended to be greater with cooler temperatures with the lightest kernels occurring in the warm soil temperature treatment.

There were no significant differences in the means of BIOMASS and NEARS among the soil temperature treatments. Neither was there a trend in biomass from cooler to warmer soil temperature treatments. NEARS showed slightly more ears per plant under the cooler temperature treatments (ambient and cool).

3.1.3. Growth and Development

Soil temperature treatments affected the developmental rate of the com plants. For DOP 1, under the warm treatment the 5-leaf stage was reached 4 days before the ambient treatment, and 8 days before the cool treatment (Table 5). Furthermore, that developmental delay was maintained throughout the season even though the soil temperature treatments were shut off after the 5-leaf stage (Figure 3). Thus the plants reached tasseling with the same differences in days among the treatments (Table 5), However, when development was plotted as a function of GDD (Figure

4), the number of GDD required to reach the 5-leaf stage and tasseling were less in the cool treatment compared to the ambient and warm treatments (Table 6). The ambient treatment also needed fewer GDD than the warm to reach comparable stages.

Similar plant developmental behavior was observed during the second planting date. The differences in developmental rate based on Julian dates among the treatments was less than for DOP 1. However, accumulated GDD to reach each were basically the same in each treatment for both planting dates.

For both planting dates maximum leaf area was attained earlier by the plants under warm treatment compared to ambient and cool. However any leaf area in the cool treatment was reached with fewer GDD compared to the ambient (Figure 5), and in the same way the ambient needed fewer GDD than the warm. For DOP 1, the cool treatment had the greatest maximum leaf area (Table 7). In addition, the maximum leaf area under the warm treatment was the smallest. For DOP 2 the largest maximum leaf area was under the ambient treatment and the smallest in the warm. There were no significant differences in the total number of leaves per plant among treatments at both planting dates. In addition, the number of leaves in DOP 1 and DOP 2 were basically the same.

The plants in the cool treatment needed fewer GDD to get to the final mean height compared to the ambient, and warm treatments (Figure 6). The plants behaved the same for both planting dates. In the first planting date the plants under the cool treatment were taller than in the ambient and warm treatments (Table 8). Furthermore, plants in the ambient treatment were taller than in the warm treatment. There were no substantial differences in final mean heights among the treatments for DOP 2. However, the mean final heights in DOP 2 were significantly taller than in DOP 1.

3.1.4. Growing Season Weather.

The weather that affected the crop during the periods from planting to 5-leaf stage, 5-leaf stage to tasseling, and tasseling to harvest is shown in Table 9. Solar radiation and potential evaporation are summed over the periods. The other weather variables are the means of the different growth periods. Soil temperature is reported for the first growth stage only. Precipitation is not included because the plots were kept well watered throughout the growing season by irrigation.

Although there were fewer soil temperature growing degree days accumulated in the cooler soil temperature treatments, the cooler soil temperatures resulted in more days required to reach the 5-leaf stage. Therefore the total solar radiation received during the period from planting to 5-leaf stage is greater under the cooler temperatures. The three soil temperature treatments were all planted on the same day. However, the weather experienced by the three treatments during their different growth stages was not the same.

During the planting to 5-leaf stage, air temperature experienced by the warm treatment averaged 1°C less than in the cool soil temperature treatment of the first planting date, but only 0.3°C less in the second planting date. Between planting dates, the second planting date was 2.2°C warmer than the first planting date. Total solar radiation received at the surface was greater for the cool treatments than for the ambient and warm treatments during both planting dates. Because solar radiation can be utilized by the plant only after it has emerged, the total solar radiation for the period had to be adjusted to account for the solar radiation received only between emergence and the 5-leaf stage (Table 9).

During the period from 5-leaf stage to tasseling (May 9 date of planting), and tasseling to maturity (both dates of planting), the total solar radiation (Table 8) received at the surface by the warm soil temperature treated plants was greater than for the cool treated plants. Other weather variables were relatively constant for the different temperature treatments during these last two periods. However, air temperature growing degree days were somewhat variable with the ambient treatment accumulation slightly more growing degree days during the period from 5-leaf stage to tasseling, and the warm treatment accumulation more from tasseling to maturity.

3.2. Rainfall during Different Growth Stages.

The water applied to the com plots in the mobile shelters on each "rain" day are shown in Table 11. Table 12 shows the total amount of water applied to the plots during the various growth stages. The plot that was well watered from planting to maturity is the only plot that received the total amount of rainfall shown in table 12. Other plots received less water depending upon which growth stage they were to be watered in, and one plot received no water from planting to maturity. Heavy rains during the month of July resulted in flooding of some of the plots. The flooding resulted in water being received by some to the plots that should have been dry during the growth stage that existed at the time of the flooding.

Preliminary regression analysis revealed that the fractional factorial experiment design separated the effects of rainfall in any given growth stage from the other stages. Table 3 shows the linear response coefficients for final grain yield (Mg ha^{-1}), the number of kernel rows per ear, the number of kernels per row, kernel mass, and vegetative mass. The statistical significance of the various rainfall response of the number of kernel rows per ear, kernel mass, vegetative mass, and total grain yield can not be explained using just one year of data. Additional years of data must be obtained to determine the true response of the corn crop to rainfall during the different growth stages.

4. DISCUSSION

The results of the two studies in 1992 are inconclusive at this point. More years of data are needed to verify the observations of the past year. The summer of 1992 was abnormally cool throughout the season and went from extremely dry in May and June to record rains in July. Rainfall on the soil temperature experiment was not an issue because the plots were irrigated to ensure adequate soil moisture throughout the growing season. The record rains had a negative

effect on the mobile shelter plots where the effect of rainfall in various growth stages was being studied. Both experiments were conducted in the summer of 1993. If similar results are observed, then the experiments will be stopped or modified.

4.1 Soil Temperature Treatments

The effects of soil temperature on corn growth and development experiment is unique because it was conducted in the natural environment, while the soil temperature at the growing point was controlled. The design of the soil temperature control system provided relatively good average soil temperature control throughout first date of planting of the experiment. Errors in the control of the soil temperature differences during the second date of planting were caused by attempting to control both dates of planting soil temperatures at the same time.

Because of delays in getting the control system constructed, the first date of planting was delayed beyond the end of April. The first date of planting delay plus the cool temperatures experienced during May would have resulted in planting the second date of planting after June 10. Such a delay would have resulted the second date of planting not maturing before frost. Therefore, the second date of planting was established before treatment of the first date of planting was terminated.

With only one temperature control system, the average ambient temperature was computed as the mean of the two dates of planting ambient temperatures. However, the surface of the soil under the first date of planting was shaded by the com canopy while the surface of the soil in the second date of planting plots were exposed to full sunlight. This resulted in an average ambient temperature different from the actual ambient soil temperature of either the first or second date of planting plots. This different was as large as 5°C (Figure 2b). The end effect was that the last several days of treatment of the first date of planting's cool and heated plots were warmer than desired, and the treatments of the second date of planting's cool and heated plots were cooler than desired.

Inspite of these error sources the temperature control was such that differences in the temperature at the growing point of the corn plants was observed. The different temperatures experienced by the plants from planting to the 5-leaf stage resulted in measurable differences in the yield, yield components, and the growth and development of the corn crop.

The delayed emergence of leaves under cooler temperatures was expected. However, this delay was not expected to persist through out the growing season. The number of days, and growing degree units for the different soil temperature treated plants to go from 5-leaf stage to tasseling were the same (46 days) in the first planting and differed only by 1 day (42 and 41 days) in the second planting date. This observation showed that the plants under the different treatments responded the same once the temperature treatments were removed.

Growing degree units have been used to time the development of com plants. It is generally assumed that the number of growing degree days to go from one stage to another is constant

regardless of the temperature regime experienced by the crop. The results here indicate that this assumption is invalid. As the growing point temperature under which the plants were developing decreased, the total number of growing degree days to reach the 5-leaf stage decreased. This provides a partial explanation of why the corn crop in the abnormally cool growing season of 1992 matured before the normal number of growing degree days to maturity had accumulated.

The results of the first year experiment did not confirm the observation of the previous experiments (Hollinger and Changnon, 1993) that yields were greater under cooler temperatures. In fact the cool treated plots were the lowest yielding. This was confirmed in the yield component analysis which showed the cool treated plants produced fewer kernel rows per ear and fewer kernels per row. However the cool treated plants had larger kernels, and a larger leaf area index.

The data collected from these experiments will allow it to be used to evaluate the effect of leaf area interception of solar radiation over the growing season on final yield and the yield components. These studies are planned for the second year of the project along with collection of a second year of data and analysis of both years data.

5. LITERATURE CITED

Banwart, W. 1987. The acid rain test plot facility. Agric. College Rep., University of Illinois, Agronomy Dept., Urbana, Illinois. 36 pp.

Banwart, W. L. 1988. Field evaluation of an acid rain drought stress interaction. Environ. Pollution 53: 123-133.

Changnon, S. A., and S. E. Hollinger. 1988. Use of unique field facilities to simulate effects of enhanced rainfall on crop production. J. Weather Modification 20: 60-66.

Coelho, D. T., and R. F. Dale. 1980. An energy crop growth variable and temperature function for predicting corn growth and development: Planting to silking. Agron. J. 72: 503-510.

Cross, H. Z., and M. S. Zuber, 1972. Prediction of flowering date in Maize based on different methods of estimating thermal units. Agron. J. 64: 351-355.

Herrero, M. P., and R. R. Johnson. 1980. High temperature stress and pollen viability of Maize. Crop Sci. 30: 796-800.

Hollinger, S. E., and S. A. Changnon, 1993. Response of corn and soybean yields to precipitation augmentation, and implications for weather modification in Illinois. Illinois State Water Survey Research Bulletin 73, Illinois State Water Survey, Champaign, Illinois.

Huff, F. A. and S. A. Changnon. 1972. Evaluation of potential effects of weather modification on agriculture. J. Appl. Metero. 11: 376-384.

Jones, R. J., B. G. Gengenbach, and V. B. Cardwell. 1981. Temperature effects on in vitro kernel development of maize. Crop Sci. 21: 761-766.

Jones, R. J., S. Ouattar, and R. K. Crookston. 1984. Thermal environment during endosperm cell division and grain filling in maize: Effects on kernel growth and development in vitro. Crop Sci. 24: 133-137.

Jones, R. J., J. Roessler, and S. Ouattar. 1985. Thermal environment during endosperm cell division in maize: Effects on number of endosperm cells and starch granules. Crop Sci. 25: 830-834.

Lehenbauer, R. A. 1914. Growth of maize seedlings in relation to temperature. Physiol. Res. 1: 247-288.

McKee, G. W. 1964. A coefficient for computing leaf area in hybrid corn. Agron. J. 56:240-241.

Runge, E. C. A. 1968. Effects of rainfall and temperature interactions during the growing season on corn yield. Agron. J. 60: 503-507.

Table 1. Climatic sequence of rain days and dry days in Champaign-Urbana used to select water application dates for the rain effects in different corn growth stages.

Day of Month	May	June	July	August	September	October
1	Dry	Dry	Dry	Dry	Dry	Dry
2	Rain	Rain	Rain	Rain	Dry	Rain
3	Rain	Dry	Dry	Rain	Rain	Dry
4	Dry	Dry	Dry	Dry	Dry	Dry
5	Dry	Dry	Dry	Dry	Dry	Dry
6	Dry	Rain	Rain	Dry	Dry	Dry
7	Rain	Dry	Rain	Rain	Rain	Dry
8	Dry	Dry	Dry	Dry	Rain	Rain
9	Dry	Rain	Dry	Dry	Dry	Rain
10	Rain	Dry	Dry	Dry	Dry	Dry
11	Rain	Dry	Dry	Dry	Dry	Dry
12	Dry	Dry	Dry	Rain	Dry	Dry
13	Dry	Dry	Rain	Rain	Dry	Dry
14	Dry	Rain	Rain	Dry	Rain	Rain
15	Dry	Rain	Dry	Dry	Dry	Dry
16	Rain	Dry	Dry	Dry	Dry	Dry
17	Dry	Dry	Dry	Dry	Dry	Dry
18	Dry	Dry	Dry	Dry	Dry	Rain
19	Dry	Rain	Rain	Rain	Rain	Rain
20	Rain	Rain	Dry	Dry	Dry	Dry
21	Dry	Dry	Dry	Dry	Dry	Dry
22	Dry	Dry	Dry	Dry	Dry	Rain
23	Rain	Rain	Dry	Dry	Rain	Dry
24	Rain	Dry	Rain	Rain	Dry	Dry
25	Dry	Dry	Dry	Dry	Dry	Dry
26	Dry	Dry	Dry	Dry	Dry	Dry
27	Dry	Rain	Dry	Rain	Dry	Rain
28	Dry	Rain	Dry	Dry	Rain	Dry
29	Rain	Dry	Rain	Dry	Rain	Dry
30	Dry	Dry	Dry	Dry	Dry	Dry
31	Dry		Dry	Dry		Dry

Table 2. Maximun, minimum and mean difference between the cool and ambient soil temperatures and the warm and ambient soil temperature in the second date of planting plots for various periods of the total treatment time.

	Cool				Warm			
Date	Mean (°C)	Std. Dev. (°C)	Max. (°C)	Min. (°C)	Mean (°C)	Std. Dev. (°C)	Max. (°C)	Min. (°C)
Jun 4-Jun 8	-6.39	2.47	-2.26	-13.17	4.14	138	6.87	0.44
Jun 9 - Jun 15	-4.14	1.59	-0.23	-7.91	5.41	1.30	8.82	1.70
Jun 16 - Jun 23	-4.51	1.84	2.03	-9.14	6.26	1.93	15.26	1.44
Jun 24-Jun 29	-4.74	1.18	-1.19	-8.98	5.68	1.19	11.78	3.08
Jun 30-Jul 2					6.01	1.75	12.72	3.42
Jun 30-Jul 4	-4.74	1.13	030	-7.15				

Table 3. Planting date effect on overall yield, biomass, number or rows (NROWS), number of kernels per row (NKERN), weight of 100 kernels (W100KERN), number of ears per plant (NEARS), total ear weight (TEARW), and total kernel weight (TKERNELW) for the 1992 field experiment.

Variable	Date of Planting		
	First	Second	Prob>F[§]
Yield (kg/ha)	8.52	6.28	**
Biomass (g/plant)	828.0	875.0	NS
NROWS	15.1	13.9	*
NKERN	36.3	31.9	*
Wl00KERN(g)	34.3	32.1	*
NEARS	1.3	1.2	NS
TEARW (g/ear)	240.0	180.0	**
TKERNELW (g/ear)	210.0	150.0	**

[§] the prob>F for the effect of planting date for each variable.
*, ** significant at the 0.05, and 0.01 probability levels respectively; NS = not significant.

Table 4. Temperature treatment effect on overall yield, biomass, number or rows (NROWS), number of kernels per row (NKERN), weight of 100 kernels (W100KERN), number of ears per plant (NEARS), total ear weight (TEARW), and total kernel weight (TKERNELW) for the 1992 field experiment.

	Treatment			
Variable	Cool	Ambient	Warm	lsd[§]
Yield (kg/ha)	6.5b	7.9a	7.9a	1.11
Biomass (g/plant)	901.0a	816.0a	837.0a	120.0
NROWS	14.1b	14.7a	14.8a	0.57
NKERN	31.4b	34.6a	36.5a	3.18
W100KERN(g)	34.2a	32.8b	327.0b	1.18
NEARS	1.3a	1.3a	1.2a	0.2
TEARW (g/ear)	191.0b	212.0ab	216.0a	21.5
TKERNELW(g/ear)	163.0b	183.0a	188.0a	20.3

[§] lsd @ a = 0.05

Table 5. Temperature treatment effect on plant development rate based on the day of the year at which the 5-leaf and tasseling stages were reached for the 1992 field experiment.

	5-Leaf		Tasseling	
Treatment	DOP 1	DOP 2	DOP 1	DOP 2
	Day of Year			
Cool	168	185	214	227
Ambient	164	182	210	224
Warm	160	180	206	221

DOP = Planting date

Table 6. Temperature treatment effect on plant development based on the GDD necessary to reach the 5-leaf and tasseling for the 1992 field experiment.

	5-Leaf		Tasseling	
Treatment	DOP 1	DOP 2	DOP 1	DOP 2
	Day of Year			
Cool	221.4	224.8	737.3	710.2
Ambient	303.7	315.6	838.3	818.9
Warm	369.6	394.5	901.4	891.3

DOP = Planting date

Table 7. Mean maximum leaf areas as affected by temperature treatments at both planting dates for the 1992 field experiment.

	Maximum leaf area (cm^2)	
Treatment	DOP 1	DOP 2
Cool	7897	7839
Ambient	7492	8032
Warm	7081	7429

DOP = planting date

Table 8. Mean maximum heights as affected by temperature treatments at both planting dates for the 1992 field experiment.

	Maximum height (cm)	
Treatment	DOP 1	DOP 2
Cool	217	226
Ambient	207	233
Warm	182	230

DOP = planting date

Table 9. Mean wind speed, air temperature, relative humidity, dew point temperature, barometric pressure, maximum air temperature, minimum temperature, soil temperature, and total solar radiation, air temperature growing degree days, soil temperature growing degree days, and evaporation during the period from planting to the 5-leaf stage, 5-leaf stage to tasseling, and tasseling to maturity.

Date of Plant	Soil Temp. Treat.	Wind Speed (m/s)	Solar Rad. (MJ/m^2)	Max. Air Temp. (°C)	Min. Air Temp. (°C)	Mean Air Temp. (°C)	Rel. Hum. (%)	Dew Point Temp. (°O)	Potential Evap. (mm)	Baro-metric Press. (mb)	Soil Temp. (°C)	Air Deg. Days (°C)	Soil Deg. Days (°C)
						Planting to 5-Leaf Stage							
May 9	Cool	1.71	752.10	24.4	13.3	18.9	70.7	12.8	6.39	990.7	15.4	327.6	220.4
	Amb	1.73	668.40	23.8	12.7	18.3	70.0	12.0	5.63	991.1	19.7	272.9	304.9
	Warm	1.76	563.50	23.4	12.4	17.9	72.1	12.1	4.70	991.2	24.1	226.9	369.6
June 4	Cool	1.76	714.30	26.5	15.3	21.1	57.7	14.2	6.24	986.5	17.4	334.0	225.5
	Amb	1.71	652.10	26.3	14.9	20.9	66.1	13.7	5.69	986.7	22.0	295.7	315.1
	Warm	1.78	600.20	26.1	14.9	20.8	66.5	13.6	5.22	986.8	27.2	270.1	394.5
						5-Leaf Stage to Tasseling							
May 9	Cool	1.79	961.3	26.1	16.5	21.4	79.4	17.1	8.38	987.8		533.9	
	Amb	1.74	982.0	26.5	16.6	21.7	77.5	17.0	8.60	987.6		547.9	
	Warm	1.72	1,012.7	26.5	16.3	21.5	75.1	16.3	8.86	987.8		541.3	
June 4	Cool	1.74	832.2	25.9	17.1	21.6	85.9	18.9	7.25	989.8		497.1	
	Amb	1.69	840.0	26.5	17.4	22.0	85.8	19.2	7.37	989.1		514.2	
	Warm	1.63	819.2	26.3	17.0	21.7	85.0	18.7	7.16	988.9		490.4	
						Tasseling to Maturity							
May 9	Cool	2.07	1,620.7	22.5	11.7	17.1	76.8	12.4	13.49	992.4		690.5	
	Amb	2.07	1,691.7	22.7	11.9	17.2	77.4	12.7	14.11	992.2		732.7	
	Warm	2.05	1,756.5	22.7	12.1	17.4	77.9	13.0	14.67	992.2		779.3	
June 4	Cool	2.14	1,329.8	22.0	11.0	16.4	75.7	11.5	11.48	992.5		542.7	
	Amb	2.13	1,394.9	22.1	11.1	16.5	75.5	11.6	11.59	992.5		572.8	
	Warm	2.12	1,463.6	22.4	11.5	16.9	75.9	12.0	12.02	992.4		621.8	

Table 10. Total solar radiation received by the cool, ambient, and warm soil temperature treated corn plots from emergence to the 5-leaf stage.

	First Date of Planting		Second Date of Planting	
Treatment	Date of Emergence (DOY)	Solar Radiation (MJ/m^2)	Date of Emergence (DOY)	Solar Radiation ($MJ/^2$)
Cool	145	534.4	164	529.0
Ambient	140	450.7	161	466.8
Warm	138	345.8	160	414.9

Table 11. Actual rain days, potential evapotranspiration between rain days, growth stage of the crop, and total water applied to the 50 percent and 100 percent of evapotranspiration plots.

Rain Day	Growth Stage	Potential Evapo-transpiration (nun)	50 % of Potential Evapotranspiration (nun)	100 % of Potential Evapotranspiration (nun)
Jun 4	Planting to Tassel initiation			
Jun 9	Planting to Tassel initiation	20		10.0
Jun 15	Planting to Tassel initiation	35		1Z5
Jun 19	Planting to Tassel initiation	22		11.0
Jun 23	Planting to Tassel initiation	20		10.0
Jun 27	Planting to Tassel initiation	23		11.5
Jul 2	Tassel initiation to Ear initiation	30		15.0
Jul 6	Ear initiation to End of row set	20		14.0
Jul 13	Ear initiation to End of row set	26		18.2
Jul 19	End of row set to silking	26	13.0	26.0
Jul 24	End of row set to silking	19	*9.5*	19.0
Jul 29	End of row set to silking	22	11.0	220
Aug 3	End of row set to silking	21	10.5	21.0
Aug 7	End of row set to silking	22	11.0	22.0
Aug 12	End of row set to silking	26	13.0	26.0
Aug 19	Silking to End of lag phase	30	15.0	30.0
Aug 24	End of lag phase to Maturity	27	13.5	27.0
Aug 27	End of lag phase to Maturity	14	7.0	14.0
Sep 3	End of lag phase to Maturity	27	13.5	27.0
Sep 8	End of lag phase to Maturity	22	11.0	22.0
Sep 14	End of lag phase to Maturity	25	12.5	25.0
Sep 19	End of lag phase to Maturity	20	10.0	20.0
Sep 23	End of lag phase to Maturity	11	5.5	11.0
Sep 28	End of lag phase to Maturity	17	8.5	17.0
Oct 2	End of lag phase to Maturity	16	8.0	16.0
Oct S	End of lag phase to Maturity	21	10.5	21.0
Oct 14	End of lag phase to Maturity	17	8.5	17.0

Table 12. Total water applied to the various mobile shelter corn plots during the different growth stages.

Growth Stage	50% of Potential Evapotranspiration (nun)	100% of Potential Evapotranspiration (mm)
Planting to Tassel Initiation		55.0
Tassel Initiation to Ear Initiation		15.0
Ear Initiation to End of row set		3Z2
End of row set to Silking	68.0	136.0
Silking to End of lag phase	15.0	30.0
End of lag phase to Maturity	108.5	217.0

Table 13. Response coefficients of total grain yield, the number of kernels rows per ear, the number of kernels per row, kernel mass, and vegetative mass to water applied in different growth stages.

Growth Stage	Number of Kernel Rows per Ear (rows/mm)	Number of Kernels per Row (kernels/mm)	Kernel Mass (mg/mm)	Vegetative Mass (g/mm)	Total Grain Yield (kg/ha/mm)
Planting to Tassel Initiation	0.088	0.296	-0.230	265.8'	751.6'
Tassel initiation to Ear initiation	0.501	-1.663	-0.365	-12.9	441.7
Ear initiation to End of row set	-0.254	0.876	1.385'	275.7'	-414.6
End of row set to Silking	-0.159'	0.077	0.048	79.4'	134.8
Silking to End of lag phase	-0.493'	1.321	-0.630	-33.4	98.2
End of lag phase to Maturity	0.003	0.120	0.111'	69.5'	222.9'

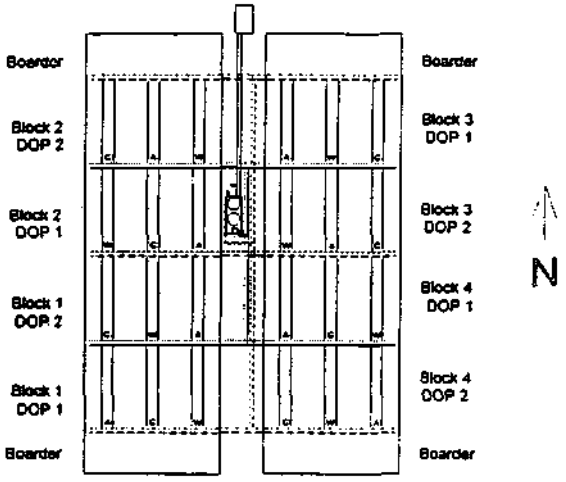

Figure 1. Field plot design of the soil temperature effect on corn growth, development, and yield.

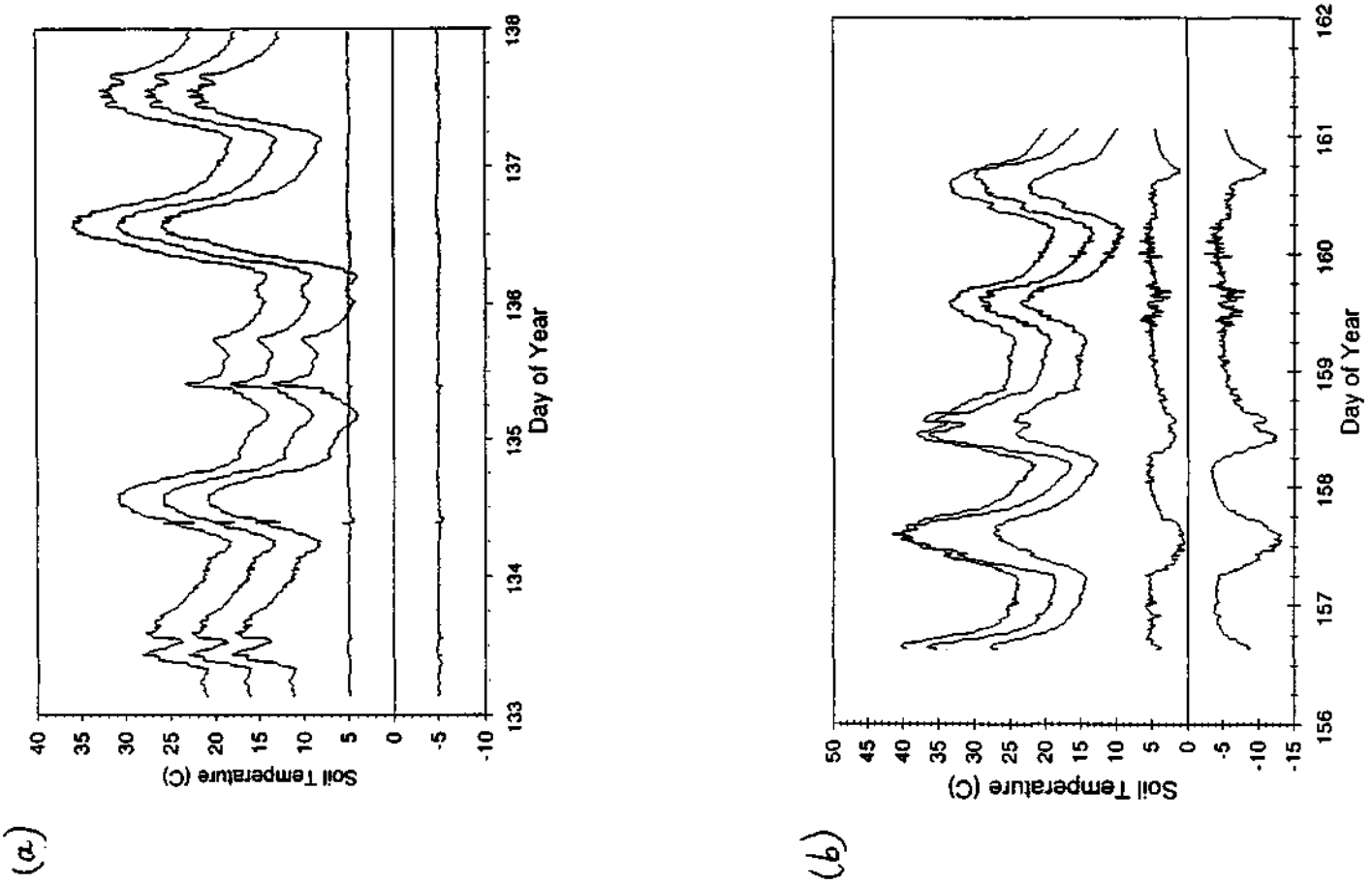

Figure 2. Cool, warm, and ambient soil temperatures, and deviation of the cool (variation about -5°C offset from ambient: (a) the first date of planting for the period May 29 (148) to June 1 (153); (b) second date of planting for the period June 4 (156) to June 8 (161).

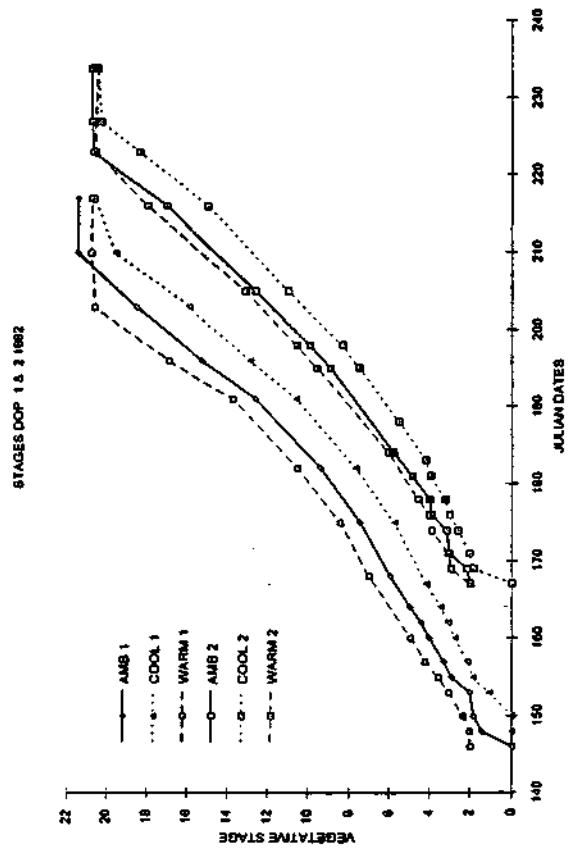

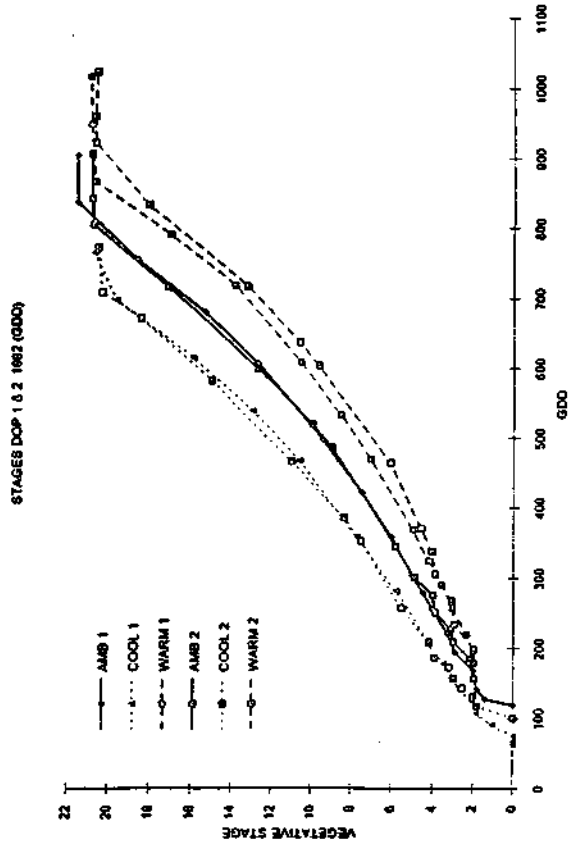

Figure 3. Vegetative development stages as a function of the day of the year (Julian Day).

Figure 4. Response of vegetative development rate as a function of soil temperature growing degree days to the 5-leaf stage and air growing degree day accumulation from the 5-leaf stage to the 21-leaf stage (tasseling).

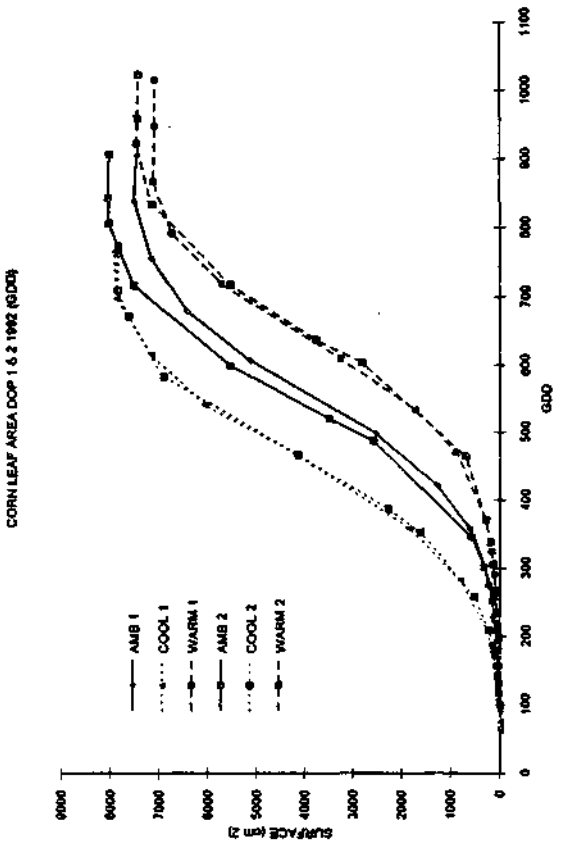

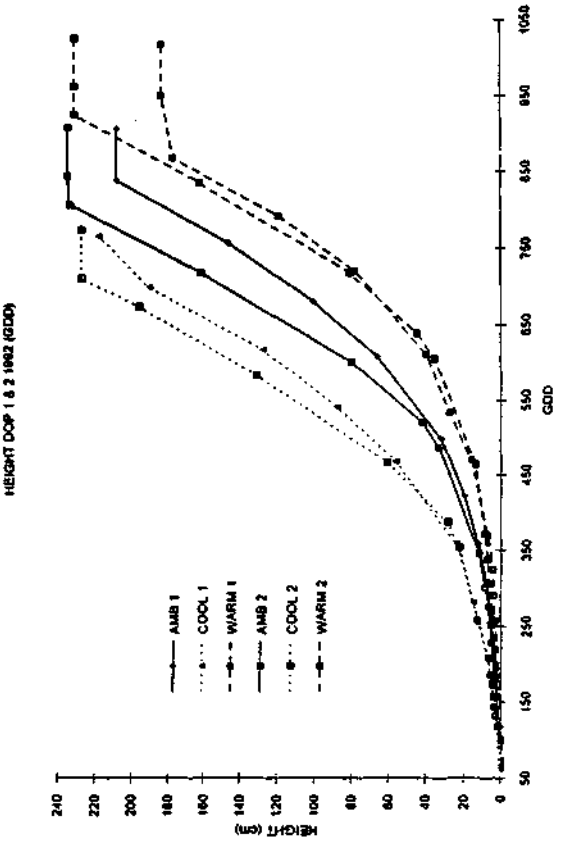

Figure 5. Rate of total leaf area development as a function of soil growing degree day accumulation from planting to 5-leaf stage and air growing degree day accumulation from the 5-leaf stage to the 21-leaf stage (tasseling).

Figure 6. Effect of soil temperature treatments on the height of corn relative to soil growing degree day accumulation from planting to 5-leaf stage and air growing degree day accumulation from the 5-leaf stage to the 21-leaf stage (tasseling).

Chapter 10. Economic Effects of Weather Modification and Seasonal Forecasts in Illinois Agriculture

Summary

Results from the investigations of crop yield shifts produced by simulated summer rain increases done in 1987-1991 were coupled with summer rainfall forecasts to assess the possible economic outcomes of using forecasts to select the level of rain change for a given summer. This research was done as part of Task 11. Simulated rain increases to actual rain amounts tested ranged from 10 to 40 percent. These values are not scientifically established as possible from midwestern cloud seeding, but were chosen to provide a wide range of conceivable changes. The yields of corn and soybeans, under these different levels of simulated rain increases, and grown under various growing season conditions experienced during the five-year agricultural plots experiment, varied considerably.

The value of using a summer rain forecasts (above, below, or near average amounts) made on June 1, and with an accuracy of 60 percent, was assessed. The skill level was used as a guide to select the amount of rain change to use in each of the five test years. Then, the distribution of the financial gain from the crop yields obtained was computed.

The use of the summer rain forecasts to decide whether to increase rainfall and by how much showed an expected gain in 85 percent of the annual cases studied. Use of this forecasting skill (and hence less than perfect choice of level of precipitation augmentation to use in a given year), produced a gain in revenue expected over the five-year test period of 1.6 percent of the crop value, a possible maximum gain of 3.8 percent, and a possible maximum loss of 0.6 percent. Rain increase applied without use of summer rain predictions (and based on use of the added rain level found best for continuous use in all five years) provided a revenue gain of only 0.4 percent, considerably less than the value obtained with the forecasts. If perfect rain forecasts existed, the expected gain would be 4.5 percent of the crop value. Even with a rain modification technology that could deliver 10, 25, or even 40 percent rain increases in any given summer, the agricultural value of rain augmentation in Illinois done over a series of years is relatively small, even when coupled with summer rain forecasts. Results indicated that most of the gain achievable from added rainfall came in the dry summers. The results of this study appear in the *Journal of Applied Meteorology,* 1993.

Chapter 11. Effects of Drought on the Surface Energy Budget

Summary

A combination of tools were used to derive large-area estimates of mid-summer sensible heat flux in the midwestern United States. This was Task 12 in the proposed research. These tools included field measurements of the surface energy budget during the 1988 and 1991 droughts in Illinois, diagnostic analysis of upper air (radiosonde) data, and a model of the surface energy budget that assumes a surface cover of corn. The field measurements indicated that midday Bowen ratios of around 1.0 were present during mid-summer drought, compared to values of 0.2 to 0.3 expected when adequate soil moisture conditions existed These field measurements were successfully simulated using the CERES-Maize model, after a modification to the root growth parameterization.

A diagnostic analysis of radiosonde data for the period 1957-1989 was performed to examine the effect of soil moisture deficiencies on boundary layer heating. Estimates of surface sensible heat flux from this analysis are within a factor of two of the estimates using the CERES-Maize model.

Large-area estimates of sensible heat flux covering the United States Cora Belt during July 1 - August 18 for the period 1949-1991 were made by driving the CERES-Maize model with historical climate data. These model estimates show rather small year-to-year variability. However, in a very dry year like 1988, the model-estimated sensible heat flux is about 30 W/m^2 greater than the long-term mean. This value was adjusted based on the radiosonde model data comparison. A revised value of 20 W/m^2 was obtained. This value is sufficiently large to cause an increase in daytime maximum temperatures of about 2°K on days with very dry soil moisture, compared to wet soil conditions, assuming that initial conditions are similar. This may in part explain the excessive high temperatures during these droughts, and in turn help explain persistence of hot-dry conditions in droughts. The results of this study will appear in an article on *Boundary Layer Meteorology*.

Chapter 12. Urban and State Responses to Global Warming

W. Henry Lambright
Syracuse Research Corporation

1. INTRODUCTION

This report concerns findings regarding the project, "Urban Response to Global Warming: The Case of Chicago." It represents research during the period October 1992 through May 1993. This project was Task 13 in the planned research, but its scope was reduced.

This report covers activities that were steps in a direction of uncovering the way climate change is being dealt with in the State of Illinois and City of Chicago. There are four activities discussed: (1) interviews with key individuals involved climate change in the Chicago area; (2) monitoring of developments regarding a multi-institutional research project on climate change impacts in the Chicago area; (3) monitoring of state policy activity in Illinois; and (4) a survey of policy activity in other cities and states to place Chicago and Illinois findings in a broader context.

2. INTERVIEWS WITH KEY INDIVIDUALS ON CLIMATE CHANGE IN THE CHICAGO AREA

In the previous year, we had surveyed a range of functions of local government in the Chicago area, getting diverse perspectives on the climate change problem. These interviews marked a continuation of the process, extending our reach to others who were concerned with the impacts of climate change but who were not public officials. One interview was with a utility and the other with a local public interest research group.

a. Commonwealth Edison

We interviewed a senior official with the Environmental Department of Commonwealth Edison, the principal power company in the Chicago area. Commonwealth Edison is the most nuclear-intensive utility in the country. Hence, its plants do not contribute to the CO_2 problem to the degree many midwestern plants relying mainly on coal do. Commonwealth Edison is concerned with the global warming issue, but it is not an urgent issue for the organization.

The climate change concern most important to Commonwealth Edison is the impact of global warming on its ability to deliver power. If global warming comes, the Chicago area will get hotter and the demand will soar. There is a risk that commonwealth Edison might not be able to meet the demand. The company is having financial problems. There are lay-offs and the company is even going to have to drop out of EPRI as part of cost-saving strategies. The state regulatory agency does not want it to add new capacity. It does not want the utility to over-build. It wants the utility to plan for a bad situation — but not necessarily global warming conditions.

The worst situation Commonwealth Edison faced recently was in 1988. The company did not have to use all its capacity then. It did not have to shut off lights. But what if 1988 happened again and again? What if the situation was even worse than 1988 and created a demand that was beyond that for which the utility was prepared? The impacts of the greenhouse effect could be dire for Commonwealth Edison, and even more so for other utilities that do not have nuclear power. The implication is that utilities need to plan for worst cases of a greenhouse world, but they are not being allowed to build to meet that world. Needless to say, the regulators would have a different perspective.

Conservation is one possible answer to the utility's capacity problem, and the company is working on this. There is also the possibility of enhancing the generating capacity through sharing power from other utilities, perhaps even from other states. But other utilities are not necessarily going to be in a future position to share power. Commonwealth Edison has fewer problems than other utilities (because of its nuclear capacity). But it still sees global warming as a problem and the concern is that if global warming is real, the capacity to meet demand would not be there.

b. Chicago Lung Association

The Chicago Lung Association is very interested in the greenhouse issue. It is an active interest in those areas where air pollution and health come together. It sees global warming as an environmental health issue. Global warming will increase the ozone (smog) pollution problem. Chicago already has ozone problems, and global warming would make them worse. This would affect people of all ages, especially those afflicted with lung conditions, such as asthma. What is to be done? Chicago will have to reduce emissions, and that means transportation issues. The Chicago Lung Association sees transportation agencies as a critical point of local decision-making for climate change.

The Association sees the Clean Air Act as a force to deal with ozone and thus with global warming, since dealing with ozone means cutting back on automobile use. Smog is pacing local decision-making for climate change in certain respects, or at least providing models. Thus, because air travels across state boundaries, there are states getting together to study their collective smog problems. Michigan, Illinois, Wisconsin, and Indiana are currently involved in the Lake Michigan Ozone Study. This will help understand common problems and common solutions. If states can learn to work together to deal with smog, they can learn to deal with other regional environmental threats, such as the greenhouse effect on climate.

However, the Chicago Lung Association is not sanguine about policy action in regard to the greenhouse effect. It feels the year 1988 was a harbinger: "our worst ozone summer." People became ill, asthma attacks increased. There was an upsurge of visits to hospitals for lung problems. If greenhouse comes, it could bring a new order of magnitude to environmental health cases in Chicago, and no one is ready.

3. "CHICAGO PROJECT:" A MULTI-ORGANIZATION RESEARCH PROJECT

During the course of the year, we monitored the initial steps in the development of the "Chicago Project." This was an attempt by the Illinois State Water Survey to develop a project that would use Chicago as a case study of the urban impacts of changed climate conditions. The study would examine comprehensively all the impacts in great depth. This would be a good project for Chicago, Illinois, and the nation. It would take an interdisciplinary approach and use various institutional capabilities. The Chicago Project was seen as a potential model for the country, a pioneering venture.

A number of meetings were held and representatives from various research and governmental institutions attended. In addition to the Water Survey, Argonne National Laboratory took an early interest. Officials from the state and city governments attended. Early on, I attended a meeting myself involving an economist from the University of Illinois to discuss facets of the project.

The strategy of the project's leaders was to obtain a start-up grant to get the activity under way. The basic idea remains sound, and the reasons for slow action appear to have less to do with substance and more with a traditional political wariness between state and city leaders.

4. STATE ACTIVITY BY ILLINOIS IN REGARD TO GLOBAL WARMING

The State of Illinois was becoming more active in global warming issues, and this was tracked The principal manifestation of this heightened Illinois interest was a new state task force on global climate change. The task force was operational in 1993 and had the opportunity to anticipate issues and steer Illinois in a sound direction, leading to possible mitigation and/or adaptation policies. There were various interests represented on the task force, such as the coal industry, farmers, water management, scientists, and environmentalists.

I had the opportunity to meet with Stanley Changnon, who was the scientist-advisor to the task force, and Robert Lieberman, who is principal staff director for the task force. We discussed what might be expected from the task force, and the need for continuing study of global warming issues in Illinois. There was likelihood of growing political and economic conflict in the future regarding global warming, due to conflicting interests in energy and water use.

5. A SURVEY OF OTHER STATES AND CITIES

A fifth activity was a survey of what other states and cities were doing in climate change so as to put the Illinois/Chicago developments in perspective.

a. Cities

With respect to cities, we contacted the International Council for Local Environmental Initiatives (IGLEI) with whom we had earlier established communication. ICLEI has been conducting an

urban CO_2 reduction project. This "consists of a select group of cities committed to providing leadership at the local government level in the development of urban strategies reducing emissions of carbon dioxide." Among the cities are: Portland, San Jose, Denver, Minneapolis-St. Paul, Dade County-Miami, the City of Toronto, Metropolitan Toronto, Helsinki, Copenhagen, Hannover, Saarbrucken, Bologna, and Ankara. The goal is to develop a strategy and take action for a 20 percent reduction in urban CO_2. The research results thus far indicate "that long-term reductions in CO_2 emissions will only be possible if there is greater attention paid to urban energy patterns and if there is a much greater role for local governments in developing and implementing CO_2 reduction strategies" (Torrie, 1993).

As the ICLEI project has evolved, some cities have moved more quickly and smoothly in developing urban CO_2 reduction policies. Toronto has apparently done well, as have Minneapolis-St. Paul and Portland. Among those United States urban areas having difficulty are Denver, San Jose, and Dade County. One of the issues in Dade County is the reluctance of Florida Power and Light to agree that there is an urban CO_2 problem.

Chicago is not involved in the urban CO_2 reduction project, but it is a participant in another related ICLEI project called the Great Lakes Municipal Energy Collaboration.

b. States

We have been in communication with EPA, which maintains information on state responses to climate change. As Sibold (1992, p. i) writes: "States are important players in the climate change area due to their influence and authority over utilities, land use, transportation, taxation, and environmental programs and policies." According to EPA (1992, p. 1), the following states have "broad-based climate change response measures:" Alaska, California, Connecticut, Iowa, and Oregon. Among the states that have apparently done the most are Connecticut and Oregon. In 1990, Connecticut passed a law which:

> Establishes a broad range of energy efficiency measures. Included are building code changes maximizing energy savings and calls for purchase of energy efficient appliances and vehicles. Also mandated: goals for improving public transportation and Connecticut Public Transportation Commission (CPTC) monitoring of progress toward these goals. The Act appropriates $80,000 from the Special Transportation Fund for CPTC. It also allows the state Environmental Protection Agency (EPA) to require tree/grass planting in connection with air discharge permits. Another aspect of the Act weakens municipality plans that give tax breaks to multi-level parking garages (EPA, 1992, p.1).

In 1989, Oregon passed a law that "requires the Oregon Department of Energy (ODOE) to develop strategies to reduce greenhouse gas emissions. The study target is to cut 1988 emissions levels 20 percent by 2005. Priority is placed on conservation, renewable resources, and alternative fuels" (EPA, 1992, p. 2).

This document reveals considerable activity similar to that in Illinois regarding state task forces in these states with "broad based climate change measures." If we go beyond "climate change" policy to consider such related climate-intensive policy areas as energy and transportation, the list of actions by states across the country grows substantially.

Also, this EPA report contains information on adaptation measures at the state level. A number of states are engaged in planning activities related to anticipated effects, such as sea level rise. There is also study underway in certain states concerning coastal erosion due to climate change effects.

What this survey makes clear is that climate change is on the agenda of a number of states, sometimes using the label of climate change and sometimes under related policy labels. There are many states that have moved further and faster than Illinois to plan for the climate change contingency.

The work we have done was just a start. Nevertheless, we trust that this report is useful.

6. REFERENCES

Sibold, Katherine D., 1992. Foreword, Selected Summary of Current State Responses to Climate Change. EPA, Washington, DC.

Torrie, Ralph, 1993. "Findings and Policy Implications from the Urban CO_2 Reduction Project." ICLEI, Toronto.

U.S. Environmental Protection Agency, 1992. Selected Summary of Current State Responses to Climate Change. EPA, Washington, DC. pp. 1-2.

Chapter 13. Hydrologic Responses to Changes in Climate and Land Use

1. INTRODUCTION

In a recent hydrologic study related to landscape functions of wetlands (Demissie and Khan, 1993), it was determined that flooding has been increasing in northeastern Illinois in recent years. Nine out of the eleven river gaging stations in northeastern Illinois showed increasing trends in flood peaks for the period of data collection. The initial assumption as to the cause of the increased flooding was the major land use changes, especially wetland drainage, that were taking place in northeastern Illinois. However, further analysis showed that precipitation also has been increasing over the same period of time. Therefore, the increase of flooding in northeastern Illinois is not only due to land use changes but also due to changes in the climate, primarily precipitation.

This pilot project has been designed to quantify the relative contribution of the different factors leading to increased flooding in northeastern Illinois. Watersheds with similar land use practices were compared to evaluate the impacts of climate variability on the trends in flooding. Similarly, watersheds with similar climate conditions but different land use practices are compared to evaluate the impact of land use changes on the trend in flooding. The general approach was to compare the hydrologic response of pairs of watersheds with similar drainage areas and soils but different land use or climatic conditions.

The following are the original tasks that were proposed for this project:

1. Select stream gaging stations in watersheds located in northeastern Illinois such that a wide range of drainage areas, land covers and soils are covered and such that each stream flow record has at least 20 years of data. Obtain relevant data on streamflow, soils, land use and precipitation for the selected watersheds.

2. Analyze trends and relations in annual mean flows, annual peakflows, time to peakflow, annual mean precipitation and peak precipitation corresponding to the annual peakflows. Also analyze trends in the flood unit hydrograph by examining the flood's peakflow, duration and volume.

The progress so far includes the determination of trends in annual mean flow and annual peakflow for streamflow records of 28 stations for a period of 40 years, and the determination of trends in the residual of annual mean flow and annual peakflow for four stations for a 50-year period of records. The residual trend analysis is used as a tool to detect trends in streamflow fluctuation that are not due to the effect of climate variability.

2. DESCRIPTION OF DATA

Twenty-eight streamgaging stations which have 20 or more years of records are used in the trend analysis. The gaging stations fall within the area considered as northern Illinois which is the section of the state above the 40 degree latitude. The location of these

stations are shown in figure 1 and the period of record for the stations are listed in table 1. A breakdown of the stations in term of drainage areas is as follows:

Drainage area (A) (sq mi)			*No. of stations*
	A	<50	8
50	<A	<500	11
500	<A		9

The analysis involves the detection of trends in the annual mean flow and annual peakflow for the 28 stations. The analysis was for a period of 40 years which covers 1951 to 1990.

The streamflow records for the following four stations were also selected for analysis of trends in the residual of the annual streamflow between 1941 and 1990.

Streamflow station	*Drainage area (sq mi)*	*Precipitation station*	*Precipitation region/state*
Kankakee River at Momence	2294	Wheatfield 2 NNW (129511)	1, Indiana
Iroquois River at Chebanse	2901	Watseka (119021)	5, Illinois
Des Planes River at Riverside	630	Chicago O'Hare (111549)	2, Illinois
Du Page River at Shorewood	324	Kankakee (114603)	5, Illinois

The four precipitation recording stations that are within the drainage area of each of the streamgaging stations are listed above. The precipitation records include annual mean precipitation and annual peak precipitation. The annual peak precipitation values were obtained from storms which occurred within six days prior to the corresponding annual peakflows.

The rank correlation analysis shows increasing trends in the mean flow record of 13 stations and at 11 stations for the peak flow. The only exception was the peakflow record for Elkhorn Creek (near Penrose) where a decreasing trend was observed. The minimum rank correlation coefficient for significant trends at the 95 percent level of confidence appears to be 0.19 for the streamflow records. The linear regression approach, on the other hand, indicated significantly increasing trends in the mean flow and peakflow data of 11 and 8 stations, respectively.

5. TRENDS IN STREAMFLOW RESIDUALS

In estimating the magnitude of hydrological changes caused by human modification of the landscape, it is difficult to distinguish between the effect of the human-induced changes and changes due to climate variability. However, we can attempt to determine if the observed hydrological changes are due to human effects or climate induced hydrological variability through statistical analysis. One approach is to use a linear regression equation to determine the relations between streamflow and precipitation. Then a non-parametric statistical method such as the Kendall Rank Correlation test is performed on the residual streamflow, i.e. the difference between the measured and predicted streamflow values.

The following steps were used in the residual trend analysis for the streamflow records:

1) Evaluate trends in the annual series of mean precipitation and peak precipitation for the precipitation-recording stations within or near the watershed corresponding to each of the streamgaging stations. The linear regression trend method is then used to predict the magnitude of the trend in the series.

2) Perform linear regression analysis of mean flow and peakflow against mean precipitation and peak precipitation in order to evaluate the component of the streamflow trend that can be attributed to the effect of trends in precipitation.

3) Analyze residual mean flow and peak flow after removing the effect of precipitation so that trends that are due to other factors such as changes in land use can be detected.

The above procedure has been completed for four selected streamflow stations and the corresponding precipitation stations. The results are shown in figures 2-9. The procedure listed above has been completed for the four streamflow stations and their corresponding precipitation stations. The results are shown in figures 2-9 for Kankakee, Iroquois, Des Plaines, and Du Page Rivers, respectively. The Kendall Rank Correlation coefficient for the streamflow and precipitation parameters are shown in table 3.

Table 3: Results of Kendall Rank Correlation and Linear Regression Tests

Station	*Mean flow*	*Peak-flow mean*	*Residual flow*	*Residual peak flow*	*Mean precipitation*	*Peak precipitation*
Kankakee	0.22	0.30	0.00	-0.09	0.27	0.26
Iroquois	0.30	0.24	0.38	0.15	0.25	0.23
DesPlaines	0.48	-0.09	0.50	0.26	0.11	-0.11
Du Page	0.25	0.01	0.11	0.25	0.11	0.10

Increasing trends are observed in the annual mean flow for the four stations. However, only Kankakee and Iroquois show significant upward trends in peakflow at the 95 percent confidence interval. Also, only the two stations show increasing trends in residual mean flow and residual peakflow.

In table 4, it is observed that the percentage of the variability in the streamflow that can be attributed to fluctuations in precipitation increases is in the following order: Iroquois, Kankakee, Du Page and Des Plaines. This coincidentally, is the order in which urbanization and storm drainage have affected the streamflow in these rivers. The Kankakee and Iroquois Rivers drain predominantly agricultural watersheds, whereas the Du Page River and the Des Plaines River flow partly through urbanized watersheds.

Table 4: Coefficient of Determination (Percent)

Station	*Mean Flow*	*Peakflow*
Kankakee	34.6	5.7
Iroquois	28.2	25.3
Des Plains	60.9	45.1
Du Page	37.0	29.6

The absence of significant trends in the residual streamflow for the Du Page and Des Plaines gaging stations can be attributed to the fact that the land use pattern in the Chicago area has not changed significantly in the last 50 years. However, the annual

flow has been steadily increasing with an increase in the observed annual precipitation for the region. The Des Plaines has experienced the highest increasing trend in annual mean flow with a rank correlation coefficient of 0.48.

Since only 34.6 percent and 28.2 percent of the mean flow and 5.7 percent and 25.3 percent of the peakflow in the Kankakee and Iroquois can be attributed to the fluctuation in precipitation based on linear regression relations, the remaining portion of the fluctuation in the streamflow, which has been shown to exhibit significantly increasing trends in the residual streamflow, are due to other factors which will include changes in land use such as drainage of wetlands for agriculture and urbanization which has taken place in these watersheds in the last 50 years.

6. CONCLUSIONS

This study has demonstrated that the annual streamflow in northern Illinois has been increasing in the last 40 to 50 years. The greatest increase in streamflow variation is observed to be occurring in the northeast corner of the state.

Linear regression relations between streamflow and precipitation were used to show that the fluctuation in the streamflow of two rivers draining watersheds in the highly urbanized northeastern region of the state is largely due to the corresponding increasing trends in precipitation variation in the region. However, two other rivers, Kankakee and Iroquois, have been experiencing increasing annual flow due to changes in land use shifts and other factors, which have occurred in the last 50 years.

7. REFERENCES

Alley, W.M. 1988. *Using Exogenous Variables in Ttesting for Monotonic Trends in Hydrologic Time Series.* Water Resources Research 24(11):1955-1961.

Demissie, M., and A.Q. Khan. 1993. *Evaluation of Ttrends in Streamflow Due to Wetland Drainage.* Illinois State Water Survey Contract Report ###, Champaign, Illinois.

Kendall, M.G. 1975. *Rank Correlation Methods.* 4th ed., Charles Griffin, London.

Mann, H.B. 1945. *Non-Parametric Test Against Trend.* Econometrica, vol. 13, pp. 245-259.

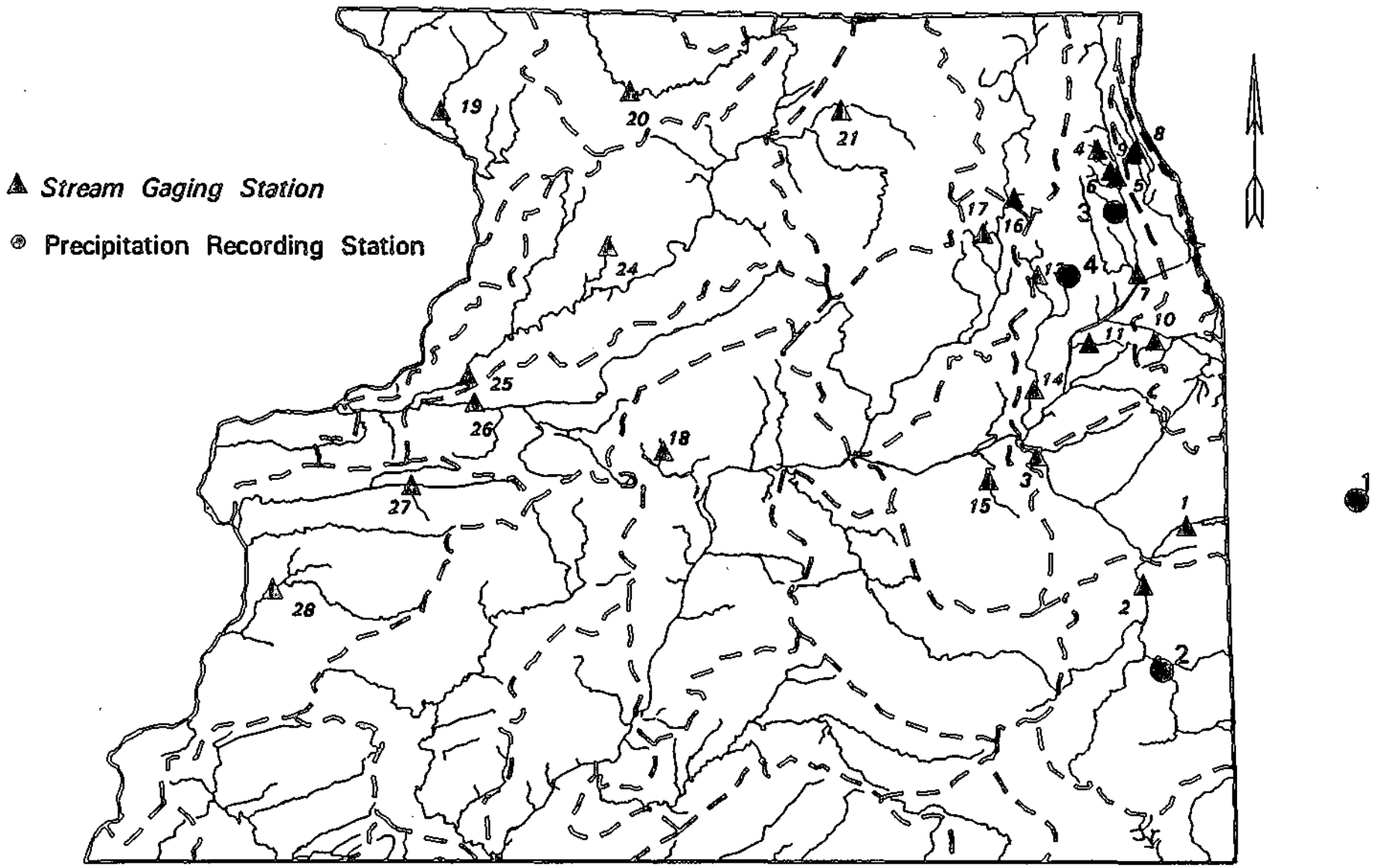

Figure 1. Location of streamgaging stations and precipitation recording stations in Northern Illinois

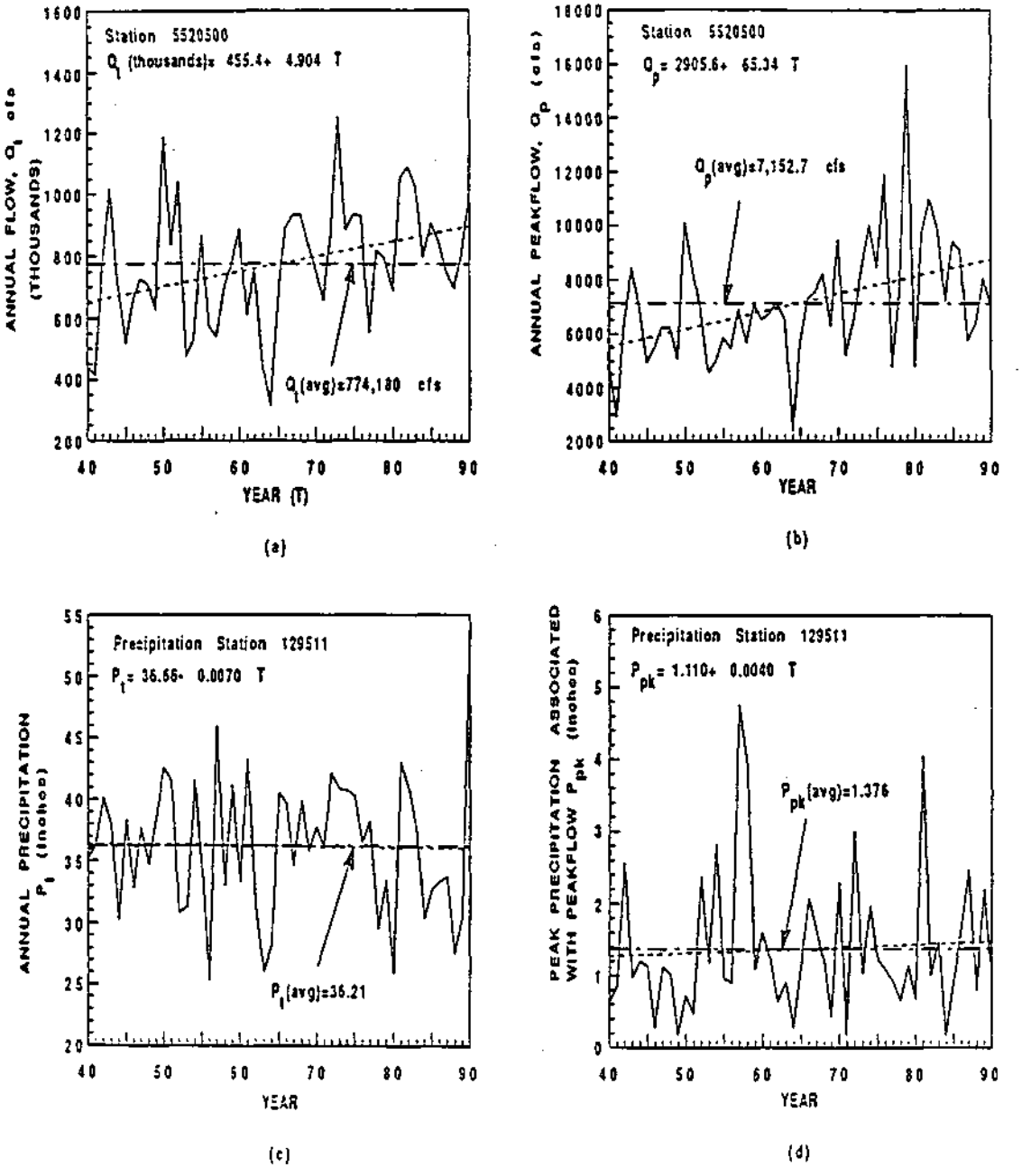

Figure 2. Trends in a) annual mean flow, b) annual peakflow, c) annual mean precipitation and d) peak precipitation associated with peakflow for the Kankakee River at Momence, Illinois

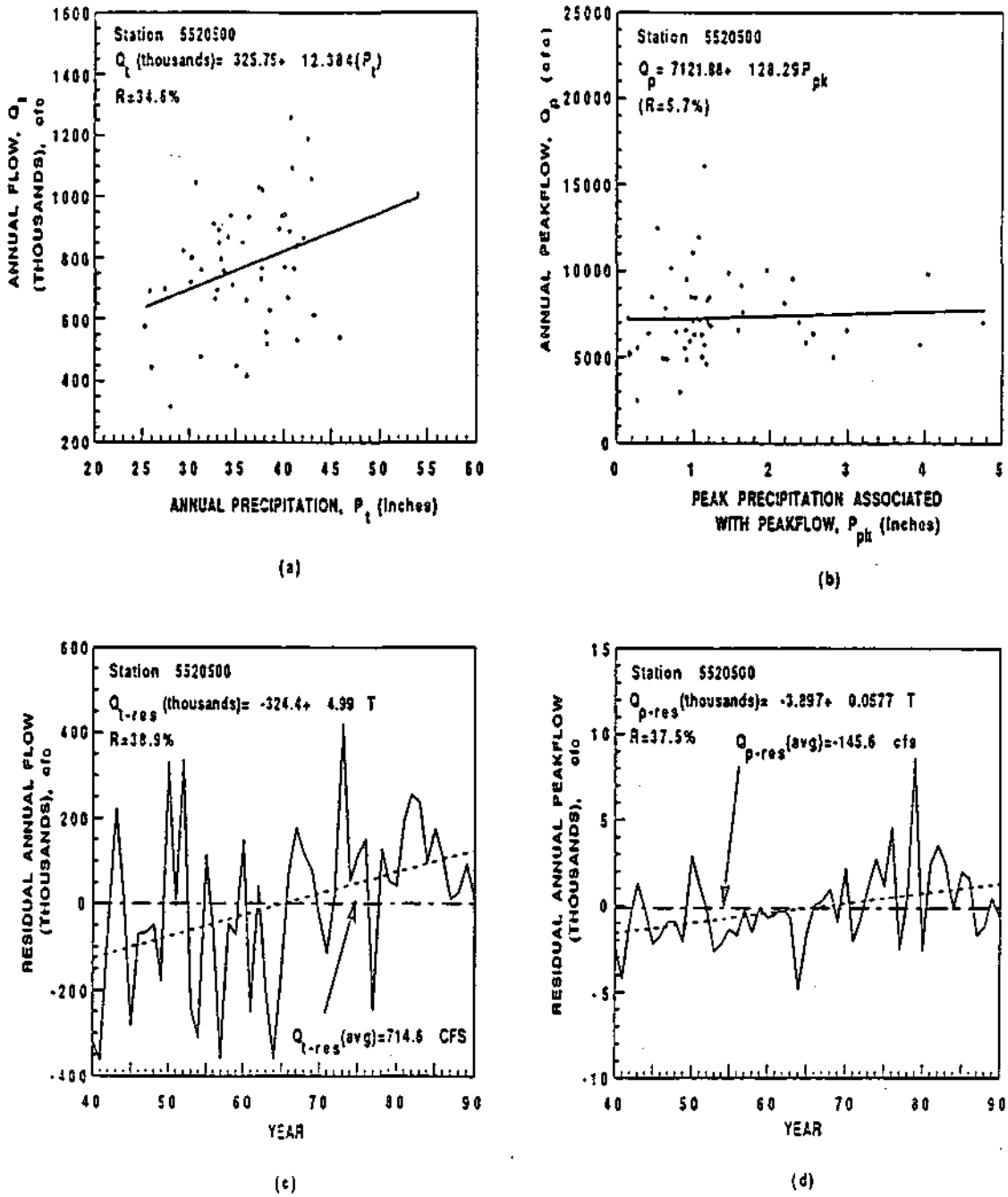

Figure 3. a) Linear regression of annual mean flow with annual mean precipitation, b) Linear regression of annual peakflow with the associated peak precipitation, c) Trends in residual annual mean flow and, d) Trends in residual annual peakflow for the Kankakee River at Momence, Illinois

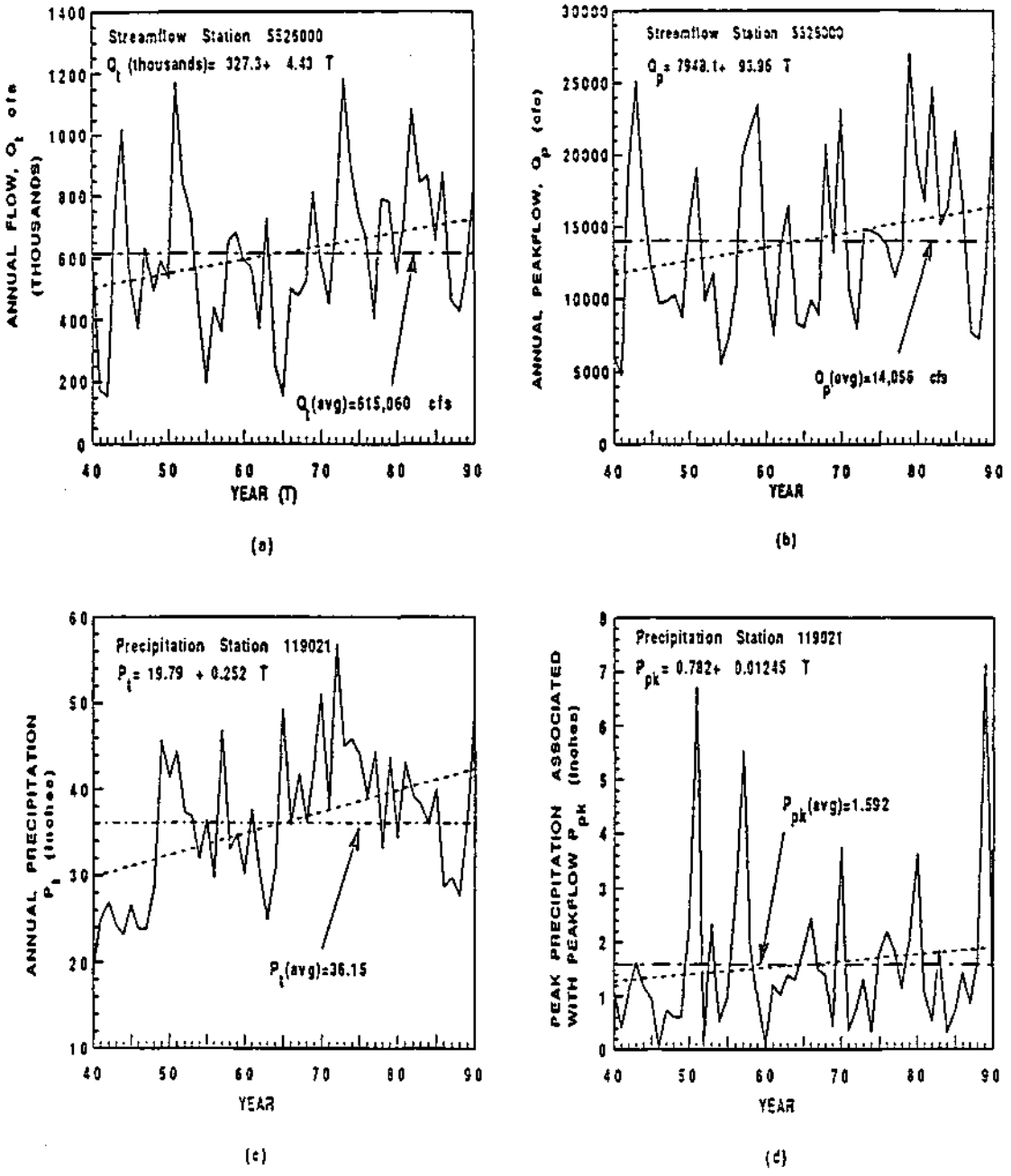

Figure 4. Trends in a) annual mean flow, b) annual peakflow, c) annual mean precipitation and d) peak precipitation associated with peakflow for the Iroquois River at Chebanse, Illinois

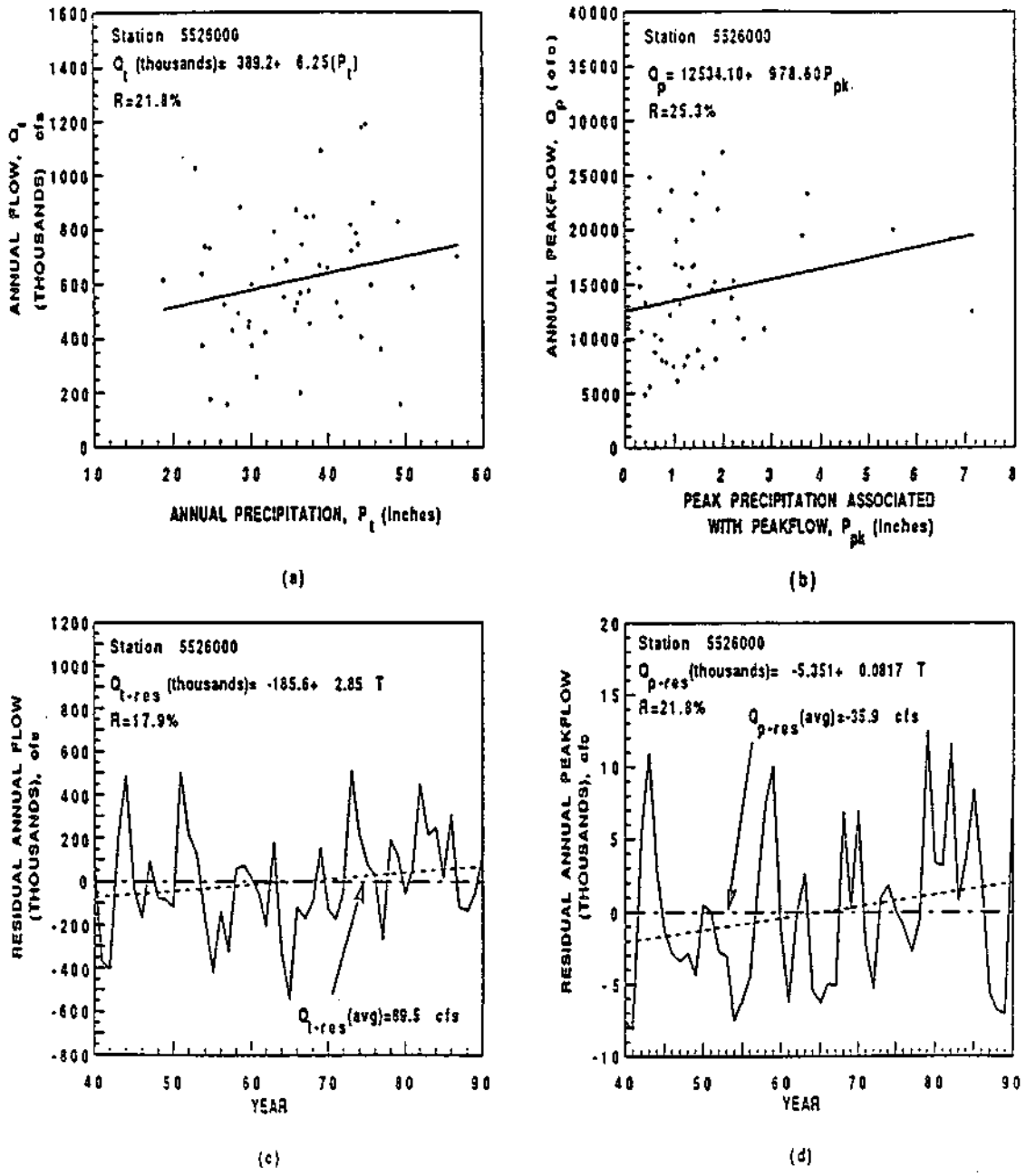

Figure 5. a) Linear regression of annual mean flow with annual mean precipitation, b) Linear regression of annual peakflow with the associated peak precipitation, c) Trends in residual annual mean flow and, d) Trends in residual annual peakflow for the Iroquois River at Chebanse, Illinois

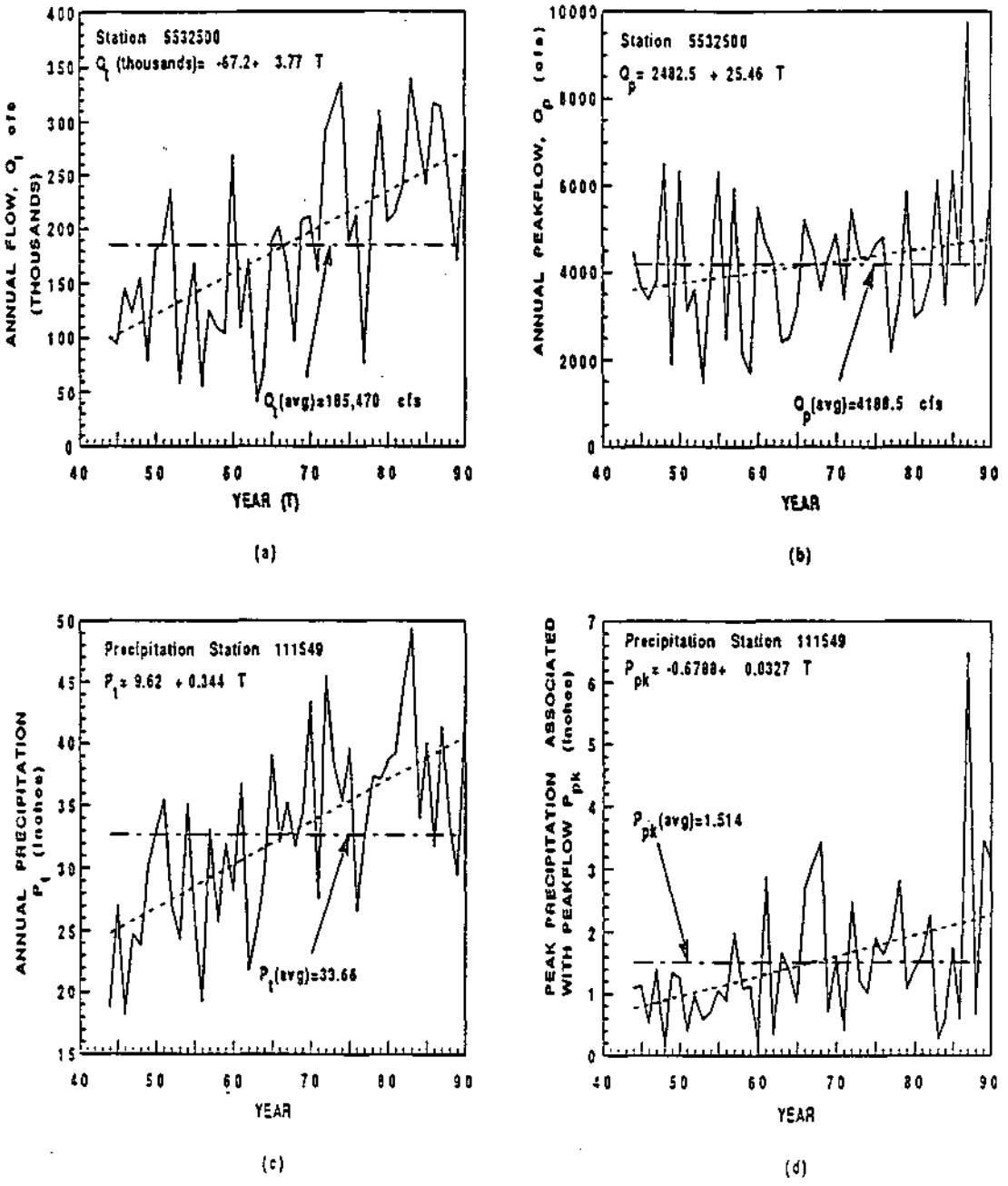

Figure 6. Trends in a) annual mean flow, b) annual peakflow, c) annual mean precipitation and d) peak precipitation associated with peakflow for the Des Plaines River at Riverside, Illinois

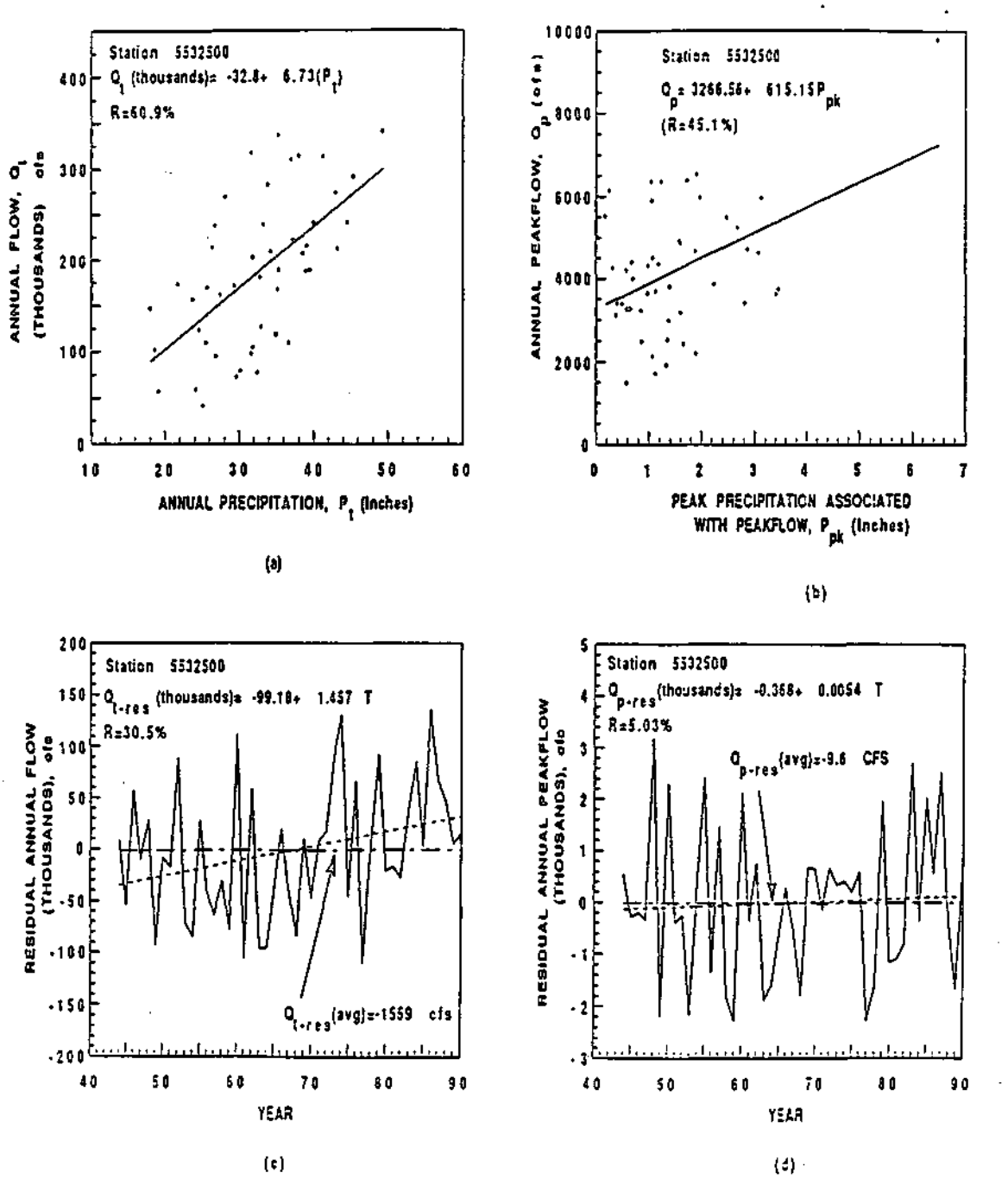

Figure 7. a) Linear regression of annual mean flow with annual mean precipitation, b) Linear regression of annual peakflow with the associated peak precipitation, c) Trends in residual annual mean flow and, d) Trends in residual annual peakflow for the Des Plaines River at Riverside, Illinois

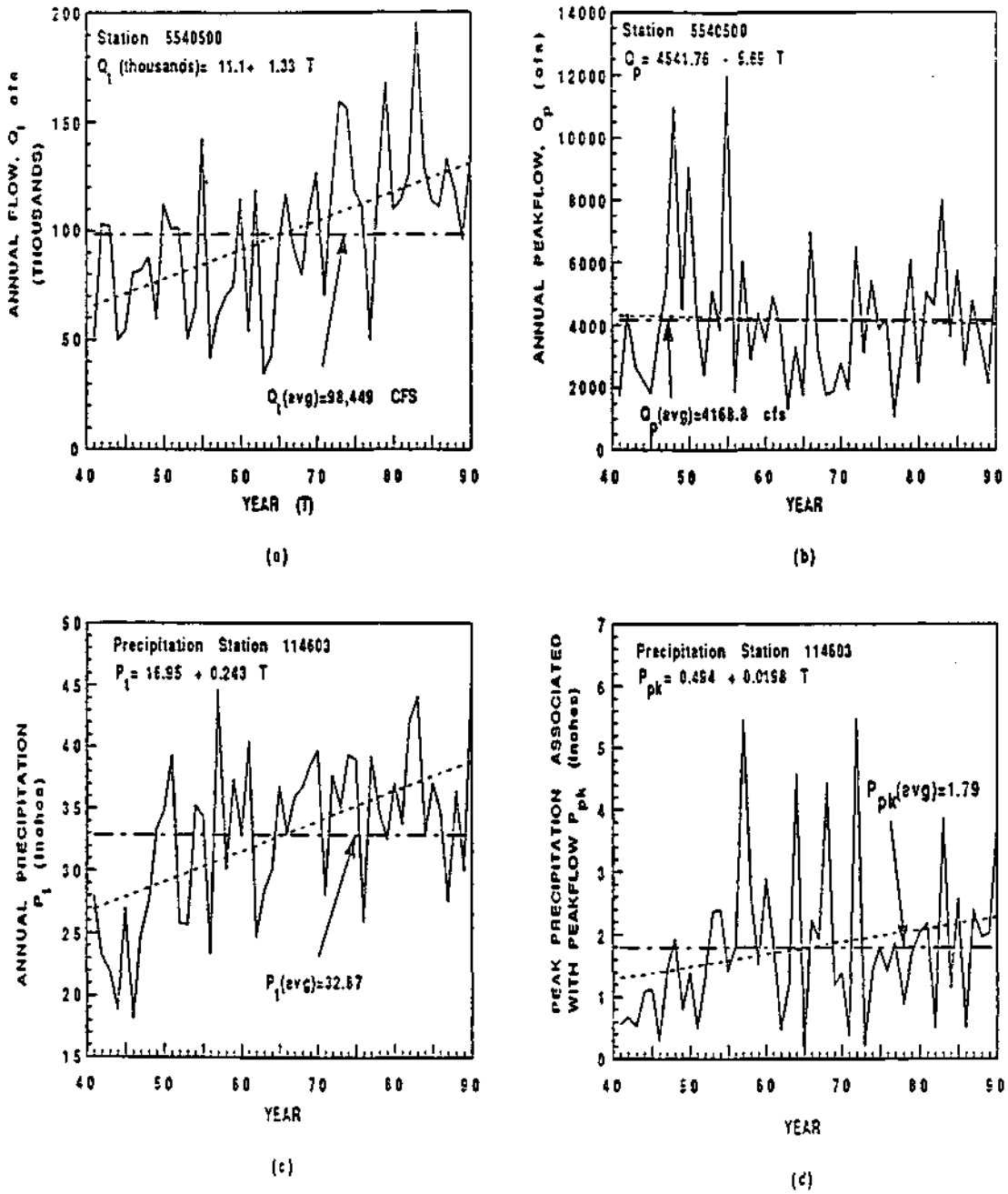

Figure 8. Trends in a) annual mean flow, b) annual peakflow, c) annual mean precipitation and d) peak precipitation associated with peakflow for the Du Page River at Shorewood, Illinois

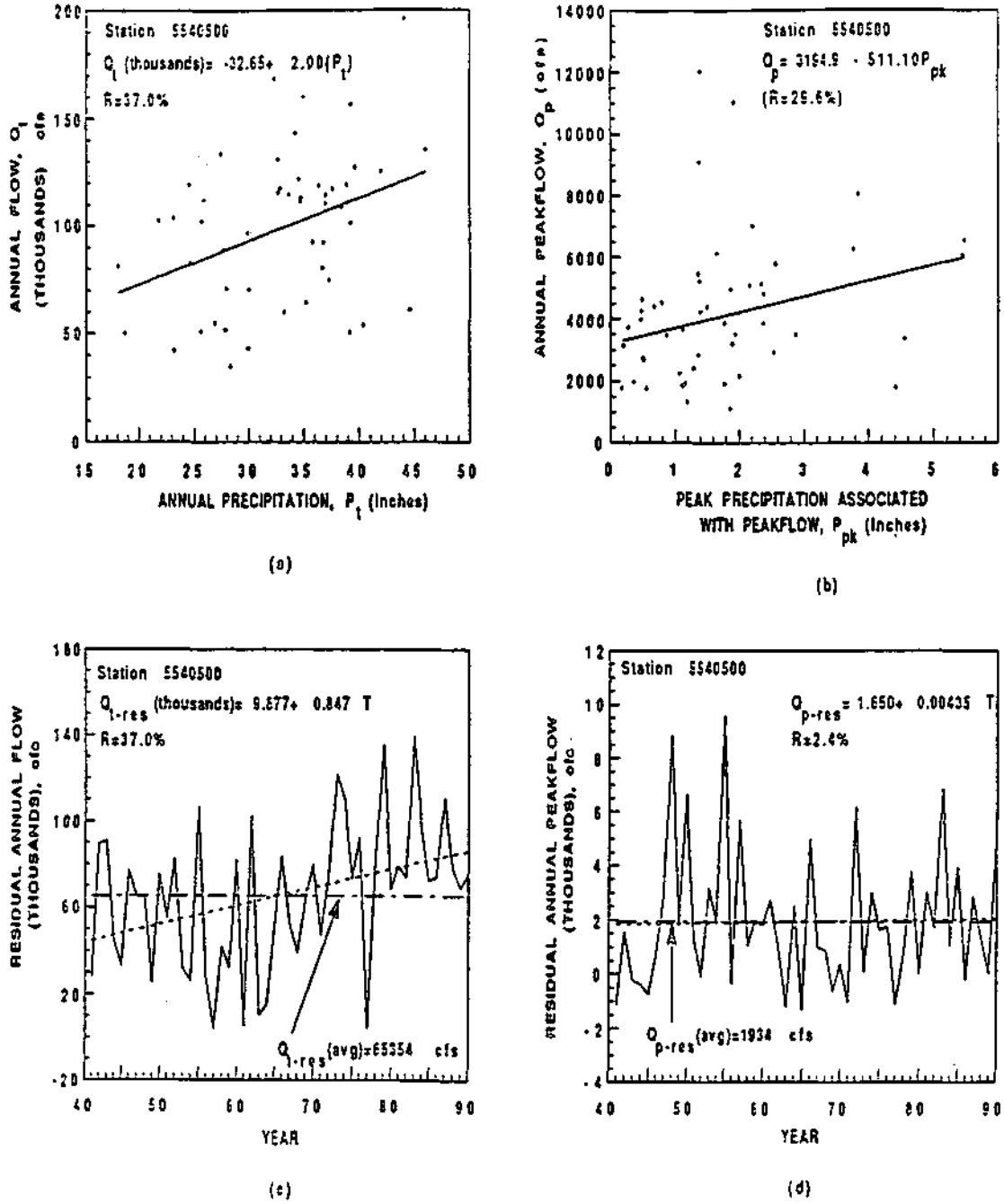

Figure 9. a) Linear regression of annual mean flow with annual mean precipitation, b) Linear regression of annual peakflow with the associated peak precipitation, c) Trends in residual annual mean flow and, d) Trends in residual annual peakflow for the Du Page River at Shorewood, Illinois